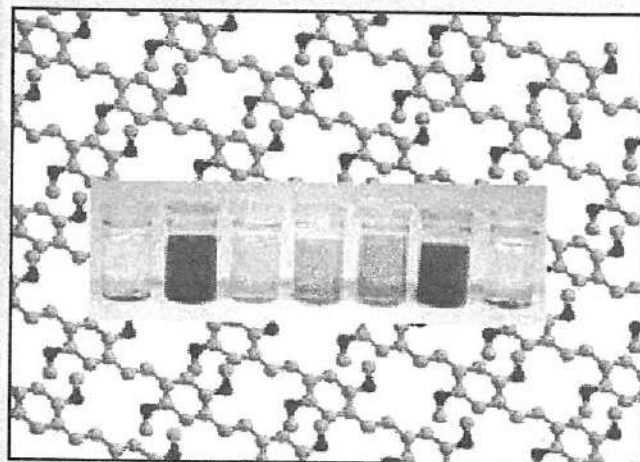


DOCTORAATSPROEFSCHRIFT

2007 | Faculteit Wetenschappen



Spectroscopy, Electrochemistry and Spectro-Electrochemistry of PPV and PTV Derivatives; the Effect of Backbone Structure and Side Chain Polarity on the Optoelectronic Properties of Conjugated Polymers

Proefschrift voorgelegd tot het behalen van de graad van
Doctor in de Wetenschappen, scheikunde, te verdedigen door:

Sofie FOURIER

Promotor: prof. dr. T.J. Cleij
Copromotor: prof. dr. J. Yperman

universiteit
hasselt

INSTITUUT VOOR
MATERIAALONDERZOEK

541.69



070539



10 APR 2007

541.64
FOUR
2007

uhasselt

DOCTORAATSPROEFSCHRIFT

2007 | Faculteit Wetenschappen

**Spectroscopy, Electrochemistry and Spectro-Electrochemistry
of PPV and PTV Derivatives; the Effect of Backbone Structure
and Side Chain Polarity on the Optoelectronic Properties of
Conjugated Polymers**

Proefschrift voorgelegd tot het behalen van de graad van
Doctor in de Wetenschappen, scheikunde, te verdedigen door:

Sofie FOURIER

070539

Promotor: prof. dr. T.J. Cleij

Copromotor: prof. dr. J. Yperman



10 APR 2007

↑
↑
universiteit
hasselt

INSTITUUT VOOR
MATERIAALONDERZOEK

D/2007/2451/14

Dankwoord

Vier jaar, het lijkt een lange tijd voor je doctoraatsonderzoek. Maar voor je het weet zit je te ploeteren op de tekst en de indeling van je thesis. Het uiteindelijke resultaat is natuurlijk niet alleen de prestatie van mij maar een samenspel van factoren. Gelukkig stelt mij een dankwoord in de gelegenheid om diegenen te bedanken die zijn steentje heeft bijgedragen tot het voltooien van deze thesis in de afgelopen vier jaar. Ik wil hier dan ook graag beginnen met het vragen van vergeving aan allen die ik niet bij naam noem.

Allereerst en bovenal gaat mijn dank uit naar mijn promotor en copromotor.

Mijn promotor Prof. Thomas Cleij wil ik bedanken voor de wetenschappelijke ideeën en daarbij horende discussies die verwerkt zijn in dit doctoraatswerk. Ik denk met plezier terug aan vele interessante gesprekken, niet alleen over het onderzoek maar tal van andere activiteiten. Thomas, zonder jou was mijn doctoraat nooit gelukt. Dank je wel! Daarnaast wens ik jou en Jennifer nog veel geluk met jullie twee kindjes, het zijn toch twee grote schatjes. Hopelijk kunnen onze kindjes nog veel samen spelen in de toekomst!

Mijn copromotor Prof. Jan Yperman wil ik graag bedanken voor het vertrouwen en de steun die hij me altijd heeft gegeven en voor de vrijheid om mijn eigen weg te zoeken in dit onderzoek. Ik ben hem daarbij ook dankbaar dat hij me de gelegenheid heeft gegeven om een doctoraat aan te vatten in zijn onderzoeksgroep.

Dankwoord

Daarnaast wil ik Prof. Dirk Vanderzande bedanken voor het uitschrijven van mijn projectvoorstel en het verder begeleiden samen met Dr. Laurence Lutsen. Mijn tijd in Universiteit Hasselt zou nooit zo leuk zijn geweest zonder de vele collega's die gedurende (een deel van) de periode 2002-2006 mijn verblijf verlevendigden. Laat mij eerst beginnen met de groep mensen die al een tijdje Universiteit Hasselt heeft verlaten: Jos, Hilde, Filip, Roel en Anja. Jos, ik heb je stoel bij je vertrek mogen warm houden, dank je hiervoor! Hilde, bij u kon steeds terecht voor een rustige babbel en nuttige tips voor het aggregaat. Filip, ik ben veel in je grapjes getrapt maar dat maakte de korte tijd dat we samen mochten beleven des te plezieriger. Roel, jij was steeds bereid om iets te gaan drinken in de cafetaria. Anja, je hebt me bij het aanvatten van mijn doctoraat goed opgevangen en in looppas het secretariaat gewezen voor het halen van mijn eerste laboboek. Vervolgens hebben we de vaste garde die ik graag wil bedanken: Veerle, Iris, Liesbet en Wibren. Veerle, dank je wel voor de mooie trouwfoto's en trouwalbum. Bij u kon ik altijd terecht voor een plezierige babbel. Nog veel succes met je bouw. Iris, mijn buurvrouwje op de 'kleine' bureau, het was aangenaam om de uurtjes op de bureau te mogen delen naast je. Je was steeds een luisterend oor. Liesbet, ook bij u kon ik steeds terecht om een leuke babbel te slaan. Nog veel plezier met de kindjes! Wibren, bij u kon ik steeds terecht als ik vragen had over de vacuümstikstof lijn. Bedankt! Vervolgens wil ik mijn studiegenoten Lien, Kristof en Ine bedanken. Lien en Kristof, we zijn samen begonnen aan ons doctoraat, we hebben samen vier toffe jaren beleefd. Veel succes bij jullie nieuwe job. Ine, we hebben 8 mooie jaren achter de rug, veel toffe gesprekken in de auto op weg naar Leuven, een mooie tijd om nooit meer te vergeten. Dank je wel, lieve vriendin (en natuurlijk voor heel lang) en denk eraan: de eerste donderdag van de maand is het onze avond! Raoul, we hebben heel wat samen mogen les geven aan BMW, amai, wat hebben we daar toch allemaal meegemaakt! Zarina, nog veel succes dit jaar bij het behalen van jouw doctoraat. Het was tof om u te leren kennen en veel mooie momenten gewenst met je metekindje, stuur me regelmatig een foto door hé! Fateme, good luck for your PhD work, you are a nice person! Jimmy, bij u kon ik

Dankwoord

steeds terecht als ik een probleem had bij de computer. Arne, het is toch beter dat je naar de kapper gaat in plaats van je haren te laten knippen door Veerle, Lien en Ine. Bert, Jan, Frederik, Hanne en Joke, jullie heb ik niet zo goed leren kennen aangezien onze tijd samen zeer kort was, maar ik wens jullie fijne doctoraatsjaren toe en natuurlijk mooie resultaten! Daarnaast wil ik ook alle mensen van Toegepaste Scheikunde bedanken. Tom, het was zeer fijn om gedurende drie jaren samen met u het labo te mogen delen, je zorgde altijd voor de nodige sfeer. Amai, je kon soms stinken! Caroline, jij kon soms ook goed stinken in ons labo. Martine, bedankt voor het aanleren van IR en Raman spectroscopie en natuurlijk ook voor de lange aangename babbels! Tot slot wil ik de andere mensen van TOES en AS bedanken voor de lekkere taart en de vele gesprekken in de koffiekamer.

Ik wil ook graag de mensen op de achtergrond bedanken. Niet alleen alle mensen van het secretariaat, ook Christel Rappoort en Steven Nijs, bedankt voor het steeds opnieuw bezorgen van de bestellingen, Koen Van Vinckenroye, redder in nood bij het crashen van mijn computer en Jos Kaelen voor het maken van de complexe cellen gebruikt in dit doctoraatswerk.

Voor mijn doctoraatsonderzoek heb ik veel medewerking gehad van mensen uit het buitenland. Zo mocht ik genieten van een uitstapje naar Milaan en Kassel om er samen te werken met Marinella Cattelani, Sylvia Lutzati (ISMAL-CNR in Milaan) en Prof. Josef Salbeck en Irina Suske uit Kassel. Bedankt allen voor het aanleren van in situ UV-Vis spectro-electrochemie. Ook wil ik Prof. Michael Deleuze bedanken voor de theoretische berekeningen op het einde van dit werk.

Universiteit Hasselt ben ik dankbaar voor de financiële steun gedurende vier jaar doctoreren.

Tot slot wil ik mijn familie bedanken voor gewoon alles! Allereerst mijn allergrootste dank naar mama en pokke voor wat ze me hebben meegegeven, de jarenlange steun en bezorgdheid, de liefde en onmisbare raad. Bedankt dat jullie me de kans hebben gegeven om verder te studeren: hoewel het soms vanzelfsprekend is, besef ik nu wel dat het niet zo is. Verder wil ik mijn broers en

Dankwoord

zussen (samen met de partners) bedanken voor de fijne jaren: Ilse, Kristof (pète) en Mieke, Jeroen en Sofie, Ietse en Greet met Fleurkje, Jef, Marieke (Tita) en Nick. Bomma, ook jij mag niet in mijn lijstje ontbreken. Je hebt nooit gesnapt wat ik nu eigenlijk deed in Diepenbeek, ik gaf soms les aan studenten, ik stond in een labo, ik studeerde en ik verdiende geld. Dat kon je niet altijd volgen. Nu zie je wel wat het eigenlijk is. Maar je moest ons plots verlaten een paar maanden voor het beëindigen van mijn doctoraat. Bomma, ik had zo graag dat je erbij was!

Erik, gedurende de vier doctoraatsjaren, zijn onze levens heel wat veranderd. We leerden elkaar kennen, gingen samenwonen, trouwden en kregen ons eerste kindje, en dit allemaal in vier jaar. Tja, een tijd om nooit meer te vergeten. Bedankt dat je er steeds was in moeilijke tijden en de tripjes naar het buitenland voor mijn doctoraat samen met ons hondje Wiebel.

Niemke, mijn allerliefste schatteboutje. Je bent nog zo klein en toch heb je een grote inbreng gedaan in mijn leven en bij het schrijven van dit werkje. Je hebt mijn ogen opengetrokken dat er ook nog een leven is zonder de scheikunde. Niemke, je bent het allermooiste wat me overkomen is in mijn leven. We gaan nog vele mooie momenten samen beleven.

Nu rest mij alleen nog te zeggen: "Het gaat u goed en dank je wel!"

Liefs,

Sofie

Table of Contents

Dankwoord

Table of Contents

Chapter 1: Introduction: Conjugated Polymers

1.1 Introduction	1
1.2 Charge Transport	3
1.3 Doping in Conjugated Polymers	5
1.4 Charges in Conjugated Polymers: Solitons, Polarons and Bipolarons	9
1.5 Aim and Outline	13
1.6 References	15

Chapter 2: Electrochemistry: Cyclic Voltammetry

2.1 Introduction	21
2.2 Experimental	25
2.3 Estimation of HOMO-LUMO Energy Levels	26
2.4 Determination of the Band Gap E_g	34
2.5 Accuracy of CV- Measurements	36

Table of Contents

2.5.1 Reversibility of an Electrochemical Process	36
2.5.2 Impurities	38
2.5.3 Ion transport through the Polymer Film	40
2.5.4 Arbitrary Choice of Onset	41
2.6 Electrochemical Properties of PPV Derivatives	42
2.6.1 Non-substituted poly(<i>p</i> -phenylene vinylene) (PPV)	42
2.6.2 Poly(2,5-di-alkoxy substituted <i>p</i> -phenylene vinylene)	44
2.6.3 PPV-type polymers with more complex aromatic cores	61
2.7 Electrochemical Properties of PTV Derivatives	69
2.7.1 <i>Non-substituted</i> poly(thienylene vinylene) (PTV)	69
2.7.2 Poly(3,4-substituted thienylene vinylene)	71
2.8 Electrochemical Properties of bis-(1-cyano- 2-thienylvinylene) phenylene derivatives	77
2.9 Electrochemical Properties of Reference Compounds	83
2.10 Typical trends observed for various types of conjugated polymers	87
2.10.1 Poly(<i>p</i> -phenylene vinylene) derivatives	87
2.10.2 Poly(thienylene vinylene) derivatives	92
2.11 Conclusions	94
2.12 References	95

Chapter 3: UV-Vis-NIR Absorption Spectroscopy

3.1 Introduction	103
3.2 Experimental	106
3.3 Thin Film UV-Vis-NIR Absorption Spectroscopy	107
3.4 Thin Film Thermochromism of PPV-Type Polymers	110

Table of Contents

3.4.1 Temperature Dependent Thin Film UV-Vis	
Absorption Spectra of PPV-type Polymers	111
3.4.2 Temperature Dependent Thin Film UV-Vis	
Absorption Spectra of PTV-type Polymers	119
3.5 Thin Film Ionochromism of PPV-type Polymers	123
3.6 Solution UV-Vis-NIR Absorption Spectroscopy	128
3.7 Solution Thermochromism in Selected Solvents	139
3.8 Conclusions	158
3.9 References	160

Chapter 4: *In Situ* Spectro-Electrochemistry

4.1 Introduction	165
4.2 <i>In situ</i> UV-Vis-NIR Spectro-Electrochemistry	168
4.2.1 Introduction	168
4.2.2 Experimental	169
4.2.3 <i>In Situ</i> UV-Vis-NIR Spectro-Electrochemistry of MDMO-PPV	170
4.2.4 <i>In Situ</i> UV-Vis-NIR Spectro-Electrochemistry of MTEM-PPV and BTEM-PPV	176
4.2.5 <i>In Situ</i> UV-Vis-NIR Spectro-Electrochemistry of NTEM-PPV	178
4.2.6 <i>In Situ</i> UV-Vis-NIR Spectro-Electrochemistry of PTV and DiPh-PTV	183
4.2.7 Conclusions	186
4.3 <i>In Situ</i> ATR-IR Spectro-Electrochemistry	187
4.3.1 Introduction	187
4.3.2. Experimental	189
4.3.3 <i>In Situ</i> ATR-IR Spectro-Electrochemistry of PPV	190

4.3.4 <i>In Situ</i> ATR-IR Spectro-Electrochemistry of MDMO- PPV	196
4.3.5 <i>In Situ</i> ATR-IR Spectro-Electrochemistry of PTV	202
4.3.6 <i>In Situ</i> ATR-IR Spectro-Electrochemistry of DiPh-PTV	206
4.3.7 Conclusions	211
4.4 <i>In Situ</i> Raman Spectro-Electrochemistry	212
4.4.1 Introduction	212
4.4.2 Experimental	215
4.4.3 <i>In situ</i> Raman Spectro-Electrochemistry of MDMO-PPV	217
4.4.4 <i>In Situ</i> Raman Spectro-Electrochemistry of PTV	222
4.4.5 Conclusions	226
4.5 Theoretical Calculations	227
4.5.1 Introduction	227
4.5.2 Experimental	228
4.5.3 Theoretical Vibrations of PPV-7	231
4.5.4 Theoretical Vibrations of OCC-PPV-7	238
4.5.7 Conclusions	245
4.6 References	246
Summary	251
Samenvatting	257
List of Abbreviations	263

Chapter 1

Introduction: Conjugated Polymers

1.1 Introduction

The beginning of conjugated polymer research occurred nearly a quarter of a century ago, when thin films of poly(acetylene) were found to exhibit profound increases in electrical conductivity when exposed to iodine vapor¹⁻³. This was the first report of polymers with high electrical conductivity ($\sigma = 10^{-9}$ S/cm for pristine films and $\sigma = 38$ S/cm for exposed films). The procedure for synthesizing poly(acetylene) was based upon a route discovered in 1974 by Shirakawa and coworkers (figure 1-1) through serendipitous addition of 1000 times the normal amount of catalyst during the polymerization of acetylene⁴. For this discovery, they were awarded the Nobel Prize for chemistry in 2000.



Figure 1-1: Alan MacDiarmid (left), Hideki Shirakawa (center), Alan Heeger (right)

Typical π -conjugated polymers consist of alternating single (σ) and double (π) bonds. The π electrons are highly delocalized and readily polarizable; features that play important roles in their electrical and optical properties. Examples of conjugated polymers include poly(acetylene) (PA), poly(*p*-phenylene vinylene) (PPV), poly(ethylenedioxythiophene) (PEDOT), polythiophene (PT), poly(thienylene vinylene) (PTV) (figure 1-2).

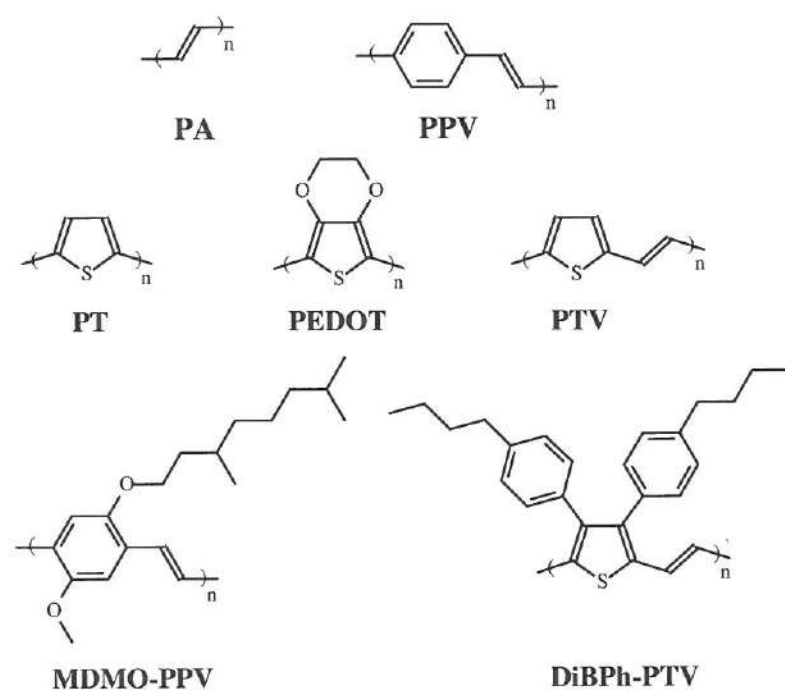


Figure 1-2: The chemical structure of some conjugated polymers

Like many other conjugated polymers, PPV and PTV are, insoluble and infusible, which results in an unsatisfactory processibility^{5,6}. As a result, soluble alternatives have been developed such as poly(2-methoxy-5-(3,7-dimethyloctyloxy)-1,4-phenylenevinylene) (MDMO-PPV) and poly(3,4-bis(4-butylphenyl)-2,5-thienylenevinylene) (DiBPh-PTV), typical derivatives with side groups attached to the conjugated backbone⁷⁻⁹ (figure 1-2). Current research focuses on the synthesis of new conjugated polymers and a further optimization of their solubility, as well as

their optical and electronic properties to make them suitable for various applications. The list of investigated applications includes polymer batteries¹⁰⁻¹⁵, smart windows¹⁶⁻¹⁹, polymeric actuators²⁰, field-effect transistors (FET)^{19, 21-26}, sensors^{19, 27-30}, photodiodes^{31, 32}, lasers³³⁻³⁸, solar cells^{32, 39-42}, light-emitting diodes (LEDs)^{7, 43-46} and light-emitting electrochemical cells (LECs)⁴⁷⁻⁵².

1.2 Charge Transport

Ever since the discovery of conjugated polymers, theorists have tried to explain the fundamental mechanism of their unusual conductivity. In figure 1-3, the molecular structure of trans poly(acetylene) is depicted as a chain of carbon atoms with attached hydrogen atoms. Like most conjugated polymers, this structure is π -conjugated, *i.e.* the bonds between adjacent carbon atoms alternate between single (σ) bonds and double (σ and π) bonds. The π -electrons are not very tightly bound, and they can become delocalized along the polymer chain.



Figure 1-3: trans poly(acetylene)

Study of one-dimensional metals became of interest in the 1950s when it was found that it is energetically favorable for such a chain to distort spontaneously, creating a gap between the filled valence band (VB) and the unfilled conduction band (CB). In poly(acetylene), this distortion causes alternating pairs of carbon atoms to move closer to one another. A band gap (E_g) develops between the filled valence band and empty energy levels (conduction band) (figure 1-4A). If the band gap is large, *e.g.* 10 eV, electrons are difficult to excite into the conduction band, and an *insulator* is obtained at room temperature. If the gap is small, *e.g.* 1.0 eV, electrons may be excited from the valence band into the conduction band by processes such as thermal excitation, vibrational excitation, or excitation by photons. The resulting charge carriers exhibit mobility and the material can be

classified as a ‘semiconductor’ (figure 1-4B). For conduction to take place in conventional, inorganic semiconductors, electrons must generally be excited from the valence to the conduction band. Thermal excitation at room temperature gives rise to some conductivity in many semiconductors. Doping is an efficient way to create additional charge carriers and thus obtain an enhanced conductivity. “Doped” conjugated polymers, when in an appropriate oxidized or reduced state (*vide infra*), are semiconductors with a significant conductivity because of their unique, extended π -conjugation. In these polymers, the extended-overlapping π -orbitals become the valence band and the π^* -orbitals become the conduction band. In most conjugated polymers the band gap is larger than 1 eV (figure 1-4C). Finally, if the band gap vanishes, overlap between the valence and conduction bands occurs, with the latter now partially being filled, leading to *metallic* properties (figure 1-4D).

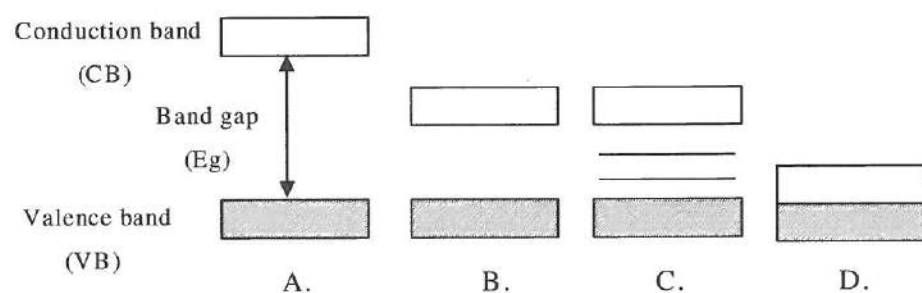


Figure 1-4: Schematic overview of the band model.

A: Band structure for insulators

B: Band structure for non-doped semiconductors, e.g. a pristine conjugated polymer

C: Band structure for doped semiconductors

D: Band structure for metals

To obtain the value of the band gap energy E_g , several techniques can be applied. Predictions of the band gap can be made by theoretical calculations. For example, a method, which has been widely used to predict the band structure of conjugated polymers, is the Valence Effective Hamiltonian (VEH) pseudo potential technique.

On the other hand, the experimental determination can be performed amongst others by electrochemistry (cyclic voltammetry) and ultraviolet-visible (UV-Vis) spectroscopy. Both experimental techniques can give a straightforward and rapid estimation of the band gap energy of conjugated polymers.

The value of the band gap E_g varies depending on several parameters and can be controlled to a certain extent by molecular design.⁵³⁻⁵⁷ Equation (i) describes the band gap in the bulk as the sum of five contributions.

$$E_g = E_{\Delta r} + E_{Res} + E_{\theta} + E_{Sub} + E_{Int} \quad (i)$$

$E_{\Delta r}$ is the energy contribution of the bond length alternation, E_{Res} is the resonance stabilization energy, E_{θ} the energy contribution caused by the interring torsion angle, E_{Sub} the influence of substituents and E_{Int} the intermolecular or inter-chain coupling in the solid state. These five different parameters are evidently often related to each other. Especially, UV-Vis absorption spectroscopy is a suitable experimental method to observe changes in the contributions of these five parameters. For example, thermochromic and solvatochromic effects are correlated with changes in E_{θ} and aggregation phenomena influence E_{Int} .

1.3 Doping in Conjugated Polymers

Pristine conjugated polymers exhibit a low conductivity because of the absence of charge carriers. Their typically high conductivity arises only after the generation of additional charge carriers in the backbone. These charge carriers can be added using a variety of typical ‘doping’ and charge injection processes, during which the redox state of the polymer changes. The term ‘doping’ is generally correct, as a small quantity of a dopant gives rise to disproportionally large change in the properties of the material. The doping of conjugated polymers is essentially a charge transfer reaction that results in a partially oxidized or reduced polymer.⁵ This removal or addition of electrons leads to the presence of charges on the

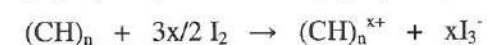
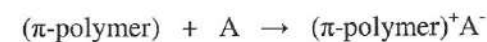
conjugated polymer. In most conjugated polymers, these charges are strongly delocalized over several monomer units, *i.e.* the conjugation length. The charges also cause a relaxation of the geometry of the (charged) polymer to a more energetically favored conformation.

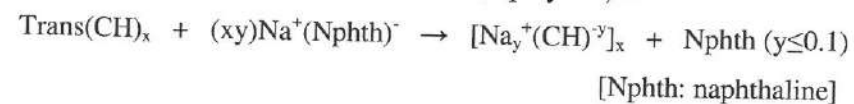
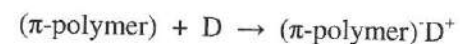
Doping of pristine conjugated polymers can be accomplished *chemically*, *e.g.* by exposure to a solution or vapor of the dopant, or *electrochemically*, by subjecting the conjugated polymer to an applied potential. Oxidation of the polymer is referred to as p-doping (in analogy to inorganic semiconductors). Similarly n-doping results in partial reduction of the polymer chain.

✓ Chemical doping

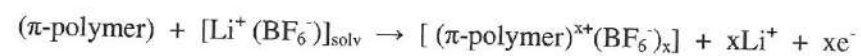
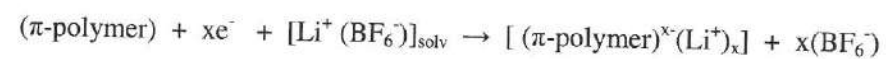
In chemical doping, the dopant, *i.e.* the oxidizing or reducing agent, should have a redox potential suitable for the oxidation/reduction of the conjugated polymer. Concomitantly, the ionization potential (or electron affinity) of the conjugated polymer should be small enough (or large enough) to facilitate the doping process. For instance, in chemical doping of pristine (undoped or neutral) poly(acetylene) by I_2 , the I_2/I_3^- redox potential is such that oxidation of poly(acetylene), *i.e.* p-doping can take place. Thus, simple exposure of pristine poly(acetylene) to I_2 vapor yields a p-doped conjugated polymer with iodine ions being formed at the same time. Alkali-metals for example Na^+ can be used for the n-doping of a conjugated polymer. During the doping/dedoping processes, the dopant physically moves in and out of the conjugated polymer lattice. This leads to physical, volumetric strains on the conjugated polymer, such as swelling and shrinking.

p-doping:



n-doping:✓ *Electrochemical doping*

When a positive potential is applied to a thin film of a conjugated polymer, immobilized on an inert electrode, the dopant anion moves from the solution into the film towards the delocalised positively charged sites of the polymer and anionic doping occurs. This anionic doping is usually referred to as p-type doping. Similarly, if a negative potential is applied, a cation would move in from the solution into the conjugated polymer film. This would be referred to as cationic, or n-type doping. The basic processes are exemplified by the following two reactions.

p-doping:n-doping:

Chemical and electrochemical doping generally give similar results, since similar charge carriers are obtained. The main advantage of electrochemical doping over the chemical way is the control of the doping level⁵⁸. This can easily be done electrochemically *via* the applied voltage giving highly reproducible results, whereas with chemical doping attempts to reach intermediate doping levels often results in inhomogeneous doping.

In all chemical and electrochemical p- and n-doping processes discussed thus far in the context of conjugated polymers, counter “dopant” ions are introduced, which stabilize the charges on the polymer backbone. However, the doping concept

extends considerably beyond that, since also “doping” processes exist in which no counter dopant ions are involved. These are typically processes in which transitory “doped” species are produced, which have similar spectroscopic signatures to polymers containing dopant ions. Examples include “photo-doping” and “charge-injection doping”.

When trans poly(acetylene) for example, is exposed to radiation of energy greater than its band gap, electrons are promoted across the band gap and the polymer undergoes “photo-doping”. Under appropriate experimental conditions, spectroscopic signatures characteristic of, for example, solitons (bond alternation defects) can be observed. They disappear rapidly because of the recombination of electrons and holes when irradiation is discontinued. If a potential is applied during irradiation, then the electrons and holes separate and photoconductivity is observed.

Charge-injection doping is possibly the most important form of doping, because it forms the basis for many current optical and electronic applications of conjugated polymers. Application of an appropriate potential across the structure can give rise, for example, to a surface charge layer, the “accumulation” layer. Such layers have been extensively investigated for conjugated polymers. The resulting charges in the polymer are present without any associated dopant ion. The spectroscopic properties of the charged species so formed can therefore be examined in the absence of dopant ion. Using this approach, spectroscopic studies of poly(acetylene) demonstrate the presence of similar absorption bands as observed for chemically and electrochemically doped polymers.

1.4 Charges in Conjugated Polymers: Solitons, Polarons and Bipolarons

✓ Solitons

Trans poly(acetylene) is a polymer with a degenerate ground state since the double and single bonds can be interchanged without changing the ground state energy. Therefore, the ground state has two configurations with the same energy (figure 1-5A). If both of the energetically equivalent configurations coexist on the same chain, an obvious disturbance in the standard conjugation pattern occurs. The appearing bond alternation defect is known as neutral soliton (figure 1-5B). This kind of quasi-particle has an unpaired electron that can extend over approximately ten carbon atoms^{59, 60} but is electrically neutral and is iso-energetically mobile along the polymer chain in both directions.

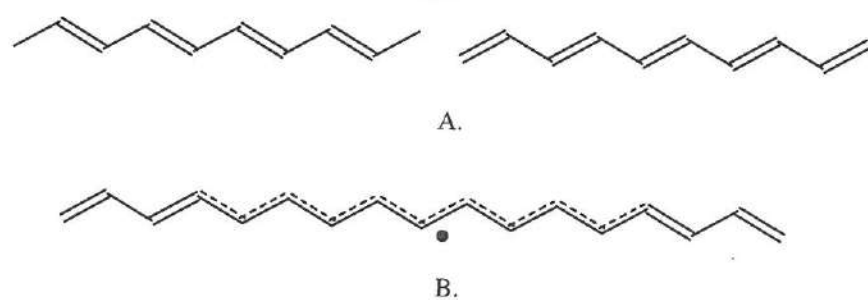


Figure 1-5: trans poly(acetylene)

A. Structure of two equivalent trans poly(acetylene) chains

B: Neutral soliton of trans poly(acetylene)

This soliton give rise to a state in the middle of the otherwise empty energy gap E_g that can be occupied by zero, one or two electrons, depending on the actual charge on the polymer chain (figure 1-6).

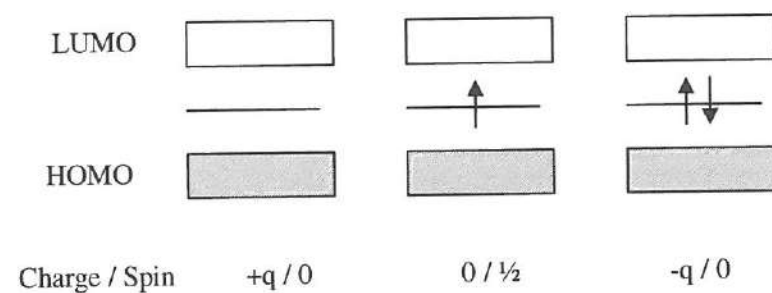
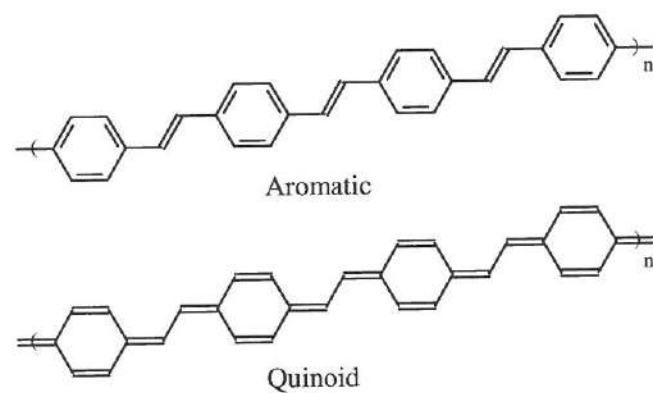


Figure 1-6: Three types of solitons,

✓ Polarons and bipolarons

If one looks at the non-degenerate case instead of the degenerate ground state case a slightly different picture emerges. Most conjugated polymers have non-degenerate ground states since their possible structures are not energetically equivalent. A typical example of this are the aromatic and quinoid forms of poly(*p*-phenylene vinylene) (PPV) as shown in figure 1-7. The quinoid structure is less stabilized and therefore higher in energy than the benzenoid form.

Figure 1-7: Aromatic and quinoid form of poly(*p*-phenylene vinylene)

Lowest ground state energy is that of the aromatic form of PPV

One can now consider a similar, but local, geometric distortion of the ground state in a conjugated polymer. The localized distortion, requiring distortion energy, gives rise to new localized electronic states within the band gap and are observable

via optical transitions with well defined energies. The removal of an electron from this localized state, *i.e.* oxidizing or “p-doping” of the conjugated polymer, results in a band structure as depicted in figure 1-8A. The entity in figure 1-8A is called a polaron, a term again borrowed from condensed matter physics. In this example the polaron is a radical cation (one unpaired electron), which is locally associated with a structural distortion in the conjugated polymer. In other words, a polaron is a charge in an extended lattice, which is stabilized by a local distortion of that lattice.

If one now considers the removal of a second electron from the conjugated structure, this process possibly could occur through formation of a second polaron at some other location in the conjugated polymer chain, *i.e.* the coexistence of two polarons. The second electron however could also be removed from the polaron itself, generating a bipolaron, and it is essential to determine whether this process or the formation of two polarons is more favorable. For both processes the formation energies are predicted to be roughly the same, but the ionisation energy for bipolaron formation should be substantially lower. Therefore one bipolaron is thought to be thermodynamically more stable than two coexisting polarons⁶¹, despite the coulombic repulsion. Figure 1-8 depicts an example of the actual structure that polarons and bipolarons represent in a typical conjugated polymer chain. It can be seen that the polaron/bipolaron in general represents a domain of a conjugated polymer in which the normal, aromatic structure of an uncharged conjugated polymer is interrupted in a significant way. For example, in several conjugated polymers the aromatic ring, *i.e.* the benzenoid (or benzoid) type structure, is replaced by a quinonoid (or quinoid) type structure.

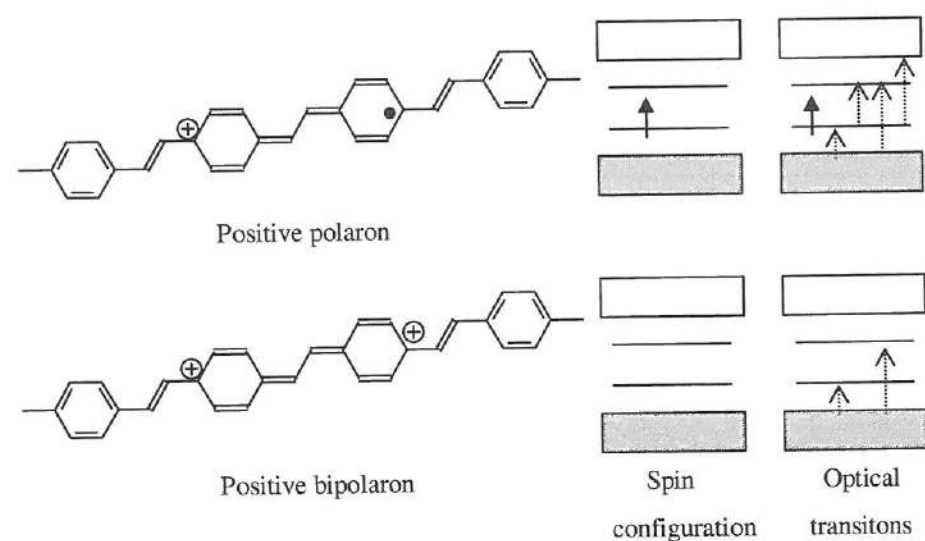


Figure 1-8: Structure, spin configuration and optical transitions for the positive polaron and bipolaron

The above discussion focuses on the generation of positively charged polarons and bipolarons, *i.e.* p-doping or oxidation, with an anion accepting the removed electrons from the conjugated polymer chain. In addition to this, also “n-doping” can occur, *i.e.* reduction or donation of electrons to the conjugated polymer chain. This would result in negatively charged polarons and bipolarons (figure 1-9). It is noteworthy that apart from these positively and negatively charged polarons and bipolarons, the neutral polarons and bipolarons are just the corresponding structural distortions before removal of electrons. However, such structures exist only hypothetically. Another important feature to note regarding the bipolaron levels is that they are either empty (p-type doping) or fully occupied (n-type doping), and thus do not have an associated spin.

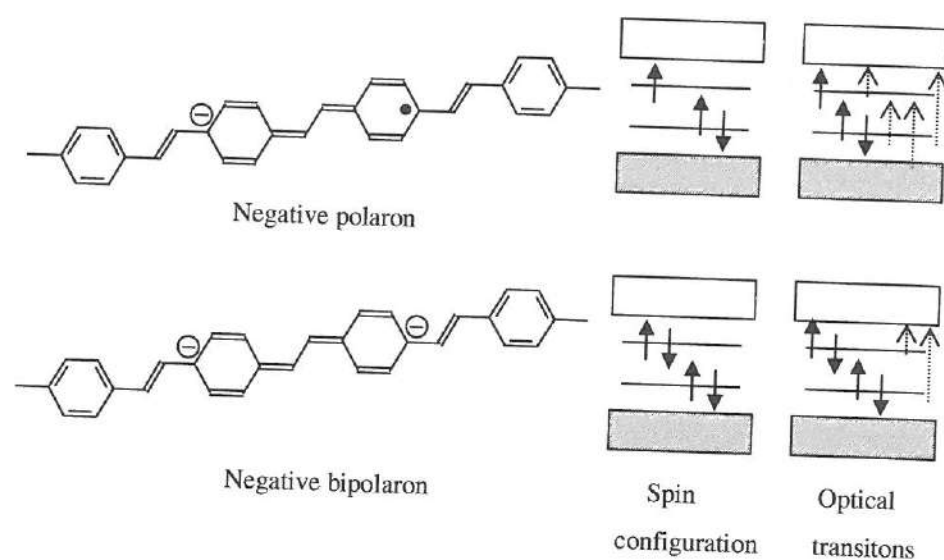


Figure 1-9: Structure, spin configuration and optical transitions for the negative polaron and bipolaron

1.5 Aim and Outline

In this thesis, an evaluation of a selection of relevant structure-property relationships of conjugated polymers is presented. The relationship between structural polymer characteristics and opto-electronic properties attracts attention from academia as well as industry. Various techniques, which situate themselves at the interface of chemistry and physics, have been employed to study these relationships. Electrochemical measurements give insight in valuable parameters such as oxidation and reduction potentials (*i.e.* the band gap energy levels), the band gap energy itself and the structure and stability of charge carriers. *In situ* techniques, in which the electrochemical measurements are coupled with UV-Vis-IR or Raman spectroscopy, can give a deep insight in the physical processes related to charge carrier formation and transport. In this respect, electrochemistry is an indispensable discipline to every research group strongly involved in the design, synthesis and evaluation of conjugated polymers. To further complement the

electrochemical and spectro-electrochemical measurements, different optical properties of conjugated polymers, such as solvatochromic and thermochromic effects, are examined in this thesis as well. The result is a comprehensive overview of the optical and electrochemical characteristics of a representative selection of conjugated polymers. Understanding the factors influencing the opto-electronic properties may provide the means to enhance the performance of opto-electronic devices based on this class of polymers.

More specifically, **chapter 2** focusses on the determination of the band gap energy levels associated with the valence and the conduction band of different PPV and PTV conjugated polymers. This is an important parameter, as it allows for the construction of an energetic scheme for a photovoltaic device, which is essential for the successful design of such devices. A comparison of the optical and electrochemically determined values of the gap is given. The chapter concludes with an attempt to identify the relationship between the chemical structure and the band gap in conjugated polymers. It is well known that modification of the side groups of a conjugated polymer can have a substantial impact on the HOMO and LUMO levels and thus affect the band gap.

Chapter 3 describes the thermochromic and solvatochromic behavior of various conjugated polymers. The thermochromic effects of conjugated polymers are studied with temperature dependent UV-Vis spectroscopy. For these studies a representative selection of four 2,5-di-alkoxy-substituted PPV polymers with various side chains is used. The thermochromic effect is demonstrated in polymer solutions as well as thin films. The thermochromic effects can be directly correlated to the segmental motions in the conjugated backbone. Based on the observed thermochromic properties a novel method is developed, which allows for a direct determination of previously inaccessible glass temperature (T_g) values. Furthermore, the solvatochromism of conjugated polymers is studied and it is

demonstrated that, as expected, aggregation phenomena have a large impact on the optical properties of conjugated polymers.

Chapter 4 focuses on the combination of electrochemistry and optical spectroscopy. The combination of these two characterization techniques provides additional relevant information on the opto-electronic properties of the polymer systems studied. Experimental measurement cells have been developed to perform *in situ* UV-Vis-NIR-, *in situ* ATR-IR- and *in situ* Raman- spectro-electrochemical measurements. With these measurements, charge carriers can be identified in electrochemically doped polymers. For selected polymers, the observed vibrational frequencies which occur as a result of the doping process, are compared with frequencies obtained from *ab initio* calculations.

1.6 References

- 1 H. L. Shirakawa, A. G. Macdiarmid, C. K. Chiang and A. J. Heeger, *Journal of the Chemical Society-Chemical Communications*, 16, **1977**, 578.
- 2 C. K. Chiang, C. R. Fincher and Y. W. Park, *Physical Review Letters*, 39, **1977**, 1098.
- 3 C. K. Chiang, M. A. Druy, S. C. Gau, A. J. Heeger, E. J. Louis, *Journal of American Chemical Society*, 100, **1978**, 1013.
- 4 T. Ito, H. Shirakawa and S. Ikeda, *Journal of Polymer Science Part a-Polymer Chemistry*, 12, **1974**, 11.
- 5 A. J. Heeger, *Journal of Physical Chemistry B*, 105, **2001**, 8475.
- 6 C. J. Brabec, F. Padinger and N. S. Sariciftci, *Journal of Applied Physics*, 85, **1999**, 6866.
- 7 D. Braun and A. J. Heeger, *Applied Physics Letters*, 58, **1991**, 1982.
- 8 F. Wudl and G. Sardanov, *US Patent*, 189, **2000**, 136.

- 9 H. Becker, H. Spreitzer, W. Kreuder, E. Kluge, H. Schenk, *Advanced Materials*, 12, **2000**, 42.
- 10 C. Arbizzani, M. Mastragostini and B. Scrosati, *Handbook of Organic Conductive Molecules and Polymers*, Vol 4, Ed. H.S. Nalwa (John Wiley & Sons, New York, 1997), **1997**, 595.
- 11 T. Sato, K. Banno, T. Maruo and R. Nozu, *Journal of Power Sources*, 152, **2005**, 264.
- 12 X. Yu, J. Xie, Y. Li, H. Huang, C. Lai, *Journal of Power Sources*, 146, **2005**, 335.
- 13 J. Wang, *Advanced Materials*, 14, **2002**, 963.
- 14 P. J. Nigrey, D. MacInnes, D. P. Nairns, A. G. Mac Diarmid and A. J. Heeger, *Journal of Electrochemical Society*, 128, **1981**, 1651.
- 15 J. Miller, *Advanced Materials*, 5, **1993**, 671.
- 16 W. A. Gazotti, G. Casalbore-Miceli, A. Geri and M.-A. De Paoli, *Advanced Materials*, 10, **1998**, 60.
- 17 R. Wisnieff, *Nature*, 394, **1998**, 225.
- 18 S. Sindhu, K. Narasimha Rao, S. Ahuja, A. Kumar and E. S. R. Gopal, *Materials Science and Engineering: B*, 1-2, **2006**, 39.
- 19 S. Roth, *One-Dimensional Metals*, Weinhiem VCH, **1995**, 209.
- 20 T. F. Otero, *Handbook of Organic Conductive Molecules and Polymers*, Vol. 4, Ed. H.S. Nalwa (John Wiley & Sons, New York), **1997**, 517.
- 21 Y. Yang and A. J. Heeger, *Nature*, 372, **1994**, 344.
- 22 A. van Breemen, P. T. Herwig, C. H. T. Chlon, J. Sweelssen, H. F. M. Schoo, *Advanced Functional Materials*, 15, **2005**, 872.
- 23 G. Horowitz, *Advanced Materials*, 10, **1998**, 365.
- 24 C. D. Dimitrakopoulos and R. L. Malenfrant, *Advanced Materials*, 14, **2002**, 99.
- 25 A. Tsumura, H. Koezuka and T. Ando, *Applied Physics Letters*, 49, **1986**, 1210.
- 26 J. H. Burroughes, C. A. Jones and R. H. Friend, *Nature*, 355, **1988**, 137.

- 27 W. Göpel and K.-D. Schierbaum, *Handbook of Organic Conductive Molecules and Polymers*, Vol 4, Ed. H.S. Nalwa (John Wiley & Sons, New York), Chap. 12, **1997**, 621.
- 28 W. Mac Diarmid, W. Zhang, Z. Huang, P. C. Wang, F. Huang, *Polymer Preprint*, 11, **1997**, 333.
- 29 B. Crone, A. Dodabalapur, A. Gelperin, L. Torsi, H. E. Katz, *Applied Physics Letters*, 78, **2001**, 2229.
- 30 D. T. McQuade, A. E. Pullen and T. M. Swager, *Chemical Reviews*, 100, **2000**, 2537.
- 31 J. J. M. Halls, C. A. Walsh, N. C. Greenham, E. A. Marseglia, R. H. Friend, *Nature*, 376, **1995**, 498.
- 32 C. J. Brabec, N. S. Sariciftci and J. C. Hummelen, *Advanced Functional Materials*, 11, **2001**, 15.
- 33 F. Hide, M. Diaz-Garcia, D. Schwartz, M. Anderson, Q. Pei, *Science*, 273, **1996**, 1833.
- 34 M. Diaz-Garcia, F. Hide, B. J. Schwartz, M. R. Anderson, Q. Pei, *Synthetic Metals*, 84, **1997**, 455.
- 35 N. Tessler, F. R. Denton and R. H. Friend, *Nature*, 382, **1996**, 695.
- 36 B. J. Schwartz, M. Diaz-Garcia, F. Hide, M. Anderson, Q. Pei, *Polymer Preprint*, 38, **1997**, 325.
- 37 N. Tessler, *Advanced Materials*, 11, **1999**, 363.
- 38 M. McGehee and A. J. Heeger, *Advanced Materials*, 12, **2000**, 1655.
- 39 S. E. Shaheen, C. J. Brabec, N. S. Sariciftci, F. Padinger, T. Fromherz, *Applied Physics Letters*, 78, **2001**, 841.
- 40 F. Padinger, R. S. Rittberger and N. S. Sariciftci, *Advanced Functional Materials*, 13, **2003**, 85.
- 41 J. J. M. Halls, C. A. Walsh, N. C. Greenham, E. A. Marseglia, R. H. Friend, *Nature*, 376, **1995**, 498.
- 42 G. Yu, J. Gao, J. C. Hummelen, F. Wudl and A. J. Heeger, *Science*, 270, **1995**, 1789.

- 43 J. H. Burroughes, D. D. C. Bradley, A. R. Brown, R. N. Marks, K. Mackay, *Nature*, 347, **1990**, 539.
- 44 R. H. Friend, R. W. Gymer, A. B. Holmes, J. H. Burroughes, R. N. Marks, *Nature*, 397, **1999**, 121.
- 45 S. J. Campbell, S. Carter, S. Karg and M. Angelopoulos, *Polymer Preprint*, 38, **1997**, 384.
- 46 P. K. H. Ho, J.-S. Kim, J. H. Burroughes, H. Becker, S. F. Y. Li, *Nature*, 404, **2000**, 481.
- 47 Y. Yang and Q. Pei, *Journal of Applied Physics*, 81, **1997**, 3294.
- 48 L. Holzer, F. P. Wenzl, S. Tasch, G. Leising, B. Winkler, *Applied Physics Letters*, 75, **1999**, 2014.
- 49 Q. Pei, G. Yu, C. Zhang, Y. Yang and A. J. Heeger, *Science*, 269, **1995**, 1086.
- 50 D. J. Dick, A. J. Heeger, Y. Yang and Q. Pei, *Advanced Materials*, 8, **1996**, 985.
- 51 Y. Yang and Q. Pei, *Polymer Preprint*, 38, **1997**, 335.
- 52 L. Holzer, B. Winkler, F. P. Wenzl, S. Tasch, L. Dai, *Synthetic Metals*, 100, **1999**, 71.
- 53 M. Kertesz, J. Koller and A. Azman, *Journal of Chemical Physics*, 67, **1977**, 1180.
- 54 J. P. Lowe and S. A. Kafafi, *Journal of American Chemical Society*, 106, **1984**, 5837.
- 55 J. L. Bredas, G. B. Street, B. Themans and J. M. Andre, *Journal of Chemical Physics*, 83, **1985**, 1323.
- 56 Y.-S. Lee and M. Kertesz, *Journal of Chemical Physics*, 88, **1988**, 2609.
- 57 J. Roncali, *Chemical Reviews*, 97, **1997**, 173.
- 58 P. J. Nigrey, A. G. Macdiarmid and A. J. Heeger, *Journal of the Chemical Society-Chemical Communications*, 14, **1979**, 594.
- 59 M. J. Rice, *Physical Letters A.*, 71, **1979**, 152.

- 60 W. P. Su, J. R. Schrieffer and A. J. Heeger, *Physical Review Letters*, 42, **1979**, 1698.
- 61 J. L. Bredas and G. B. Street, *Accounts of Chemical Research*, 18, **1985**, 309.

Chapter 2

Electrochemistry: Cyclic Voltammetry

2.1 Introduction

Electrochemistry of conjugated polymers can be carried out in nonaqueous systems. It may be carried out in two-electrode mode (working and counter electrodes) or three electrode mode (working, counter and reference electrodes), the latter is typically better for accurate potential control, while the former may more correctly emulate certain practical applications such as electrochromic devices.

The *working electrode* is the electrode where the potential is controlled and where the current is measured. For many electrochemical experiments, the working electrode is an inert conductive material such as gold, platinum, indium tin oxide (ITO) or glassy carbon. The conjugated polymers are typically directly prepared on or cast onto the conductive substrate. Alternatively, the conjugated polymers can be dissolved in the electrolyte solution. In all cases, the working electrode serves as the surface at which the electrochemical reaction takes place. The *counter electrode* or the auxiliary electrode is a conductor that completes the cell circuit. The counter electrode in laboratory experiments is generally an inert conductor like

platinum or graphite with the stipulation that it is generally larger in area than the working electrode, so that electrochemical reactions on its surface are not limiting. A device known as a potential/galvanostat is used for control of potential (potentiostatic mode) or current (galvanostatic mode) applied to the working electrode and monitoring of the resultant current or potential. The current that passes through the electrochemical cell is measured between the working electrode and the counter electrode. An electrolyte of adequate conductivity, generally an ionic salt in a solvent, gel or polymer matrix, is required for the charge transport and is therefore necessary for the observation of any electrochemical phenomena. For the three-electrode mode, the working electrode potential is controlled with respect to the *reference electrode*. This electrode should have a constant electrochemical potential as long as no current flows through it. The most common reference electrodes are the Saturated Calomel Electrode (SCE), the Normal Hydrogen Electrode (NHE) and the Silver/Silver Chloride (Ag/AgCl) electrodes. A silver wire (Ag) can also be used as a pseudo-reference electrode. Electrochemical potentials can only be measured relatively to each other. Therefore one has to apply a reference system. For the calculations presented in this chapter, it is important to understand the most basic types of reference electrode systems.

The *Normal Hydrogen Electrode* (NHE) is the primary standard in electrochemistry. It is based on the following reversible equilibrium:



The standard hydrogen electrode consists of a platinum wire or a platinum sheet covered with platinum black (*i.e.* platinised) and an electrolyte solution containing hydronium ions (H_3O^+). The hydrogen gas is usually continuously supplied. By definition, the potential of this electrode is zero at all temperatures.

The *Saturated Calomel Electrode* (SCE) or the *Calomel Electrode* was introduced by Ostwald in 1890. In the simplest case, a single drop of mercury is placed in a small tube and is covered by mercury (I) chloride (calomel, Hg_2Cl_2). Another possibility is to fill a small glass tube with a paste of mercury, mercury (I) chloride

and potassium chloride solution. The paste is in contact with a potassium chloride solution of constant activity. Mostly, a saturated potassium chloride solution is used and the paste additionally contains solid potassium chloride. The electrode net reaction can be written in the following way:



The Silver / Silver Chloride electrode (Ag/AgCl) is the most frequently used reference electrode in practical measurements, because the construction is very simple. The potential is very well reproducible and this electrode does not contain mercury, as was used in the SCE. Normally, a silver wire is covered with silver chloride. The electrode net reaction is:



As an alternative, a silver wire can be placed in a silver nitrate electrolyte solution (Ag/AgNO_3). This latter electrode configuration is in general more stable in non-aqueous media. This is important, since the electrolyte solution typically used to measure the electronic properties of conjugated polymers is non-aqueous acetonitrile.

The normal hydrogen electrode (NHE) is the universally accepted reference electrode in aqueous solutions. Unfortunately, such a universal reference electrode does not exist for non-aqueous solutions. By using aqueous reference electrodes like SCE or Ag/AgCl , an unknown liquid-junction potential is introduced into the measurements. There has been great interest in finding a reference redox couple of which the potential is independent of the solvent. It has been shown that compounds containing large ligands and a transition metal ion, *e.g.* ferrocene (Fc) and its derivatives, are most suitable. The well-defined one-electron system Fc/Fc^+ is now widely used in cyclic voltammetric studies in highly resistive organic solvents as a reference potential. When a reference compound like ferrocene is used, the procedure in cyclic voltammetry is that the formal potential of the Fc/Fc^+ system is measured as the mid-peak potential. The characteristic potentials of all other voltammetric signals are then related to the formal potential of Fc/Fc^+ . The

general formula $E^f = 1/2 (E_{p(\text{anodic})} + E_{p(\text{cathodic})})$ allows for the calculation of formal potentials of electrochemical processes¹.

A typical electrochemical experiment often employed to study conjugated polymers is cyclic voltammetry. In a cyclic voltammetry experiment, a potential is applied to the system, and the faradaic current response is measured (a faradaic current is the current due to a redox reaction). The current response over a range of potentials (a potential window) is measured, starting at an initial value and varying the potential in a linear manner up to a pre-defined limiting value. At this potential (often referred to as a switching potential), the direction of the potential scan is reversed, and the same potential window is scanned in the opposite direction (hence the term cyclic). This means that, for example, species formed by oxidation on the first (forward) scan can be reduced on the second (reverse) scan. This technique is commonly used, since it provides a fast and simple method for initial characterization of a redox-active system. In addition to providing an estimate of the redox potential, it can also provide information about the rate of electron transfer between the electrode and the analyte, and the stability of the analyte in the electrolyzed oxidation states (*e.g.*, do they undergo any chemical reactions). During a cyclic voltammogram, the doping/dedoping process can sometimes be observed visually, a process usually referred to as electrochromism. Electrochromism is the change of color or spectral signature with applied voltage (or equilibrium potential of chemical potential). Conjugated polymers possess the unique property that their color changes with redox state, which in turn is nearly always related to doping level of the conjugated polymer.

In this chapter the determination of the energetic positions of the edges of the valence band (HOMO) and the conduction band (LUMO) levels are presented as well as the band gap E_g of different kinds of conjugated polymers by applying the method of cyclic voltammetry. Optical absorption measurements are used for comparison the optical band gap with the electrochemically obtained value. At the

end of this chapter, typical trends observed for various types of conjugated polymers are discussed.

2.2 Experimental

All electrochemical experiments were carried out in a conventional three-electrode cell with using 0.1 M tetrabutylammoniumhexafluorophosphate (TBAPF₆) in anhydrous acetonitrile as the supporting electrolyte. The working electrode was a platinum disk electrode or an Indium-Tin-Oxide (ITO) coated glass substrate. The counter electrode was a platinum wire, which was placed in a separate compartment with a semi-porous frit. As a reference electrode, a silver wire in a 0.1 M AgNO₃ containing electrolyte solution was used ('quasi reference electrode' denoted later as Ag/AgNO₃). After each measurement the reference electrode was calibrated with ferrocene (which under standard conditions has an E⁰ in the range 0.03 - 0.07 V *vs.* Ag/AgNO₃). For all measurements an Eco Chemie Autolab PGSTAT 20 galvanostat-potentiostat was used. Cyclic voltammetry measurements were performed on polymer films under N₂ atmosphere with a potential sweep rate of 50 mV/s. All electrochemical experiments were carried out at room temperature. (figure 2-1)

The conjugated polymer films were drop-coated from a chloroform solution (5 mg/mL) onto the Pt working electrode or spin-coated onto the ITO coated glass substrate. When the conjugated polymer was not soluble in a chloroform solution, the precursor polymer was spin-coated from a chloroform solution onto the ITO working electrode and subsequently converted to its corresponding conjugated form by thermal treatment under a continuous flow of N₂.

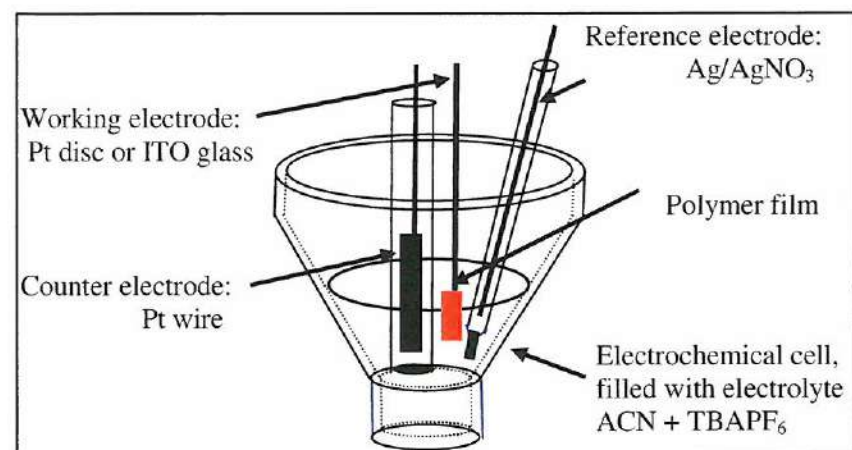


Figure 2-1: Electrochemical cell.

2.3 Estimation of HOMO-LUMO Energy Levels

The oxidation process corresponds to the removal of electrons from the highest occupied molecular orbital (HOMO) (a process associated with the ionisation potential IP), whereas the reduction cycle corresponds to the filling by electrons of the lowest unoccupied molecular orbitals (LUMO) (electron affinity EA). The onset oxidation and reduction potentials are closely related to the energies of the HOMO and LUMO levels of an organic molecule and thus can provide important information regarding the magnitude of the energy gap. The onset potentials were determined from the intersection of the two tangents drawn at the rising current and baseline charging current of the CV traces. (figure 2-2) Electrochemical band gap is directly derived from the HOMO and LUMO values.

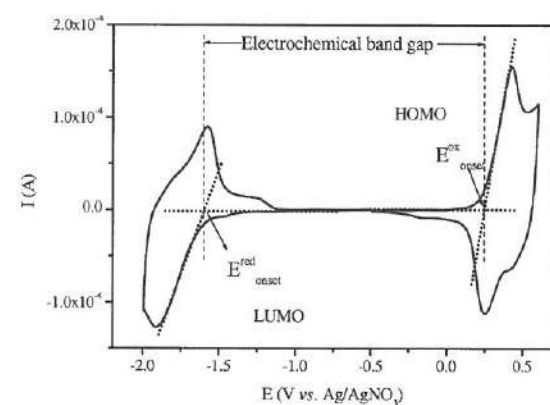


Figure 2-2: Determination of the HOMO and LUMO energy levels with the electrochemical band gap from a cyclic voltammogram

Efficient charge transfer from a donor to an acceptor is an important requirement for the design of organic solar cells. In this regard, electrochemical data can give valuable information, since they allow the estimation of the relative position of HOMO/LUMO levels of the investigated materials. The knowledge of these values allows for the selection of suitable donor-acceptor pairs with energy levels, which potentially will facilitate the charge transfer process.

As mentioned above, the oxidation and reduction onset potentials have been determined from a cyclic voltammogram. For the conversion from the oxidation and reduction potentials in Volt (vs. the reference electrode Ag/AgNO₃ obtained from a non-aqueous acetonitrile-solution) to an energy level in eV (vs. the vacuum level), a large variety of calculation methods can be found in the literature. All these methods share a common practice, that after each measurement the reference electrode is calibrated with ferrocene as an internal standard (*vide infra*). In order to select a correct conversion method, first the calculation methods found in the literature will be reviewed.

✓ Literature Method 1

As mentioned before, usually the ferrocene/ferrocenium redox couple is used as an internal standard. According to literature method 1, the potential values obtained versus Fc/Fc^+ were converted to the saturated calomel electrode (SCE) scale (SCE electrode is an aqueous electrode) by adding a constant of 0.16 V to them. The conversion is based on the following reduction potentials from literature sources: (1) the reduction potential of ferrocene *versus* NHE (aqueous electrode) is 0.4 V and (2) the reduction potential of SCE *versus* NHE is 0.24 V. To transpose the measured redox behavior into estimates for the ionization potential IP and electron affinity EA, it is necessary to relate the electrochemical potentials to the vacuum level relative to which IP and EA are defined. An empirical relationship between SCE and the vacuum level has been proposed by Brédas *et al.*² on the basis of a detailed comparison between valence effective Hamiltonian calculations and experimental electrochemical measurements.

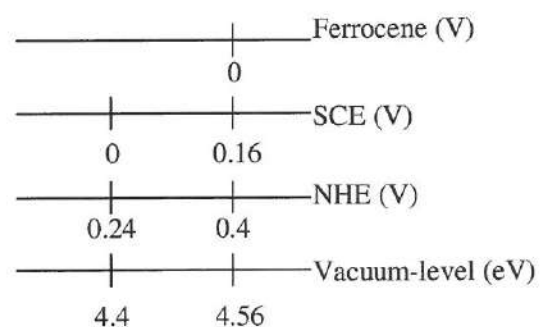
$$\text{IP (E}_{\text{HOMO}}) = -(E_{\text{ox}} + 4.4) \text{ eV}$$

$$\text{EA (E}_{\text{LUMO}}) = -(E_{\text{red}} + 4.4) \text{ eV}$$

With the onset potentials for the oxidation and reduction given *versus* SCE.

It should be noted that in solid state physics the vacuum level of an electron just outside the surface is taken as a reference point. With respect to this vacuum level all other energies are taken as negative values.

This calculation method can be summarized by the following scheme:



Example: $E_{\text{ox}} = 1.10 \text{ V vs. SCE}$
 $\text{HOMO} = -(1.10 + 4.4) \text{ eV} = -5.5 \text{ eV}$

According to this method, therefore the reduction potential of Ferrocene is located at 4.56 V vs. Vacuum.

Various research groups use this model to calculate the HOMO and LUMO values of a conjugated polymer: Examples include Ahn and Koo (South Korea), Agrawal, Jenekhe and Yang (USA), Li and Xiao (USA), Kwon and Tonzola (USA) and De Leeuw (Netherlands).³⁻¹²

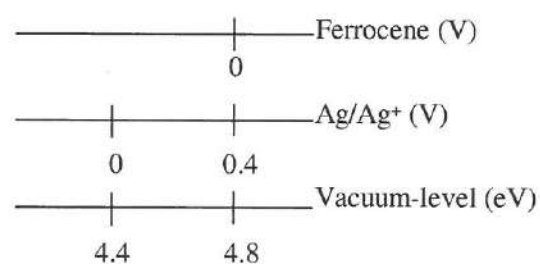
✓ *Literature Method 2*

This calculation method is comparable with the first method, the only difference is the use of the reference electrode. The expectation is that:

$$\text{IP} = E_{\text{HOMO}} = -(E_{\text{ox}} + 4.4) \text{ eV}$$

$$\text{EA} = E_{\text{LUMO}} = -(E_{\text{red}} + 4.4) \text{ eV}.$$

where E_{ox} and E_{red} are, respectively, the onset potentials for oxidation and reduction relative to a Ag/AgCl reference electrode. This last reference electrode is calibrated using ferrocene/ferrocenium redox couple as an external standard, and the $E_{1/2}$ of the Fc/Fc⁺ redox couple was found to be 0.4 V vs. the Ag/AgCl reference electrode.



Example: $E_{\text{ox}} = 0.55 \text{ V vs. Ag/Ag}^+$
 $\text{HOMO} = -(0.55 + 4.4) \text{ eV} = -4.95 \text{ eV}$

According to this method, therefore the reduction potential of Ferrocene is located at 4.80 V vs. Vacuum.

Various research groups use this model to calculate the HOMO and LUMO values of a conjugated polymer: Examples include Al-Abraham and Janietz, Pommerehne (Germany), Chen, Wang, and Yang (China), Cervini and Morgado (UK), Cho and Kin (South Korea) and a variety of other groups.¹³⁻³³

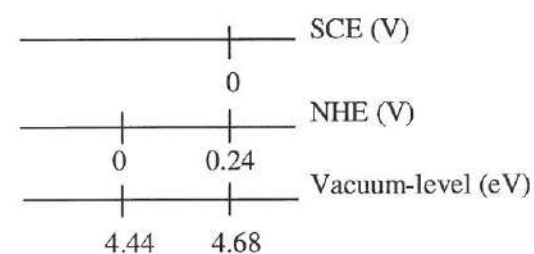
✓ Literature Method 3

The energy parameters IP (HOMO) and EA (LUMO) are related to the measured redox potentials by:

$$IP = E_{\text{HOMO}} = -(E_{\text{ox}} + 4.44) \text{ eV}$$

$$EA = E_{\text{LUMO}} = -(E_{\text{red}} + 4.44) \text{ eV}$$

where E_{ox} and E_{red} are the oxidation and reduction potentials in volts *versus* the NHE potential. This value is virtually identical with the value calculated by Gomer and Tryson³⁴, Gurevich and Pieskov (-4.43 eV), by Lohmann³⁵ (-4.48 eV) and Trassati³⁶. Thus we now have five estimates of the absolute value of $\mu_{\text{H}^+/\text{H}_2}$ which lie very close together and for this conversion -4.44 eV is used as the reasonable average of these values. For further reference, the well established reduction potential of the reference electrode SCE is 0.24 V vs. NHE³⁷.

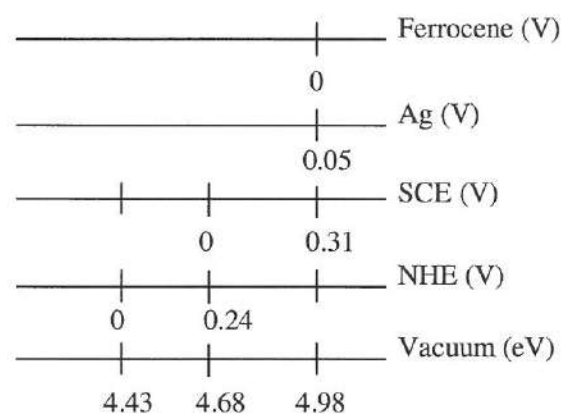


Example: $E_{\text{ox}} = -0.37 \text{ V vs. SCE}$
 $\text{HOMO} = -(-0.37 + 4.682) \text{ eV} = -4.272 \text{ eV}$

Also this method is used by a large variety of research groups: Bard (USA), Brédas (Belgium/USA), Shi, Tian and Wu (China), Trassati (Italy), Kotz (Switzerland), Reis (USA) and Ozkan (USA).^{2, 36, 38-45}

Based on the significant amount of theoretical work supporting this conversion method, this calculation method is deemed significantly more reliable than the other models. The connection to the Ag/AgNO₃ scale and ferrocene can readily be established from the work of Allen J. Bard³⁷, an important electrochemist, who found that reduction potential of ferrocene/ferrocenium in acetonitrile is 0.31 V vs. SCE.

This leads to a general scheme for the calculation of HOMO and the LUMO values of conjugated polymers, which will be used for the studies presented in this thesis. Since in the electrochemical cell, which is used for our investigations, the reduction potential of ferrocene is in the range 0.03 - 0.07 V (average 0.05 V) vs. Ag/AgNO₃, the scheme is as follows (with the exact conversion depending on the actually measured ferrocene value):



Example: $E_{\text{ox}} = 0.5 \text{ V vs. Fc/Fc}^+$
 $\text{HOMO} = -(0.5 + 4.982) \text{ eV} = -5.483 \text{ eV}$

According to this method therefore the reduction potential of Ferrocene is located at 4.98 V vs. Vacuum.

✓ Literature Method 4

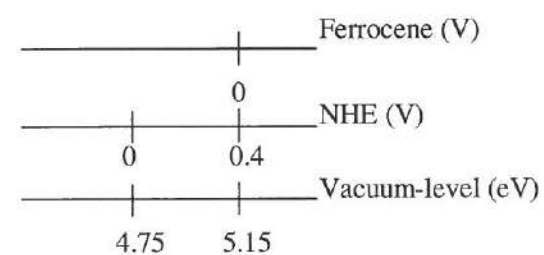
In the research using this method it was assumed that ferrocene has a reduction potential of 0.4V vs. NHE (see also method 1). Using this value, the determined oxidation and reduction onset potentials in the cyclic voltammogram were corrected to NHE and subsequently recalculated to eV by using the assumption that NHE is located at -4.75 V vs. the vacuum level. So, the equation for the calculation of HOMO and LUMO is:

$$\text{HOMO} = -(E_{\text{onset}}^{\text{ox}} + 4.75) \text{ eV}$$

$$\text{LUMO} = -(E_{\text{onset}}^{\text{red}} + 4.75) \text{ eV}$$

With the onset potentials expressed *versus* NHE.

This calculation method is only used at the university of Linz⁴⁶⁻⁴⁹.



Example: $E_{\text{ox}} = 0.795 \text{ V vs. NHE}$
 $\text{HOMO} = -(0.79 + 4.75) \text{ eV} = -5.54 \text{ eV}.$

According to this method, therefore the reduction potential of Ferrocene is located at 5.15 V vs. Vacuum.

✓ Other Literature Methods

In the literature, a significant amount of alternative methods and errors can be found, which are associated with the lack of knowledge of the various reference

electrode systems. A typical example, is the method employed by Jégou (USA) and Wan (China).^{50, 51}

According to Jégou⁵⁰: The electron affinity (LUMO level) is estimated from the onset reduction potential by using a value of -4.8 eV for the SCE energy level relative to the vacuum level. This calculation method is similar to the previously presented second literature method. However, erroneously instead of the ferrocene level, the SCE energy level is used. In another example, according to Wan⁵¹: HOMO and LUMO energy levels are calculated assuming that the Ag/Ag⁺ reference electrode is positioned at 4.7 V vs. Vacuum. This calculation method is comparable to the previously presented third literature method, but also in this case, the wrong reference electrode is used (*i.e.* SCE is positioned at *circa* 4.7 V vs. Vacuum).

✓ Conclusions

Electrochemistry is an indispensable discipline to every research group to determine the energetic positions of the edges of the valence band and the conduction band of conjugated polymers. However, in literature several methods to calculate these energy values from experimental data can be found. This makes a comparison of experimentally found electrochemical data with literature values troublesome. The various methods yield highly varying results. As a result, for the reduction potential of ferrocene in acetonitrile the values of 4.56 eV, 4.80 eV, 4.98 eV and 5.15 eV are found when, respectively the first, second, third and fourth calculation method are used. The difference between the lowest and the highest value is 0.59 eV! This means that dependent on the calculation method a reported HOMO or a LUMO position of a polymer can shift more than 0.5 eV.

Summarizing, after a careful analysis of the various conversions the HOMO and LUMO energy levels of the different conjugated polymers calculated in this work, is based on the reduction potential of ferrocene located at 4.98 V vs. vacuum-level.

This assumes that the conversion from NHE reference electrode to the vacuum energy level is 4.43 ± 0.05 V and that the reduction potential of the SCE vs. NHE reference electrode is 0.24 V. The conversion from SCE in aqueous environment to Ag/AgNO₃ in non-aqueous (acetonitrile) environment can be made using ferrocene. The reduction potential of ferrocene/ferrocenium in acetonitrile is well known and equal to 0.31 V vs. SCE. The last important reduction potential is ferrocene vs. Ag/AgNO₃ which in our laboratory has been estimated at 0.05 V.

2.4 Determination of the Band Gap E_g

To obtain the value of the band gap energy, several techniques can be applied. Predictions of the band gap can be made by theoretical calculations. A method that has been widely used to predict the band structure of conjugated polymers is the valence effective Hamiltonian (VEH) pseudo potential technique⁵². The band gaps, which have been calculated in this way, are usually in reasonable agreement with experimental data. The experimental determination can amongst others be performed by electrochemistry (cyclic voltammetry) and ultraviolet-visible (UV-Vis) spectroscopy.

As mentioned above, the electrochemical band gap is directly derived from the HOMO and LUMO values obtained in a cyclic voltammogram. The difference between the HOMO and the LUMO is the electrochemical band gap.

To determine the optical band gap of a conjugated polymer from a UV-Vis spectrum, the tangent on the low energetic side of the absorption spectrum is drawn. The intersection of this tangent and the abscissa gives a value for the optical band gap (figure 2-3).

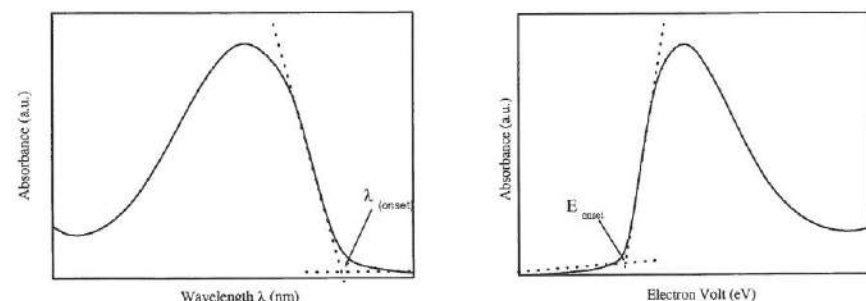


Figure 2-3: Determination of the optical band gap from an UV-Vis spectrum

In an UV-Vis spectrum, the absorbance is measured as a function of the wavelength of the absorbed lights. To make the conversion from nanometers (nm) to electron volt (eV), one can use the equation of Planck.

$$E = h\nu = hc/\lambda$$

In this equation, E is the energy (in J), h is the Planck constant (6.626×10^{-34} Js), c is the speed of light (3×10^8 ms $^{-1}$), ν is the frequency (in s $^{-1}$ or Hz) and λ is the wavelength (in m). Since 1 eV equals 1.602×10^{-19} J, the conversion from nm to eV can be straightforwardly accomplished using a simple conversion equation.

$$E \text{ (eV)} = 1240.8/\lambda \text{ (nm)}$$

Several reports can be found in literature in which the optical and the electrochemical band gap of a conjugated polymer are compared^{20, 53-56}. A clear trend, which can be observed both in the literature and in the experiments reported in this chapter, is that the electrochemical band gap is always slightly larger than the optical band gap. A possible explanation for this observation is that the optical band gap can be considered the 'pure' HOMO-LUMO transition, while in the electrochemical data generally an interface barrier for charge injection between different materials can play a role.⁵⁶ Such a barrier could occur at the interface between the working electrode and the polymer film and therefore increase the observed value. Hence, it can be expected that the electrochemical system is much

more comparable to the actual conjugated polymer based devices, such as polymer LEDs and organic solar cells.

2.5 Accuracy of CV- Measurements

In this work, the exact determination of the HOMO and LUMO position of a polymer is an essential concept. This raises the question what the actual accuracy of a CV experiment is and whether it is possible to compare HOMO and LUMO values of different kinds of polymers. There are different factors that can be influence the accuracy namely:

- ✓ Reversibility/irreversibility of the electrochemical processes
- ✓ Impurities in the electrolyte solution or the polymer films
- ✓ Ion transport through the polymer films
- ✓ Arbitrary choice of onset

As a result of these factors, the accuracy with which HOMO and LUMO energy levels can be estimated based on electrochemical measurements is somewhat limited. However, in almost all cases it is possible to obtain values for these levels at an accuracy of ± 0.10 V or better. This value is the margin of error for all electrochemical derived data in this thesis. Detailed knowledge of the factors influencing the accuracy of the measurements is often essential to understand the observed electrochemical behavior. To this end, a number of illustrative examples are presented below.

2.5.1 Reversibility of an Electrochemical Process

- ✓ *Reversibility/quasi-reversibility/irreversibility*

For a redox reaction to be reversible, the concentrations of the oxidized and reduced species at the electrode surface must be maintained at the values required

by the Nernst equation. In practical terms, a redox reaction is reversible if the rate of electron transfer is fast relative to the scan rate (the rate of change of potential) and if the oxidized and reduced species are stable on the experimental time scale (*i.e.*, they do not undergo any significant chemical reactions). One advantage of cyclic voltammetry is that it is relatively straightforward to see from a cyclic voltammogram whether a system is reversible. The peak potential difference for a reversible system is 60 to 70 mV (the theoretical value is about 59 mV, depending on the temperature and the switching potential), and the peak currents are equal (figure 2-4A). In electrochemistry the kinetics are called irreversible when the charge transfer step is very slow or one of the electrochemical species decomposes during the measurement. In this case, the anodic and cathodic reactions are never of similar size and shape (figure 2-4B). When the electrode process is neither very facile nor very slow we speak of quasi-reversible behavior (figure 2-4B).

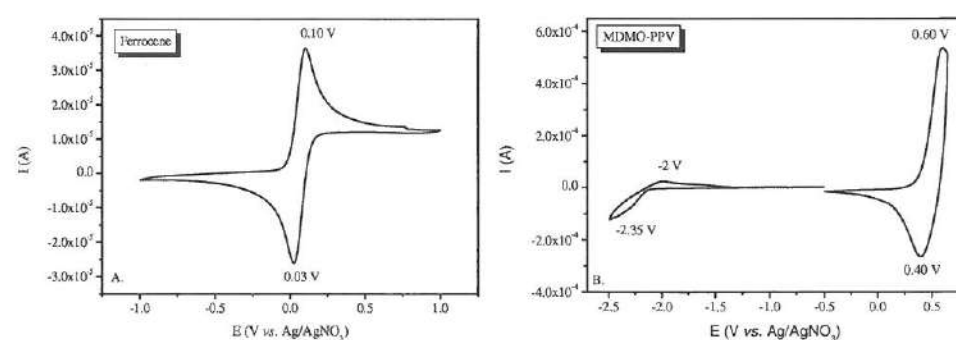


Figure 2-4: Cyclic voltammograms of ferrocene and MDMO-PPV.

A. Ferrocene/ferrocenium is a reversible process.

B. Oxidation of MDMO-PPV is quasi-reversible, the reduction irreversible.

The accuracy of a cyclic voltammetry experiment is higher when the studied redox process is reversible or quasi-reversible. The above is illustrated by the cyclic voltammogram of MDMO-PPV (Figure 2-4B). The oxidation peak of MDMO-PPV (right side of the figure) is quasi-reversible with a peak potential difference of 0.2 V. This means that the species formed by oxidation can be reduced on the

reverse scan. Through this, the calculation of the HOMO is more accurate. The reduction peak of MDMO-PPV at the left side of the figure 2-4B is irreversible because on the reverse scan only a minimal current for the oxidation of the species formed by reduction can be seen. Hence, the obtained LUMO value will be significantly less reliable.

2.5.2 Impurities

The purity of the solvents and the electrolytes strongly influences the potential range, which can be used for experiments. Careful drying and purification of the solvents and the electrolyte considerably improve the quality of the voltammograms. Otherwise, electrochemically active impurities could possibly undergo certain undesired reactions at the electrodes, leading to higher currents, which would obscure the behavior of the actual species studied. To remove the cathodically active oxygen the solution in the electrochemical cell is purged with nitrogen or argon.

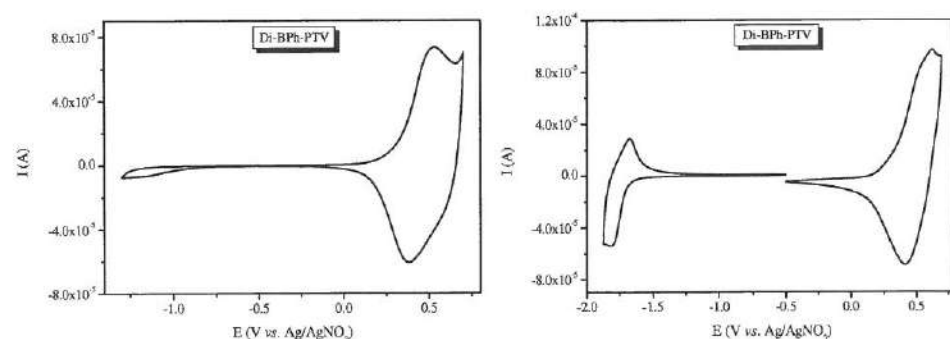


Figure 2-5: A cyclic voltammogram of Di(phenylbutyl)-PTV

A: The polymer contains moisture: no clear reduction peak

B: The polymer is dry: a clear reduction peak

An example of a cyclic voltammogram of an insufficiently dried polymer is shown in figure 2-5. When the polymer is wet, there is no reversible reduction peak

observed (figure 2-5A) and as a result, the LUMO energy level can not be derived from the measurement. After the same polymer is subjected to additional drying in a vacuum oven (figure 2-5B), a reversible reduction peak is observed and the LUMO energy level can readily be obtained.

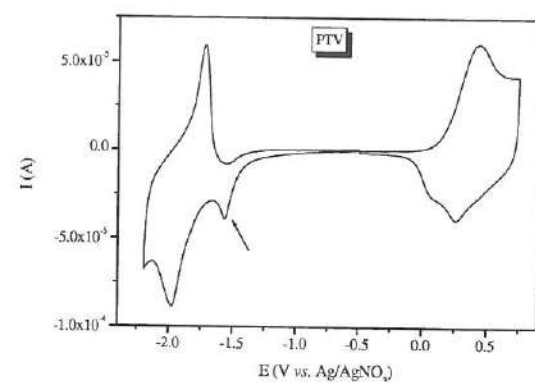
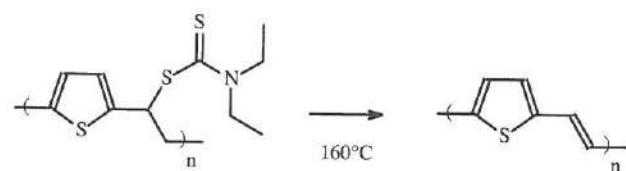


Figure 2-6: A cyclic voltammogram of PTV

Another example of the disturbing presence of impurities can be found in the cyclic voltammogram shown in figure 2-6. At a potential of -1.5 V vs. Ag/AgNO₃, a shoulder is observed. During the synthesis of this particular polymer, a conversion step of a non-conjugated precursor polymer into its conjugated form is needed (Scheme 2-1). This process takes place at elevated temperatures. However, it is not uncommon that decomposition fragments of the leaving groups do not fully evaporate from the film. Since this leaving group is electrochemically active, an additional peak is observed in the cyclic voltammogram.



Scheme 2-1: Conversion step of a non-conjugated PTV precursor polymer into its conjugated PTV.

2.5.3 Ion transport through the Polymer Film

The ohmic potential drop or the iR drop is the potential drop due to solution resistance as well as the resistance of the polymer films covering the electrode. This is the difference in potential required to move ions through the solution and polymer film. The major effects of iR drop in cyclic voltammetry include shift in peak potential, decrease in magnitude of current and increase in peak separation. The reactions of interest occur at the surface of the working electrode. The polymer film is coated on this electrode. As mentioned before, charge carriers appear during the doping process. Those charge carriers give rise to a negative or positive delocalized charge on the polymer backbone. As a result of this, the anions or cations present in the electrolyte solution move into the conjugated polymer film towards these delocalised charge sites to stabilize the charge. The ease with which these movements occur, depends on the type of side chains attached to the polymer backbone. When the side chains are too apolar like MDMO-PPV, it is difficult to migrate the very polar electrolyte-ions to these charged sites on the polymer backbone. Because of this, a higher potential (overpotential) is needed to oxidize or reduce the polymer. Resulting in a shift of the HOMO and LUMO energy levels. When the polymer has a polar side chain like MTEM-PPV, the charges are more readily stabilized due to the incorporation of the electrolyte ions and there is no significant potential shift. This is exemplified by Table 2-1. Both MDMO-PPV and MTEM-PPV have very similar electronic properties. This is reflected in their virtually identical optical band gap. However, the apparent electrochemical band gap of MDMO-PPV is significantly larger than that of MTEM-PPV. It appears that both the HOMO and the LUMO have shifted as a result of the above described effect of the ion mobility in the polymer film. Hence, it is important to calculate the electrochemical band gap after every measurement and compare it with optical band gap.

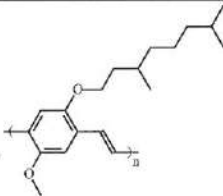
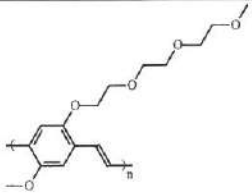
Polymer	MDMO-PPV	MTEM-PPV
Structure		
HOMO (eV)	-5.32	-5.05
LUMO (eV)	-2.78	-2.95
Electrochem.	2.54	2.10
Band gap (eV)		
Optical	2.12	2.10
Band gap (eV)		

Table 2-1: HOMO, LUMO and band gap of MDMO-PPV and MTEM-PPV

2.5.4 Arbitrary Choice of Onset

As mentioned above, the onset potentials are determined from the intersection of the two tangents drawn at the rising current and baseline charging current of the CV traces. Sometimes, it is difficult to draw an accurate tangent. For example in figure 2-7, we can draw two separate tangents at the oxidation peak in the cyclic voltammogram of MTEM-PPV. The difference between the two intersects is 0.2 V. The intersection at 0.1 V vs. Ag/AgNO₃ is chosen for the HOMO and LUMO calculations. In this chapter always the first intersection in a cyclic voltammogram is used for the determination of the HOMO-LUMO values, since at this point the onset of oxidation/reduction occurs for the most conjugated segments of a polymer.

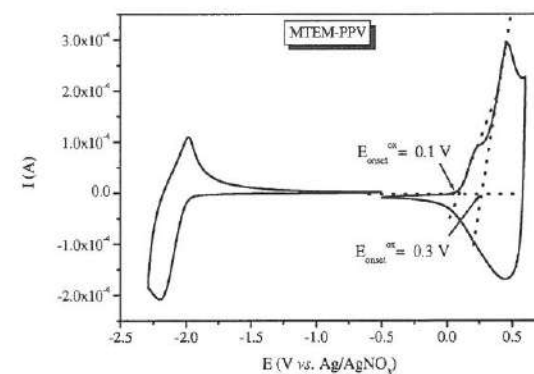


Figure 2-7: A cyclic voltammogram of MTEM-PPV

2.6 Electrochemical Properties of PPV Derivatives

2.6.1 Non-substituted poly(*p*-phenylene vinylene) (PPV)

The non-substituted poly(*p*-phenylene vinylene), abbreviate as PPV, is the parent conjugated polymer of a class of PPV-type polymers with phenylene rings that are connected in *para* by vinylene bonds. PPV is a polymer with a very low solubility in commonly used organic solvents, which makes it rather difficult to process. A methodology that avoids this problem is to use a precursor route. The PPV, which is used in this work, is synthesized with the sulfinyl precursor route. This precursor polymer, which exhibits excellent solubility in organic solvents, can thermally be converted into the corresponding conjugated polymer. In order to carry out the cyclic voltammogram, the precursor polymer solution (CHCl_3) was deposited onto the ITO glass by spin-coating. The obtained thin film was converted into PPV at a typical temperature of 120°C under a nitrogen atmosphere (scheme 2-2) ⁵⁷.



Scheme 2-2: Conversion step of a non-conjugated PPV precursor polymer into its conjugated PPV.

The cyclic voltammogram of PPV is demonstrated in figure 2-8. The starting potential is -0.5 V *vs.* Ag/AgNO₃. The potential is swept from -0.5 to +1.2 V *vs.* Ag/AgNO₃. In this potential window, an oxidation wave is observed. The maximum current occurs at 1.0 V *vs.* Ag/AgNO₃. Upon reversal of the sweep back to -0.5 V *vs.* Ag/AgNO₃ virtually no reduction (re-oxidation) wave is observed. This anionic doping is termed p-type doping. Similarly, if a negative potential is applied, n-type doping is observed. In the potential window from -0.5 V to -2.2 V *vs.* Ag/AgNO₃, the maximum current of the reduction peak occurs at -2.1 V *vs.* Ag/AgNO₃. Also in this potential window virtually no oxidation (re-reduction) is observed. As mentioned before, the onset potentials of the n- and p-doping can be used to determine the HOMO and LUMO energy levels of PPV and the potential difference can be used to estimate the energy gap of the polymer. The onset potential of the oxidation (p-doping) is 0.64 V *vs.* Ag/AgNO₃, which corresponds to a HOMO energy level of -5.58 eV. The onset potential of the reduction occurs at -1.82 V *vs.* Ag/AgNO₃, which corresponds to a LUMO energy level of -3.12 eV. The electrochemical band gap is 2.46 eV, which is identical to the optical band gap^{15, 53, 58}.

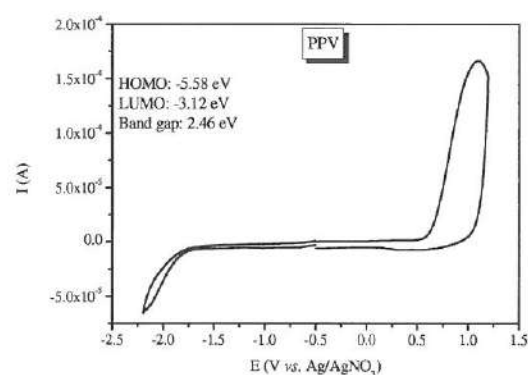


Figure 2-8: Cyclic voltammogram of a thin film of PPV on an ITO substrate.

2.6.2 Poly(2,5-di-alkoxy substituted *p*-phenylene vinylene)

The rigid conjugated structure of PPV results in an insoluble polymer. To obtain soluble conjugated polymers, long and flexible alkyl and/or alkoxy side chains on the polymer backbone are often attached^{59, 60, 61, 62}.

✓ MDMO-PPV

Poly[2-methoxy-5-(3,7-dimethyloctyloxy)-*p*-phenylene vinylene] (MDMO-PPV) is a soluble polymer due to the branched octyloxy side chain at position 5 and a methoxy group at position 2 of the polymer backbone (structure figure 2-9). The MDMO-PPV studied, was synthesized *via* the sulfinyl precursor route⁵⁹. This conjugated polymer was directly spin-coated from a CHCl₃ solution (5 mg/mL) onto the Pt working electrode.

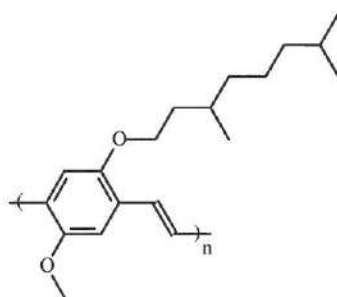


Figure 2-9: Poly[2-methoxy-5-(3,7-dimethyloctyloxy)-*p*-phenylene vinylene]
(MDMO-PPV)

Figure 2-10 shows the cyclic voltammogram of MDMO-PPV. The observed p-doping process (oxidation) is fully reversible. The reduction process of MDMO-PPV is mostly irreversible and no large n-doping peak has been observed. This means that MDMO-PPV shows a stronger tendency to be charged through p-doping process rather than n-doping. The oxidation potential of MDMO-PPV is 0.6 V *vs.* Ag/AgNO₃. However, the HOMO energy level is more accurately determined from the onset of oxidation. In this anodic scan the onset of oxidation of MDMO-PPV occurs at 0.4 V *vs.* Ag/AgNO₃, which corresponds to a HOMO energy level

of -5.32 eV. The onset potential of the reduction peak is -2.14 V vs. Ag/AgNO_3 , which corresponds to a LUMO energy level of -2.78 eV. The electrochemical band gap is 2.54 eV. The optical band gap obtained *via* UV-Vis measurements is 2.12 eV. The difference between the electrochemical and the optical band gap is significant. This is due to the previously mentioned hampered charge transport of the electrolyte solution through the apolar polymer film as a result of the longer or bulky side chains on the working electrode.⁶³ The calculated HOMO and LUMO levels are comparable with data from the literature^{11, 13, 15, 21, 48, 64-68}.

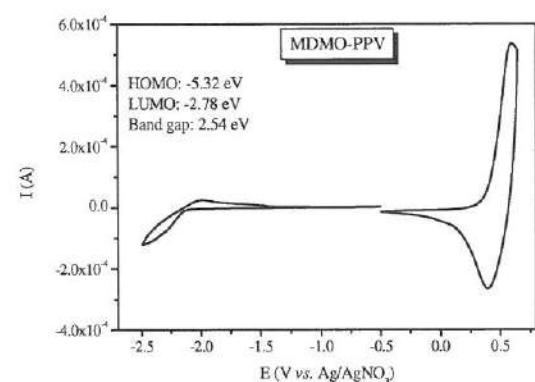


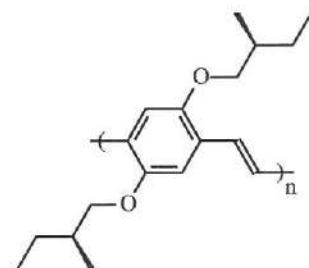
Figure 2-10: Cyclic voltammogram of a thin film of MDMO-PPV on a Pt electrode.

✓ BMB-PPV and BN-PPV

Two additional PPV derivatives with apolar side chains are poly[2,5-bis((S)-2-methylbutoxy)-*p*-phenylene vinylene] (BMB-PPV) and poly[2,5-bis(nonyloxy)-*p*-phenylene vinylene] (BN-PPV) (figure 2-11). These polymers have been developed since it is generally observed that the introduction of chiral or linear side chains attached onto the phenylene core can increase the charge carrier mobility as a result of better stacking and additional structural ordering. A precursor approach is preferred to synthesize these polymers, since this class of conjugated polymers exhibits comparatively poor solubility. For the synthesis of the polymers described in this section again the sulfinyl precursor route was used.

Since BMB-PPV and BN-PPV are indeed not soluble in chloroform, their precursor polymer solutions (CHCl_3) were deposited onto ITO glass substrates by spin-coating. The obtained thin films were converted into the conjugated polymers BMB-PPV and BN-PPV at a temperature of 110 °C and 115 °C respectively under a nitrogen atmosphere. The color of both conjugated polymers is orange.

BMB-PPV



BN-PPV

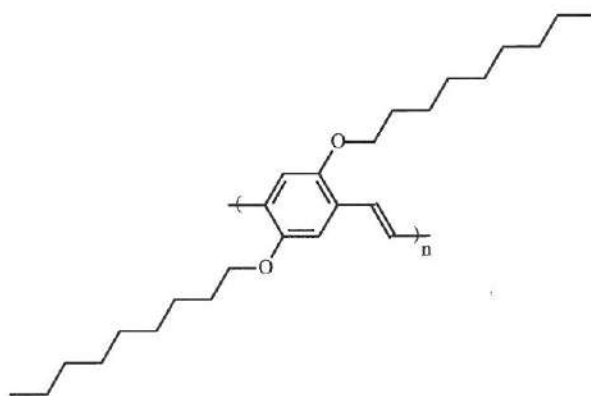


Figure 2-11: Molecular structure of
poly[2,5-bis((S)-2-methylbutoxy)-p-phenylene vinylene] (BMB-PPV)
and *poly[2,5-bis(nonyloxy)-p-phenylene vinylene]* (BN-PPV)

The cyclic voltammograms from BMB-PPV and BN-PPV are displayed in figure 2-12 and indicate that the electrochemical oxidation is mostly reversible in both cases but the reduction process is not. The latter is quasi-reversible for the BMB-PPV and irreversible for BN-PPV. The poorly defined reduction process of BN-PPV is possibly associated with traces of impurities associated with the leaving

group of the sulfinyl precursor route. This is corroborated by the fact that a similar reduction behavior was observed for the precursor polymer itself.

It is observed that, in the oxidation process the onset oxidation potential is 0.35 V vs. Ag/AgNO₃, which corresponds to a HOMO level of -5.27 eV. The onset potential of the reduction of BMB-PPV is -1.88 V vs. Ag/AgNO₃, which corresponds to a LUMO level of -3.04 eV. The electrochemical band gap is 2.23 eV, this value is only slightly larger than the optical band gap of 2.12 eV. Surprisingly, ion mobility issues are much less important for this polymer than for MDMO-PPV. Apparently, the polymer film of BMP-PPV is sufficiently permeable for electrolyte ions. The onset potential for oxidation of BN-PPV is 0.34 V vs. Ag/AgNO₃, which corresponds to a HOMO level of -5.28 eV. Since the reduction process is poorly defined, an electrochemical LUMO estimation is not possible. Therefore, the electrochemical data are combined with data of the UV-Vis characteristics (the optical band gap of BN-PPB is 2.11 eV), to give an estimate of the LUMO energy level of BN-PPV, *i.e.* -3.17 eV.

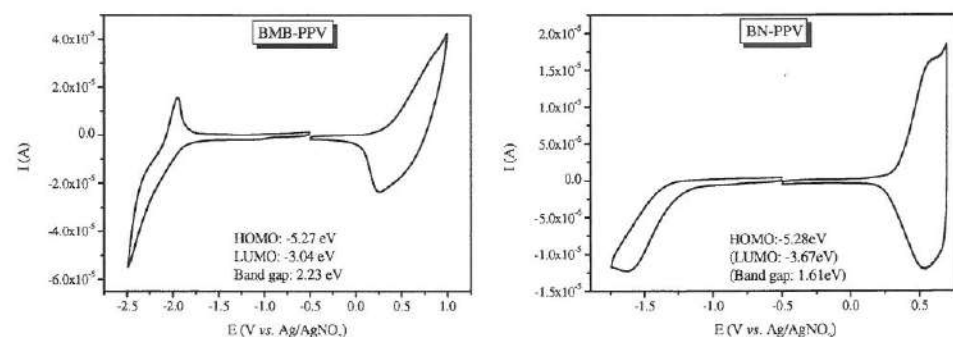


Figure 2-12: Cyclic voltammograms of thin films of BMB-PPV and BN-PPV on ITO glass working electrodes.

In table 2-2, there is an overview of the HOMO and LUMO energy levels of the two apolar PPV derivatives, compared with the energy levels of the also apolar MDMO-PPV. It appears that the HOMO-energy levels of the three polymers are almost identical. This indicates that the type of apolar side chains attached to the

phenylene ring does not have a substantial impact on the redox properties of the PPV derivatives. However, different side chains can lead to different packing in the polymer films and, as a result, different permeability for electrolyte ions. This is reflected in the different LUMO values found for MDMO-PPV and BMB-PPV.

Polymer	HOMO (eV)	LUMO (eV)	Electrochemical band gap (eV)	Optical band gap (eV)
BMB-PPV	-5.27	-3.04	2.23	2.12
BN-PPV	-5.28	(-3.17)	-	2.11
MDMO-PPV	-5.32	-2.78	2.54	2.12

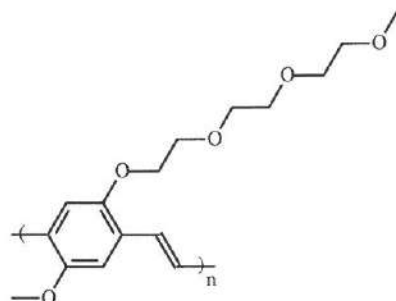
Table 2-2: HOMO and LUMO energy levels as well as the optical band gap of selected apolar PPV derivatives (the value between brackets is an estimate).

It should be noted that the oxidation process of both polymers can also be observed visually. For both polymers, a color change of the films from orange to colorless was observed upon oxidation. Subsequently, in the reverse process upon dedoping the color of the film returned to orange. This observation further confirms the reversibility of the p-doping process.

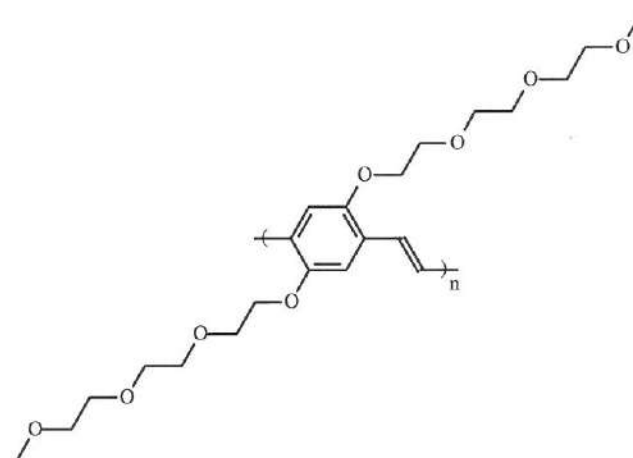
✓ *MTEM-PPV, BTEM-PPV and NTEM-PPV*

Poly[2-methoxy-5-(triethoxymethoxy)-*p*-phenylene vinylene] (MTEM-PPV), poly[2,5-bis(triethoxymethoxy)-*p*-phenylene vinylene] (BTEM-PPV) and poly[2-(*n*-nonyloxy)-5-(triethoxymethoxy)-*p*-phenylene vinylene] (NTEM-PPV) (structure figure 2-13) are three 2,5-di-substituted polar PPV derivatives. The effect of side chain polarity on the optical and electronic properties has been investigated (see also Chapters 3 and 4). All three polar functionalized 2,5-substituted conjugated polymers have been prepared *via* the sulfinyl precursor route ⁶⁹. The resulting polymers are excellently soluble in chloroform. The polymers were directly drop-coated from a CHCl₃ solution (5 mg/mL) onto the Pt working electrode.

MTEM-PPV



BTEM-PPV



NTEM-PPV

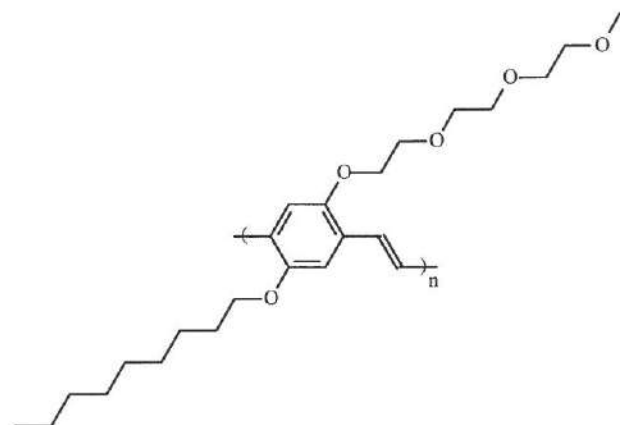


Figure 2-13: Molecular structure of

Poly[2-methoxy-5-(triethoxymethoxy)-p-phenylene vinylene] (MTEM-PPV)
Poly[2,5-bis(triethoxymethoxy)-p-phenylene vinylene] (BTEM-PPV) and
Poly[2-(n-nonyloxy)-5-(triethoxymethoxy)-p-phenylene vinylene] (NTEM-PPV)

Figure 2-14 shows the redox properties of the polymers MTEM-PPV, BTEM-PPV and NTEM-PPV respectively, as determined from their cyclic voltammograms. Both p- and n-doping processes are reversible under the electrochemical conditions employed. It can be seen from figure 2-14 that these polymers exhibit a good redox reversibility. The three functionalized polymers can be repeatedly 'doped-dedoped' without changes in its oxidation and reduction peak characteristics. Therefore, electrochemically determined band gaps, can be deduced with only a minimal error.

MTEM-PPV exhibits typical oxidation peak potentials of 0.24 V and 0.47 V *vs.* Ag/AgNO₃ and reduction peak potentials at -2.21 V *vs.* Ag/AgNO₃. The onset potentials of oxidation and reduction of MTEM-PPV have been determined as 0.10 and -2.00 V *vs.* Ag/AgNO₃, respectively. As a result, the HOMO energy level is -5.05 eV and the LUMO -2.95 eV. The difference between the two onset potentials, *i.e.* the electrochemical band gap, of this polymer is 2.10 eV. This value is identical to the energy corresponding to the onset of the optical absorption (2.10 eV) of MTEM-PPV film^{70, 71}.

The oxidation peak potentials of BTEM-PPV and NTEM-PPV are 0.37 V and 0.61 V *vs.* Ag/AgNO₃, respectively. The reduction peak potentials of these two polymers are -2.12 V and -2.19 V *vs.* Ag/AgNO₃, respectively. The more relevant onset oxidation potentials of BTEM-PPV and NTEM-PPV are 0.21 V and 0.17 V *vs.* Ag/AgNO₃, which correspond to HOMO energy levels of -5.15 eV for BTEM-PPV and -5.09 eV for NTEM-PPV. The onset reduction potentials are -1.97 V and -2.02 V *vs.* Ag/AgNO₃, which correspond to LUMO levels of -2.97 eV for BTEM-PPV and -2.90 eV for NTEM-PPV. As a result, the electrochemical band gaps are 2.18 eV and 2.19 eV, respectively. These values are also only slightly larger than the optical band gaps of the polymers (2.10 eV and 2.12 eV)⁷¹.

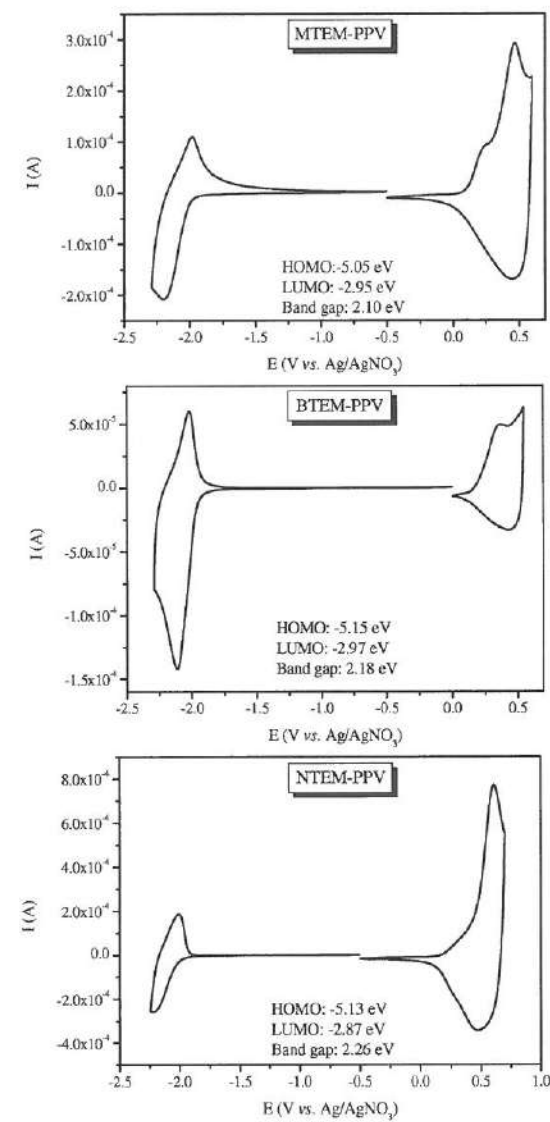


Figure 2-14: Cyclic voltammograms of thin films of three 2,5-substituted polar PPV derivatives on Pt working electrodes.

In table 2-3, there is an overview of the HOMO and LUMO energy values of the three polar PPV derivatives, as well as the earlier discussed MDMO-PPV. From this table it is evident that the HOMO and LUMO values of the three polar

polymers are essentially identical, within the margin of error. Apparently, the exact structure of the polar side chain attached to the phenylene ring is also in this case not very important for the redox properties. Instead, the general alkoxy character dominates the electronic properties. It should be noted that the HOMO and LUMO values for MDMO-PPV deviate as a result of ion transport effects (*vide supra*).

Polymer	HOMO (eV)	LUMO (eV)	Electrochemical band gap (eV)	Optical band gap (eV)
MTEM-PPV	-5.05	-2.95	2.10	2.10
BTEM-PPV	-5.15	-2.97	2.18	2.10
NTEM-PPV	-5.09	-2.90	2.19	2.12
MDMO-PPV	-5.32	-2.78	2.54	2.12

Table 2-3: HOMO and LUMO energy levels as well as the electrochemical and optical band gap of three polar functionalized PPV derivatives and MDMO-PPV.

As mentioned before, the p-doping/dedoping and n-doping/dedoping are reversible for the three polar conjugated PPV derivatives, but there is some difference in the size of the actual n-doping peaks of the three polymers. The areas under the n-doping peaks of MTEM-PPV and NTEM-PPV are much smaller than that of BTEM-PPV, which means that the amount of charge consumed in the n-doping for MTEM-PPV and NTEM-PPV is less than that of the BTEM-PPV polymer. The difference between the three conjugated polymers is the chemical structure. BTEM-PPV has two oligo(oxyethylene) side chains, whereas MTEM-PPV and NTEM-PPV have only one (figure 2-1). During the n-doping process, negative charges are created. The positive cation TBA^+ from the electrolyte solution (TBAPF_6) is needed to stabilize the negative charge carriers. In the case of MTEM-PPV and NTEM-PPV, there is only one oligo(oxyethylene) side chain per repeating unit. This side chain facilitates the formation of a complex with the electrolyte cation TBA^+ (figure 2-15). In this way, the negative charge is better stabilized during the reduction of the polymer, which accounts for the distinct

reversible n-doping peak. In the case of BTEM-PPV, which has two oligo(oxyethylene) chains, this electrolyte-ion-polymer interaction is further enhanced and the stabilization of the negative charge is larger than observed for MTEM-PPV and NTEM-PPV (figure 2-16). This results in an increase in size of the n-doping peak. In contrast, the negative charges created during the reduction of MDMO-PPV can not as readily be stabilized, since this polymer only has apolar side chains. These side chains cannot form a complex with the electrolyte cation TBA^+ . In chapter 3 of this work, the complexation of various ions will be studied with UV-Vis spectroscopy in more detail. In conclusion, the presence or absence of electrochemical reversibility in conjugated polymers is not only associated with the possibility of a polymer to be n- and/or p-doped but also with its ability to facilitate sufficient stabilization of the electrolyte counter ion in the polymer film.

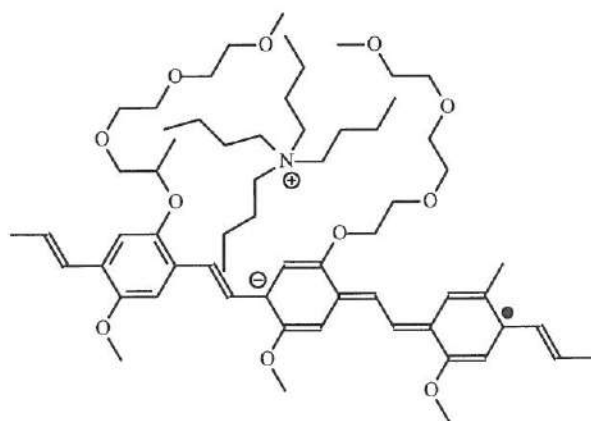


Figure 2-15: Impression of a possible structure of the complex of a TBA^+ cation of the electrolyte solution with the oligo(oxyethylene) side chains of MTEM-PPV and NTEM-PPV during the electrochemical reduction.

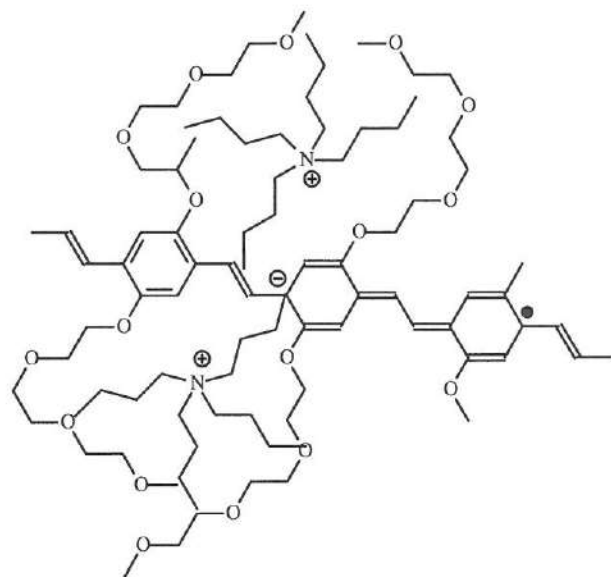


Figure 2-16: Impression of a possible structure of the complex of TBA^+ cations of the electrolyte solution with the oligo(oxyethylene) side chains of BTEM-PPV during the electrochemical reduction

✓ *Para-phenylene crown ethers*

In the previous paragraph, the complexation of the electrolyte cation TBA^+ with oligo(oxyethylene) side chains of neighboring monomer units is observed during the reduction process. In an attempt to further tune this complexation behavior and to verify whether a polymer with crown ether side chains can also complex the electrolyte cation TBA^+ within one repeating unit, two *para*-substituted macrocyclic polyethers namely *p*-phenylene-20-crown-6 and *p*-phenylene-23-crown-7 were introduced into the polymer backbone (figure 2-17). Both polymers have been synthesized *via* the Gilch route and are soluble in chloroform. The polymers have been drop-coated onto a Pt working electrode to form thin films suitable for electrochemical measurements.

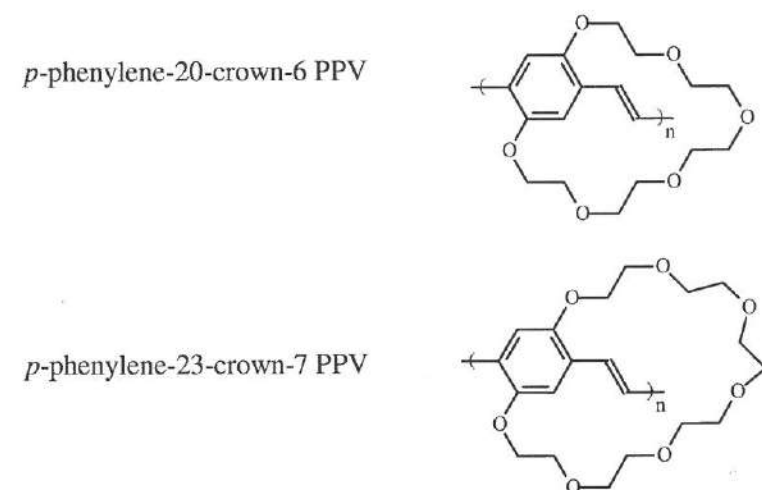


Figure 2-17: Molecular structures of the crown ether containing PPV derivatives.

The cyclic voltammetric behavior of the crown ether containing PPV derivatives was studied (figure 2-18). The oxidation of both PPV derivatives (p-doping) exhibits an irreversible electrochemical response. However, the observed response is likely not the electrochemical behavior typically for this polymer. Traces of contaminants from the synthesis of the crown ethers, such as alkali-metal salts, which form a complex with the crown ether and hence are difficult to remove, as well as their counter ions dominate the oxidation characteristics. Surprisingly, the reduction of both polymers (n-doping) also exhibits an irreversible electrochemical doping/dedoping process (figure 2-18). Hence, it can be concluded that the TBA⁺ cation is too large to form a complex with the crown ether in a similar way as observed for BTEM-PPV. Since there is no extra stabilization of the negative charge and an irreversible n-doping peak is observed ⁷².

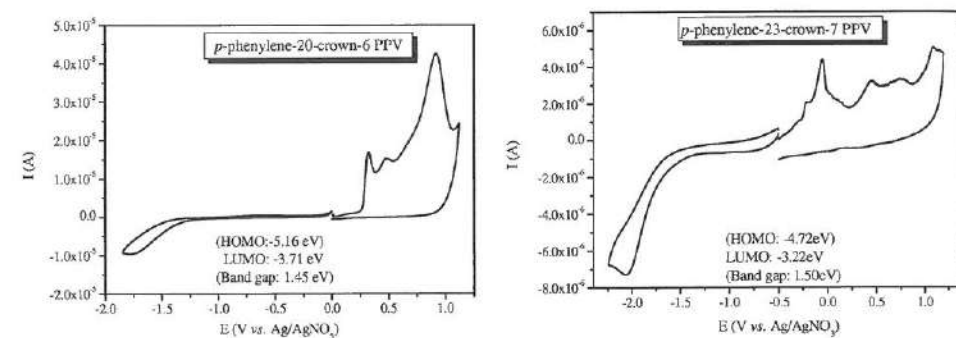


Figure 2-18: Cyclic voltammograms of thin films of the crown ether containing PPV derivatives on Pt working electrode in 0.1 M TBAPF₆ in dry acetonitrile electrolyte solution.

It is also possible to use another electrolyte solution, containing a smaller cation, *i.e.* Li⁺. When as the electrolyte solution 0.1 M LiClO₄/anhydrous acetonitrile is used, a modified cyclic voltammetric behavior of the crown ethers containing PPV derivatives is observed. (figure 2-19)

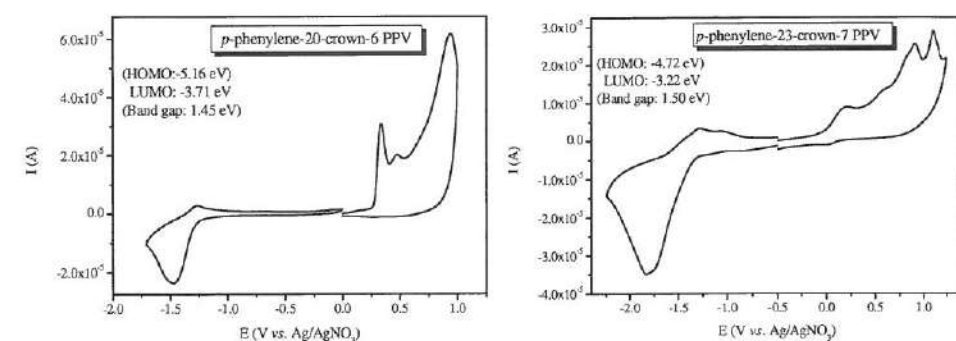


Figure 2-19: Cyclic voltammogram of thin films of the crown ether containing PPV derivatives on Pt electrodes, using an alternative 0.1 M LiClO₄ in dry acetonitrile electrolyte solution.

Using this electrolyte, the oxidation of the crown ether containing PPV derivatives (p-doping) still exhibits the previously mentioned irreversible electrochemical response. However, the reduction of both polymers (n-doping) displays a different

electrochemical response, which represents a quasi-reversible electrochemical doping/dedoping process (figure 2-19). This is indicative of some form of stabilization of the cation.

For both *para*-phenylene crown ethers PPV derivatives, no accurate HOMO energy level can be calculated electrochemically. Only the LUMO level can be estimated. While sweeping cathodically in the presence of the LiClO₄ electrolyte, both polymers showed a reduction peak with an onset potential at -1.20 V vs. Ag/AgNO₃ for *p*-phenylene-20-crown-6 containing PPV and at -1.69 V vs. Ag/AgNO₃ for *p*-phenylene-23-crown-7 containing PPV. This corresponds to a LUMO value of -3.71 eV for the small crown ether polymer and -3.22 eV for larger one. With the help of the optical band gap, an estimation of the HOMO energy levels can be made. For the *p*-phenylene-20-crown-6 containing PPV the optical band gap is 2.3 eV, giving a HOMO energy level estimate of -6.01 eV. Finally, for the *p*-phenylene-23-crown-7 containing PPV, the optical band gap is 2.23 eV, giving a HOMO energy level estimate of -5.45 eV. These values are different, as compared to previously discussed *p*-alkoxy PPV-type polymers. Possibly, this is a result of complexation phenomena or steric interactions of the bulky crown ether group.

To conclude this paragraph, complexation of electrolyte cation TBA⁺ with the two studied oxyethylene crown ether containing PPV-derivatives is not observed during the reduction process. Apparently, TBA⁺ is too large to form such complexes and an irreversible reduction is observed. When a smaller cation, *i.e.* Li⁺, is used, this cation can form a complex with the crown ether and a quasi-reversible reduction peak is observed. However, the complexation of Li⁺ with the crown ethers is not as strong as the complexation of TBA⁺ with the oligo(oxyethylene) side chains of BTEM-PPV, NTEM-PPV and MTEM-PPV, which is reflected in the absence of full reversibility of the reduction process in the crown ether containing PPV derivatives.

✓ Copolymers of MDMO-PPV and BTEM-PPV

An interesting approach for tuning the physical and chemical properties of conjugated polymers is the synthesis of copolymers. Various parameters can be manipulated in this way and polymers with intermediate and/or improved properties often arise. Emission maxima, solubility, film forming and redox properties can all be changed significantly as was demonstrated in various literature reports^{22, 73}. However, it is noteworthy in this context that a large dissimilarity between the employed monomers may also lead to charge localization and reduction of charge mobility.⁷⁴ However, this is probably not the case for the two copolymers described in this section, since both monomers induce a very similar conjugated backbone structure.

The first copolymer (copolymer **1**) is copoly(2-methoxy-5-(hydroxy-triethoxy)-*p*-phenylene vinylene/2,5-bis(triethoxymethoxy)-*p*-phenylene vinylene), abbreviate as (MHTE-BTEM)-PPV (figure 2-20). This copolymer is prepared to improve the solubility of the homopolymer MHTE-PPV. This copolymer is synthesized *via* the sulfinyl precursor route using both the monomer towards the alcohol-functionalized PPV derivative and the monomer towards BTEM-PPV. The molar monomer feed ratio of the copolymerization is 3 BTEM-PPV / 1 MHTE-PPV. The second copolymer (copolymer **2**) is copoly(2-methoxy-5-(2-(*N*-butyl-*N*-amino-*p*-nitrobenzene)-ethoxy)-*p*-phenylene vinylene / 2-methoxy-5-(3,7-dimethyloctyl oxy)-*p*-phenylene vinylene) ((MBNB-MDMO)-PPV) (figure 2-20). MBNB-PPV polymer is insoluble in the common organic solvents. Copolymerization reaction between the monomer towards MBNB-PPV and the monomer towards MDMO-PPV in the ratio of 1:1 yields a soluble conjugated PPV-type copolymer **2**. The copolymers **1** and **2** are soluble in chloroform and for the electrochemical measurements thin films of these polymers have been cast onto Pt electrodes from chloroform solutions.

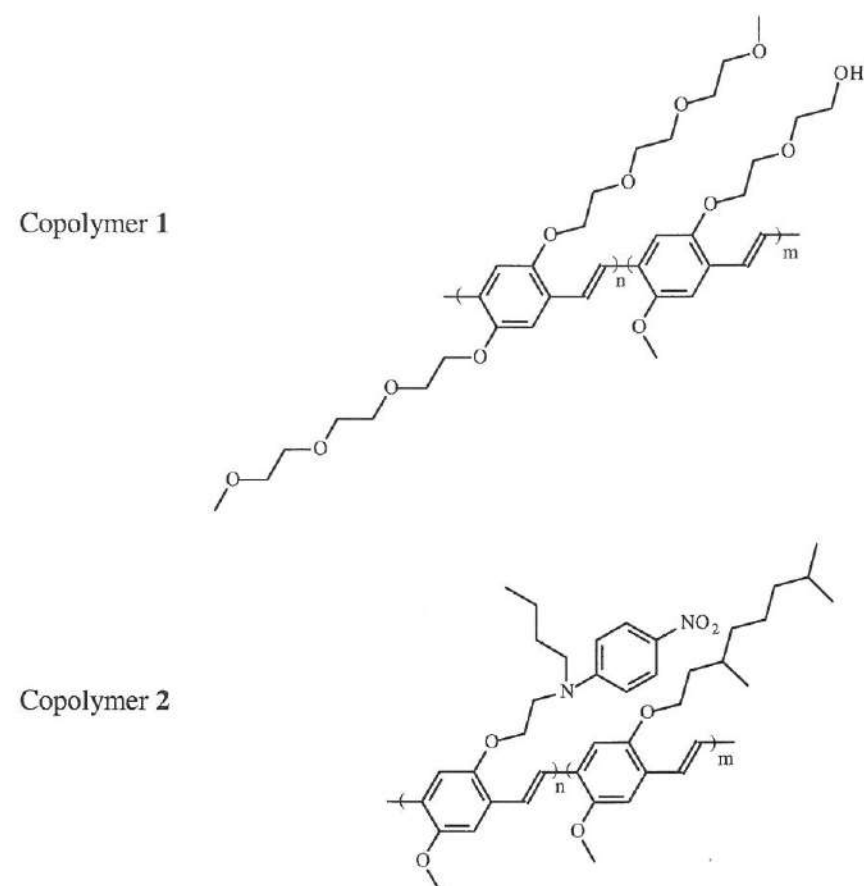


Figure 2-20: Molecular structure of Copolymer 1 and Copolymer 2

The cyclic voltammograms of copolymer 1 and 2 display distinct oxidation and reduction processes (Figure 2-21). As observed in the cyclic voltammograms, the electrochemical properties of copolymer 1 are comparable with those of BTEM-PPV and copolymer 2 with MDMO-PPV. For copolymer 1 the HOMO and LUMO energy levels are indeed almost identical to those of BTEM-PPV. The LUMO energy level of MDMO-PPV is not comparable because the ion transport through the polymer films plays an important role (table 2-4). Apparently this transport more readily occurs in the copolymer film.

Remarkably, the electrochemical properties of the *p*-nitroaniline side chain of copolymer **2** do not manifest themselves in the cyclic voltammogram of this copolymer (figure 2-21B). At a reduction potential of about -0.126 V vs. SCE, *i.e.* -0.386 V vs. Ag/AgNO₃, the reduction of the *p*-nitro group could have been expected. The oxidation of the amino group was anticipated at an oxidation potential of about 0.536 V vs. SCE, *i.e.* 0.276 V vs. Ag/AgNO₃.⁷⁵ However, both peaks are absent in copolymer **2**. This implies that the *p*-nitroaniline is either absent or due to an unknown reason, no longer electrochemically active.

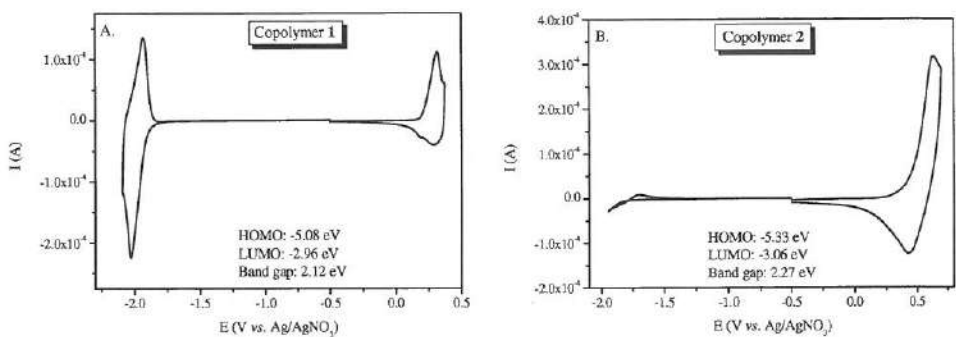


Figure 2-21: Cyclic voltammogram of copolymers **1** and **2** on Pt working electrode.

Polymer	HOMO (eV)	LUMO (eV)	Electrochemical Band gap (eV)	Optical Band gap (eV)
BTEM-PPV	-5.15	-2.97	2.18	2.10
Copolymer 1	-5.08	-2.96	2.11	2.10
MDMO-PPV	-5.32	-2.78	2.54	2.12
Copolymer 2	-5.33	-3.06	2.27	2.14

Table 2-4: HOMO, LUMO energy levels of BTEM-PPV, MDMO-PPV and copolymers **1** and **2** with the optical and electrochemical band gap.

2.6.3 PPV-type polymers with more complex aromatic cores

The electrochemical properties of a selection of conjugated polymers with a backbone containing larger or more exotic aromatic structures have been studied as well. In all polymers the PPV base structure remains readily recognizable.

✓ Poly(*p*-naphthalene vinylene) PNV

It is generally observed that in conjugated polymers the charge carrier mobility is correlated with the structural order of the polymer films. A possible approach is the development of polymeric materials with extended conjugated systems. An example of such an extended aromatic core derivative, *i.e.* poly(*p*-naphthalene vinylene) (PNV, figure 2-22), has been prepared *via* the dithiocarbamate route. Since similar to PPV, also PNV is insoluble in organic solvents like chloroform, a precursor polymer solution in chloroform has been made and spin-coated onto an ITO glass substrate. The obtained thin films have been converted into the conjugated form at a temperature of 190 °C under a nitrogen atmosphere.

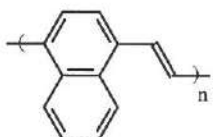


Figure 2-22: Molecular structure of poly(*p*-naphthalene vinylene) (PNV)

The cyclic voltammogram of PNV (figure 2-23) shows quasi-reversibility upon oxidation and irreversibility upon reduction. The onset of oxidation of PNV can be observed at 0.71 V *vs.* Ag/AgNO₃ whereas the onset of reduction is observed at -1.30 V *vs.* Ag/AgNO₃. This corresponds with a HOMO energy level of -5.42 eV and a LUMO energy level of -3.41 eV. The optical and electrochemical band gap are reasonably close, 2.18 eV and 2.01 eV, respectively. When these results are compared with those of *non-substituted* PPV polymer, it can be concluded that by introduction of an extended aromatic core like a naphthalene ring in the polymer

backbone, a band gap reduction is observed from 2.46 eV for PPV to 2.01 eV for PNV. This reduction is mostly associated with a large shift of the LUMO energy level from -3.12 eV for PPV to -3.41 eV for PNV. The HOMO energy level is much less affected.

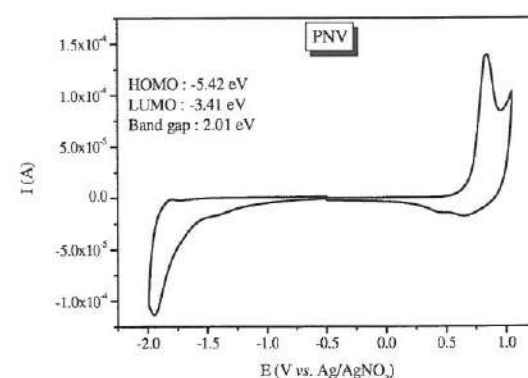


Figure 2-23: Cyclic voltammograms of a thin film of PNV on an ITO working electrode.

✓ Poly(*p*-fluoranthene vinylene) PFV

Poly(*p*-fluoranthene vinylene) (PFV) (figure 2-24) has a backbone architecture containing non-alternant polycyclic aromatic hydrocarbon repeating units, in which the base structure of poly(*p*-phenylene vinylene) PPV remains readily recognizable⁷⁶. This novel material was inspired by the field of organic solar cells. In such solar cells, a p-type conjugated polymer such as MDMO-PPV is combined with a soluble derivative of C₆₀, PCBM as the electron acceptor (*vide infra*). However, an alternative for PCBM is of interest to facilitate the formation of an optimal morphology. PFV was chosen because of the fact that fluoranthene is a substructure of C₆₀. Since PFV is like most other substituted conjugated polymers insoluble in common organic solvents, a dithiocarbamate precursor polymer was employed. Subsequently, this precursor polymer has been transformed into the corresponding conjugated polymers by thermal treatment. An ITO glass has been

used as working electrode and the conversion has been done at a temperature of 190 °C under N₂ atmosphere.

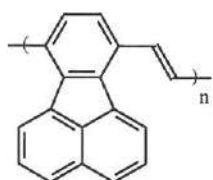


Figure 2-24: Molecular structure of poly(*p*-fluoranthene vinylene) (PFV)

Thin film cyclic voltammetry was employed to investigate the electrochemical behavior of PFV and to estimate the position of its lowest occupied molecular orbital (LUMO) energy level. The cyclic voltammogram of PFV displays a distinct reduction process (Figure 2-25), *i.e.* n-doping. In contrast, no reversible p-doping has been observed. This suggests that this new polymer under the applied electrochemical conditions acts as an n-type conjugated polymer. Such polymers are quite rare and highly desired for applications⁷⁷. The observed unusual n-type behavior originates from the non-alternant polycyclic aromatic hydrocarbon units in the backbone. The peak potential of the reduction of PFV is -2.14 V *vs.* Ag/AgNO₃. The conduction band edge energy level is accurately determined from the onset of reduction at -1.83 V *vs.* Ag/AgNO₃, which corresponds to a LUMO energy level of -3.10 eV. The valence band edge energy level is determined from the onset of oxidation at 0.71 V *vs.* Ag/AgNO₃, which corresponds to a HOMO energy level of -5.64 eV. The difference between the onset reduction and onset oxidation potential give an estimation of the electrochemical band gap, *i.e.* 2.54 eV. The optical band gap is somewhat smaller at 2.34 eV.

It should be noted that the peak potential of the reduction peak of pure fluoranthene is -2.18 V *vs.* Ag/AgNO₃.⁷⁸ This is comparable with the observed reduction peak of PFV polymer. As a result, the measured HOMO and LUMO energy levels of PFV may well be those of the fluoranthene unit itself. If this would be true, the conjugated structure (*i.e.* the vinylene bonds) has no impact on the position of the

HOMO and LUMO energy levels. However, additional measurements on this novel material are needed to confirm this.

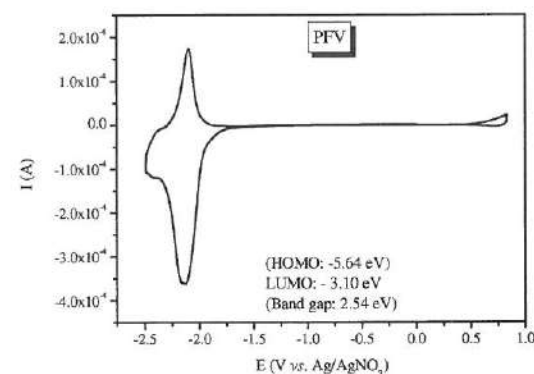


Figure 2-25: Cyclic voltammogram of a thin film of PFV on an ITO working electrode.

✓ Poly(quinoxaline vinylene) PQV

Most conjugated polymers synthesized to date have low electron affinity, despite the advantages of high electron affinity for many applications. One example is in light-emitting diodes (LEDs), where a high electron affinity would allow for the fabrication of LEDs in which good electron injection can be achieved by stable cathodes such as aluminum, rather than the low work function metals required for more electron-rich polymers. Other possible applications are n-type field effect transistors (FETs) or the use of such polymers as the electron accepting material in photodiodes or solar cells. A possible method to get a polymer with a high electron affinity is to introduce an electron-deficient heterocyclic unit in the polymer backbone for example pyridine, pyrimidine, quinoline, oxadiazole or quinoxaline^{79, 80}. To study the electronic properties of such a material, a conjugated polymer, poly(quinoxaline vinylene) PQV, has been synthesized, which has quinoxaline units incorporated in the backbone (figure 2-26).

PQV is insoluble in common organic solvents, but similarly to PFV the dithiocarbamate precursor polymers can be readily transformed into the

corresponding conjugated polymers by thermal treatment in a thin film. For the conversion, an ITO glass is used as working electrode and, the conversion is done with a temperature of 260 °C under N₂ atmosphere.

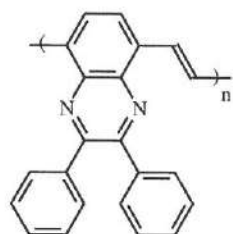


Figure 2-26: Molecular structure of Poly(quinoxaline vinylene) (PQV)

The cyclic voltammogram of PQV is shown in figure 2-27. For PQV, the reduction peak is seen at -1.69 V vs. Ag/AgNO₃ and the re-oxidation at -1.52 V vs. Ag/AgNO₃. The reduction process is quasi-reversible and can be repeated many times without any large degradation being noticed. The oxidation of PQV is irreversible. The onset potentials for the oxidation and the reduction are 0.42 V vs. Ag/AgNO₃ and -1.28 V vs. Ag/AgNO₃, respectively, which corresponds to a HOMO energy level of -5.35 eV and a LUMO energy level of -3.65 eV. The band gap calculated from the onset reduction and oxidation potential is 1.70 eV, which is slightly lower than the optical band gap (1.83 eV). This is possibly due to the low accuracy of the calculated HOMO level, since this is an irreversible oxidation peak. According to these electrochemical results, it can be concluded that the LUMO of PQV (-3.65 eV) is lower in energy than that of the other conjugated polymers studied in this work (PPV: -3.1 eV, 2,5-substituted di-alkoxy-PPV: -2.8 to -3.0 eV, PNV: -3.4 eV and PFV: -3.1 eV). That means that the electron affinity of PQV is higher than that of the previously mentioned conjugated polymers, as was anticipated based on the introduction of the quinoxaline units. This result is important for the application of PQV as an acceptor material in optoelectronic devices.

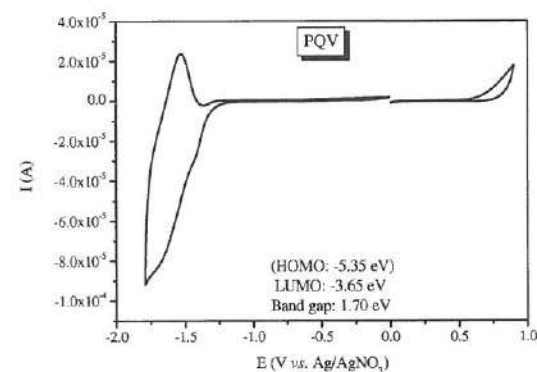


Figure 2-27: Cyclic voltammogram of a thin film of PQV on an ITO working electrode.

✓ Poly(triptycenevinylene) PTTyV

The polycyclic triptycene unit (9,10-dihydro-9,10-*o*-benzenoanthracene) is electron rich and it is believed to induce a 3D-porosity structure when incorporated in polymers. A triptycene containing conjugated polymer, *i.e.* poly(triptycenevinylene) (PTTyV) (figure 2-28) has been prepared *via* the dithiocarbamate precursor route. Similar to several other discussed polymers, PTTyV is insoluble in chloroform and for that reason, the precursor polymer has been spin coated on an ITO working electrode. Subsequently, a thermal conversion is done at a temperature of 220 °C under nitrogen atmosphere.

The cyclic voltammogram of the triptycene polymer PTTyV shows that the oxidation wave is quasi-reversible and the reduction irreversible (Figure 2-29). From this measurement, the onset values for oxidation and reduction have been determined at 0.94 V *vs.* Ag/AgNO₃ and -1.42 V *vs.* Ag/AgNO₃. This gives directly the electrochemical band gap E_g of 2.36 eV, which is smaller than the optical bandgap of 2.6 eV. The band edges for the HOMO and LUMO can be estimated at -5.87 eV and -3.51 eV, respectively.

PTTyV is a PPV derivative with bulky side chains. When these electrochemical results are compared with the HOMO and LUMO energy level of *non-substituted*

PTTyV / 1 MDMO-PPV. The molecular structure of the copolymer **3** is shown in figure 2-30.

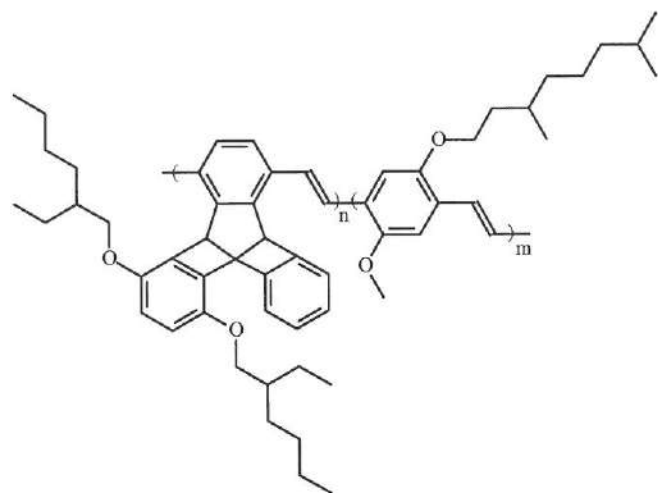


Figure 2-30: Molecular structure of Copolymer **3**

The incorporation of the MDMO-PPV subunits has the desired effect and this copolymer is indeed soluble in chloroform. To obtain a cyclic voltammogram of copolymer **3**, the solution was drop casted on a Pt working electrode. The cyclic voltammograms of copolymer **3** display distinct oxidation and reduction processes (Figure 2-31). Similar to the homopolymer, the reduction of the copolymer is irreversible, whereas the oxidation is a quasi-reversible electrochemical doping/dedoping process. The onset oxidation and reduction potentials of copolymer **3** are 0.39 V and -1.69 V vs. Ag/AgNO₃. This corresponds with a HOMO energy level of this copolymer at -5.30 eV and the LUMO at -3.22 eV. The electrochemical band gap of copolymer **3** is 2.08 eV, which is slightly smaller than the optical band gap of 2.2 eV. It appears that the electrochemical properties of this copolymer **3** are a reasonable average between the properties of PTTyV and a typical *p*-alkoxy-PPV type polymers.

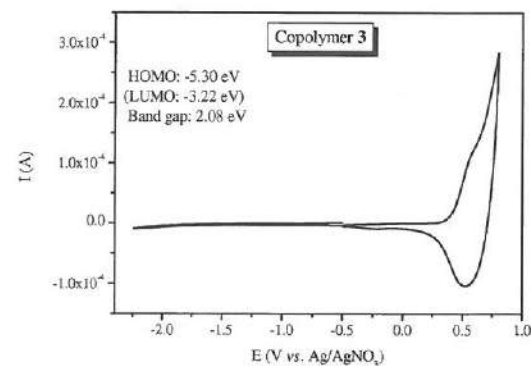


Figure 2-31: Cyclic voltammogram of a thin film of copolymer 3 on a Pt working electrode.

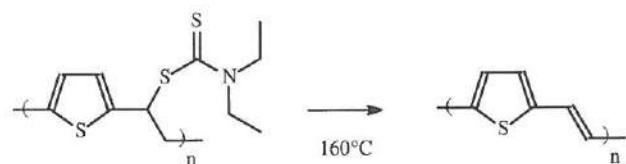
2.7 Electrochemical Properties of PTV Derivatives

Another class of conjugated polymers are the poly(thienylene vinylene) derivatives. This polymer can be regarded as an alternating copolymer of thiophene and vinylene. Due to the extra vinylene double bond in PTV, the band gap of PTV is smaller than that of polythiophene (PT). This is the result of two effects (1) a decrease in the overall aromatic character of the π -conjugated system, allowing a better delocalization of π -electrons over the whole polymer chain, and (2) a limitation in rotational disorder due to the presence of ethylenic linkages of defined configuration⁸¹. In this section, the electrochemical behavior of selected PTV derivatives will be discussed.

2.7.1 Non-substituted poly(thienylene vinylene) (PTV)

The non-substituted PTV (scheme 2-3), which was used for the electrochemical experiments, has been synthesized *via* the dithiocarbamate precursor route. PTV is not soluble in chloroform. For that reason, the precursor polymer is spin-coated onto an ITO working electrode. By heating the thin film until 160 °C under

nitrogen atmosphere, the dithiocarbamate leaving group is eliminated from the precursor polymer and the conjugated PTV polymer is obtained.



Scheme 2-3: Conversion step of a non-conjugated PTV precursor polymer into its conjugated PTV.

The electrochemical behavior of poly(thienylene vinylene) derivatives is very sensitive to contaminations, such as water, in the electrolyte solution or in the polymer. In figure 2-32, two cyclic voltammograms of the same polymer (PTV) are shown. In figure 2-32A, a quasi reversible p-doping process and a small irreversible n-doping are observed. In marked contrast, a quasi reversible p- and n-doping peak are observed in the measurements represented by figure 2-32B. The only difference between these two measurements is the presence/absence of traces of water in the conjugated polymer. The cyclic voltammogram in figure 2-32B is obtained after drying the polymer during one night under vacuum and by working with very pure and dry solvents during the synthesis. This means that it is essential to work under inert conditions with PTV derivatives!

As shown in the cyclic voltammogram in figure 2-32B, purified PTV has partial reversible n-doping and p-doping processes. The oxidation and reduction peak potentials are 0.44 V vs. Ag/AgNO₃ and -1.98 V vs. Ag/AgNO₃, respectively. The onset oxidation and reduction potentials are determined to be 0.15 V vs. Ag/AgNO₃ and -1.66 V vs. Ag/AgNO₃, from which the HOMO and LUMO energy levels could be estimated as -5.08 eV and -3.27 eV, respectively. Hence, the electrochemical band gap is 1.81 eV. This band gap is comparable to the optical band gap, which has been determined from the absorption edge of a polymer thin film, *i.e.* 1.75 eV. These results indicate that PTV polymer is a low band gap

material⁸². The small peak observed in figure 2-32B at a potential of -1.57 V vs. Ag/AgNO₃ is likely associated with polymer defects and traces of impurities like the dithiocarbamate leaving group⁸³.

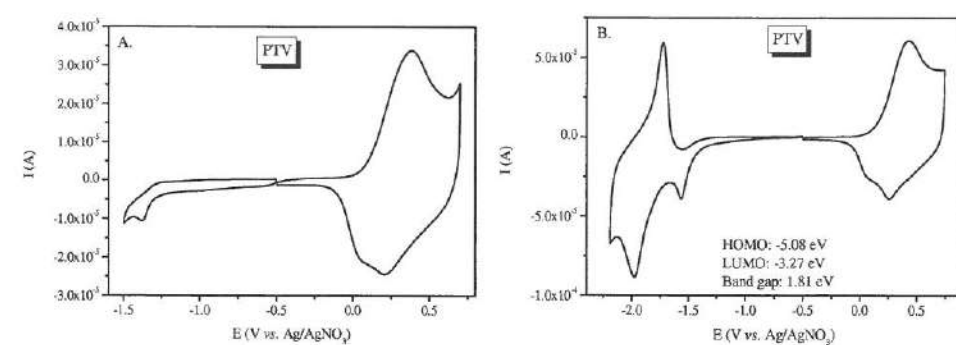


Figure 2-32: Cyclic voltammograms of thin films of PTV on ITO working electrodes (left as prepared; right after purification).

2.7.2 Poly(3,4-substituted thienylene vinylene)

✓ H-PTV and BH-PTV

By introduction of alkyl side chains, it is often possible to increase the solubility of a conjugated polymer. In the following two conjugated polymers, one or two hexyl side chains have been attached to the third and fourth position of the thiophene ring. Poly[3-hexyl-2,5-thienylene vinylene] (H-PTV) and poly[3,4-bis(hexyl)-2,5-thienylene vinylene] (BH-PTV) have been synthesized *via* the dithiocarbamate precursor route. The molecular structure is shown in figure 2-33. Both polymers are soluble in common organic solvents, such as chloroform and were cast on the Pt working-electrode from a chloroform solution^{64, 84}.

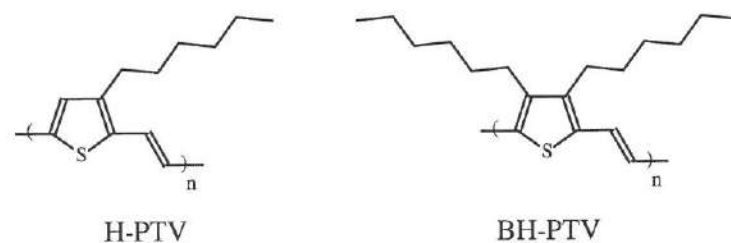


Figure 2-33: Molecular structure of
Poly[3-hexyl 2,5-thienylene vinylene] (H-PTV)
and poly[3,4-bis(hexyl) 2,5-thienylene vinylene] (BH-PTV)

The cyclic voltammogram of H-PTV is depicted in figure 2-34A. H-PTV can be both oxidized and reduced with a p-doping/dedoping onset potential of 0.19 V and an n-doping/dedoping onset potential of -1.74 V vs. Ag/AgNO₃. Both the p- and n-doping characteristics are quasi-reversible. The energy levels of the HOMO and the LUMO of H-PTV are estimated at -5.17 eV and -3.24 eV. The electrochemical band gap is therefore 1.93 eV. The optical band gap, as determined from UV-Vis spectroscopy, is 1.7 eV.

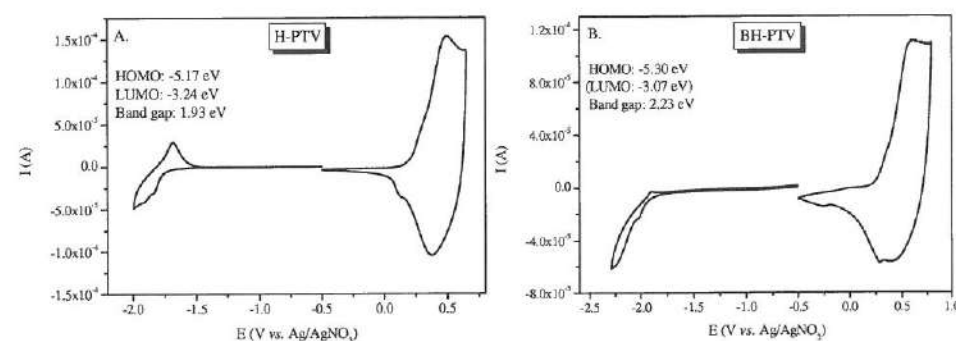


Figure 2-34: Cyclic voltammograms of thin films of H-PTV (left) and BH-PTV (right) on Pt working electrodes.

Figure 2-34B shows the cyclic voltammogram of the BH-PTV film on Pt electrode. The p-doping/dedoping process at positive potential range is reversible, whereas the n-doping/dedoping processes at negative potential range is irreversible. The

oxidation peak potential is 0.61 V vs. Ag/AgNO₃. The onset reduction potential and onset oxidation potential of the polymer are -1.91 V and 0.32 V vs. Ag/AgNO₃, respectively. From the $E_{\text{onset}}^{\text{red}}$ and $E_{\text{onset}}^{\text{ox}}$ values, the LUMO and HOMO energy levels of -3.07 eV and -5.30 eV can be obtained. The energy gap of BH-PPV calculated from the electrochemical measurement is 2.23 eV, which is significantly larger than the optical energy band gap of 1.67 eV.

For both polymer H-PTV and BH-PTV, there is a large difference between the optical and electrochemical band gap. A possible reason is also in this case the difficult electrolyte ion-transport through the dense conjugated polymer film. This is caused by the side chains of H-PTV and BH-PTV, which are apolar, a feature previously observed for MDMO-PPV. Due to this reason, it may be better to calculate the LUMO position by using the optical band gap, *i.e.* -3.47 eV and -3.63 eV for H-PTV and BH-PTV respectively.

Polymer	HOMO (eV)	LUMO (eV)	Electrochemical Band gap (eV)	Optical Band gap (eV)
PTV	-5.08	-3.27	1.81	1.75
H-PTV	-5.17	-3.24	1.93	1.7
BH-PTV	-5.30	-3.07	2.23	1.67

Table 2-5: HOMO, LUMO energy levels of PTV, H-PTV and BH-PTV with the optical and electrochemical band gap.

As shown in table 2-5, the introduction of a hexyl side chains onto the thiophene ring enlarge the electrochemical band gap, whereas the optical band gap remains unchanged. Both HOMO and LUMO energy level shift due to the incorporation of one or two hexyl side chains. Since the optical band gap remains essentially the same, this effect can solely be explained by the difficult electrolyte ion-transport through the dense conjugated polymer film.

✓ *DiPh-PTV and DiBPh-PTV*

Another example of a substituted PTV derivative is poly[3,4-diphenyl-2,5-thienylene vinylene] (DiPh-PTV) and poly[3,4-bis(4-butylphenyl)-2,5-thienylene vinylene] (DiBPh-PTV) (figure 2-35). It is anticipated that in this particular derivative, the steric hindrance of the reactive 3- and 4-position by the two phenyl rings will lead to a higher stability than its unsubstituted analogue, which is advantageous for applications. Additionally, it is expected that the introduction of phenyl substituents will lead to a decrease in the band gap, which would increase the applicability of this class of conjugated materials in photovoltaic applications. The introduction of butyl side chains in the latter leads to excellent solubility in common organic solvents⁸⁵.

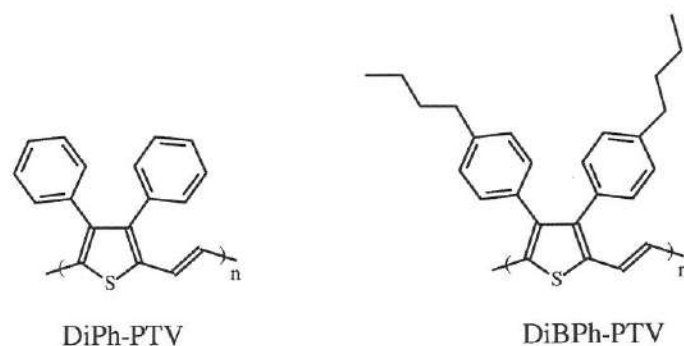


Figure 35: Molecular structure of
Poly[3,4-diphenyl-2,5-thienylene vinylene] (DiPh-PTV) and
Poly[3,4-bis(4-butylphenyl)-2,5-thienylene vinylene] (DiBPh-PTV)

DiPh-PTV and DiBPh-PTV are prepared *via* the dithiocarbamate precursor route. DiPh-PTV is insoluble in chloroform. For the electrochemical measurements, the precursor polymer of DiPh-PTV is spin-coated onto the ITO glass working electrode and heated until 175 °C in nitrogen atmosphere to convert it into the conjugated DiPh-PTV. DiBPh-PTV is a soluble PTV derivative due to the introduction of butyl side chains and can be directly spin-coated on the ITO glass working electrode.

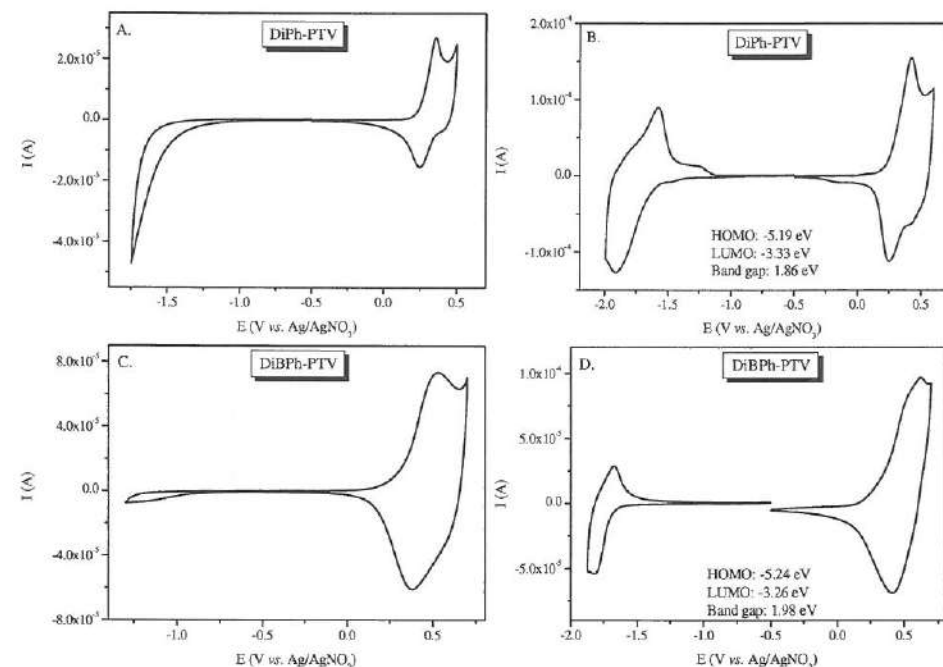


Figure 2-36: Cyclic voltammograms of thin films of DiPh-PTV (top) and DiBPh-PTV (bottom) on ITO working electrodes (left as prepared; right after purification).

The cyclic voltammograms of DiPh-PTV and DiBPh-PTV display distinct oxidation and reduction processes (Figure 2-36). Whereas the oxidation process of as prepared conjugated polymers is directly associated with the conjugated structure, *i.e.* p-doping, the reduction process is irreversible and poorly defined and associated with polymer defects and traces of impurities (figure 2-36A and C). Hence, also in this case, special care was taken during the synthesis to obtain improved purity polymer films. When the polymers are synthesized with anhydrous solvents and are thoroughly dried after the polymerization reaction under vacuum, the reduction process is also reversible and distinct n-doping characteristics are observed (figure 2-36B and D). The observed p- and n-doping process are in all cases quasi-reversible. The LUMO energy level is determined from the onset of reduction. In the cathodic scan the onset of reduction of DiPh-PTV is -1.62 V vs. Ag/AgNO₃, which corresponds to a LUMO energy level of -

3.33 eV. The onset of reduction of DiBPh-PTV is -1.69 V vs. Ag/AgNO₃, giving a LUMO energy level of -3.26 eV. In the anodic scan the onset of oxidation of DiPh-PTV occurs at 0.24 V vs. Ag/AgNO₃, which corresponds to a HOMO energy level of -5.19 eV. The onset of oxidation of DiBPh-PTV occurs at 0.29 V vs. Ag/AgNO₃, which corresponds to a HOMO energy level of -5.24 eV (table 2-6). The optical band gaps of both polymers are somewhat smaller than their electrochemical band gaps. The optical band gap of DiPh-PTV is 1.74 eV, the electrochemical band gap 1.86 eV. These values are almost identical to those observed for PTV, *i.e.* 1.75 eV (optical band gap) and 1.81 eV (electrochemical band gap). Apparently, no reduction in band gap is observed as a result of phenyl substitution, possibly as a result of competing steric effects. The optical band gap of DiBPh-PTV is 1.8 eV and the electrochemical band gap is 1.98 eV. This increase in band gap, as compared to DiPh-PTV is opposite to what can be expected for the introduction of lightly electron donating substituents. Apparently also in this case the alkyl groups reduce the ion-mobility in the films.

Polymer	HOMO (eV)	LUMO (eV)	Electrochemical Band gap (eV)	Optical Band gap (eV)
DiPh-PTV	-5.19	-3.33	1.86	1.74
DiBPh-PTV	-5.24	-3.26	1.98	1.8
PTV	-5.08	-3.27	1.81	1.75

Table 2-6: HOMO, LUMO energy levels of DiPh-PTV, DiBPh-PTV and PTV with the optical and electrochemical band gap.

It should be noted that also for these polymers the oxidation process can be observed visually. For both DiPh-PTV and DiBPh-PTV a color change of the films from blue to light yellow was observed upon oxidation. Subsequently, in the reverse process upon dedoping the color of the film returned to blue. This observation further confirms the reversibility of the p-doping process.

It is noteworthy that upon application of increased bias (*i.e.* scanning to 1.0 V vs. Ag/AgNO₃), a second and a third oxidation process can be observed for DiPh-PTV (Figure 2-37). Similarly to the first oxidation process, which is associated with the HOMO energy level, the second oxidation process with an oxidation potential of circa 0.7 V vs. Ag/AgNO₃ (-5.4 eV) is quasi-reversible. This process is possibly associated with the oxidation of the phenyl rings. In contrast, the third oxidation process with an oxidation potential of circa 0.9 V vs. Ag/AgNO₃ (-5.6 eV) is irreversible and results in an irreversible degradation of the conjugated system.

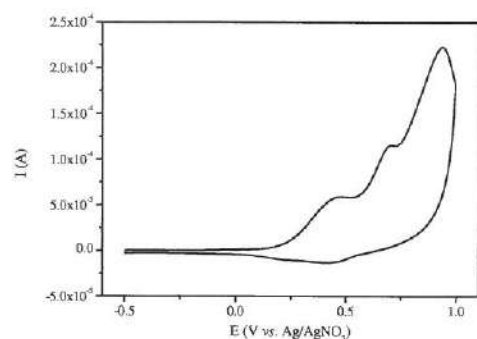


Figure 2-37: Cyclic voltammogram of a thin film of DiPh-PTV on an ITO working electrode upon application of increased bias.

2.8 Electrochemical Properties of bis-(1-cyano-2-thienylvinylene) phenylene derivatives

In this section a selection of six conjugated polymers based on the bis-(1-cyano-2-thienylvinylene) phenylene subunit are presented. The structure consists of a central dialkoxy-phenylene core p-disubstituted by two thiophene derivatives through a cyanovinylene linker. In figure 2-38, the molecular structures of the six derivatives are shown. The polymers were synthesized via an oxidative polymerization with FeCl₃^{28, 86, 87}. Subsequently the electrochemical behavior of the different soluble polymers has been compared. The aim of these measurements

is to investigate the influence of the effect of side group substitutions at the thiophene ring on the energy levels of the polymers.

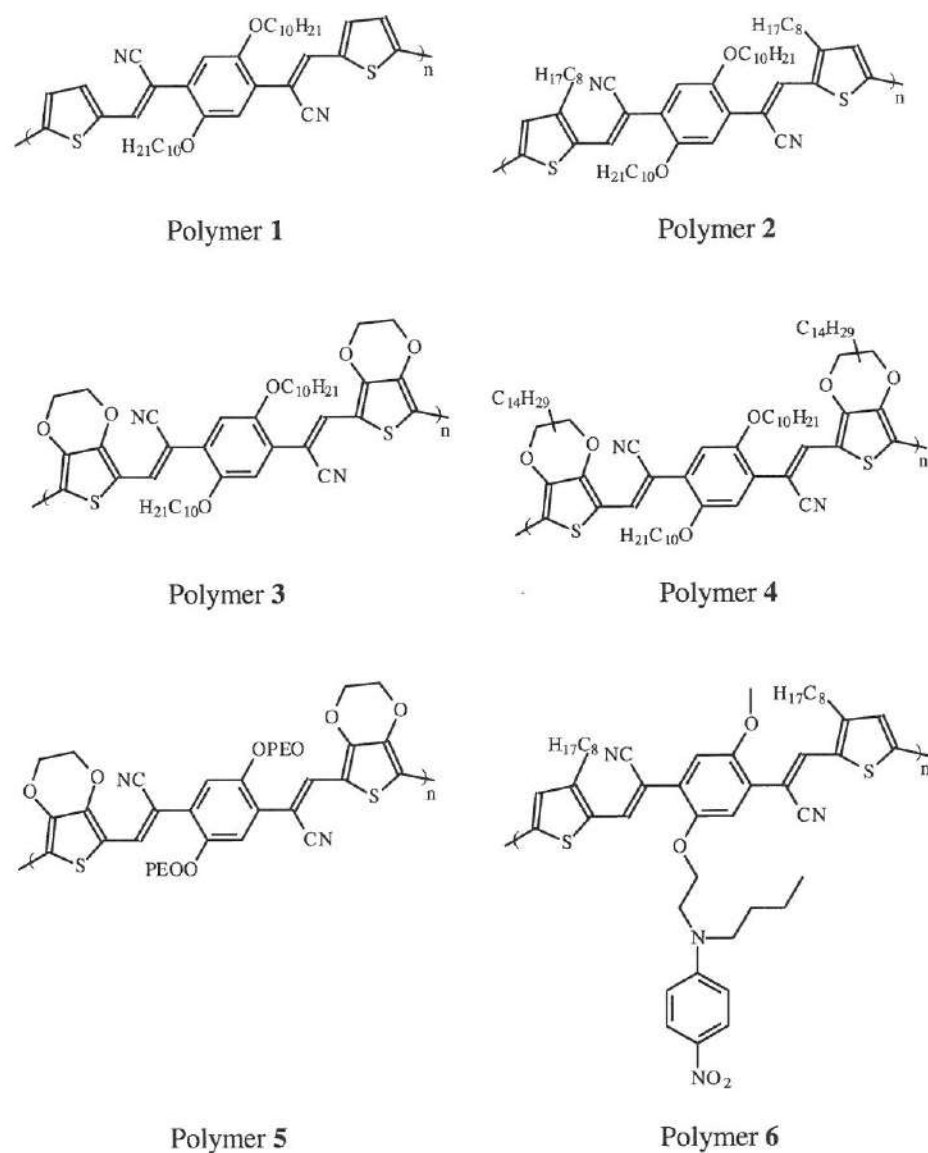


Figure 2-38: Molecular structures of bis-(1-cyano-2-thienylvinylene) phenylene derivatives 1-6

The cyclic voltammograms of polymers **1-4** display quasi reversible oxidation and reduction processes (Figure 2-39) and the onsets of oxidation and reduction potentials are gathered in table 2-6 with the HOMO and LUMO energy level.

With an ethylenedioxy group incorporated in polymer **a** a decrease in electrochemical band gap of *ca.* 0.5 eV and in optical band gap of *ca.* 0.2 eV was found on going from polymer **1** to **3**. Due to the introduction of the ethylenedioxy group attached onto the thiophene ring, the oxidation onset of the polymer **3** decreases, *i.e.* the HOMO level decrease whereas there is only a comparatively small effect on the reduction onsets, *i.e.* the LUMO levels. As a result, a electron donating group like an ethylenedioxy group lower the band gap energy significantly.

The effect of alkyl side chain substitution on the oxidation and reduction process of the polymers can also be compared by using the values of polymer **1** and **2** reported in table 2-6. The onset oxidation and reduction potentials, *i.e.* the HOMO and LUMO energy levels, do not exhibit significant changes when an octyl side chain is attached onto the thiophene ring. The redox potentials of polymer **3** and **4** can also be compared (table 2-6). Polymer **4** has an alkyl substitution into the ethylenedioxy group of polymer **3**. This alkyl substitution in polymer **4** increases the oxidation potentials as compared with their non-substituted analogues polymer **3**. Since the electrochemical band gap in going from **3** to **4** changes significantly, but the optical band gap remains very close for both polymers, it can be expected that ion transport issues play also in this case a role. If this is indeed the case, than apparently the introduction of the long alkyl side chain in **4**, effectively hampers the ion transport through the film. Another explanation could be the decreased coplanarity of the molecules imparted by the alkyl chains, but this seems unlikely.

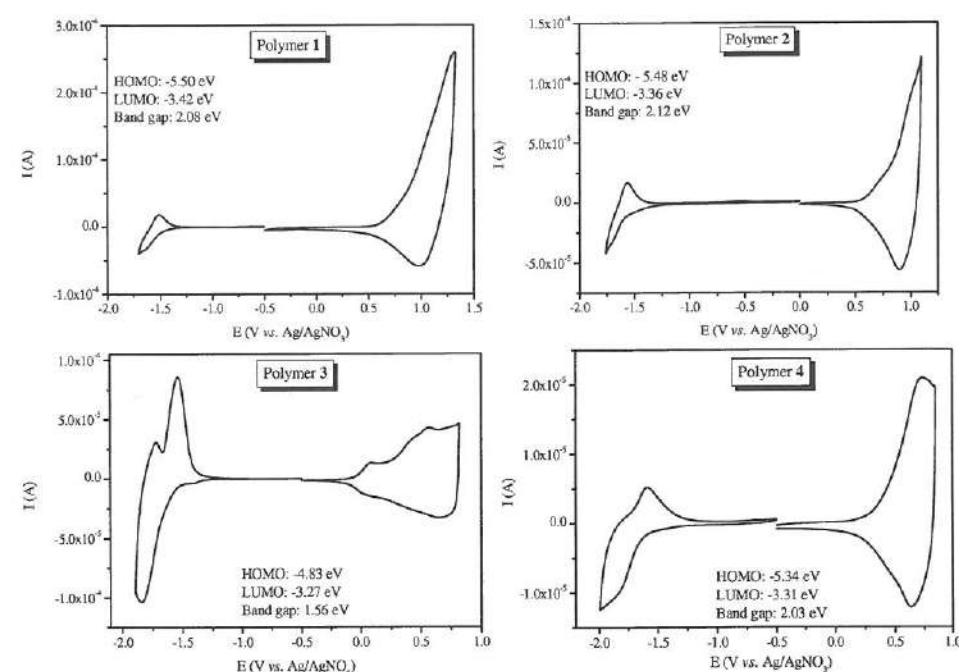


Figure 2-39: Cyclic voltammograms of thin films of the bis-(1-cyano-2-thienylvinylene) phenylene derivatives **1-4** on Pt working electrodes.

The selected group of polymers unfortunately does not give any insight into the question whether the influence of the cyano-vinylene linkage has an impact on the electrochemical properties. To answer this question, a reference polymer without the cyano group is needed. However, from the data it appears that the reduction is mainly dominated by the presence of the cyano-vinylene bond, *viz.* the LUMO energy level in table 2-6 of the four polymers does not exhibit significant variation. The changes in the band gap are mainly determined by the HOMO of the polymer. This could point to a strong localization of the LUMO on the cyano-vinylene group, instead of delocalization.

It should be noted that the oxidation process can also be observed visually. A color change of the films from blue to light yellow was observed upon oxidation.

Subsequently, in the reverse process upon dedoping the color of the film returned to blue. This observation further confirms the reversibility of the p-doping process.

	$E_{\text{ons}}^{\text{ox}}$ (V)	$E_{\text{ons}}^{\text{red}}$ (V)	HOMO (eV)	LUMO (eV)	Electroch. Band gap (eV)	Optical
P 1	0.62	-1.46	-5.50	-3.42	2.08	1.8
P 2	0.57	-1.55	-5.48	-3.36	2.12	1.7
P 3	-0.04	-1.60	-4.83	-3.27	1.56	1.6
P 4	0.40	-1.63	-5.34	-3.31	2.03	1.7
P 5	-0.02	-1.46	-4.82	-3.38	1.44	1.6
P 6	0.72	-1.45	-5.62	-3.45	2.17	2.2

Table 2-6: Reduction and oxidation onset potentials of bis-(1-cyano-2-thienylvinylene) phenylene derivatives 1-6 (expressed in V vs. Ag/AgNO₃), as well as the HOMO, LUMO with the optical and electrochemical band gap.

Polymers **5** and **6** are examples of the further tuning of the properties of this class of polymers. Polymer **5** is comparable to polymer **3** of the previous paragraph. The only difference between polymer **3** and **5** is that in polymer **3** the alkoxy side chains on the phenylene core have been replaced by polar oligo(oxyethylene) side chains (figure 2-38). Polymer **6** is comparable to polymer **2**, with the difference being that in polymer **6** one of the alkoxy side chains on the phenylene core has been replaced by an alkoxy side chain with an attached donor-acceptor moiety with NLO properties (figure 2-38).

The electrochemical data of polymer **5** and **6** are listed in table 2-6. Figure 2-40 shows the quasi-reversible oxidation and reduction behavior of polymers **5** and **6**. Polymer **5** oxidizes at a potential ($E_{\text{onset}}^{\text{ox}} = -0.02$ V vs. Ag/AgNO₃) comparable with the oxidation potential of polymer **3**. The HOMO energy level is estimated at -4.82 eV. The reduction potential of polymer **5** is -1.46 V vs. Ag/AgNO₃. This

value is in the same order of magnitude as the reduction potential of polymer **3**. The LUMO energy level is estimated at -3.38 eV. Hence, it can be concluded that the electrochemical behavior of polymers **3** and **5** is very similar. Apparently, the influence of the exact nature of the alkoxy side chain has no significant effect on the HOMO and LUMO energy level. This was previously observed for the PPV-type polymers (*vide supra*). The first atom attached onto the phenylene ring is evidently most important for the measured electrochemical properties.

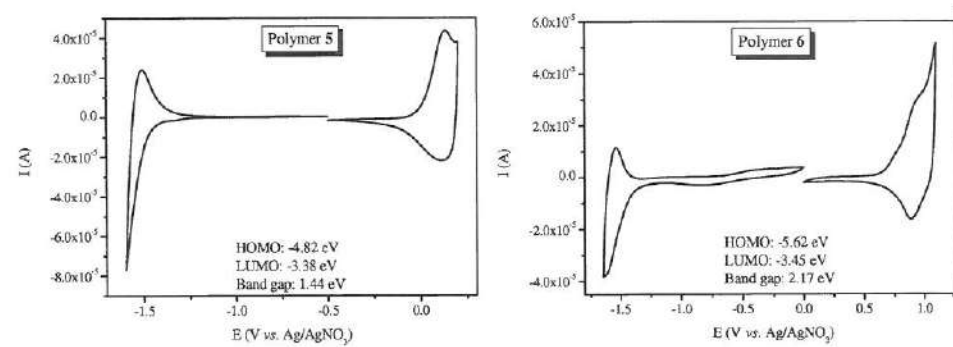


Figure 2-40: Cyclic voltammograms of thin films of the bis-(1-cyano-2-thienylvinylene) phenylene derivatives **5** and **6** on Pt working electrodes.

Similar conclusions can be made when the electrochemical properties of polymer **2** and **6** are compared (table 2-6). Polymer **6** oxidizes at a potential of 0.72 V vs. Ag/AgNO₃. This onset oxidation potential is higher than the oxidation potential of polymer **2**. This means that the incorporation of a big sidechain with NLO properties increases the HOMO energy level of polymer **6**. The reduction potential of polymer **6** is -1.45 V vs. Ag/AgNO₃. This value is in the same order of magnitude as the reduction potential of polymer **2**. The LUMO energy level is estimated at -3.45 eV. Surprisingly also in this case, the electrochemical properties of the attached donor-acceptor *p*-nitroaniline moiety of polymer **6** do not manifest themselves in the cyclic voltammogram. This is comparable with copolymer **2**.⁷⁵

Finally, it is worth mentioning that the results for solar cells performance are disappointing. The solar cells made of these polymers exhibit low efficiencies, which can be attributed to the low hole mobilities observed in the pure polymer films. This may well corroborate the earlier statement that strong localization at the vinylene-cyano group occurs. For that reason, the bis-(1-cyano-2-thienylvinylene) phenylene derivatives will not be referred to in the general discussion on the typical electrochemical trends observed for various types of conjugated polymers (*cf.* section 2.10).

2.9 Electrochemical Properties of Reference Compounds

✓ P3HT and PCBM

Plastic electronics based on organic semiconductors comprise a very promising technology to enter the electronic market. For example, organic solar cells, which typically use conjugated polymers as electron donors in combination with an organic n-type acceptor, can be processed from solution or dispersion using conventional thin film technology. The discovery of ultrafast charge transfer in p-conducting polymer/fullerene composites in 1992⁸⁸ brought a crucial milestone in the field of polymer solar cells. Regioregular poly(3-hexylthiophene) (P3HT) is currently one of the most attractive materials for such devices. It combines commercial availability with sufficient solubility, a reasonably low band gap and a high degree of intermolecular order leading to high charge carrier mobilities. 1-(3-methoxycarbonyl)-propyl-1-phenyl-(6,6) C₆₀ (PCBM) is a soluble fullerene derivative, which is commonly employed as the acceptor in these bulk heterojunction organic solar cells. The chemical structures of PCBM and P3HT are shown in figure 2-41^{49, 89}.

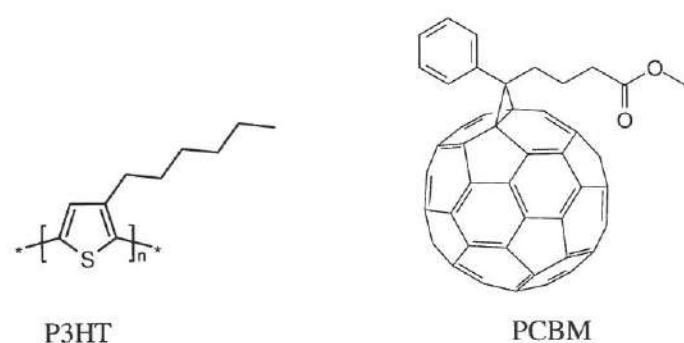


Figure 2-41: Molecular structure of poly(3-hexyl thiophene) (P3HT) and 1-(3-methoxycarbonyl)-propyl-1-phenyl-(6,6) C₆₁ (PCBM)

Efficient charge transfer from donor to acceptor, effective charge transport and charge injection into the electrodes are important parameters for the design and optimization of organic solar cells. In this regard, electrochemical data can give valuable information, since they allow the estimation of the relative position of HOMO/LUMO levels of the investigated materials. The knowledge of these values is essential for finding suitable donor-acceptor pairs. In the previous sections the electrochemical properties of many conjugated polymers have been reported, all of which have been prepared within the research group Organic and Polymer Chemistry of Hasselt University. However, since P3HT and PCBM comprise important materials for solar cells, additional samples of these materials were obtained.⁹⁰⁻⁹³ Subsequently, for reference purposes their electrochemical characteristics were measured in thin films, which were prepared by dropping a solution on a platinum working electrode. Table 2-7 contains the HOMO and LUMO values of P3HT and PCBM. Figure 2-42 shows the cyclic voltammograms of these materials.

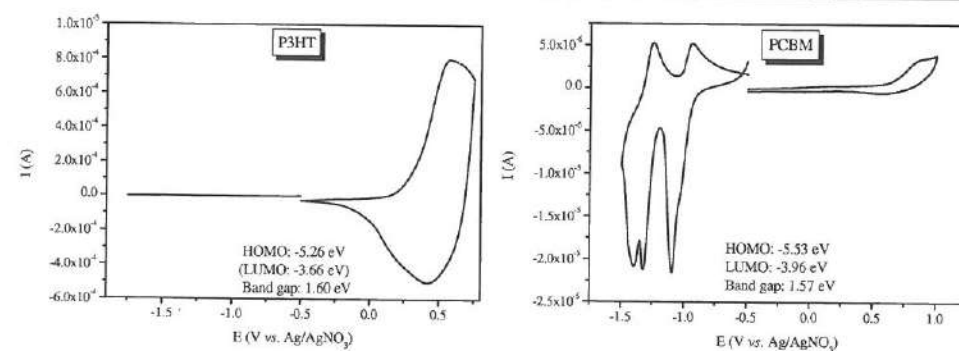


Figure 2-42: Cyclic voltammograms of thin films of P3HT and PCBM on Pt working electrodes.

Material	$E_{\text{onset}}^{\text{ox}}$ (V)	$E_{\text{onset}}^{\text{red}}$ (V)	HOMO (eV)	LUMO (eV)	Electrochemical band gap (eV)
P3HT	0.28	-1.32	-5.26	-3.66	1.60
PCBM	0.55	-1.02	-5.53	-3.96	1.57

Table 2-7: Cyclic voltammetry data: Reduction and oxidation onset potentials (expressed in V vs. Ag/AgNO₃) as well as the HOMO and LUMO energy levels with the electrochemical band gap of P3HT and PCBM

For estimation of the HOMO and LUMO of PCBM, the onset values of oxidation and reduction were used, in a similar fashion as was done for all previously discussed polymers. This will allow for a fair comparison. However, this also means that the table does not contain the formal potentials. As expected, the LUMO of P3HT is higher in energy than that of PCBM. That means that the electron affinity of PCBM is higher than that of P3HT. The electrochemical band gap of P3HT is equal to 1.60 eV and is clearly lower than the optical band gap (1.93 eV). The electrochemical value is in accordance with literature data^{94, 95}.

Figure 2-43 shows the resulting energy diagram of a P3HT/PCBM organic solar cell in relation to the work functions of the commonly employed ITO and aluminum (Al) electrodes. The relative position of donor LUMO and acceptor LUMO is crucial to achieve the desired charge transfer. Figure 2-43 shows that there is a difference 0.3 eV between the LUMO of P3HT and that of PCBM. The HOMO of P3HT polymer is clearly higher in energy than the HOMO of PCBM. Under the resulting conditions it is energetically favorable for the photoexcited P3HT to transfer an electron to PCBM. Therefore P3HT can be used as an electron donor with PCBM as an electron acceptor to prepare donor/acceptor solar cells⁹⁶.

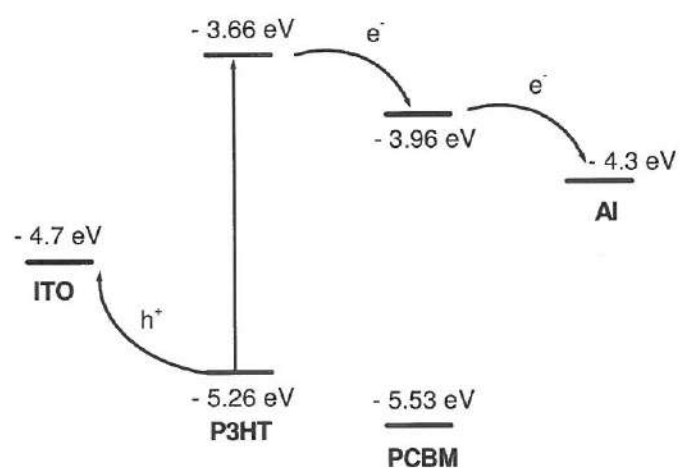


Figure 2-43: Energy diagram of a typical organic solar cell consisting of P3HT as the donor and PCBM as the acceptor. Also the work function of the typical ITO and Al electrodes are given.

As demonstrated in the above energy diagram of P3HT and PCBM, the functioning of the organic solar cell can be predicted when the relative HOMO and LUMO energy levels of each conjugated material are known. These values give valuable information, which donor materials can or should preferably be combined with which acceptor for a promising fabrication of polymer solar cell devices. Obviously, the relative LUMO position of the acceptor material should be lower in

energy than the LUMO position of the donor material. With the help of this chapter which lists the HOMO and LUMO energy levels of different types of conjugated polymers, the selection of suitable materials is facilitated.

2.10 Typical trends observed for various types of conjugated polymers

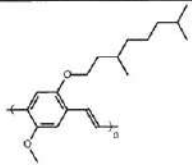
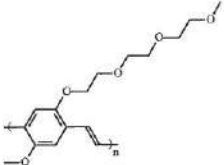
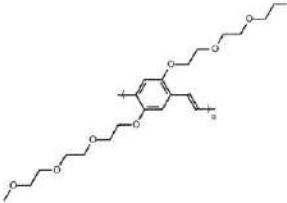
In the previous sections it has been demonstrated that the optical and electrochemical properties of various conjugated polymers exhibit as expected a strong dependence on the changes in main chain structure as well as the attached side chains. It has been demonstrated that the band gaps of these polymers can readily be adjusted in the window from 1.5 eV to 3 eV. This is a result of the fact that the modification of the main chains and/or side chains with a variety of electron-withdrawing or electron-donating groups enables the tuning of HOMO and LUMO energy levels in a wide range.

2.10.1 Poly(*p*-phenylene vinylene) derivatives

In this chapter, three different types of PPV derivatives have been discussed, namely non-substituted PPV, 2,5 di-alkoxy substituted PPV derivatives and PPV-type polymers with larger and/or more complex aromatic cores. An overview of the HOMO and LUMO energy levels of all relevant 2,5 di-alkoxy substituted PPV derivatives is presented in table 2-8.

From the data of table 2-8, it can be seen that the HOMO energy level of the polar 2,5-substituted di-alkoxy PPV derivatives (MTEM-PPV, BTEM PPV and NTEM-PPV) is positioned at -5.10 ± 0.05 eV. The LUMO energy level of the same polymers is positioned at -2.95 ± 0.05 eV. The resulting electrochemical band gap for these polymers is 2.15 ± 0.10 eV. The optical band gap for all polar and apolar

discussed 2,5-substituted di-alkoxy PPV derivatives is 2.10 ± 0.05 eV. Hence, for polar substituted PPV derivatives the optical and electrochemical band gaps are comparable within the margin of error. This is not the case for the apolar 2,5-substituted di-alkoxy PPV derivatives (MDMO-PPV, BN-PPV and BMB-PPV), which have significantly shifted HOMO and LUMO energy levels. It can be concluded that this must be due to the apolar alkoxy side chains, which dominate the thin film properties. As a result, the ion transport of the electrolyte solution through the polymer film is difficult, which directly affects the measured electrochemical properties.

Alkoxy PPV Polymers	HOMO level (eV)	LUMO level (eV)	Electro. Band gap (eV)	Optical Band gap (eV)	Structure of polymer
MDMO- PPV	-5.32	-2.78	2.54	2.12	
MTEM- PPV	-5.05	-2.95	2.10	2.10	
BTEM- PPV	-5.15	-2.97	2.18	2.10	

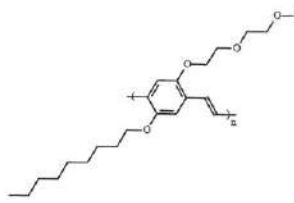
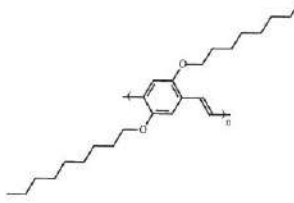
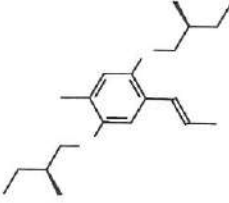
NTEM-PPV	-5.09	-2.90	2.19	2.12	
BN-PPV	-5.28	-3.67	1.61	2.11	
BNB-PPV	-5.27	-3.04	2.23	2.12	

Table 2-8: The HOMO and LUMO energy levels, the electrochemical band gap, the optical band gap and the structures of various 2,5-di-alkoxy substituted PPV derivatives.

Based on this assessment and a thorough analysis of the optical and electrochemical data it can hence be concluded that in the studied series of polymers there is no significant effect of the type of side chains attached to the phenylene ring in the PPV backbone. Apparently, the first atom(s) attached to the phenylene ring dominate the optoelectronic properties. In the above series this is at the 2- and 5-position of the phenylene ring an oxygen atom. For comparison, the HOMO energy level of unsubstituted PPV is -5.6 ± 0.1 eV and the LUMO is -3.1 ± 0.1 eV. This demonstrates that the introduction of the two alkoxy groups significantly decreases the oxidation onsets of the polymers *i.e.* the HOMO levels decrease, whereas there is only a minimal effect on the reduction onsets, *i.e.* the LUMO levels remain comparatively unchanged. As a result, alkoxy groups in the 2,5-position of the phenylene unit lower the band gap energy significantly. The

reason for this is the fact that the alkoxy group is an electron donating group, which provides additional electron density to participate in the conjugated system.^{66, 97, 98}

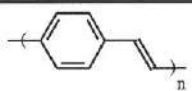
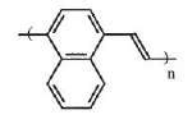
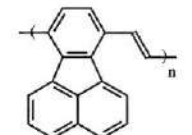
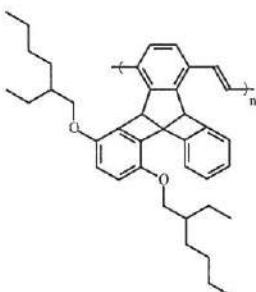
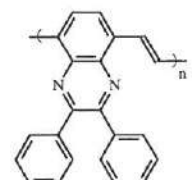
Alkyl PPV Polymers	HOMO level (eV)	LUMO level (eV)	Electro. Band gap (eV)	Optical Band gap (eV)	Structure of polymer
PPV	-5.58	-3.12	2.46	2.46	
PNV	-5.42	-3.41	2.01	2.18	
PFV	-5.64	-3.10	2.54	2.34	
PTTyV	-5.87	-3.51	2.36	2.60	
PQV	-5.35	-3.65	1.70	1.83	

Table 2-9: The HOMO and LUMO energy levels, the electrochemical band gap, the optical band gap and the structures of various PPV derivatives with larger and/or more complex aromatic cores.

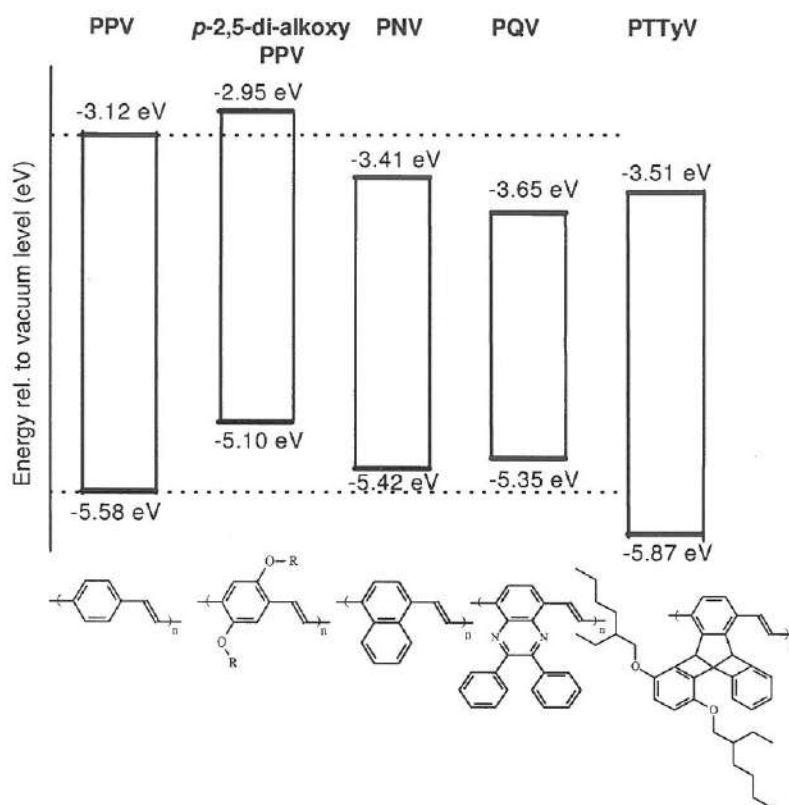


Figure 2-44: Structures and HOMO and LUMO energy levels of selected types of PPV-polymers

As mentioned above, the nature of the alkoxy substituents has no significant impact on the electrochemical properties of the conjugated polymers studied. Another issue of interest is whether an extension of the conjugated system will have marked impact on the optoelectronic properties. Two examples include PNV and PFV (table 2-9). Whereas it appears that the extension of the conjugated system in PFV has only minimal impact on the optoelectronic properties, *i.e.* the additional cyclopenta fused naphthalene unit is apparently electronically mostly decoupled, in the case of PNV a band gap reduction is observed, which is mostly associated with a shift of the LUMO energy level. Introduction of a hetero-aromatic system, *e.g.* PQV, leads to a further band gap reduction. It can be expected that in PPV

derivatives with bulky side chains, the HOMO and LUMO will be changed due to steric effects. This is exemplified by PTTyV, for which polymer indeed significantly changed HOMO and LUMO energy levels are observed.

Figure 2-44 is another way to demonstrate the different HOMO and LUMO levels. In this figure, the effect of 2,5-alkoxy substitution, extension of the aromatic system and steric effects are readily discernible.

2.10.2 Poly(thienylene vinylene) derivatives

In table 2-10 the HOMO and LUMO energy levels of various PTV derivatives are compared. *Non-substituted* PTV has a HOMO level of about -5.1 eV and a LUMO energy level of -3.3 eV. The electrochemical band gap is 1.8 eV. This means that PTV is a low band gap polymer. When grafting one or two *alkyl* side chains to the thiophene unit (H-PTV), the positions of the HOMO and the LUMO somewhat change and the electrochemical band gap incrementally increases to 2.2 eV. This increase in band gap probably is a result of a combination of a steric effect as a result of the substituents and the previously discussed hampered ion transport through thin films of conjugated polymers with apolar alkyl side chains. The latter may be most important, since no significant changes in the optical band gap are observed. This is corroborated by the fact that when the thiophene ring is substituted by an even more bulky group, *e.g.* the phenyl or the butylphenyl side chain, the effect on the band gap remains small, with the largest increase again being observed for the alkyl substituted representative. Furthermore, it is noteworthy that the phenyl substituents appear to be electronically decoupled from the conjugated system. In this context it is interesting to compare the electrochemical behavior of the PTV derivatives with those of the previously discussed PPV derivatives. Similarly to PPV derivatives, steric and ion-conductivity effects play an important role in PTV-type polymers. No substituent effect has been investigated for the PTV-derivatives since alkoxy substituted

examples are not yet available for electrochemical studies. It can be anticipated that in such PTV derivatives the band gap will be significantly further reduced, while the increased flexibility of the ether group will minimize steric effects.

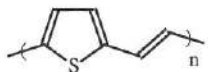
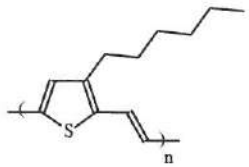
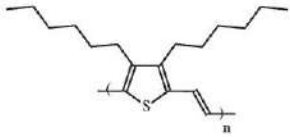
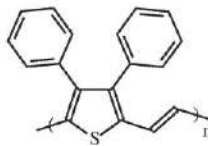
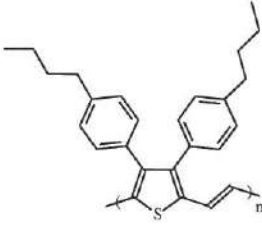
Alkyl PTV Polymers	HOMO level (eV)	LUMO level (eV)	Electro. Band gap (eV)	Optical Band gap (eV)	Structure of polymers
PTV	-5.08	-3.27	1.81	1.75	
H-PTV	-5.17	-3.24	1.93	1.7	
BH-PTV	-5.30	-3.07	2.23	1.67	
DiPh- PTV	-5.19	-3.33	1.86	1.74	
DiBPh- PTV	-5.24	-3.26	1.98	1.8	

Table 2-10: The HOMO and LUMO energy levels, the electrochemical band gap, the optical band gap and the structures of various PTV derivatives.

2.11 Conclusions

In this chapter, the electrochemical properties are presented of different PPV and PTV derivatives. Estimates of the highest occupied (HOMO) and lowest unoccupied molecular orbitals (LUMO) energy levels have been derived for all polymers studied. Especially the effect on the electronic properties of the introduction of side chains has been studied. The introduction of long alkyl or alkoxy-side groups to conjugated polymers is important for the solubility and processability of PPV and PTV derivatives. It can be concluded that the HOMO energy level is changed by the introduction of alkoxy-side groups, while the LUMO remains almost unchanged. As a result the electrochemical band gap decreases. In contrast, alkyl substitution has only minimal effects on the energy levels. Bulky side groups can impact both the HOMO and the LUMO levels. The same holds true for modifications to the aromatic system, for example by extension of the aromatic system. However, it is important to realize that the exact position of electrochemically determined HOMO and LUMO energy levels is dependent on various factors, which are not always directly a result of the optoelectronic properties of the conjugated backbone. Especially the ability of electrolyte ion transport through the thin conjugated polymer films is important, since otherwise an additional resistance is introduced, which can create a significant additional error in the electrochemical measurements. The presence or absence of electrochemical reversibility in conjugated polymers is not only associated with the possibility of a polymer to be n- and/or p-doped but also with its ability to facilitate sufficient stabilization of the electrolyte counter ion in the polymer film.

At Hasselt University, a large variety of conjugated polymers has been developed. By careful adjustments to the conjugated system it is possible to modify the HOMO and LUMO energy levels over a wide range. The LUMO values of the materials presented in this thesis range from about -2.9 eV to -3.7 eV and HOMO values range from about -5.0 eV to -5.9 eV. Summarizing, the HOMO and LUMO

values for the main three polymer classes studied are listed in table 2-11. Substitution with electron donating/accepting or bulky groups can be utilized to further tailor these levels.

Type of Material	HOMO (eV)	LUMO (eV)
2,5-OR-PPV	-5.10	-2.95
PPV, PFV (alkyl-PPV)	-5.6	-3.1
PTV, alkyl-PTV	-5.1	-3.3

Table 2-11: Overview

2.12 References

- 1 A. M. Bond and R. Colton, *Coordination Chemistry Reviews*, 166, **1997**, 161.
- 2 J. L. Bredas, R. Silbey, D. S. Boudreaux and R. R. Chance, *Journal of the American Chemical Society*, 105, **1983**, 6555.
- 3 T. Ahn, S.-G. Lee and H.-K. Shim, *Optical Materials*, 21, **2002**, 191.
- 4 A. K. Agrawal and S. A. Jenekhe, *Chemistry of Materials*, 8, **1996**, 579.
- 5 H. W. Chen. Z.-K. Wang L.-H, Kang E.-T, *Macromolecules*, 33, **2000**, 9015.
- 6 S. M. M. J. de Leeuw. D.M., Brown A.R., Einerhand R.E.F, *Synthetic Metals*, 87, **1997**, 53.
- 7 T. W. Kwon, M. M. Alam and S. A. Jenekhe, *Chemistry of Materials*, 16, **2004**, 4657.
- 8 S. W. Ko, B. J. Jung, N. S. Cho and H. K. Shim, *Bulletin of the Korean Chemical Society*, 23, **2002**, 1235.
- 9 Y. F. Li, Y. Cao, J. Gao, D. L. Wang, G. Yu, *Synthetic Metals*, 99, **1999**, 243.

- 10 C. J. Tonzola, M. M. Alam, W. Kaminsky and S. A. Jenekhe, *Journal of the American Chemical Society*, 125, **2003**, 13548.
- 11 Y. Xiao, W. L. Yu, J. Pei, Z. K. Chen, W. Huang, *Synthetic Metals*, 106, **1999**, 165.
- 12 C. J. Yang and S. A. Jenekhe, *Macromolecules*, 28, **1995**, 1180.
- 13 M. Al-Ibrahim, A. Konkin, H. K. Roth, D. A. M. Egbe, E. Klemm, *Thin Solid Films*, 474, **2005**, 201.
- 14 P. H. Aubert, M. Knipper, L. Groenendaal, L. Lutsen, J. Manca, *Macromolecules*, 37, **2004**, 4087.
- 15 R. Cervini, X. C. Li, G. W. C. Spencer, A. B. Holmes, S. C. Moratti, *Synthetic Metals*, 84, **1997**, 359.
- 16 Y. Chen and S. P. Lai, *Journal of Polymer Science Part A-Polymer Chemistry*, 39, **2001**, 2571.
- 17 H. J. Cho, B. J. Jung, N. S. Cho, J. Lee and H. K. Shim, *Macromolecules*, 36, **2003**, 6704.
- 18 T. J. Dingemans, A. Bacher, M. Thelakkat, L. G. Pedersen, E. T. Samulski, *Synthetic Metals*, 105, **1999**, 171.
- 19 C.-C. Ho, K.-M. Yeh and Y. Chen, *Polymer*, 45, **2004**, 8739.
- 20 S. Janietz, D. D. C. Bradley, M. Grell, C. Giebeler, M. Inbasekaran, *Applied Physics Letters*, 73, **1998**, 2453.
- 21 J. H. Kim and H. Lee, *Synthetic Metals*, 139, **2003**, 471.
- 22 Y. Z. Lee, X. W. Chen, S. A. Chen, P. K. Wei and W. S. Fann, *Journal of the American Chemical Society*, 123, **2001**, 2296.
- 23 Y. Liu, M. S. Liu and A. K. Y. Jen, *Acta Polymerica*, 50, **1999**, 105.
- 24 J. P. Lu, Y. Tao, M. D'Iorio, Y. N. Li, J. F. Ding, *Macromolecules*, 37, **2004**, 2442.
- 25 J. Morgado, F. Cacialli, R. H. Friend, B. S. Chuah, H. Rost, *Macromolecules*, 34, **2001**, 3094.
- 26 Z. H. Peng, Z. N. Bao and M. E. Galvin, *Chemistry of Materials*, 10, **1998**, 2086.

- 27 J. Pommerehne, H. Vestweber, W. Guss, R. F. Mahrt, H. Bassler, *Advanced Materials*, 7, **1995**, 551.
- 28 P. Wagner, P. H. Aubert, L. Lutsen and D. Vanderzande, *Electrochemistry Communications*, 4, **2002**, 912.
- 29 B. H. Wang, J. Yin, M. Z. Xue, J. L. Wang, G. Y. Zhong, *Thin Solid Films*, 424, **2003**, 186.
- 30 B. H. Wang, J. Yin, M. Z. Xue, J. L. Wang, G. Y. Zhong, *Synthetic Metals*, 132, **2003**, 191.
- 31 L. Yang, J.-K. Feng and A.-M. Ren, *Journal of Molecular Structure: Theochem*, 758, **2006**, 29.
- 32 N. C. Yang, S. M. Lee, Y. M. Yoo, J. K. Kim and D. H. Suh, *Journal of Polymer Science Part A-Polymer Chemistry*, 42, **2004**, 1058.
- 33 X. W. Zhan, S. Wang, Y. Q. Liu, X. Wu and D. B. Zhu, *Chemistry of Materials*, 15, **2003**, 1963.
- 34 R. Gomer and G. Tryson, *Journal of Chemical Physics*, 66, **1977**, 4413.
- 35 F. Lohmann, *Zeitschrift fur Naturfosch: Teil A*, 22, **1967**, 843.
- 36 S. Trasatti, *Electrochimica Acta*, 28, **1983**, 1083.
- 37 A. J. Bard and L. R. Faulkner, *Electrochemical Methods: Fundamentals and Applications*, second edition, **2001**, Wiley.
- 38 A. J. Bard, R. Memming and B. Miller, *Pure and Applied Chemistry*, 63, **1991**, 569.
- 39 E. R. Kotz, H. Neff and K. Muller, *Journal of Electroanalytical Chemistry*, 215, **1986**, 331.
- 40 M. M. Shi, H. Z. Chen, J. Z. Sun, J. Ye and M. Wang, *Chemical Physics Letters*, 381, **2003**, 666.
- 41 H. Reiss and A. Heller, *Journal of Physical Chemistry*, 89, **1985**, 4207.
- 42 W. J. Tian, J. S. Huang, Wu F., C. Q. Sun, X. Liu, *Chinese Physical Letters*, 13, **1996**, 790.
- 43 M. Ozkan, O. C.S., O. Kibar and M. M. Wang, *Iee Engineering in Medicine and Biology*, **2001**, 144.

- 44 S. C. Veenstra, W. J. H. Verhees, J. M. Kroon, M. M. Koetse, J. Sweelssen, *Chemistry of Materials*, 16, **2004**, 2503.
- 45 T. W. Wu F., Sun J., Shen J., Pan X., Su Z., *Materials Science and Engineering B*, 85, **2001**, 165.
- 46 D. A. M. Egbe, T. Kietzke, B. Carbonnier, D. Muhlbacher, H. H. Horhold, *Macromolecules*, 37, **2004**, 8863.
- 47 D. A. M. Egbe, L. Nguyen, B. Carbonnier, D. Muhlbacher and N. S. Sariciftci, *Polymer*, 46, **2005**, 9585.
- 48 D. Mühlbacher, H. Neugebauer, A. Cravino and N. S. Sariciftci, *Synthetic Metals*, 2003, **2003**, 1361.
- 49 M. C. Scharber, D. Muhlbacher, M. Koppe, P. Denk, C. Waldauf, *Advanced Materials*, 00, **0000**, 1.
- 50 G. Jegou and S. A. Jenekhe, *Macromolecules*, 34, **2001**, 7926.
- 51 J.-H. Wan, J.-C. Feng, G.-A. Wen, H.-Y. Wang, Q.-L. Fan, *Tetrahedron Letters*, 47, **2006**, 2829.
- 52 J. L. Bredas, *Handbook of Conducting Polymers*, Dekker, New York, **1986**, 859.
- 53 H. Eckhardt, L. W. Shacklette, K. Y. Jen and R. L. Elsenbaumer, *Journal of Chemical Physics*, 91, **1989**, 1303.
- 54 C. Arbizzani, M. Catellani, M. Mastragostino and M. G. Cerroni, *Journal of Electroanalytical Chemistry*, 423, **1997**, 23.
- 55 M. Catellani, R. Lazzaroni, S. Luzzati and J. L. Bredas, *Synthetic Metals*, 101, **1999**, 175.
- 56 M. Cheng, Y. Xiao, W. L. Yu, Z. K. Chen, Y. H. Lai, *Thin Solid Films*, 363, **2000**, 110.
- 57 F. Louwet, D. Vanderzande, J. Gelan and J. Mullens, *Macromolecules*, 28, **1995**, 1330.
- 58 P. Damlin, C. Kvarnstrom, H. Neugebauer and A. Ivaska, *Synthetic Metals*, 123, **2001**, 141.

- 59 L. Lutsen, P. Adriaenssens, H. Becker, A. J. Van Breemen, D. Vanderzande, *Macromolecules*, 32, **1999**, 6517.
- 60 D. Braun and A. J. Heeger, *Applied Physics Letters*, 58, **1991**, 1982.
- 61 H. Becker, H. Spreitzer, W. Kreuder, E. Kluge, H. Schenk, *Advanced Materials*, 12, **2000**, 42.
- 62 F. Wudl and G. Sardarov, *US Patent*, 189, **2000**, 136.
- 63 D. A. M. Egbe, L. H. Nguyen, H. Hoppe, D. Muhlbacher and N. S. Sariciftci, *Macromolecular Rapid Communications*, 26, **2005**, 1389.
- 64 J. H. Hou, C. H. Yang, J. Qiao and Y. F. Li, *Synthetic Metals*, 150, **2005**, 297.
- 65 H. J. Lee, S. Y. Cui and S. M. Park, *Journal of the Electrochemical Society*, 148, **2001**, D139.
- 66 J.-I. Lee, H. Y. Chu, C. M. Kim, L.-M. Do, T. Zyung, *Optical Materials*, 21, **2002**, 205.
- 67 M. M. Richter, F. R. F. Fan, F. Klavetter, A. J. Heeger and A. J. Bard, *Chemical Physics Letters*, 226, **1994**, 115.
- 68 C. H. Yang, G. F. He, R. Q. Wang and Y. F. Li, *Journal of Electroanalytical Chemistry*, 471, **1999**, 32.
- 69 I. Van Severen, M. Breselge, S. Fourier, P. Adriaenssens, J. Manca, *Macromolecular Chemistry and Physics*, 208, **2007**, 196.
- 70 G. F. He, C. H. Yang, R. Q. Wang and Y. F. Li, *Displays*, 21, **2000**, 69.
- 71 B. S. Chuah, D. H. Hwang, S. T. Kim, S. C. Moratti, A. B. Holmes, *Synthetic Metals*, 91, **1997**, 279.
- 72 B. Jousselme, P. Blanchard, E. Levillain, J. Delaunay, M. Allain, *Journal of American Chemical Society*, 125, **2003**, 1363.
- 73 R. E. Martin, F. Geneste, B. S. Chuah, C. Fischmeister, Y. G. Ma, *Synthetic Metals*, 122, **2001**, 1.
- 74 T. J. Cleij, J. K. King and L. W. Jenneskens, *Chemical Materials*, 12, **2000**, 84.

- 75 A. A. Jbarah and R. Holze, *Journal of Solid State Electrochemistry*, 10, **2006**, 360.
- 76 A. Palmaerts, M. van Haren, L. Lutsen, T. J. Cleij and D. Vanderzande, *Macromolecules*, 39, **2006**, 2438.
- 77 A. Babel and S. A. Jenekhe, *Journal of the American Chemical Society*, 125, **2003**, 13656.
- 78 C. Koper, M. Sarobe and L. W. Jenneskens, *Physical Chemistry, Chemical Physics*, 6, **2004**, 319.
- 79 M. Jonforsen, T. Johansson, O. Inganas and M. R. Andersson, *Macromolecules*, 35, **2002**, 1638.
- 80 M. J. Edelmann, J. M. Raimundo, N. F. Utesch, F. Diederich, C. Boudon, *Helvetica Chimica Acta*, 85, **2002**, 2195.
- 81 P. Blanchard, H. Brisset, B. Illien, A. Riou and J. Roncali, *Journal of Organic Chemistry*, 62, **1997**, 2401.
- 82 M. Onoda, H. Nakayama, K. Amakawa and K. Yoshino, *Ieee Transactions on Electrical Insulation*, 27, **1992**, 636.
- 83 H. Q. Xie, C. M. Liu and J. S. Guo, *European Polymer Journal*, 32, **1996**, 1131.
- 84 E. H. Elandaloussi, P. Frere, P. Richomme, J. Orduna, J. Garin, *American Chemical Society*, 119, **1997**, 10774.
- 85 A. Henckens, K. Colladet, S. Fourier, T. J. Cleij, L. Lutsen, *Macromolecules*, 38, **2005**, 19.
- 86 K. Colladet, M. Nicolas, L. Goris, L. Lutsen and D. Vanderzande, *Thin Solid Films*, 451-52, **2004**, 7.
- 87 K. Colladet, S. Fourier, T. J. Cleij, L. Lutsen, J. Gelan, *Macromolecules*, 40, **2007**, 65.
- 88 N. S. Sariciftci, L. Smilowitz, A. J. Heeger and F. Wudl, *Science*, 258, **1992**, 1474.
- 89 J. C. Hummelen, B. W. Knight, F. Lepeq, F. Wudl, J. Yao, *Journal of Organic Chemistry*, 60, **1995**, 532.

- 90 P. Vanlaeke, G. Vanhoyland, T. Aernouts, D. Cheyns, C. Deibel, *Thin Solid Films*, 511-512, **2006**, 358.
- 91 T. Munters, T. Martens, L. Goris, V. Vrindts, J. Manca, *Thin Solid Films*, 403, **2002**, 247.
- 92 P. Vanlaeke, A. Swinnen, I. Haeldermans, G. Vanhoyland, T. Aernouts, *Solar Energy Materials and Solar Cells*, 90, **2006**, 2150.
- 93 M. Reyes-Reyes, K. Kim, J. Dewald, R. Lopez-Sandoval, A. Avadhanula, *Organic Letters*, 7, **2005**, 5749.
- 94 M. Al-Ibrahim, H. K. Roth, U. Zhokhavets, G. Gobsch and S. Sensfuss, *Solar Energy Materials and Solar Cells*, 85, **2005**, 13.
- 95 M. Al-Ibrahim, H. K. Roth, M. Schroedner, A. Konkin, U. Zhokhavets, *Organic Electronics*, 6, **2005**, 65.
- 96 F. Padinger, R. S. Rittberger and N. S. Sariciftci, *Advanced Functional Materials*, 13, **2003**, 85.
- 97 M. Helbig and H. H. Horhold, *Makromolekulare Chemie-Macromolecular Chemistry and Physics*, 194, **1993**, 1607.
- 98 Y. W.-L. Liu B., Lai Y.-H., Huang W., *Chemical Materials.*, 13, **2001**, 1984.

Chapter 3

UV-Vis-NIR Absorption Spectroscopy

3.1 Introduction

The discovery of the electrical conductivity of doped polyacetylene has triggered a revolution in the perception of polymeric materials. Conjugated polymers are nowadays a major research topic, with useful technological applications materializing in many areas. The genuine interest in these polymers stems from the fact that they combine the optical and electronic properties of semiconductors, with the convenient processibility of plastics, for numerous applications in microelectronics. In this chapter, the optical properties of four selected conjugated polymers will be examined.

Conjugated polymers can be prepared with various types of side chains attached onto the polymer backbone. The introduction of substituents along the conjugated backbone can not only improve the processibility of these polymers, but can also modify their physical properties. It can even lead to physical phenomena that are not found in the parent unsubstituted polymers. Different side chains attached to

the polymer may influence interchain distance and packing and hence can affect the charge transfer between polymer chains. For instance, the optical and/or electrochemical properties of certain functionalized conjugated polymers can be strongly modified by varying temperature, pressure, solvent, electrolyte, etc. as a result of interaction involving amongst others the side chains. The first example of the transduction of physical information (temperature) into an optical signal in conjugated polymers is usually referred to as the thermochromic effect. This intriguing effect has been extensively studied and has led to the development of various thermochromic polythiophene¹⁻³, polysilane⁴⁻⁷, and polydiacetylene⁸⁻¹⁰ derivatives¹¹. Similarly, changes in the solvent can modify the conformation of the conjugated macromolecules and can result in solvatochromic effects. For instance, at room temperature, in a good solvent, poly(3-alkoxy-4-methyl-thiophene) exhibits an absorption maximum around 425 nm, which shifts to 545 nm upon addition of a poor solvent. This transition is very similar to that observed in the thermochromic experiments and therefore can also be related to a modification of the main-chain conformation. The change in the quality of the solvent seems to induce a sort of intramolecular and/or intermolecular collapse of the macromolecules with distinctly different optical properties¹¹. However in reality, conjugated polymer chains in solutions and films do not have an ideal structure because they tend to twist and coil. A suitable 'zero order' description of a conjugated polymer chain is that of a series of linked chromophores, each of which has a different extent of π -electron delocalization. The extent of conjugation of each conjugated segment is limited by larger twist and defects of the polymer backbone.¹² Environmental stimuli such as heat (thermochromism), solvent (solvatochromism), external pressure (piezochromism), light (photochromism) or the presence of ions (ionochromism) can trigger conformational changes and can modify the chain packing in films of conjugated polymers producing noticeable color changes as a sensory signal.¹³

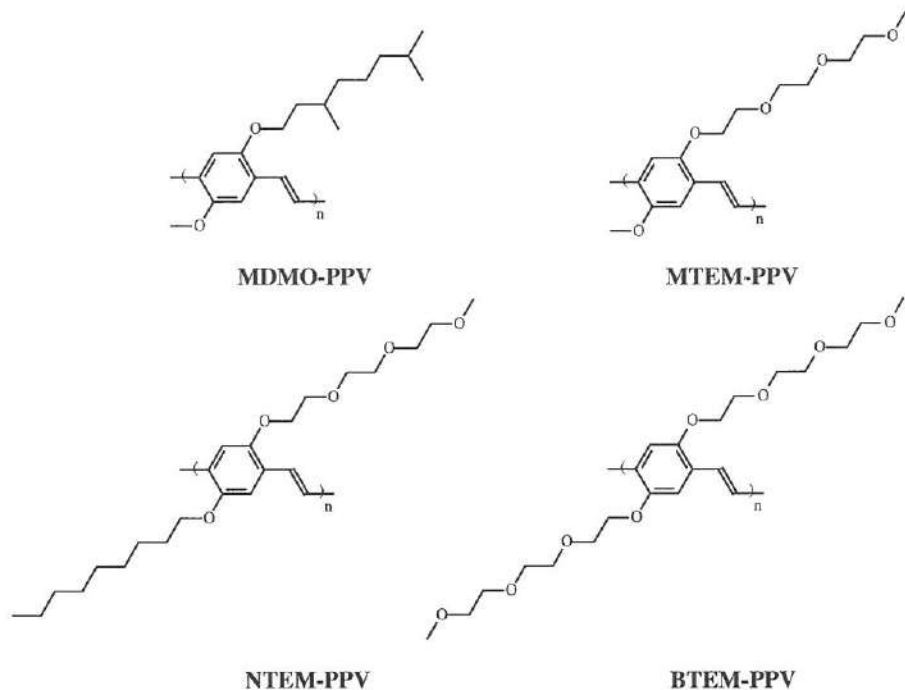


Figure 3-1: Molecular structures of the four studied 2,5-di-alkoxy substituted PPV derivatives.

This chapter focuses on the structural characterization of soluble 2,5-di-alkoxy substituted PPV polymers using ultraviolet-visible spectroscopy. These measurements lead to an understanding of the alignment and packing of the conjugated polymer main chains and side chains in thin films and solutions. Also the temperature dependences of absorption in PPV films were studied. For these studies a representative selection of four polymers with side chains with different polarities were employed, *i.e.* poly(2-methoxy-5-(3,7-dimethyloctyloxy)-*p*-phenylenevinylene) (MDMO-PPV), poly(2-methoxy-5-(triethoxymethoxy)-*p*-phenylenevinylene) (MTEM-PPV), poly(2,5-bis(tri-ethoxymethoxy)-*p*-phenylenevinylene) (BTEM-PPV) and poly(2-(*n*-nonyloxy)-5-(triethoxymethoxy)-*p*-phenylenevinylene) (NTEM-PPV) (figure 3-1). All polymers have been prepared

via the sulfinyl precursor route, which offers conjugated polymers with an enhanced purity as compared to alternative synthetic routes.¹⁴⁻¹⁶

The thermochromic, solvatochromic and ionochromic behavior of the four PPV derivatives have been studied in thin film and solution.

3.2 Experimental

Thin film UV-Vis-NIR spectroscopy was performed with a VARIAN CARY 500 UV-Vis-NIR spectrophotometer with a scan rate of 600 nm/min in a continuous run from 200 to 800 nm. For the experiments related to thin film thermochromism and ionochromism, a scan rate of 200 nm/min was used. The thin films were prepared by spin coating a CHCl_3 solution (5 mg/mL) of the respective polymer onto a quartz disc at 700 RPM. For the thin film temperature dependent UV-Vis measurements a Linkam TMS94/THMS600 controlled heating/freezing stage was employed, which was vertically positioned in the optical path of the UV-Vis-NIR spectrophotometer to allow spectra to be measured at a board range of temperatures and under nitrogen atmosphere. In the thin film thermochromism experiment, the samples were first heated to 100 °C (heating rate: 10 °C/min) and subsequently cooled (cooling rate: 5 °C/min). For measurements at sub-ambient temperatures, the stage was cooled with liquid N_2 . Spectra were taken at 20 °C temperature intervals. In the ionochromism experiments, the samples were heated from 20 to 170 °C, the soaking time was 10 min at each specific temperature, and the heating rate uses was about 10 °C/min during heating.

Solution UV-Vis absorption measurements were performed with either the previously mentioned CARY 500 UV-Vis-NIR spectrophotometer or a modular Ocean Optics spectrometer, consisting of a balanced DH2000 light source, a fiber optic arrangement for transmission measurements and a USB2000 spectrometer. The solution spectroscopy was performed in a diluted solution with a concentration

of approximately 0.1 mM based on the repeating unit of the polymer. For the temperature dependent solution measurements a transmission dip probe was employed which was fitted into a temperature controlled vessel. The polymer solutions were first heated to 60 °C with the help of a temperature controlled water bath and subsequently cooled down to room temperature. After this, the solutions were cooled down to -60 °C with CO₂/acetone. This temperature window was chosen in such a way that the boiling and freezing point of the corresponding solvents were not reached. Spectra were taken at 5 °C temperature intervals.

Differential scanning calorimetry (DSC) was performed using a DSC 2920 (TA instruments) under N₂ atmosphere. Polymer samples were sealed in aluminum pans and heated at a rate of 20 °C/min from -40 °C to 120 °C.

Fluorescence spectra were obtained with a Perkin Elmer LS-5B luminescence spectrometer. The respective polymer was dissolved in chloroform (5 mg/mL).

3.3 Thin Film UV-Vis-NIR Absorption Spectroscopy

As a reference point, the thin film UV-Vis absorption properties of four 2,5-substituted PPV derivatives (MDMO-PPV, MTEM-PPV, BTEM-PPV and NTEM-PPV) have been investigated in the absence of external stimuli. The position of the π - π^* absorption maximum of the polymer is a typical indication of the purity and defect levels of PPV-type polymers. The influence of the variation of the polarity of the side chains, *i.e.* oligo(oxyethylene) and alkyl substituents, on the optical properties has been investigated with spectroscopic measurements.

Thin films of MDMO-PPV, MTEM-PPV, BTEM-PPV and NTEM-PPV exhibit in the UV-Vis absorption spectrum a distinct absorption associated with the π - π^* transition of the polymer (figure 3-2). The exact position of this absorption

maximum is amongst others dependent on external stimuli, such as temperature, purity and defect level, *i.e.* the polymerization batch and the synthesis procedure utilized. Furthermore, the thin film morphology can play an important role. Keeping the above considerations in mind, for MDMO-PPV at ambient temperatures an absorption maximum is found in the range $\lambda_{\text{max}} = 508 - 520$ nm in a thin film. For polymers NTEM-PPV, MTEM-PPV and BTEM-PPV under the same conditions thin film absorption maxima were found in the range $\lambda_{\text{max}} = 508 - 524$ nm, $\lambda_{\text{max}} = 508 - 519$ nm and $\lambda_{\text{max}} = 509 - 518$ nm, respectively. For comparison in the literature, a typical absorption maximum of MDMO-PPV obtained from a sulfinyl precursor polymer is located at $\lambda_{\text{max}} = 514$ nm¹⁷, which is within the previously mentioned range. In table 3-1, the thin film absorption maxima of the π - π^* transition at ambient temperatures of the four polymers are given. For the measurements presented throughout this chapter the same polymerization batches have been used.

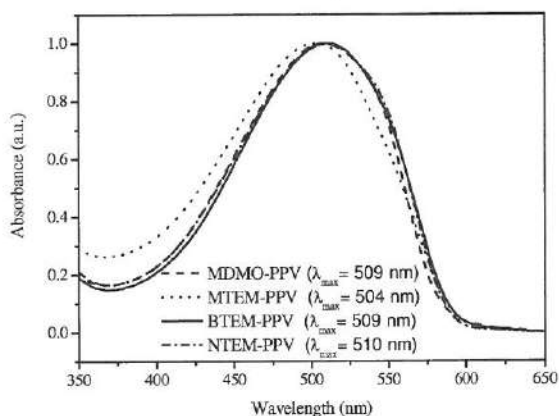


Figure 3-2: Typical UV-Vis absorption spectra of MDMO-PPV, MTEM-PPV, BTEM-PPV and NTEM-PPV in a thin film. The spectra have been normalized.

The exact position of the π - π^* absorption maximum in the UV-Vis absorption spectrum is with a measure for the effective conjugation length of a conjugated polymer. In the literature, the effective conjugation length of a PPV-type

conjugated polymer is estimated at 8 repeating units.¹⁸⁻²⁰ However, this may well be somewhat longer. During the synthesis of the different PPV derivatives, different undesired defects are incorporated in the polymer backbone, which are a result of for example, non-fully eliminated sections and side reactions. When there is more than one defect in *circa* 8 repeating units of a polymer, *i.e.* the effective conjugation length is smaller than *circa* 8 repeating units, a blue shift of the π - π^* absorption maximum is observed in the UV-Vis absorption spectrum. When the defect level of the polymer is low, (significantly more than 8 repeating units between individual defects), the π - π^* absorption maximum in the UV-Vis absorption spectrum does not change. Due to this fact, it is important to synthesize PPV derivatives with a low defect level. To avoid this problem, the PPV derivatives used in this work are synthesized *via* the sulfinyl precursor route, which gives polymers with a low intrinsic chemical defect level.¹⁶

	λ_{\max} (nm)	Optical
	Thin film	band gap (eV)
MDMO-PPV	509	2.12
MTEM-PPV	504	2.10
BTEM-PPV	509	2.10
NTEM-PPV	510	2.12

Table 3-1: The wavelengths λ_{\max} π - π^* of a thin film and the optical band gap of different 2,5-di-alkoxy-PPV derivatives

As mentioned in chapter 2, the optical band gap can be calculated using the UV-Vis absorption spectrum of a polymer film at ambient temperature. The tangent on the low energetic side of the absorption spectrum can be drawn. The intersection of this tangent and the abscissa gives a value for the band gap. In table 3-1, the optical band gap values of the four studied PPV derivatives are given. The optical band gaps of the four polymers are virtually identical. This indicates that the introduction of polar substituents in MTEM-PPV, BTEM-PPV and NTEM-PPV,

does not have a substantial impact on the optical properties of the polymers, as compared to MDMO-PPV. Small differences in the absorption maxima are partially associated with small differences in the temperature dependent conformational flexibility (*vide infra*).

It is noteworthy that the peak in the thin film absorption spectrum is broad. This is due to chain packing effects in the polymer film. While the physical properties of isolated polymers are primarily controlled by their chemical structure, these properties are drastically altered in the solid state due to electronic coupling between polymer chains as determined by their interpolymer packing and conformation¹³.

3.4 Thin Film Thermochromism of PPV-Type Polymers

Thermochromism is a unique property of a variety of conjugated polymers, which has attracted considerable attention, both from a fundamental point of view, as well as for applications such as heat sensors and indicators^{2, 3, 21-25}. Thermochromism can be defined as a change in the optical absorption spectrum, *viz.* the color, induced by a change in temperature. Thermochromism can be readily studied with temperature dependent UV-Vis absorption spectroscopy. Here, we compare the thermochromic properties of the previously mentioned four 2,5-di-alkoxy substituted PPV derivatives with various side chains, *i.e.* MTEM-PPV, BTEM-PPV, NTEM-PPV and MDMO-PPV (Figure 3-1).

The detailed study of the thermochromic properties of the above four polymers yields valuable information on the backbone flexibility and segmental motions present in these polymers at various temperatures. Whereas Differential Scanning Calorimetry (DSC) is a powerful technique for studying many polymer characteristics such as the glass transition temperatures T_g , reaction kinetics and

melting behavior,^{21, 26, 27} DSC thermograms of PPV-type polymers often do not display clear transitions even after repeated scans. Since the T_g is an essential parameter for the processing and application of conjugated polymers, alternative measurement procedures are desirable. Here we demonstrate for the first time that a careful analysis of the thermochromic behavior in PPV-type polymers gives direct information on the chain dynamics and hence the T_g. Furthermore, the formation of ground-state aggregates below the T_g is demonstrated.

3.4.1 Temperature Dependent Thin Film UV-Vis Absorption Spectra of PPV-type Polymers

✓ *Thermochromic effect in 2,5-di-alkoxy substituted PPV type polymers*

Upon heating a thin film of the conjugated polymer MDMO-PPV a distinct shift in the absorption maximum λ_{max} associated with the π - π^* transition is observed. The λ_{max} of MDMO-PPV measured in film at ambient temperature is 509 nm. Upon heating λ_{max} exhibits a hypsochromic shift of which the magnitude is dependent on the temperature. For example, when MDMO-PPV is heated to 100°C, λ_{max} shifts from 509 nm to 498 nm. After cooling the conjugated polymer back to ambient temperature, the conjugated system is fully recovered as reflected in the reoccurrence of a λ_{max} of 509 nm. In a full heating-cooling experiment the thermochromism can be visualized (Figure 3-3). In the temperature window -100 °C to 100 °C the λ_{max} of MDMO-PPV shifts from 518 nm to 498 nm, *i.e.* a reversible shift of 20 nm is observed. The thermochromism of MDMO-PPV has previously been reported and has been attributed to a trans-gauche transition of the side chains.²¹ This interpretation follows earlier observations for conjugated polymers such as polythiophenes and polysilanes, for which it has been demonstrated that side chain phase transitions play an essential role.⁷ These transitions often result in distinct, sometimes even abrupt, thermochromic shifts.

To assess whether a side chain transition is indeed responsible for the observed thermochromic effects in PPV-type polymers, the three additional polymers were studied.

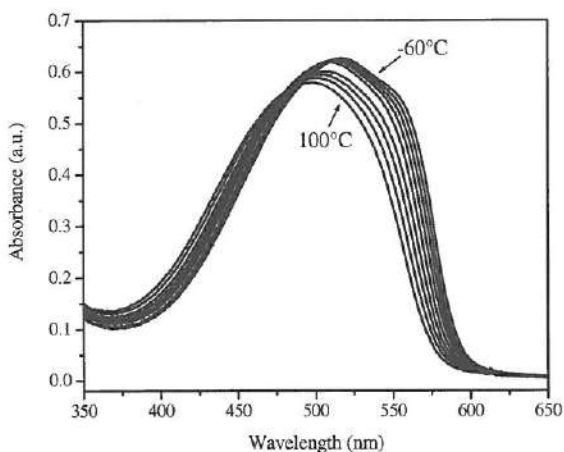


Figure 3-3: The temperature dependent UV-Vis absorption spectra of a thin film of MDMO-PPV. The starting temperature is 100 °C after which the sample is cooled down to -60 °C (cooling rate 5 °C/min; measurement intervals 20 °C)

The three polymers studied, MTEM-PPV, BTEM-PPV and NTEM-PPV contain polar oligo(oxyethylene) side chains in various arrangements. The absorption maximum of BTEM-PPV measured in a thin film at ambient temperature is 509 nm. After heating to 100°C, the λ_{max} is shifted to 495 nm (Figure 3-4). For the other two polymers similar observations can be made (Figures 3-5 and 3-6): MTEM-PPV: ambient temperature $\lambda_{\text{max}} = 504$ nm, 100°C $\lambda_{\text{max}} = 493$ nm; NTEM-PPV: ambient temperature $\lambda_{\text{max}} = 510$ nm, 100°C $\lambda_{\text{max}} = 496$ nm. Remarkably, for the above three polymers a similar behavior is observed, as was found for MDMO-PPV. Since no side chain order-disorder phenomena are expected for oligo(oxyethylene) substituents, the observed thermochromic behavior of PPV-type polymers has to have a different origin than that of, for example, polythiophenes and polysilanes.

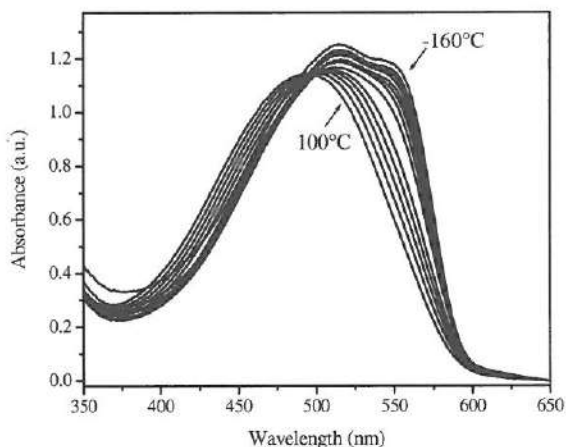


Figure 3-4: The temperature dependent UV-Vis absorption spectra of a thin film of BTEM-PPV. The starting temperature is 100 °C after which the sample is cooled down to -160 °C (cooling rate 5 °C/min; measurement intervals 20 °C).

The observed thermochromic shifts indicate that by heating PPV-type polymers, the effective conjugation length decreases. Since the thermochromic behavior is similar for all four polymers, apparently this process is related to the conjugated backbone of the polymers instead of the side chains. It is proposed that upon heating the polymers, the segmental motions present in the polymers increase in number and amplitude. As a result, also the average torsion angle of the backbone increases significantly and concomitantly the effective conjugation length decreases, as reflected in the hypsochromic shift of λ_{max} . This process is fully reversible, *viz.* by cooling down the polymer, the segmental motions in the polymer chains decrease and the effective conjugation length increases again, thus accounting for the observed bathochromic shift upon cooling. The effect of the temperature on the torsion angle was previously predicted using molecular dynamics (MD) simulations for PPV oligomers²⁸.

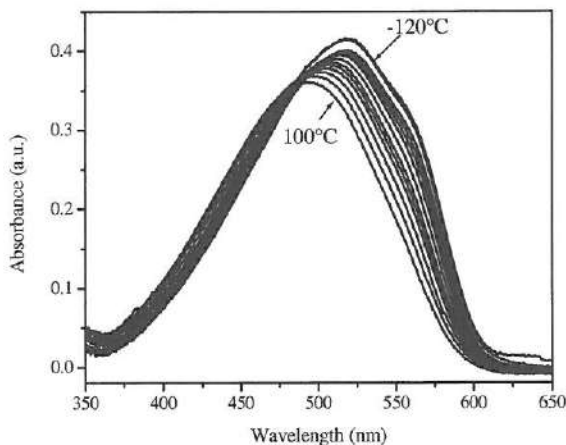


Figure 3-5: The temperature dependent UV-Vis absorption spectra of a thin film of MTEM-PPV. The starting temperature is 100 °C after which the sample is cooled down to -120 °C (cooling rate 5 °C/min; measurement intervals 20 °C).

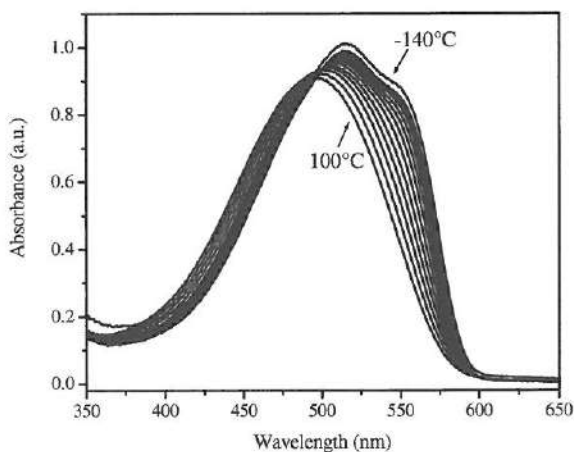


Figure 3-6: The temperature dependent UV-Vis absorption spectra of a thin film of NTEM-PPV. The starting temperature is 100 °C after which the sample is cooled down to -140 °C (cooling rate 5 °C/min; measurement intervals 20 °C)

✓ Determination of Glass Transition Temperatures

When the actual values of the energy of the π - π^* transition of the four polymers are plotted as a function of temperature, a remarkable observation can be made

(Figure 3-7). In these graphs, two linear fits with different slopes are observed. For MDMO-PPV the intersection of these two linear fits is found at 68 °C (Figure 7A; $\lambda_{\text{max}} = 505 \text{ nm}$). This temperature is in excellent agreement with the previously reported glass transition temperature (T_g) of MDMO-PPV and similar MEH-PPV (reported T_g values range from 50 °C to 75 °C).^{15, 26, 27, 29} Generally, Differential Scanning Calorimetry (DSC) is a powerful technique for studying the thermal behavior of polymeric materials. However, for PPV-type polymers such as MDMO-PPV not always a clear transition is visible in the DSC thermograms (figure 3-8), even after repeated scans, hampering an accurate determination of the T_g with this method.^{26, 27} Possibly, the presence or absence of a T_g in the DSC thermogram of MDMO-PPV is a result of small differences in, for example, morphology, purity, molecular weight and polydispersity of the employed polymers. Hence, an alternative method to obtain T_g values is of considerable interest. The presented method based on thermochromism is straightforward and predicts the T_g with considerable accuracy. This new method to obtain T_g values originates from the fact that above the T_g , the polymers have sufficient conformational flexibility to exhibit the thermochromic effect (*vide supra*), whereas below the T_g this is not the case. In this context it is noteworthy that for cyano-substituted poly(2,5-dialkoxy-*p*-phenylenes vinylene)s the thermochromic properties have been reported as well.³⁰ These polymers contain a cyano group at the vinylic double bond, which leads to a lower coplanar character.³¹ Although for these polymers also some correlations between the optical properties and the phase changes can be observed, no distinct transitions are observed in the thermochromism. This is likely either the result of their distorted character, or may also originate from their comparatively low molecular weight or insufficient purity.

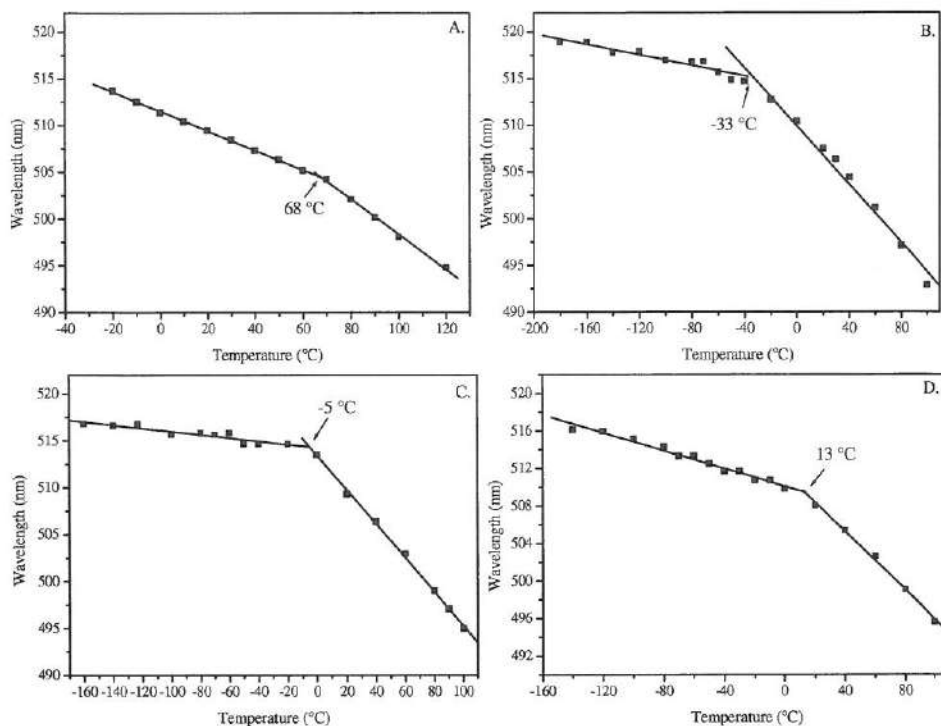


Figure 3-7: The maximum wavelength as a function of temperature of a thin film of

A. MDMO-PPV. The intersection of the two linear fits is 68 °C.

B. MTEM-PPV. The intersection of the two linear fits is -33 °C.

C. BTEM-PPV. The intersection of the two linear fits is -5 °C.

D. NTEM-PPV. The intersection of the two linear fits is 13 °C.

Whereas for MDMO-PPV a literature value for the T_g is available, our repeated conventional DSC measurements on MTEM-PPV, BTEM-PPV and NTEM-PPV did not result in the observation of a distinct T_g . Hence, the thermochromism was studied to obtain an estimate of the T_g of these polymers. The intersection of the two linear fits of BTEM-PPV (Figure 3-7C) was found at -5 °C ($\lambda_{\max} = 515$ nm), for NTEM-PPV (Figure 3-7D) at 13 °C ($\lambda_{\max} = 509$ nm) and for MTEM-PPV (Figure 3-7B) at -33 °C ($\lambda_{\max} = 515$ nm). Hence, using the thermochromism, the T_g values of these three polymers have now been accurately established. It is noteworthy that the slopes of the linear fits at temperature higher than the glass

transition temperature for all four polymers are comparable, further confirming a similar origin of the observed thermochromic effects.

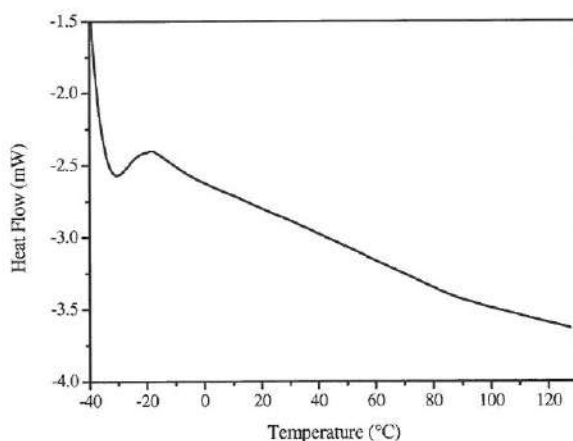


Figure 3-8: DSC of MDMO-PPV with a heating rate of 20°C/min from ambient temperature to 135°C.

The T_g values of the various PPV-type polymers are different and as expected dependent on the side chains (Table 3-2). Polymers with only oligo(oxyethylene) side chains, *i.e.* MTEM-PPV and BTEM-PPV have lower T_g values as compared to (partially) alkyl substituted polymers, *i.e.* MDMO-PPV and NTEM-PPV, reflecting the increased flexibility of these materials. Similarly, the T_g of the more flexible mono oligo(oxyethylene) substituted MTEM-PPV is lower than that of the disubstituted counterpart BTEM-PPV.

Polymers	T_g
MDMO-PPV	68 °C
NTEM-PPV	13 °C
BTEM-PPV	-5 °C
MTEM-PPV	-33 °C

Table 3-2: The glass transition temperatures (T_g) of the PPV derivatives determined via temperature dependent UV-Vis measurements

✓ *Ground state aggregation phenomena*

Close scrutiny of the temperature dependent UV-Vis absorption spectra reveals that upon cooling the shape of the UV-Vis absorption spectrum changes significantly. As a result of these changes, the apparent absorption maximum λ_{\max} of the four PPV-polymers shifts during the cooling process at temperatures lower than Tg. However, this shift does not represent thermochromic effects but the formation of an additional shoulder in the UV-Vis absorption spectrum, which causes an error when λ_{\max} is determined without deconvolution. The presence of this shoulder at low temperatures was observed for all four polymers. Remarkably, after full deconvolution of the UV-Vis absorption spectra of the four PPV-polymers below Tg, virtually identical peak maxima were observed for the π - π^* transition when the margin of error is taking into account ($\lambda_{\max} \pi$ - $\pi^* = 515$ - 518 nm; Table 3-3). Hence deconvolution unequivocally demonstrates that λ_{\max} of the π - π^* transition at temperatures lower than Tg is independent of the actual temperature and the side chains of the polymers. Apparently, a λ_{\max} of *circa* 516 nm for the π - π^* transition is a fundamental characteristic of planar 2,5 di-alkoxy substituted PPV-type chromophores. The observed change in shape of the UV-Vis absorption spectrum is a result of a second absorption at $\lambda_{\max} = \text{circa } 560$ nm, which manifests itself initially as a weak shoulder and increases in intensity at temperatures significantly below Tg.

The change in the shape of the UV-Vis spectrum of PPV-type polymers upon cooling a thin film has been observed previously and has been discussed in significant detail in literature,³²⁻³⁴ although to our best knowledge no direct connection with the relationship between the thermochromism and the Tg has been made. Also for other conjugated polymers similar phenomena have been extensively studied and the presence of red-shifted absorption bands has been interpreted both in terms of backbone planarization and ground-state aggregation.^{13, 25, 29} The occurrence of planarization indeed would result in enhanced

intramolecular conjugation and exciton delocalization over more repeating units of the polymer chain, made possible by the freezing out of molecular torsions and other low-frequency vibrational modes that distort the polymer from planarity and disrupt conjugation. However, since the $\pi - \pi^*$ transition below T_g is independent of temperature and the type of side chains, in our opinion at the T_g already a fully planar structure of the conjugated backbone has been achieved. Hence, the additional shoulder developing below T_g is a result of intermolecular ground-state aggregation phenomena, which become possible as a result of the planarization of the conjugated backbone which occurs at the T_g .

Polymers	$\lambda_{\max} \pi-\pi^*$	λ_{\max} aggregates
MDMO-PPV	518 nm	564 nm
NTEM-PPV	515 nm	557 nm
BTEM-PPV	515 nm	558 nm
MTEM-PPV	516 nm	565 nm

Table 3-3: The wavelengths $\lambda_{\max} \pi-\pi^*$ as well as the additional absorption shoulder associated with the ground-state aggregation obtained after deconvolution of the UV-Vis absorption spectra of the four PPV derivatives at temperatures below T_g

3.4.2 Temperature Dependent Thin Film UV-Vis Absorption Spectra of PTV-type Polymers

In the previous section, a new method has been developed, which allows for a direct determination of previously inaccessible T_g values from the temperature dependent UV-Vis absorption spectra. In this section, it is demonstrated that the use of this new method is not limited to PPV-type polymers but can also be utilized for other types of conjugated polymers. A prerequisite however is the fact that their thermochromism must be associated with main chain planarization processes instead of order-disorder phenomena of the side chains. As a representative

example of the thermochromic effects in different conjugated polymers, two PTV-type conjugated polymers have been studied with temperature dependent UV-Vis absorption spectroscopy. For these studies non substituted PTV (poly[2,5-thienylene vinylene]) and H-PTV (poly[3-hexyl-2,5-thienylene vinylene]) were selected (figure 3-9).



Figure 3-9: Molecular structures of the two studied PTV derivatives.

✓ *Thermochromic effect of PTV*

Figure 3-10A shows the temperature dependent UV-Vis absorption spectra of a thin film of PTV. The sample is heated until 250 °C and cooled down until -63 °C. The absorption maximum (λ_{max}) of PTV measured in a thin film at ambient temperatures is 538 nm. Upon heating the polymer film, the effective conjugation length decreases and the λ_{max} exhibits a hypsochromic shift to 528 nm at 250 °C. After cooling the conjugated polymer back to ambient temperatures, the conjugated chain is fully recovered and the λ_{max} is 538 nm. Subsequent cooling of the polymer film to -63 °C results in a bathochromic shift of λ_{max} to 560 nm. A similar behavior is also observed for H-PTV polymer (figure 3-10B). For example, in the temperature window 20 °C to 250 °C, the λ_{max} of this polymer shifts from 570 nm to 556 nm. Apparently also for PTV-derivatives by heating the conjugated polymer, the mobility of the polymer chains increases, which results in an increase of the average torsion angle. Hence, the effective conjugation length decreases, which is reflected in a blue shift of the UV-Vis absorption spectrum at elevated temperatures. Similar as observed for PPV-derivatives, this process is reversible. This implies that by cooling down the polymer, the mobility of the polymer chains decreases and the effective conjugation length increases, *i.e.* a red shift is observed

upon lowering the temperature. The fact that the thermochromic effect is also observed for unsubstituted PTV, further supports our finding that this behavior in PPV and PTV-type polymers is related to the planarization of the conjugated backbone of the polymers instead of order-disorder phenomena of the side chains.

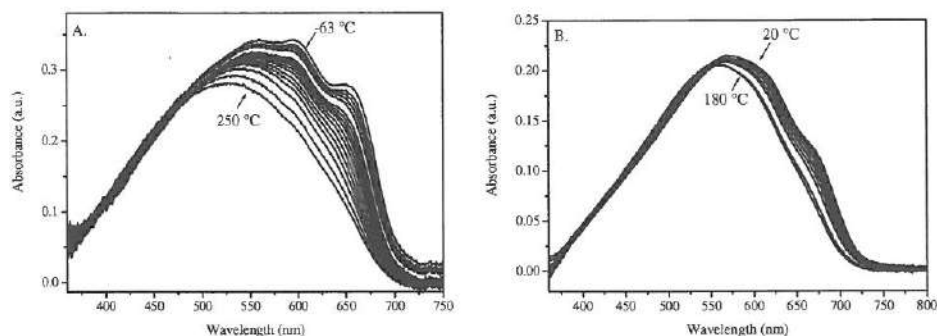


Figure 3-10: The temperature dependent UV-Vis absorption spectra of thin films of PTV and H-PTV.

✓ Determination of the Glass Transition Temperatures

The actual values of the absorption maxima of the π - π^* transition of PTV and H-PTV have been also plotted as a function of temperature. As mentioned for PPV derivatives, two linear fits with different slopes are observed. For PTV, the intersection of these two linear fits is found at 78 °C (figure 3-11A) and for H-PTV 86 °C (figure 3-11B). Also in this case it is proposed that this temperature is the glass transition temperature of the respective polymers. This is further supported by Differential Scanning Calorimetry. In contrast to PPV-type polymers, for PTV a clear glass transition is visible in the DSC thermograms (figure 3-12), *i.e.* T_g (DSC) is 69 °C³⁵. This value is in the same order of magnitude as the T_g determined with UV-Vis spectroscopy, especially in view of the fact that for both experiments different heating/cooling rates are employed.

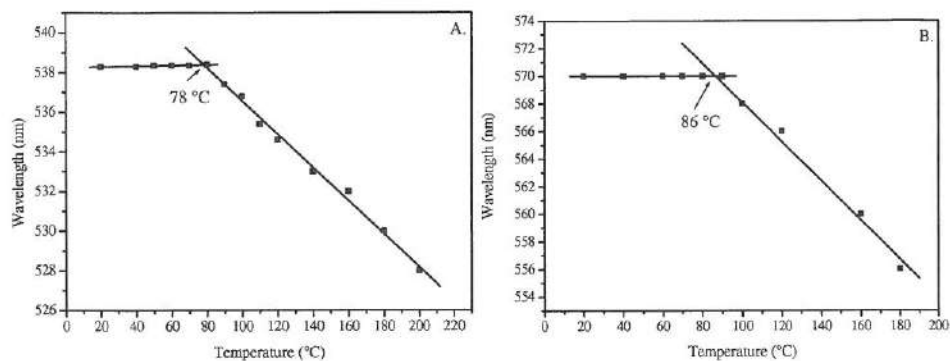


Figure 3-11: The maximum wavelength as a function of temperature of a thin film of

A. PTV. The intersection of the two linear fits is 78 °C.

B. H-PTV. The intersection of the two linear fits is 86 °C.

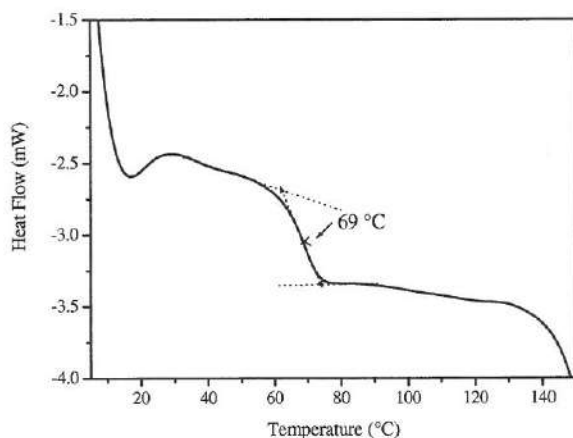


Figure 3-12: DSC of PTV (heating rate 20 °C/min).

The difference between the T_g of PTV and H-PTV is 8 °C. This is surprisingly small, since it is anticipated that the conformational flexibility of H-PTV is smaller due to the incorporation of a hexyl side chain attached onto the thiophene ring. Apparently, for the PTV derivatives addition of one side chain does not have significant impact on the conformation flexibility. It would be of interest to establish whether this is also the case for di-substituted PTV derivatives. However, these were unfortunately unavailable for these studies.

As shown in the UV-Vis absorption spectra of PTV and H-PTV, also for these polymers a formation of a shoulder is observed upon cooling. This shoulder is similar to those observed for the PPV derivatives. Hence, also for these polymers ground-state aggregation phenomena are observed below the T_g .

3.5 Thin Film Ionochromism of PPV-type Polymers

Environmental stimuli like the presence of ions can trigger conformational changes in conjugated polymers. This can produce a change in the absorption maxima of the π - π^* transition of the polymer. It is anticipated that conjugated polymers with side chains capable of complexing ions, notable changes in the temperature dependent conjugated backbone structure can be observed. It is even possible that the polymers undergo conformational changes upon coordination with ions.

To study the influence of the complexation of cations on the polymer properties, several ion containing polymer films were prepared. These films were prepared from CHCl_3 solutions of the conjugated polymer with the respective ions. The first solution is a polymer solution with one equivalent TBAPF_6 (based on the repeating unit of the polymer) added to the solution. The large TBA^+ cation was chosen because this cation was used in the electrolyte solution for cyclic voltammetry (chapter 2). It was observed that this cation was associated with the reversible n-doping peak of the polymers with polar substituents. The second prepared solution is a polymer solution with one equivalent LiClO_4 . In this experiment, Li^+ was used to investigate the scope of the ionochromism of the PPV derivatives, since the Li^+ ion is much smaller than the TBA^+ cation. For reference also a polymer solution was used without any ions present. The thin films for the UV-Vis absorption measurements were prepared from the above three solutions by spin-coating them on clean ITO glass substrates at 700 RPM.

As mentioned before, a distinct absorption associated with the π - π^* transition of the polymer in a thin film is observed in the UV-Vis absorption spectrum of PPV-type polymers. As a result of the thermochromic effect the exact position of this absorption maximum λ_{max} is dependent on the temperature. A similar thermochromic behavior is also observed for the two conjugated polymers which contain either TBAPF₆ or LiClO₄. This means that the added ions do not influence the occurrence of a thermochromic effect of a conjugated polymer. However, the exact position of λ_{max} is modified by the presence of ions. When the actual values of λ_{max} of the four PPV derivatives of the relevant films are plotted as a function of temperature, the effect of the addition of ions is more clearly visible (Figure 3-13).

For thin films of MDMO-PPV, with and without ions present, it is found that the values of λ_{max} as a function of the temperature are within the margin of error of the UV-Vis spectrophotometer. This indicates that the additional ions have no influence on the position of the absorption maxima of the π - π^* transition. This is not surprising since the structure of MDMO-PPV contains only a methyl and a longer branched alkyl side chain, which are not capable of forming any complexes with the cation Li⁺ or TBA⁺. As discussed in Chapter 2, this is the main reason that no clear n-doping phenomena are visible upon reducing thin films of MDMO-PPV in an electrochemical experiment.

In marked contrast to this the presence of the different ions does have an impact on the λ_{max} values of MTEM-PPV, NTEM-PPV and BTEM-PPV (Figure 3-13). The positions of the absorption maxima change when an ionic compound is incorporated in the polymer films. For BTEM-PPV upon addition of TBA⁺ ions, a small shift of λ_{max} from 503 nm to 508 nm can be observed at 60 °C. In contrast, when Li⁺ ions are added to BTEM-PPV, a small shift of λ_{max} to shorter wavelength, *i.e.* from 503 nm to 494 nm can be observed at 60 °C. The effect of the ions on the λ_{max} is smaller at higher temperatures. This is due to the increased flexibility of the polymer backbone at higher temperatures. Due to the additional rotational freedom

at these temperatures, it becomes increasingly difficult for the side chains to form a complex with the cation. This effect is also known for other conjugated polymers containing linear or cyclic oligo(ethylene oxide) based molecular recognition sites^{1, 36, 37}.

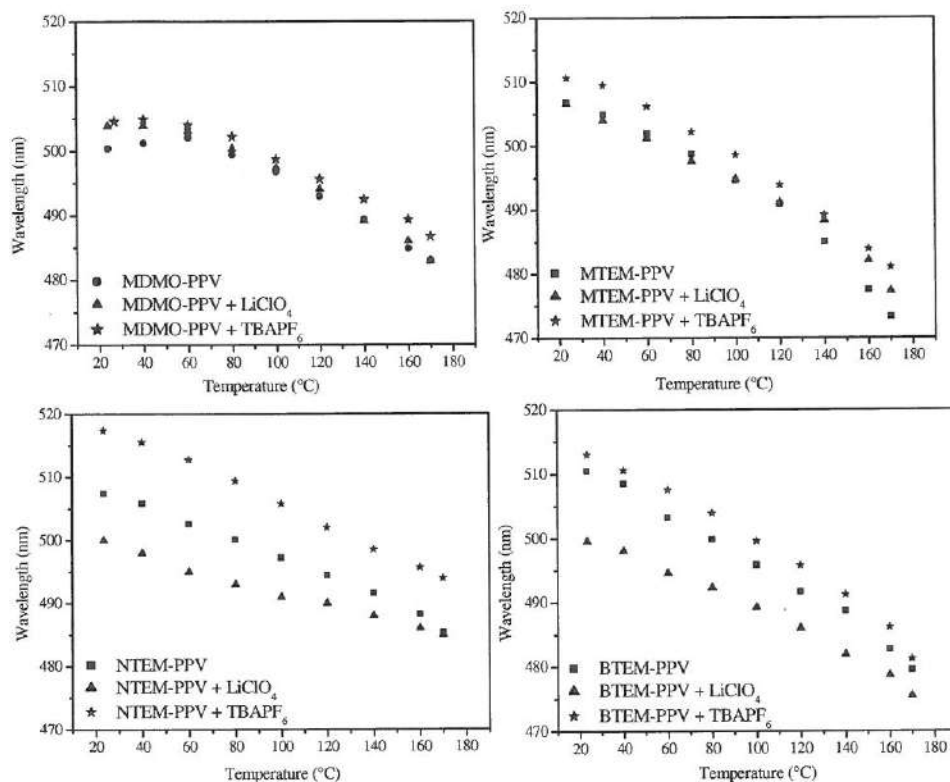


Figure 3-13: The temperature dependent UV-Vis absorption spectra of thin films of different PPV-type polymers containing different types of ions.

NTEM-PPV, MTEM-PPV and BTEM-PPV are PPV polymers with one or two oligo(oxyethylene) chains. The presence of these chains results in the occurrence of ion-polymer interactions. The most striking difference between the two added cations is their radius.

Li^+ is a rather small cation. Upon addition of Li^+ ions, λ_{max} shifts to shorter wavelength. This shift is the result of the formation of a complex between the oligo(oxyethylene) chains and the Li^+ ions (figure 3-14). The change of λ_{max} in presence of the electrolyte is the highest with BTEM-PPV. Since this polymer has two oligo(oxyethylene) side chains, more complexation sites are available.³⁷ Furthermore, it can be anticipated that both complexation within a single side chain and between two neighboring side chains will induce conformational changes of the backbone. The hypsochromic shift of λ_{max} upon addition of Li^+ reflects the small reduction in the effective conjugation length due to these conformational changes. Hence, it is not surprising that for MTEM-PPV, which is significantly less sterically crowded, due to the presence of a methoxy substituent, virtually no effect of the addition of Li^+ is observed.

In contrast to Li^+ , TBA^+ (tetrabutylammonium⁺) is a much larger cation. It can be anticipated that this cation will exhibit different complexation characteristics with the oligo(oxyethylene) chain due to steric constraints. Upon addition of TBA^+ ions, λ_{max} shifts to longer wavelength. Apparently, the introduction of these larger ions results in additional ordering phenomena, which lead to a small increase of the effective conjugation length of the polymers (figure 3-15). One can speculate that these ordering phenomena amongst others comprise the formation of sandwich-like structures consisting of alternating layers of ions and planar conjugated polymers with oligo(oxyethylene) side chains.

In this context it is noteworthy that already in chapter 2, it was explained that it is possible to form a complex between the oligo(oxyethylene) side chains and TBA^+ ions during an electrochemical reduction process. The formation of such complexes can rapidly occur in an existing polymer film because of the fact that upon reduction negative charges are placed onto the conjugated polymers backbone. These attractive ionic forces will support the formation of complexes with cations.

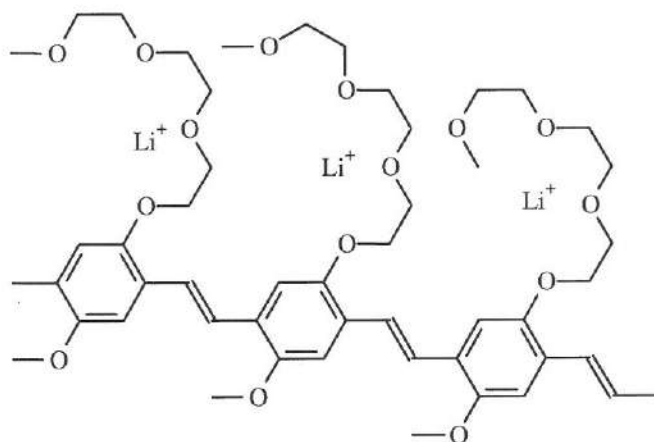


Figure 3-14: Complexation of Li^+ cation with the oligo(oxyethylene) side chains of MTEM-PPV, NTEM-PPV and BTEM-PPV

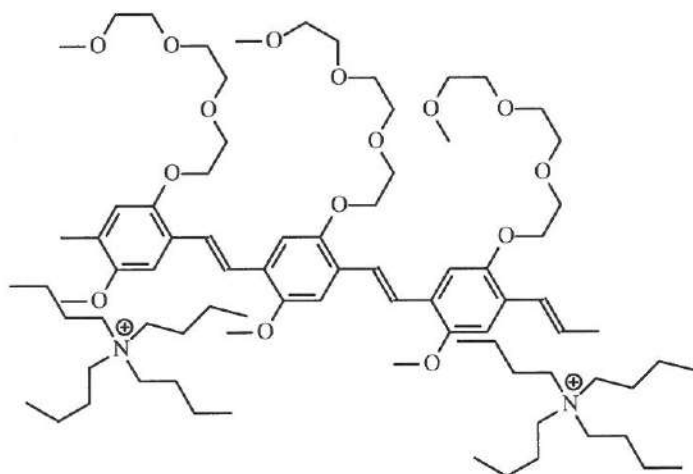


Figure 3-15: No complexation of TBA^+ cation with the oligo(oxyethylene) side chains of MTEM-PPV, NTEM-PPV and BTEM-PPV

In figure 3-16, the effect of the concentration of TBAPF_6 is shown for one of the polymers, *i.e.* BTEM-PPV. This experiment demonstrates that λ_{max} exhibits further bathochromic shifts when the concentration of the electrolyte is increased. Apparently the effective conjugation length increases upon addition of additional

TBA⁺ ions. It can be envisioned that the addition of ions to this type of polymers will be an effective method to obtain highly ordered films. Such order is important for applications in which high charge carrier mobility is desirable.

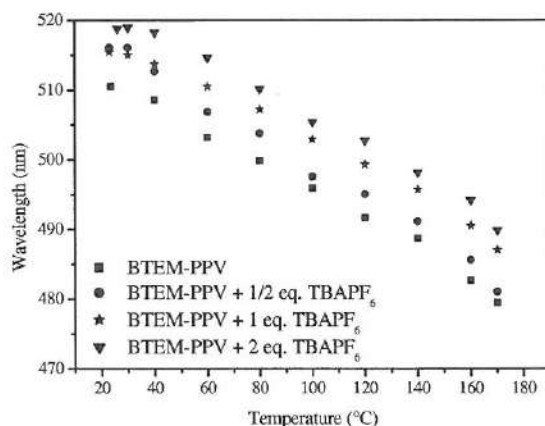


Figure 3-16: The temperature dependent UV-Vis absorption spectra of thin films of BTEM-PPV containing different concentrations of ions.

3.6 Solution UV-Vis-NIR Absorption Spectroscopy

From the selected group of four PPV-type polymers, which form the basis of this chapter, *i.e.* MTEM-PPV, BTEM-PPV, NTEM-PPV and MDMO-PPV, it is evident that by a careful choice of the substituents the polarity of the polymers can be altered without significantly affecting the thin film optical properties, which are associated with the conjugated backbone properties. In marked contrast however, this polarity change of the conjugated polymers does have a direct impact on the solubility and the solution optical properties of these polymers. In this section, the four PPV derivatives are dissolved in a wide range of solvents and the resulting UV-Vis-NIR absorption spectrum have been examined. This will allow for an assessment of the influence of the solvents on the solution properties of these polymers.

Solvent	Polarity (E _T N) ³⁸	MDMO- PPV	MTEM- PPV	BTEM- PPV	NTEM- PPV
<i>n</i> -Hexane	0.009	--	--	--	--
Toluene	0.099	±	±	±	±
Dioxane	0.164	±	+	+	±
Chlorobenzene	0.188	+	+	+	+
Tetrahydrofuran	0.207	+	+	+	±
Chloroform	0.259	+	+	+	+
Acetone	0.355	--	-	±	--
Acetonitrile	0.460	--	-	±	-
Ethanol	0.654	--	-	-	--

Table 3-4: Overview of the solubility of MDMO-PPV, MTEM-PPV, BTEM-PPV and NTEM-PPV in selected solvents

(+ completely soluble, no aggregation; ± completely soluble, aggregation observed with UV-Vis spectroscopy; - partially insoluble; -- fully insoluble).

The solution spectroscopy is performed in a diluted solution with a concentration of approximately 0.1 mM based on the repeating unit of the polymer. The solvents used in this work are *n*-hexane, toluene, dioxane, chlorobenzene, tetrahydrofuran, chloroform, acetone, acetonitrile and ethanol, arranged in order of polarity, *i.e.* E_TN values³⁸ (table 3-4).

It appears that none of the polymers are soluble in *n*-hexane, the most apolar solvent tested (Table 3-4). By using somewhat more polar solvents such as toluene and chlorobenzene, an orange or orange-red solution is obtained. At the other side of the polarity scale, all polymers are soluble in CHCl₃, but only BTEM-PPV is soluble in, for example, acetonitrile (Table 3-4). The solubility studies confirm that, as expected, the introduction of polar substituents can lead to a better solubility of the PPV-type polymers in more polar solvents

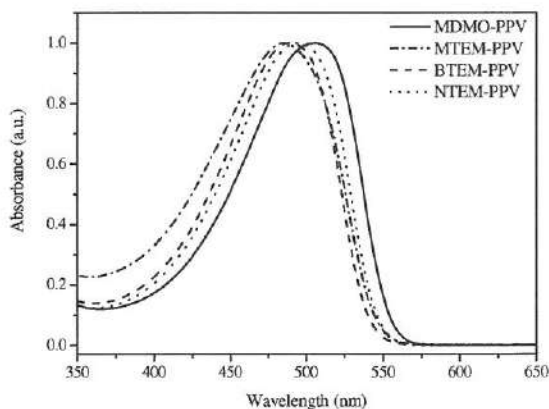


Figure 3-17: UV-Vis absorption spectrum of MDMO-PPV, MTEM-PPV, BTEM-PPV and NTEM-PPV in chloroform solution.

MDMO-PPV, MTEM-PPV, BTEM-PPV and NTEM-PPV exhibit in the UV-Vis absorption spectrum a distinct absorption associated with the π - π^* transition of the polymer (Figure 3-17). Whereas the optical properties of thin films of the four functionalized PPV derivatives are very similar, for the solution UV-Vis absorption spectra a different observation can be made. This is the result of the expected markedly different polarities of the individual polymers. For example, for a typical solvent used in the manufacturing of organic photovoltaic devices ³⁹ in which the PPV polymers readily dissolve, *i.e.* chlorobenzene, the solution absorption maxima range from $\lambda_{\text{max}} = 493$ nm for MTEM-PPV to 512 nm for MDMO-PPV (Table 3-5). Since the solution λ_{max} is generally less sensitive to external factors, as compared to the thin film λ_{max} , this large difference apparently is a result of solvatochromic effects of the PPV-type polymers.

Solvent	λ_{\max} (nm)	λ_{\max} (nm)	λ_{\max} (nm)	λ_{\max} (nm)
	MDMO-PPV	MTEM-PPV	BTEM-PPV	NTEM-PPV
Toluene	509	492	496	505
Dioxane	512	486	494	512
Chlorobenzene	512	493	498	502
Tetrahydrofuran	506	487	498	500
Chloroform	506	485	489	495

Table 3-5: Overview of solution UV-Vis absorption maxima λ_{\max} for MDMO-PPV, MTEM-PPV, BTEM-PPV and NTEM-PPV in selected solvents

A more careful analysis of the UV-Vis absorption characteristics of the solutions reveals that whereas in common solvents, such as chloroform and chlorobenzene, for all polymers a distinct transition is found in the UV-Vis absorption spectrum, at the respective edges of the polarity scale a more complex behavior is observed. Although the polymers fully dissolve, for these solvents in the UV-Vis absorption spectrum an additional absorption is found as a shoulder around $\lambda_{\max} = 560$ nm. This shoulder develops either instantaneously or over the course of a night, dependent on the particular solvent/polymer combination. The presence of a shoulder in certain solvents can be exemplified for polymer BTEM-PPV (Figure 3-18). For this polymer in toluene (at the apolar side of the polarity scale) and for acetone and acetonitrile (at the polar side of the polarity scale), such a shoulder is observed, whereas in intermediate solvents only the π - π^* transition is observed. In figure 3-19, a picture is shown of the different polymer solutions. When a shoulder is observed in the UV-Vis absorption spectra of BTEM-PPV, the color of the solution is distinctly red, whereas for solutions with only the regular transition a yellow-orange color is observed.

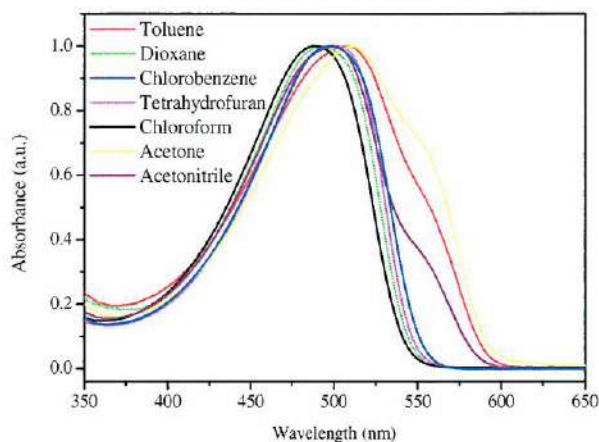


Figure 3-18: UV-Vis absorption spectra of BTEM-PPV in various solvents.



Figure 3-19: BTEM-PPV polymer in hexane, toluene, dioxane, THF, chloroform, acetone, ethanol

For the other three polymers, similar observations can be made (figures 3-20, 3-21, 3-22). The shoulders are a result of π - π stacking interactions caused by the aggregation of the conjugated systems in solution⁴⁰. Apparently at the edges of the polarity scale, aggregation of the polymers occurs, while only in good solvents the polymers remain freely solvated in solution. The aggregation effect is most pronounced for polymer NTEM-PPV, which displays in most solvents such behavior. This is presumably the result of its amphiphilic character, which results in NTEM-PPV having a high affinity to form micellar like structures.

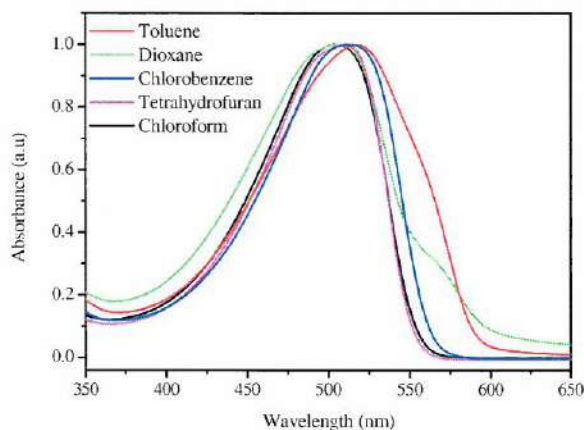


Figure 3-20: UV-Vis absorption spectra of MDMO-PPV in various solvents

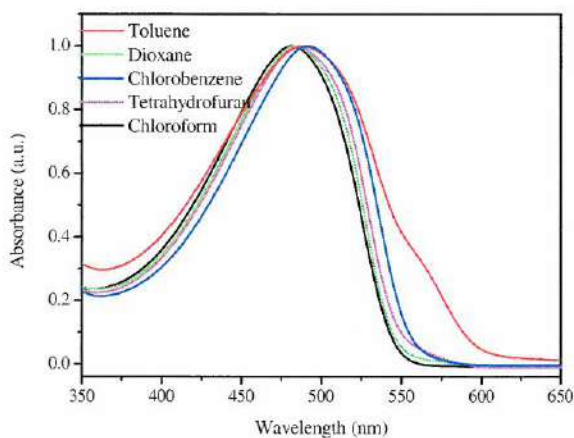


Figure 3-21: UV-Vis absorption spectra of MTEM-PPV in various solvents

When studying λ_{max} in all solvents the solvatochromic effects become apparent (Table 3-5). Apparently, the conformation of the π -conjugated backbone in solution is dependent on the specific side-chain/solvent combination. The hypsochromic shifts of λ_{max} represent increasing deviations from a fully planar structure. Similar solvatochromic effects have been previously observed for other, more flexible, conjugated polymers, such as polysilanes⁴¹.

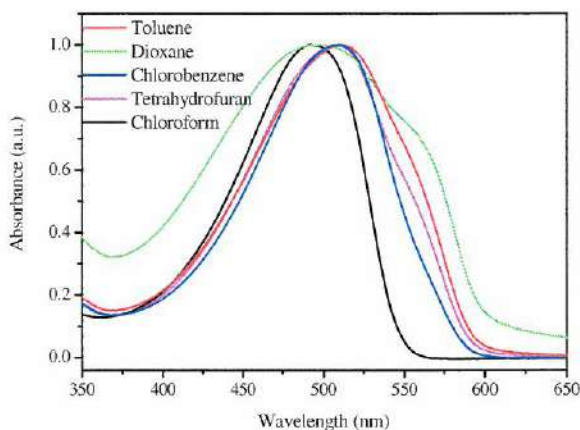


Figure 3-22: UV-Vis absorption spectra of NTEM-PPV in various solvents.

From the above studies on MTEM-PPV, BTEM-PPV, NTEM-PPV as well as MDMO-PPV it is evident that the nature of the side chains has a substantial influence on the solution properties. This will impact processes, such as various coating techniques, in which solutions play an important role. By a careful choice of substituents, PPV-derivatives can be prepared which are soluble in a wider range of solvents. This is an excellent demonstration that the applied synthetic methods are suitable to reproducibly adjust the physical properties of PPV-type polymers as desired.

✓ Concentration effect

One of the questions remaining is whether there is an effect of the concentration of the polymer solution. Figure 3-23 illustrates the spectra of BTEM-PPV solutions in two selected solvents, *i.e.* chloroform and toluene, ranging in concentration from 0.1 mM to 0.02 mM based on the repeating unit of the polymer. Chloroform is a solvent of medium polarity, which does not result in a shoulder in the UV-Vis absorption spectrum of BTEM-PPV. The color of a typical BTEM-PPV solution in chloroform is orange (figure 3-24). Toluene is a more apolar solvent on the polarity scale, and typical BTEM-solutions have a red color (figure 3-24).

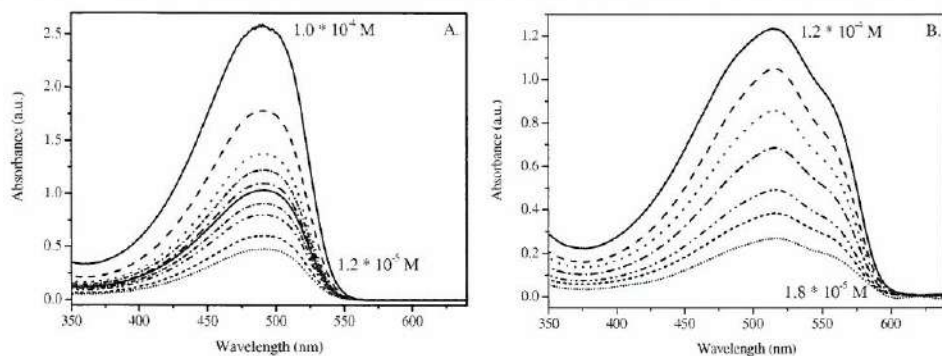


Figure 3-23: Solution UV-Vis absorption spectra of BTEM-PPV

A. in chloroform (concentration range: 0.017 mM to 0.1 mM)

B. in toluene (concentration range 0.018 mM to 0.12 mM) .

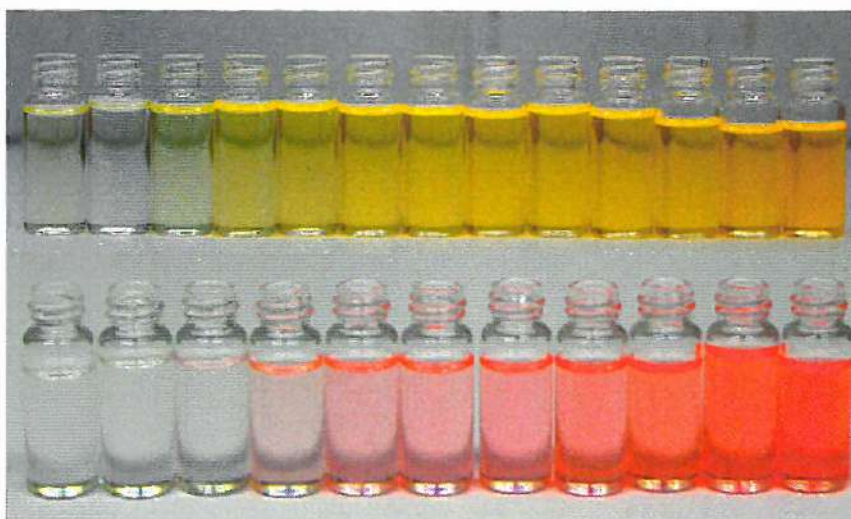


Figure 3-24: Solutions of BTEM-PPV in chloroform (top) and toluene (bottom).

The concentration range is approximately 0.02 mM to 0.1 mM.

The bottom limit of 0.02 mM has been chosen because of the fact that with our available instrumentation it is not possible to take an UV-Vis absorption spectrum of a polymer solution with a lower concentration due to the insufficient optical density. As shown in figure 3-23, varying the concentration from 0.02 to 0.1 mM does not affect the shape of the spectrum. The polymer solutions in chloroform

have a yellow-orange color, the result of a π - π^* transition centered near 500 nm, at all concentrations (figure 3-24). The color of the polymer solutions in toluene is red, even at low concentrations. Apparently, in this solvent the π - π stacking interactions occur independent of the concentration. They are a result of the complex interplay between the solvent and side chain polarities. On first glance it appears that these results are somewhat in contradiction to existing literature on this subject,⁴² in which it is claimed that the formation of PPV aggregates in solutions depends on an interplay of factors including the nature of the substituents on the polymer backbone as well as concentration and choice of the solvent. Although this concentration effect is not observed with UV-Vis absorption spectroscopy, one has to realize that this technique is limited in sensitivity. Therefore, an additional experiment has been performed using fluorescence spectroscopy.

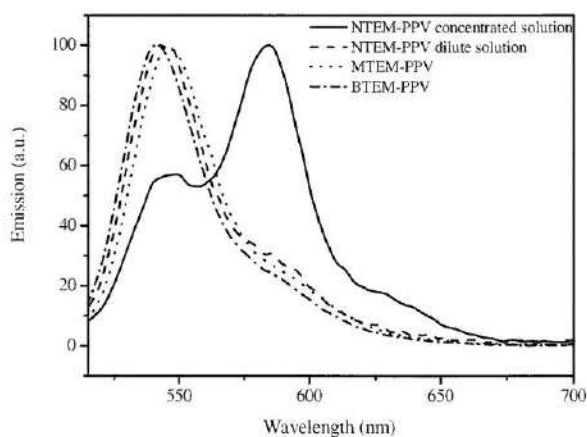


Figure 3-25: Fluorescence emission spectra of CHCl_3 solutions of MTEM-PPV, NTEM-PPV and BTEM-PPV.

Using fluorescence spectroscopy, in dilute CHCl_3 solution for NTEM-PPV, MTEM-PPV and BTEM-PPV a distinct emission is found at *circa* $\lambda_{\text{em}} = 543$ nm, (Figure 3-25), (excitation wavelength $\lambda_{\text{exc}} = 485$ nm). However, as exemplified in Figure 3-25 for NTEM-PPV, at increasing concentrations the intensity of this

emission decreases and a new red-shifted emission at $\lambda_{\text{em}} = 583 \text{ nm}$ becomes dominant. Apparently, even in CHCl_3 solution aggregation phenomena occur although to a much lesser extend as in solvents at the edges of the polarity scale and not detectable with UV-Vis absorption spectroscopy.

✓ *Time Effect*

One of the final questions remaining is how fast the aggregates develop. As previously mentioned, at the edges of the polarity scale, aggregation of the PPV polymers occurs, while only in good solvents the polymers remain freely solvated in solution. In order to study the time effect, UV-Vis absorption spectra of the different solutions have been taken directly after preparation as well as after one and three days. The resulting time dependent behavior can be exemplified for BTEM-PPV (Figure 3-26).

A shoulder develops instantaneously in the UV-Vis absorption spectrum of the BTEM-PPV in acetone and acetonitrile. Both solvents are at the polar side of the polarity scale of solvents. Apparently, aggregation phenomena already occur upon preparing the solutions. After one night, the shoulders in the acetonitrile and acetone solutions intensify, reflecting a further extension of the aggregation phenomena. Furthermore, also a shoulder, *i.e.* aggregation phenomena, occur in toluene at the apolar side of the polarity scale. The solutions of BTEM-PPV in 'good solvents' display even after 3 days only the π - π^* transition in the UV-Vis absorption spectrum. Apparently, the polymers remain freely dissolved and do not aggregate. For MDMO-PPV, MTEM-PPV and NTEM-PPV, similar observations have been made.

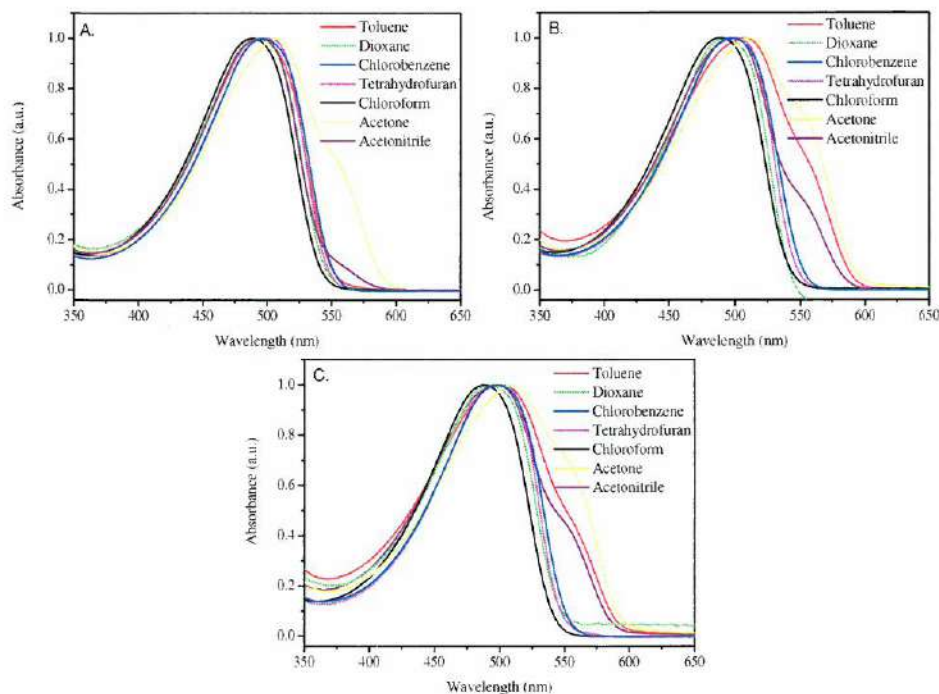


Figure 3-26: Solution UV-Vis absorption spectra of BTEM-PPV in different solvents

A. After preparing of the solution

B. After one day

C. After three days

✓ Nature of Aggregates

A final question remaining is what the structure of the formed aggregates may be. Although it should be noted that at this moment, the exact nature and structure of the aggregates remain under investigation, a brief review of the literature is at place to conclude this section. Various literature reports on conjugated polymers⁴³⁻⁴⁷ contain extensive studies describing the way in which inter- and intrachain species form in conjugated polymer solutions as the choice of solvent is varied. In all cases an increase in the spectral signatures of aggregation phenomena in solvents less able to fully dissolve the conjugated polymer have been reported, leading to the suggestion that aggregation occurs primarily between chromophores on the same polymer chain. This may well be the case for the above mentioned aggregation

phenomena in solvents at the edges of the polarity scale. However, it should be noted that the actual structure of the repeating unit is important for the shape of the resulting aggregates. This is demonstrated by another report ²⁹, which describes that symmetric substitution of the side chains attached on the phenylene ring of PPV induces the chain to adopt a conformation that is, at least over a certain length, more or less planar. Such planar structures enable the formation of interchain aggregates. Unsymmetric substitution effectively seems to prevent the formation of these interchain aggregates. In a number of cases coiled-up conformations form, which may be regarded as self- or intrachain aggregates. For example, for the asymmetric MDMO-PPV a coiled-up, spiralling conformation is observed, whereas the symmetric bis-OC₁₀-PPV adopts a more planar conformation over a certain length, which enables the formation of interchain aggregates. Especially tight coiled-up conformations, may be regarded as self- or intrachain aggregates. Not unexpectedly, there is a marked difference between the morphology of MDMO-PPV and bis-OC₁₀ PPV thin films processed from solutions. The former shows connected circular features with a typical diameter of 10 ± 2 nm, whereas the latter shows straight features with a typical length of 20-50 nm. ²⁹ It is worth mentioning that it is virtually impossible to distinguish with analytical techniques between inter- and intrachain aggregates in solution. This is different for thin films in which topographic features can be correlated to the molecular morphology using atomic force microscopy (AFM). ²⁹

3.7 Solution Thermochromism in Selected Solvents

The above discussion has provided a clear understanding to what extent the choice of solvent affects the degree of aggregation for dilute conjugated polymer solutions. The thus far presented solution UV-Vis measurements were performed at ambient temperatures. However, it can be expected that also the temperature will have a significant effect on the chain dynamics of these PPV-type polymers in

solution. The influence of temperature on the ground aggregation phenomena is demonstrated in this section for selected solvents. Since the nature of these aggregation phenomena as well as the conformation of the π -conjugated backbone in solution is dependent on the specific side-chain/solvent combination, in this section three different solvents are chosen namely chloroform, THF and toluene. The temperature dependent solution UV-Vis absorption measurements were done for the same four 2,5-dialkoxy-PPV derivatives, *i.e.* MTEM-PPV, BTEM-PPV, NTEM-PPV and MDMO-PPV, which were studied in section 3.6. Furthermore, it should be noted that in this section no distinction is made between inter- and intrachain aggregations in the polymer solution. Further research is necessary to make a difference between inter- and intrachain aggregation for PPV-type polymers in solution. In the following discussion, each polymer/solvent combination will be discussed, followed by a comparison between the various combinations.

✓ *MDMO-PPV in chloroform*

Figure 3-27 shows the optical absorption spectrum of MDMO-PPV dissolved in chloroform measured at various temperatures (range 0 – 60 °C, 10 °C intervals). The highest temperature is close to the boiling point of chloroform and forms therefore an upper limit. As can be seen, in the visible range of the absorption spectrum, *i.e.* 350-650 nm, only a single absorption is visible, which is associated with the π - π^* transition of MDMO-PPV. The absorption maximum of MDMO-PPV measured in chloroform solution at ambient temperature is 506 nm. Upon heating, the absorption maximum exhibits a hypsochromic shift. Over the entire 60° C range presented in figure 3-27, the absorption maximum of the chloroform solution of MDMO-PPV shifts from 509 nm at 0 °C to 495 nm at 60 °C. After cooling the conjugated polymer solution back to ambient temperature, the conjugated system is fully recovered as reflected in the reoccurrence of a λ_{max} of 506 nm. Such a temperature dependent shift in the λ_{max} of conjugated polymers is usually referred to as solution thermochromism. During the heating process, the

effective conjugation length decreases and the average torsion angle of the backbone increases. By cooling down the polymer, the segmental motions in the polymer chains decrease and the effective conjugation length increases again, thus accounting for the observed bathochromic shift upon cooling. The color of the polymer solution remains orange during the heating and cooling process.

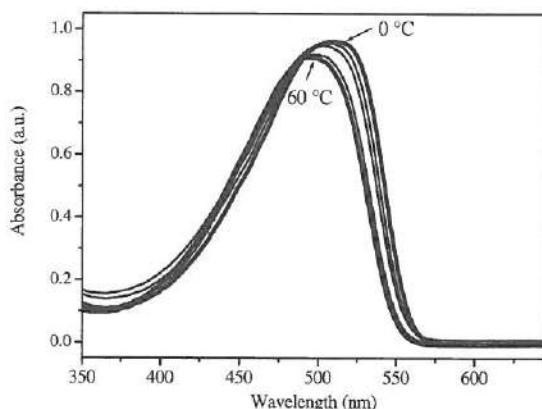


Figure 3-27: The temperature dependent UV-Vis absorption spectra of MDMO-PPV in chloroform solution.

Whereas in the above mentioned temperature range a gradual shift is observed in the absorption spectrum of MDMO-PPV dissolved in chloroform, upon lowering the temperature to $-60\text{ }^{\circ}\text{C}$ more complex behavior is observed (figure 3-28). Upon slight cooling still conventional thermochromism is observed (figure 3-28A) with λ_{max} shifting to 512 nm at $-10\text{ }^{\circ}\text{C}$. Further cooling of the MDMO-PPV solution to $-30\text{ }^{\circ}\text{C}$ (figure 3-28B), results not only a further shift of λ_{max} but also in a new absorption peak at 525 nm. Concomitantly, the intensity of the resulting broad absorption peak decreases, possibly because of the decrease in solubility of MDMO-PPV at these temperatures. The bathochromic shift of the λ_{max} associated with the π - π^* transition indicates that upon cooling the average conjugation length of the polymers increases as a result of a reduction of segmental motions. The absorption peak at 525 nm is associated with interactions between individual conjugated segments. Upon cooling below $-30\text{ }^{\circ}\text{C}$, the π - π^* transition no longer

shifts and apparently, MDMO-PPV is in a semi-planar state with a maximal effective conjugation length.⁴⁰ Due to this fact, π - π stacking phenomena become dominant at lower temperatures. This is apparent when subsequently the MDMO-PPV solution is further cooled down to -60 °C (figure 3-28C). The absorption peak at 525 nm at -30 °C is shifted to 535 nm at -60 °C and the intensity of the π - π^* transition decreases. This indicates that the interactions between conjugated segments increase in importance and possibly even the onset of aggregation is near. However, it should be noted that the color of the solution remains orange. In contrast, large scale aggregation phenomena result in more red colored solutions (*vide supra*).

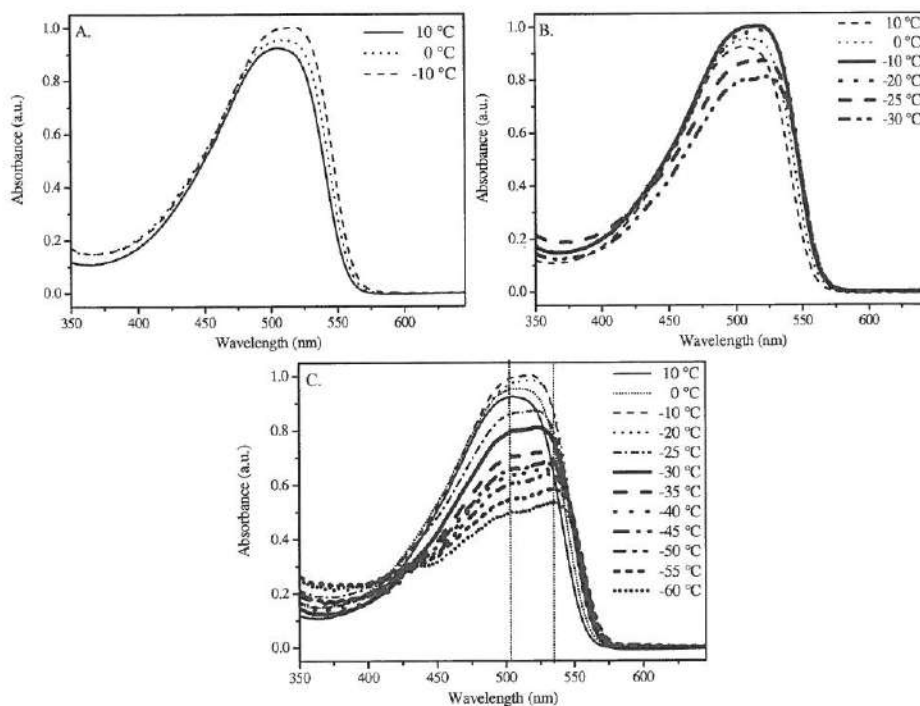


Figure 3-28: The temperature dependent UV-Vis absorption spectra of MDMO-PPV in chloroform solution (A: 10 °C to -10 °C; B: 10 °C to -30 °C; C: 10 °C to -60 °C)

✓ *MDMO-PPV in THF*

The second solvent studied is THF. The temperature-dependent UV-Vis spectra of MDMO-PPV in THF solution are very similar to those in chloroform (Figure 3-29). Upon increasing the temperature, the λ_{max} associated with the π - π^* transition of MDMO-PPV shifts 13 nm from 509 nm at 10 °C to 496 nm at 60 °C. This significant thermochromic effect is in the same order of magnitude as that observed for chloroform solutions. During the heating process the color of the THF solution remains orange.

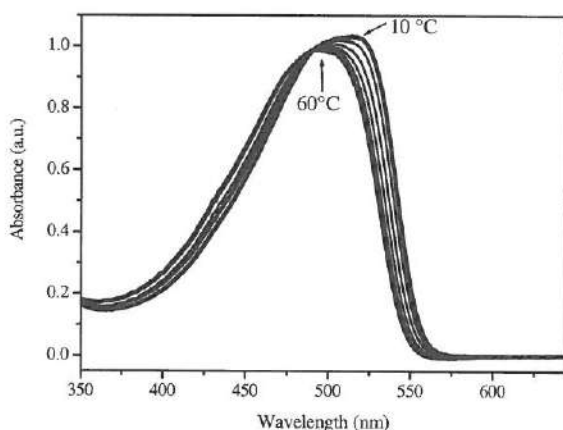


Figure 3-29: The temperature dependent UV-Vis absorption spectra of MDMO-PPV in THF solution.

Also in this case the cooling process displays a more interesting behavior. This is demonstrated in figure 3-30. In the temperature dependent UV-Vis absorption spectra in the 20 °C to -30 °C range two different effects can be seen (figure 3-30A). First of all, there is again the thermochromic effect, *viz.* upon cooling the absorption maximum of MDMO-PPV dissolved in THF exhibits a slightly bathochromic shift. This shift is difficult to observe due to the appearance of a new absorption peak at 530 nm at temperatures below -30 °C (figure 3-30B). Upon further cooling to -60 °C this new absorption peak increases in intensity and shifts to 540 nm at -60 °C. The increase in intensity is accompanied by a reduction in

peak width. Apparently, the distribution of chromophores becomes increasingly narrow at low temperatures. This is typical for thermochromic effects. This is somewhat in contrast to the chloroform solutions of MDMO-PPV, in which the absorption spectra become less well defined at low temperatures due to solubility issues. The absorption at 530/540 nm also in this case can be assigned to π - π stacking effects of conjugated segments of the polymers. Likewise during the cooling process, the color of the polymer solution remains orange, which indicates that large-scale aggregation phenomena do not occur.

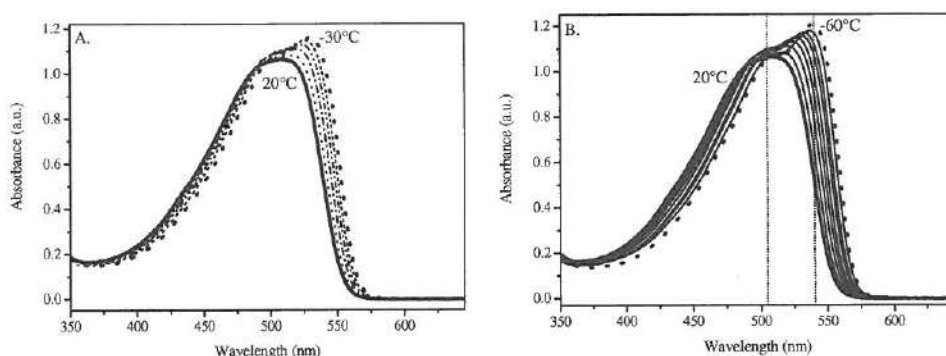


Figure 3-30: The temperature dependent UV-Vis absorption spectra of MDMO-PPV in THF solution (A: 20 °C to -30 °C; B: 20 °C to -60 °C)

✓ MDMO-PPV in toluene

As mentioned previously, when MDMO-PPV is dissolved in toluene, a reddish solution is obtained at ambient temperature as a result of aggregation phenomena. This is reflected in the UV-Vis absorption spectrum, in which an additional absorption is found as a shoulder around $\lambda_{\text{max}} = 560$ nm.

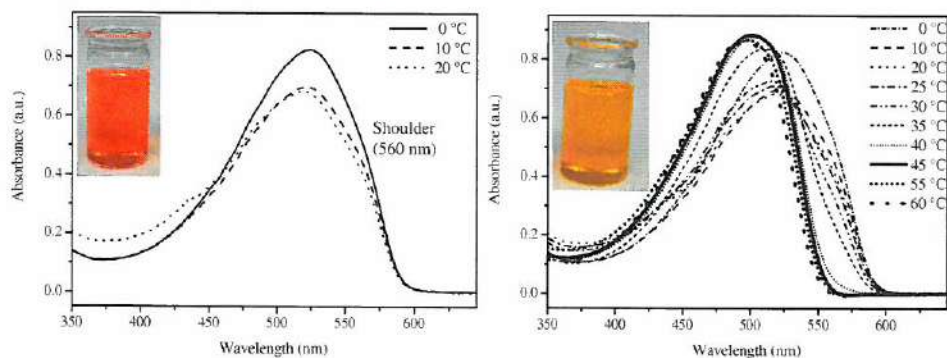


Figure 3-31: The temperature dependent UV-Vis absorption spectra of MDMO-PPV in toluene solution. (A: 0 °C to 20 °C; B: 0 °C to 60 °C)

For MDMO-PPV dissolved in toluene this shoulder is distinctly present in the temperature range 0 °C to 20 °C (figure 3-31A) and the solution has a red color. In addition, in this temperature range a small thermochromic effect is observed, with λ_{max} shifting hypsochromically from 524 nm at 0 °C to 509 nm at 20 °C. Absorption spectra at temperatures above 20 °C show the gradual disappearance of the shoulder at 560 nm while the π - π^* transition shifts to 495 nm at 60 °C (figure 3-31B).⁴⁸ At 45 °C, there is no longer a shoulder visible. Apparently, at this temperature, the aggregates have fully dissociated and the π - π stacking interactions no longer are of significant importance. As a result of this, the color of the polymer solution changes from red at 20 °C to reddish orange at 35 °C to orange at temperatures above 45 °C.

Upon cooling down the toluene solution of MDMO-PPV a broad featureless peak is obtained in the UV-Vis absorption spectrum (figure 3-32). This peak is composed of the original π - π^* transition, which has decreased in intensity, as well as the previously mentioned shoulder associated with the aggregates. Close scrutiny of this shoulder indicates that it is composed of two optical transitions. Not only the 560 nm transition associated with the red color and long range aggregates is present but also a transition at *circa* 520 nm. This peak is also observed during the cooling process of MDMO-PPV in chloroform and THF (*vide supra*).

Apparently the gradual planarization of the conjugated backbone initially results in π - π stacking effects of conjugated segments of the polymers ($\lambda_{\max} \approx 520$ nm), followed by the formation of long range aggregates ($\lambda_{\max} \approx 560$ nm).

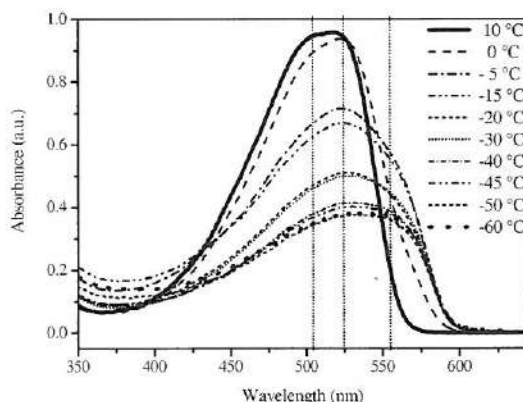


Figure 3-32: The temperature dependent UV-Vis absorption spectra of MDMO-PPV in toluene solution

✓ Solution thermochromic effects of the polar PPV derivatives

The three functionalized PPV polymers studied, MTEM-PPV, BTEM-PPV and NTEM-PPV contain a polar oligo(oxyethylene) side chains in various arrangements. Figures 3-33, 3-34 and 3-35 illustrate the absorption spectra of MTEM-PPV, BTEM-PPV and NTEM-PPV dissolved in chloroform, THF and toluene as a function of temperature (temperature range *circa* 0 °C to 60 °C). In all cases upon heating a thermochromic effect occurs. Please note that the small variations in intensity of the π - π^* transition as observed in these spectra are within the measurement error. The thermochromic effect is most clearly visible in chloroform solution. In this solvent, for MTEM-PPV λ_{\max} π - π^* shifts by 9 nm from 487 nm at 10 °C to 478 nm at 60 °C. For the other two polymers similar observations can be made. The λ_{\max} of BTEM-PPV at 10 °C is 491 nm and at 60 °C 481 nm. For NTEM-PPV the λ_{\max} at 10 °C is 497 nm and at 60 °C 487 nm. A similar trend is observed for the optical absorption maximum of the UV-Vis

spectra for the four PPV polymers dissolved in toluene and THF. It appears that for the above three polymers a similar behavior is observed, as was found for MDMO-PPV. The observed thermochromic shifts are a result of the fact that upon heating, the segmental motions present in the polymers increase in number and amplitude. As a result, also the average torsion angle of the backbone increases significantly and concomitantly the effective conjugation length decreases, as reflected in the hypsochromic shift of λ_{max} . This process is fully reversible and very comparable to the previously described thin film thermochromism (*vide supra*).

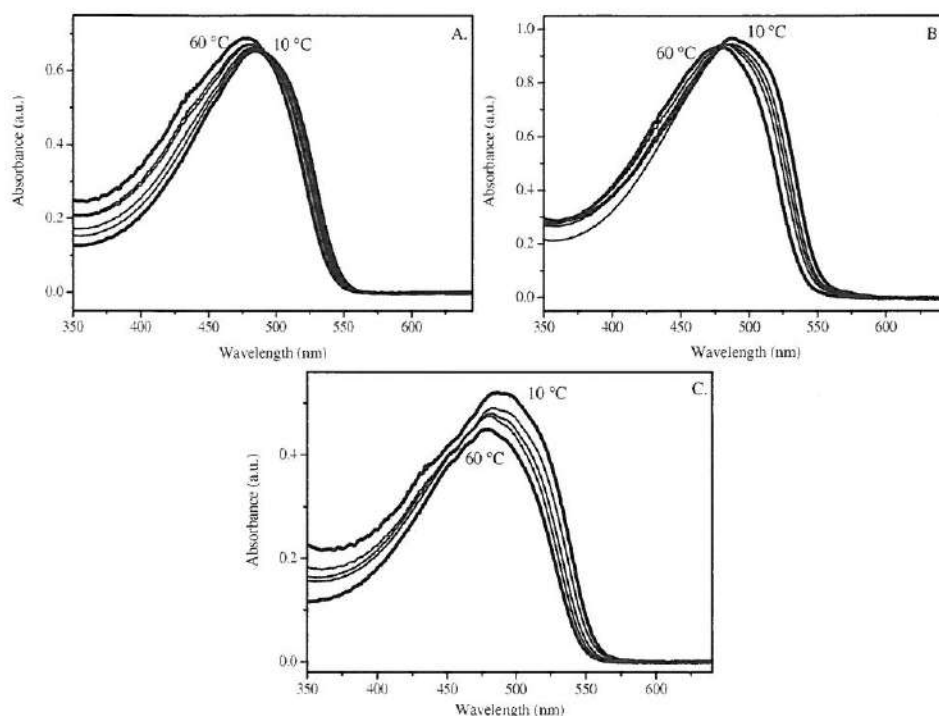


Figure 3-33: The temperature dependent UV-Vis absorption spectra of MTEM-PPV dissolved in chloroform (A), THF (B) and toluene (C).

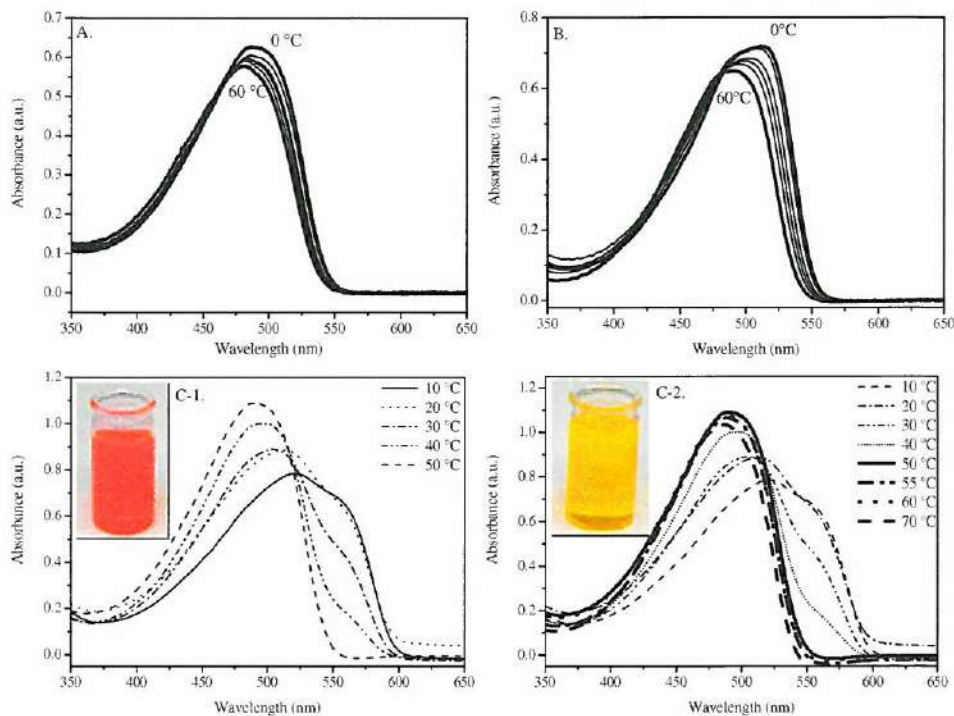


Figure 3-34: The temperature dependent UV-Vis absorption spectra of BTEM-PPV dissolved in chloroform (A), THF (B) and toluene (C1: 10 °C to 50 °C, inset solution color below 50 °C; C2: 10 °C to 70 °C, inset solution color at 60 °C).

✓ Aggregation Phenomena

In section 3.6 of this chapter, it is mentioned that the UV-Vis absorption spectra of BTEM-PPV and NTEM-PPV dissolved in a more apolar solvent like toluene not only contain the absorption associated with the π - π^* transition but also a shoulder around 550 nm (figures 3-18 and 3-22). As previously discussed, this shoulder is the result of π - π stacking interactions caused by the aggregation of the conjugated systems in solution⁴⁰. As a result the color of solutions of BTEM-PPV and NTEM-PPV in toluene is red at ambient temperatures, whereas the MTEM-PPV toluene solution is initially orange, although upon standing also here aggregation phenomena can occur (*vide supra*). When BTEM-PPV and NTEM-PPV in toluene solutions are heated to 50 °C, dissociation of these aggregates occurs. In the

temperature dependent UV-Vis absorption spectra this is notable as a disappearance of the aggregate shoulder at 550 nm. Concomitantly, λ_{\max} π - π^* becomes better defined and shifts to lower wavelength, *i.e.* 491 nm at 50 °C for BTEM-PPV and 493 nm at 50 °C for NTEM-PPV. After the dissociation of the aggregates in the polymer solution, the thermochromic effect remains active and at 60 °C, the λ_{\max} is 486 nm for both BTEM-PPV and NTEM-PPV. During the heating process, the color of the polymer solution of BTEM-PPV and NTEM-PPV change from deep red in the lower temperature range (figure 3-34C-1) to orange-red at 50 °C to orange-yellow at 60 °C (figure 3-34C-2).

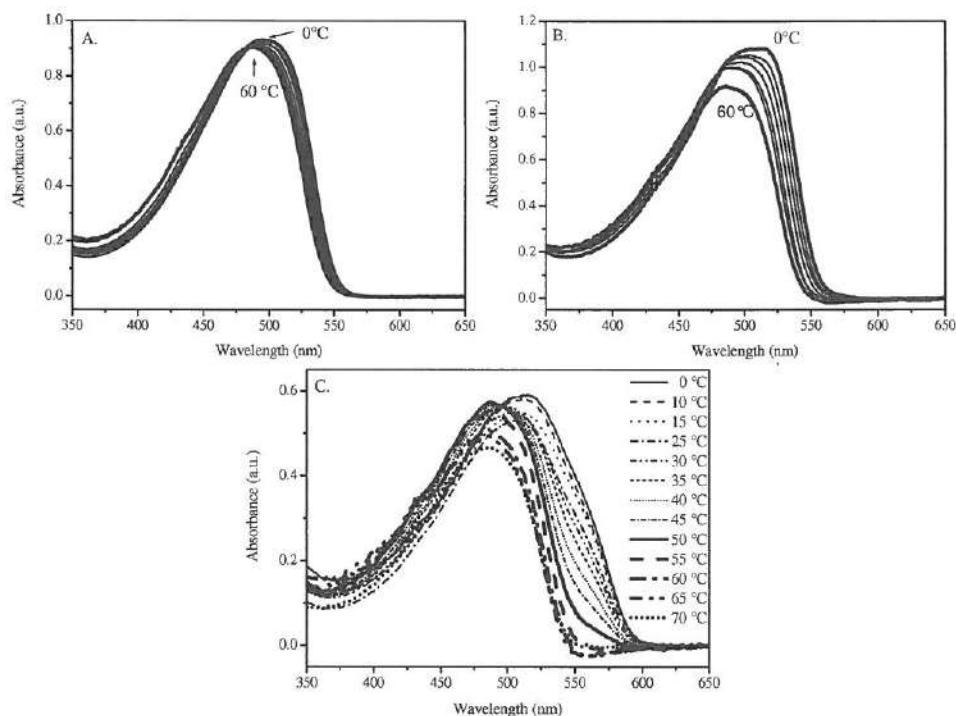


Figure 3-35: The temperature dependent UV-Vis absorption spectra of NTEM-PPV dissolved in chloroform (A), THF (B) and toluene (C).

The temperature dependent UV-Vis absorption spectra of dilute solutions of MTEM-PPV, BTEM-PPV and NTEM-PPV in chloroform, THF and toluene upon

cooling are shown in figures 3-36, 3-37 and 3-38. The spectra of the chloroform solutions of MTEM-PPV, BTEM-PPV and NTEM-PPV in the temperature range 0 °C to -60 °C (figures 3-36A, 3-37A and 3-38A) are comparable with the spectrum of MDMO-PPV under the same conditions. During the cooling process, the intensity of the absorbance decreases somewhat due to solubility issues and a new absorption appears as a poorly defined shoulder at *circa* 520 nm. At low temperatures these polymers have a reduced flexibility⁴⁰ which gives rise to interactions between individual conjugated segments.

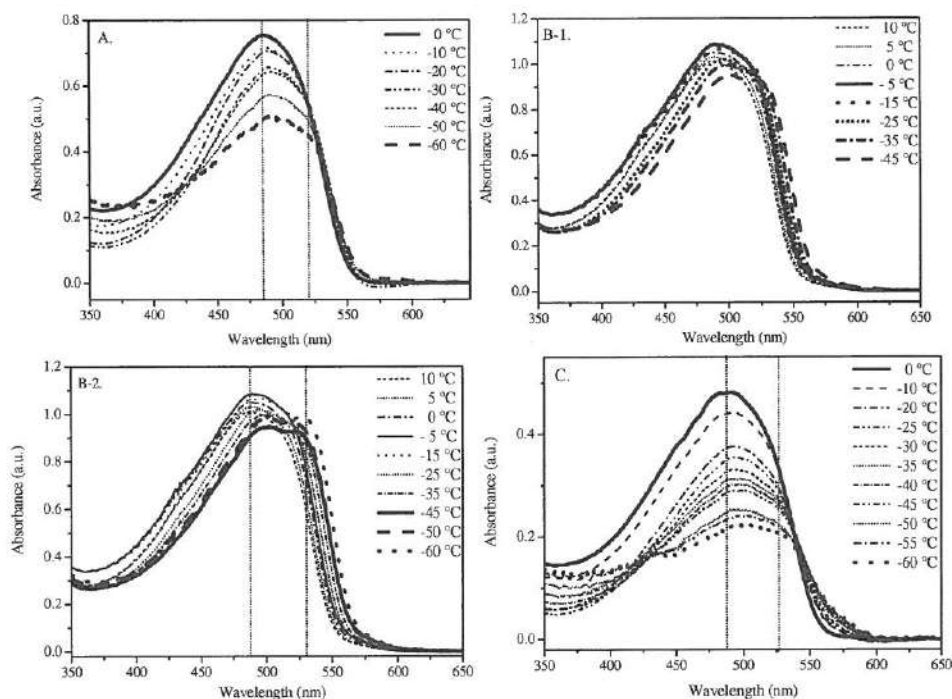


Figure 3-36: The temperature dependent UV-Vis absorption spectra of MTEM-PPV dissolved in chloroform (A), THF (B1: 10 °C to -45 °C; B2: 10 °C to -60 °C) and toluene (C).

The absorption spectra of the cooling process of solutions of MTEM-PPV, BTEM-PPV and NTEM-PPV in THF are displayed in figures 3-36B-1, -2 and 3-37B-1, -2, -3 and 3-38B-1, -2. The behavior of MTEM-PPV is similar to that of a THF

solution of MDMO-PPV. In the UV-Vis absorption spectrum of MTEM-PPV (figure 3-36B-1), the same thermochromic effect is observed between 10 °C and -5 °C as was observed during the heating process. When the polymer solution is cooled down to -45 °C, a second optical transition can be observed with a wavelength of 525 nm (figure 3-36), which is associated with interactions between individual conjugated segments. At lower temperatures, the absorbance decreases due to concentration effects. During the entire cooling process the color of the MTEM-PPV/THF solution is orange. The UV-Vis absorption spectra of the cooling processes of BTEM-PPV and NTEM-PPV (figure 3-37B-1, -2, -3 and 3-38B-1, -2) are markedly different compared to those of the THF solutions of MDMO-PPV and MTEM-PPV. Although they both also contain the typical thermochromic effects, at a temperature of -40 °C for BTEM-PPV and -45 °C for NTEM-PPV, a new absorption peak is observed with a wavelength of *circa* 550 nm (figure 3-37B-2, 3-38B-1). These peaks correspond to large-scale aggregation phenomena as a result of the planarization of the conjugated polymer backbone. At the same time also a new absorption is observed at *circa* 520 nm. This is the same transition, which is also found for MTEM-PPV and which is associated with interactions between individual conjugated segments. Upon further cooling also for these polymer solutions the intensity of the absorptions decrease due to concentration effects (figure 3-37B-3 and 3-38B-2). The large-scale aggregation phenomena are also directly visible, *i.e.* solutions of BTEM-PPV and NTEM-PPV have a red color at low temperatures.

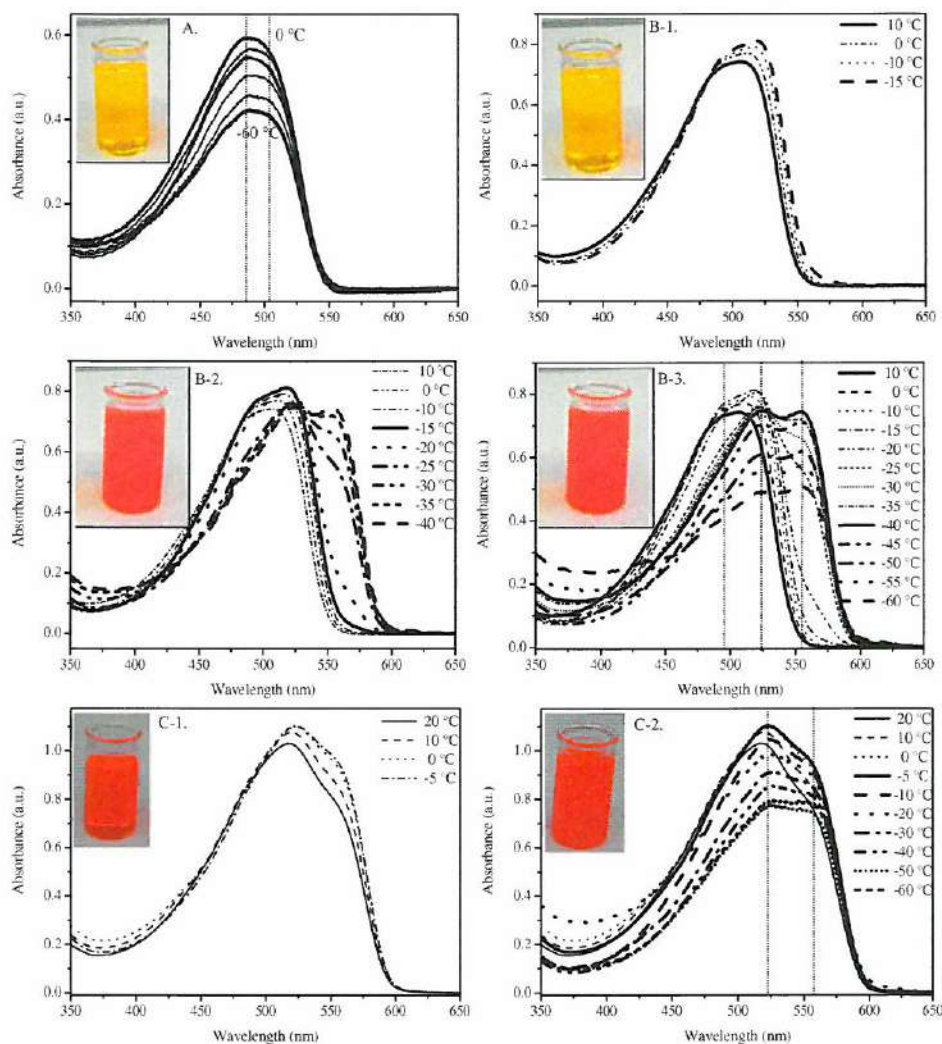


Figure 3-37: The temperature dependent UV-Vis absorption spectra of BTEM-PPV dissolved in chloroform (A, inset solution color at all temperatures), THF (B1: 10 °C to -15 °C, inset solution color at this temperature range; B2: 10 °C to -40 °C, inset solution color at this temperature range; B3: 10 °C to -60 °C, inset solution color at this temperature range) and toluene (C1: 20 °C to -5 °C, inset solution color at this temperature range; C2: 20 °C to -60 °C, inset solution color at this temperature range) solution.

The last solvent which has been used for the cooling experiments described in this section is toluene. In this solvent MTEM-PPV displays the same behavior as was observed for the other solvents. During the cooling process, a new optical transition appears at *circa* 527 nm (figure 3-36C) and concomitantly a decrease in intensity of the absorption spectrum is observed. Apparently also in this solvent, cooling of the MTEM-PPV solution results in additional interactions between individual conjugated segments. For the other two PPV derivatives, a similar behavior as MDMO-PPV is observed. Upon cooling toluene solutions of these two polymers, two new absorptions appear at *circa* 520 nm and 550 nm (figures 3-37 and 3-38), with like in the other solutions, the former being associated with interactions between individual conjugated segments and the latter being a result of true aggregation phenomena. After the formation of the two new absorption bands, the intensity decreases upon further cooling due to concentration effects (figures 3-37C-2 and 3-38C-2). For any toluene solution, in which a transition around 550 nm is observed in the UV-Vis absorption spectra (MDMO-PPV, BTEM-PPV and NTEM-PPV), the color of the solution is deep red and only the MTEM-PPV solution, which does not have this transition in this measurement set, has an orange color.

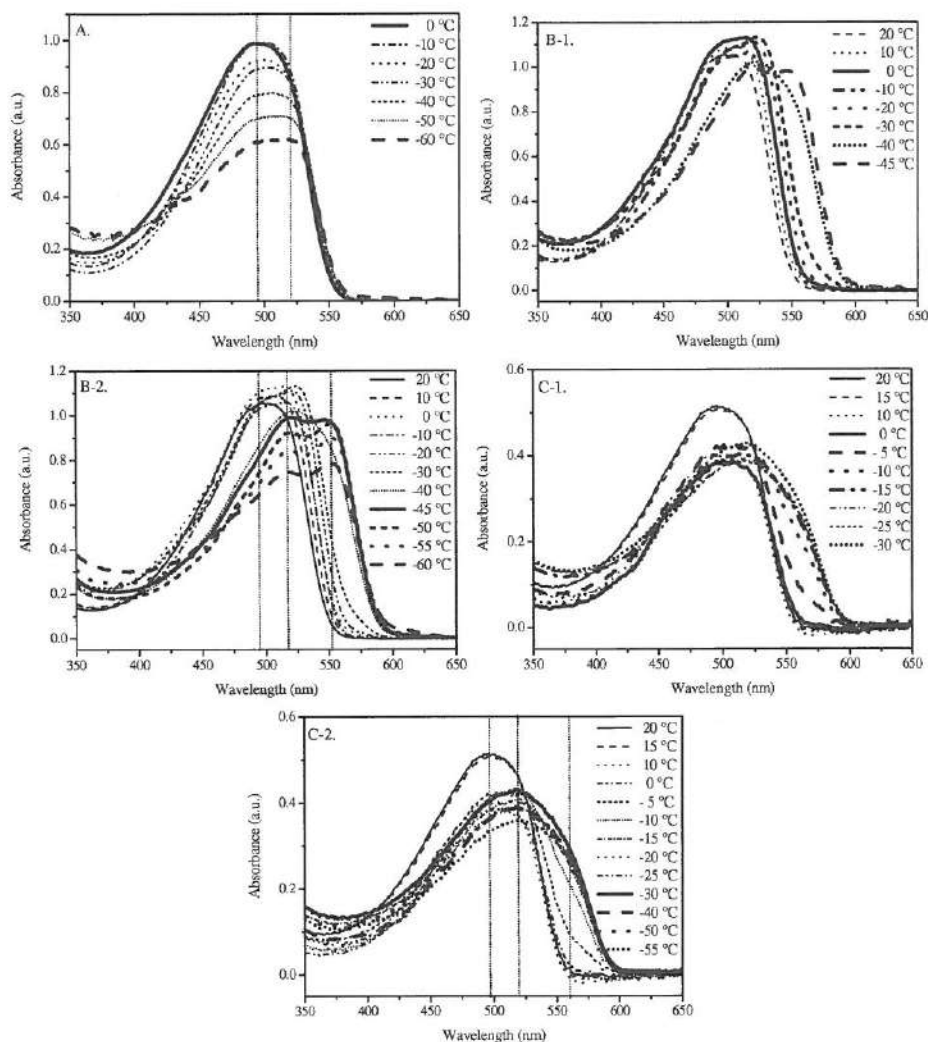


Figure 3-38: The temperature dependent UV-Vis absorption spectra of NTEM-PPV dissolved in chloroform (A), THF (B1: 20 °C to -45 °C; B2: 20 °C to -60 °C) and toluene (C1: 20 °C to -30 °C; C2: 20 °C to -55 °C).

✓ Discussion

From the above abundance of absorption spectra it may not immediately be evident what the influence is of the different side chains attached to the PPV backbone on the occurrence of interactions between conjugated polymers and the formation of

aggregates. To answer this question, an attempt will be made to summarize the temperature dependent solution UV-Vis absorption measurements for the series of four 2,5-di-alkoxy substituted PPV derivatives with different side chains, *i.e.* MDMO-PPV, MTEM-PPV, BTEM-PPV and NTEM-PPV. The first polymer is MDMO-PPV, which has a large branched decyloxy side chain on the second position of the phenylene ring and a short methoxy group on the fifth position. MTEM-PPV has the same short methoxy side chain as MDMO-PPV, but a polar linear side chain on the second position. BTEM-PPV has two polar linear side chains attached on the phenylene ring. The final polymer, NTEM-PPV, has an amphiphilic character, as a result of one linear polar and one linear apolar side chain. It should be noted that this series of polymers is not large enough to give conclusive answer conceiving all issues involving aggregation of PPV-type polymers. These four polymers have been selected because of the fact that they are readily available in high purity. In addition, they are all highly soluble in multiple organic solvents. There are a large number of factors that can influence the formation of aggregates, like the polarity of the side chain (apolar or polar), the geometry of the side chains (linear or branched) and the substitution pattern (symmetric or asymmetric). Notwithstanding, using the four PPV-derivatives, some comparisons can be made (figure 3-39). Two typical examples are:

- (1) **Effect of substitution pattern.** BTEM-PPV and MTEM-PPV can be compared, because both polymers have polar linear side chains, with BTEM-PPV having a symmetric and MTEM-PPV having an asymmetric substitution pattern (figure 3-39).
- (2) **Effect of polarity.** BTEM-PPV can also be compared with NTEM-PPV, since both polymers have long linear side chains, with BTEM-PPV having polar side chains and NTEM-PPV having one polar and one apolar side chain (figure 3-39). For this comparison, another polymer with two linear apolar side chains, *e.g.* poly[2,5-bis(nonyloxy)-*p*-phenylene vinylene] (BN-PPV) would be of interest. However, this type of polymers is not

readily soluble in organic solvents,⁴⁹ viz. apparently even more extended aggregation phenomena occur, rendering them unsuitable for this study.

The effect of geometry remains difficult to assess with the available polymers. One could compare MDMO-PPV with MTEM-PPV, but the polarity of their side chains is different and polarity issues likely will dominate the solution characteristics. Unfortunately, MDMO-PPV is currently the only available polymer with branched side chains and, for example, no polar branched representative is available. Hence, the geometry effect cannot be effectively studied until additional PPV-derivatives become available.

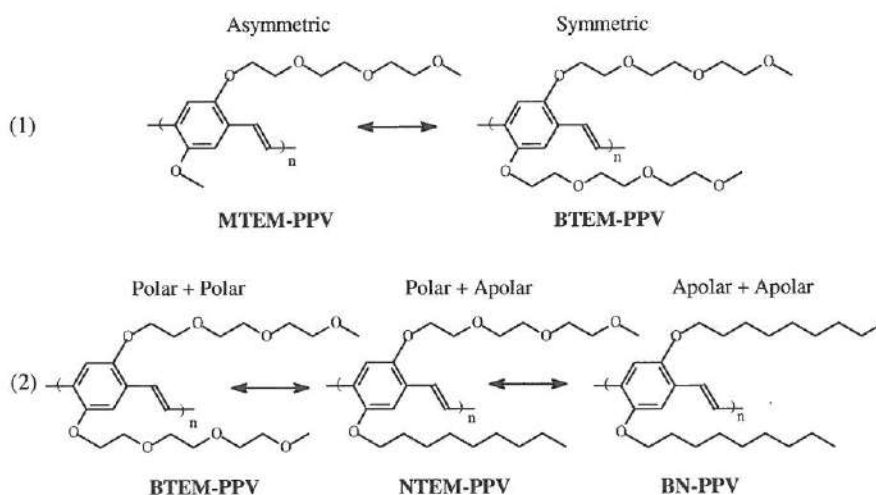


Figure 3-39: Examples of typical comparisons between various PPV-type polymers: (1) effect of substitution pattern, (2) effect of polarity.

When the behavior of solutions of MTEM-PPV is compared with that of BTEM-PPV, it can be concluded that the substitution pattern is, as expected, important for the formation of aggregates in a polymer solution. Solutions of MTEM-PPV, with its asymmetric substitution pattern, display clear signs of increasing interactions between individual conjugated segments upon cooling in the three solvents studied. However, no long-range aggregates are discernable in the studied temperature range. In contrast, upon cooling solutions of BTEM-PPV, which has a symmetric substitution pattern, not only interactions between individual conjugated segments

but also long range aggregation phenomena are observed in THF and toluene. This behavior is in agreement with the literature studies²⁹ in which it is demonstrated that symmetric substitution of the side chains attached on the phenylene ring of PPV causes the chain to adopt a conformation that is, at least over a certain strength, linear, which facilitates the formation of interchain aggregates. Unsymmetric substitution effectively seems to prevent the formation of these interchain aggregates and coiled-up conformations form, which may be regarded as self- or intrachain aggregates. However, it should be noted that the above literature statement is too generalizing. Whereas it seems that the mostly symmetrically substituted NTEM-PPV indeed also forms long-range inter-chain aggregates upon cooling, also the asymmetric MDMO-PPV seems to do this in toluene solution. A better statement would be that solutions of all PPV-type polymers display interactions between individual conjugated segments upon cooling. In addition, in poor solvents, sometimes even in the absence of cooling, long-range inter-chain aggregates are formed, which can be broken up by heating. Symmetrically substituted polymers have a higher propensity to form such long-range aggregates than asymmetrically substituted polymers.

When the issue of the polarity of the side chains is examined, it can be concluded that the polarity of the side chain is to a much lesser extent important for the formation of aggregates. BTEM-PPV and NTEM-PPV display similar behavior in the three different solvents studied (chloroform, THF and toluene). In a good solvent for both polymers, *i.e.* chloroform, upon cooling interactions between individual conjugated segments occur. Cooling of solutions of these polymers in much poorer solvents, *i.e.* THF and toluene, induces the formation of long-range inter-chain aggregates. To further support this argument, a new highly soluble PPV-type polymer is necessary with two linear apolar side chains (figure 3-39).

3.8 Conclusions

On the basis of the examples presented in this chapter, it is evident that the optical properties of functionalized conjugated polymers can be dramatically altered by several external stimuli (temperature, solvents, ions, etc.). These chromisms offer great potential for future applications. As a result of the studies presented in this chapter, the observations are now backed by a better understanding of the molecular mechanisms that drive these chromic effects.

In the beginning of this chapter, the influence of the temperature on the optical properties, *i.e.* **thermochromism**, has been demonstrated for thin films of PPV-type polymers. The thermochromic effect of four 2,5-di-alkoxy substituted PPV-type conjugated polymers with different side chains has been studied. Upon cooling these polymers, the effective conjugation length increases, which is reflected in a bathochromic shift of the λ_{max} associated with the π - π^* transition. It is demonstrated that the thermochromic effect does not depend on the nature of the side chains, as was previously reported. Instead, this effect originates from variations in the average torsion angle of the conjugated backbone repeating units. This indicates that the thermochromic effect can be directly correlated to the segmental motions present in the polymers. We have made use of this correlation and have presented a new and straightforward technique for the determination of the glass transition temperature of conjugated polymers using temperature dependent UV-Vis absorption measurements. In this way, T_g values can be obtained which are inaccessible using DSC. Above the T_g, the studied polymers exhibit virtually identical thermochromic behavior. At the T_g the backbone reaches a planar structure. Upon further cooling, the conformation of the backbone no longer changes and only ground-state aggregation phenomena are observed. It should be noted that in contrast to the thermochromic effect, the T_g of the polymers is strongly dependent on the nature of the side chains.

In the next section of this chapter, the influence of added ions on the optical properties, *i.e.* **ionochromism**, of thin films of PPV-type polymers has been examined. It appears that the optical properties of these polymer films change due to the incorporation of the added ions in the polymer film. These effects are based on the principle that the conformation of the conjugated polymer backbone can change due to complexation effects (ionochromic effects). The exact effect depends on the side of the ion. Small ions are complexed in one or more directly neighboring side chains of a single polymer, leading to additional conformational disorder due to steric hindrance. Larger ions, lead to more complex arrangements which effectively result in an increase in the effective conjugation length.

In the following section, the optical properties of PPV derivatives dissolved in different chemical solvents have been investigated. It is demonstrated that the solubility as well as solution properties are significantly affected as a result of the introduction of polar substituents. Not only is the accessible solvent range considerably expanded, *i.e.* for example, BTEM-PPV is excellently soluble in acetonitrile, but also **solvatochromism** and aggregation phenomena have been observed. It appears that PPV-type polymers when dissolved in good solvents, do not display noticeable polymer-polymer interactions. However, especially in poor solvents long-range aggregation phenomena are observed.

Finally in the last section of this chapter, the influence of the temperature onto the solution optical properties, *i.e.* **solution thermochromism**, as well as the aggregate formation process has been examined. For all solutions of PPV-type polymers, the λ_{\max} associated with the π - π^* transition displays a typical blue shift upon heating. Increasing conformational disorder is proposed to be the most important parameter responsible for this behavior. Upon cooling the conjugated polymer solutions, interactions, which are possibly intra-molecular, between individual conjugated segments become increasingly important. Dependent on the solvent/polymer combination used, a planarization of the polymer backbone can occur upon cooling

and long-range, likely inter-molecular, aggregation phenomena take place. However, it is virtually impossible to distinguish between inter- and intrachain aggregates with absorption spectroscopy. Therefore it would be of interest to study these solutions with, other techniques, such as photoluminescence spectroscopy (PL).

3.9 References

- 1 R. D. McCullough, *Advanced Materials*, 10, **1998**, 93.
- 2 S. Rughooputh, S. Hotta, A. J. Heeger and F. Wudl, *Journal of Polymer Science Part B-Polymer Physics*, 25, **1987**, 1071.
- 3 O. Inganäs, W. R. Salaneck, J. E. Osterholm and J. Laakso, *Synthetic Metals*, 22, **1988**, 395.
- 4 R. D. Miller and J. Michl, *Chemical Reviews*, 89, **1989**, 1359.
- 5 J. F. Rabolt, D. Hofer and R. D. Miller, *Macromolecules*, 19, **1986**, 611.
- 6 H. Kuzmany, J. F. Rabolt, B. L. Farmer and R. D. Miller, *Journal of Chemical Physics*, 85, **1986**, 7413.
- 7 R. D. Miller and J. Michl, *Chemical Reviews*, 89, **1989**, 1359.
- 8 H. W. Beckman and M. F. Rubner, *Macromolecules*, 26, **1993**, 5192.
- 9 A. D. Nava, M. Thakur and A. E. Tonelli, *Macromolecules*, 23, **1990**, 3055.
- 10 K. C. Lim, A. Kapitulnik, R. Zacher and A. J. Heeger, *Journal of Chemical Physics*, 82, **1985**, 516.
- 11 M. Leclerc, *Advanced Materials*, 11, **1999**, 1491.
- 12 B. J. Schwartz, *Annual Review of Physical Chemistry*, 54, **2003**, 141.
- 13 J. Kim, *Pure and Applied Chemistry*, 74, **2002**, 2031.
- 14 A. van Breemen, D. J. M. Vanderzande, P. J. Adriaenssens and J. Gelan, *Journal of Organic Chemistry*, 64, **1999**, 3106.

- 15 L. Lutsen, P. Adriaensens, H. Becker, A. J. Van Breemen, D. Vanderzande, *Macromolecules*, 32, **1999**, 6517.
- 16 H. Roex, P. Adriaensens, D. Vanderzande and J. Gelan, *Macromolecules*, 36, **2003**, 5613.
- 17 E. Kesters, D. Vanderzande, L. Lutsen, H. Penxten and R. Carleer, *Macromolecules*, 38, **2005**, 1141.
- 18 T. P. Nguyen, V. H. Tran, P. Destruel and D. Oelkrug, *Synthetic Metals*, 101, **1999**, 633.
- 19 B. Tian, G. Zerbi and K. Mullen, *Journal of Chemical Physics*, 95, **1991**, 3198.
- 20 B. Tian, G. Zerbi, H. Schenk and K. Mullen, *Journal of Chemical Physics*, 95, **1991**, 3191.
- 21 M. Onoda and K. Tada, *Thin Solid Films*, 438, **2003**, 187.
- 22 K. Yoshino, D. H. Park, B. K. Park, M. Onoda and R. Sugimoto, *Japanese Journal of Applied Physics Part 2-Letters*, 27, **1988**, L1612.
- 23 N. Hirota, N. Hisamatsu, S. Maeda, H. Tsukahara and K. Hyodo, *Synthetic Metals*, 80, **1996**, 67.
- 24 M. Leclerc, C. Roux and J. Y. Bergeron, *Synthetic Metals*, 55, **1993**, 287.
- 25 C. Roux and M. Leclerc, *Chemistry of Materials*, 6, **1994**, 620.
- 26 J. A. Mikroyannidis, P. D. Vellis, P. I. Karastatiris and L. K. Spiliopoulos, *Synthetic Metals*, 145, **2004**, 87.
- 27 S. Vaidyanathan, H. Dong and M. E. Galvin, *Synthetic Metals*, 142, **2004**, 1.
- 28 S. P. Kwasniewski, J. P. Francois and M. S. Deleuze, *Journal of Physical Chemistry A*, 107, **2003**, 5168.
- 29 M. Kemerink, J. K. J. van Duren, A. J. J. M. van Breemen, J. Wildeman, M. M. Wienk, *Macromolecules*, 38, **2005**, 7784.
- 30 S.-A. Chen and E.-C. Chuang, *Macromolecules*, 1998, **1998**, 4899.
- 31 M. Fahlman and J. L. Brédas, *Synthetic Metals*, 78, **1996**, 39.

- 32 J. Yu, M. Hayashi, S. H. Lin, K.-K. Liang, J. H. Hsu, *Synthetic Metals*, 82, **1996**, 159.
- 33 S. Lim, T. G. Bjorklund and C. J. Bardeen, *Chemical Physics Letters*, 342, **2004**, 555.
- 34 K. Pichler, D. A. Halliday, D. D. C. Bradley, P. L. Burn, R. H. Friend, *Journal of Physics-Condensed Matter*, 5, **1993**, 7155.
- 35 F. Banishoeib, A. Henckens, T. J. Cleij, L. Lutsen and D. Vanderzande, *in press*, **2006**,
- 36 L. Holzer, F. P. Wenzl, S. Tasch, G. Leising, B. Winkler, *Applied Physics Letters*, 75, **1999**, 2014.
- 37 C. Huang, W. Huang, J. S. Guo, C. Z. Yang and E. T. Kang, *Polymer*, 42, **2001**, 3929.
- 38 C. Reichardt, *Solvents and Solvent Effects in Organic Chemistry*, VCH Weinheim, **1990**, 408.
- 39 T. Munters, T. Martens, L. Goris, V. Vrindts, J. Manca, *Thin Solid Films*, 247, **2002**, 403.
- 40 M. Zheng, F. Bai and D. Zhu, *Journal of Photochemistry and Photobiology a-Chemistry*, 116, **1998**, 143.
- 41 T. J. Cleij and L. W. Jenneskens, *Journal of Physical Chemistry B*, 104, **2000**, 2237.
- 42 T. Q. Nguyen, V. Doan and B. J. Schwartz, *Journal of Chemical Physics*, 110, **1999**, 4068.
- 43 P. Wang, C. J. Collison and L. J. Rothberg, *Journal of Photochemistry and Photobiology a-Chemistry*, 144, **2001**, 63.
- 44 C. J. Collison, L. J. Rothberg, V. Treemaneeekarn and Y. Li, *Macromolecules*, 34, **2001**, 2346.
- 45 I. D. W. Samuel, G. Rumbles, C. J. Collison, S. C. Moratti and A. B. Holmes, *Chemical Physics*, 227, **1998**, 75.
- 46 J. H. Hsu, W. S. Fann, P. H. Tsao, K. R. Chuang and S. A. Chen, *Journal of Physical Chemistry A*, 103, **1999**, 2375.

- 47 R. Chang, J. H. Hsu, W. S. Fann, J. Yu, S. H. Lin, *Chemical Physics Letters*, 317, **2000**, 153.
- 48 R. Traiphol, P. Sanguansat and T. Sriksirin, *Macromolecules, American Chemical Society*, 39, **2006**, 1165.
- 49 L. Breban, L. Lutsen, G. Vanhoyland, D'Haen J, J. Manca, *Thin Solid Films*, 511, **2006**, 695.

Chapter 4

In Situ Spectro-Electrochemistry

4.1 Introduction

Poly(*p*-phenylene vinylene) (PPV) is a quite extensively studied representative of the conjugated polymers family.¹⁻⁴ Since the discovery of electroluminescence in poly(*p*-phenylene vinylene), PPV⁵, conjugated polymers have emerged as promising materials for a wide variety of optoelectronic applications. These applications range from polymeric light-emitting diodes (PLEDs) to flat panel displays, field effect transistors, (bio)sensors and photovoltaic cells.⁵⁻⁹ Hence, it is crucial to gain more insight in the electrochemical behavior and the optoelectronic properties of conjugated polymers.

Although a wide variety of electrochemical techniques are available, the most common method to investigate the electrochemical behavior of conjugated polymers is cyclic voltammetry (chapter 2). Cyclic voltammetry has been recognized as an important technique for measuring band gaps, electron affinities and ionization potentials (HOMO and LUMO energy levels). Electrochemistry is also convenient to study reactions involving electron transfer. However

electrochemical methods (e.g. cyclic voltammetry, chronoamperometry, etc.) are poor at providing structural information on the intermediate species¹⁰⁻¹⁵.

An increased understanding of redox processes can be generated by the application of *in situ* spectro-electrochemical techniques. By employing *in situ* spectro-electrochemical methods, both the electric current and the spectroscopic signal of a conducting polymer film on the surface of the working electrode can be recorded simultaneously during the electrochemical reactions. Spectroscopic investigations in the ultraviolet-visible (UV-Vis) and near infrared range (NIR) comprise the most basic form of a spectro-electrochemical method. They can give information not only on structural properties of the polymer chain but also on electronic properties of the material^{10, 11, 16}. *In situ* Fourier transform infrared spectroscopy (FTIR) in an attenuated total reflection (ATR) arrangement allows observation of structural and electronic changes taking place in the polymer film on the electrode in the mid- and near-IR regions during electrochemical reactions.¹⁷⁻¹⁹ The vibrational frequencies can be related to *ab initio* calculations allowing interpretation of the measurements at the molecular level.^{20, 21} Infrared spectroscopic signatures of electrogenerated species have been widely studied and have been the subject of several review articles.^{14, 22-24} *In situ* Resonance Raman spectroscopy is also well suited for spectro-electrochemical studies of conjugated polymers. Electrochemical doping leads to changes in chain geometry and modification of the resonance condition for Raman scattering. The dependence of the position of a Raman band on the energy of the excitation wavelength is caused by the distribution of the conjugated length in conjugated polymers.^{10, 14, 16, 17, 23}

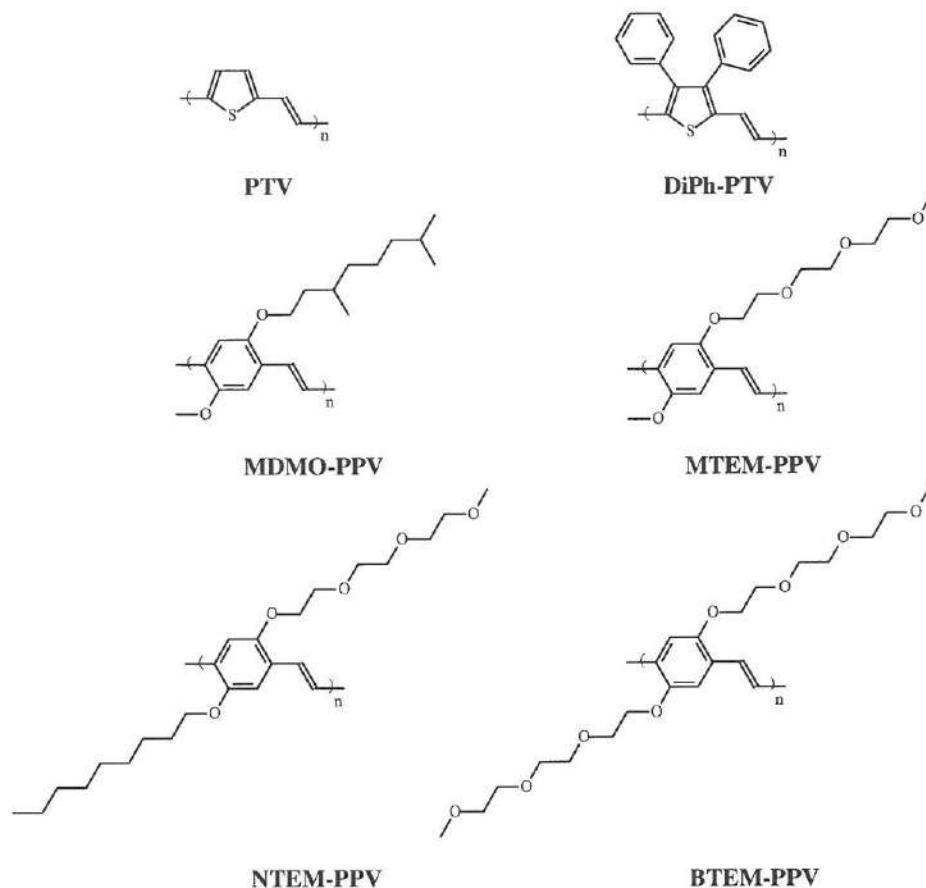


Figure 4-1: Molecular structures of the studied PTV and 2,5-alkoxy substituted PPV derivatives.

The aim of this chapter is to give a description of the modifications encountered by the conjugated structure of typical conjugated polymers upon going from a neutral to a charged (conducting) state. The previously mentioned techniques (*in situ* UV-Vis-NIR spectro-electrochemistry, *in situ* ATR-IR spectro-electrochemistry and *in situ* Raman spectro-electrochemistry) have been employed to compare the spectroscopic and electrochemical behavior of a representative selection of conjugated polymers. To this end four functionalized PPV derivatives, namely poly[2-(3',7'-di-methyloctyloxy)-5-methoxy-*p*-phenylene vinylene] (MDMO-

PPV), poly[2-methoxy-5-(methoxy triethoxy)-*p*-phenylene-vinylene] (MTEM-PPV), poly[2,5-bis(methoxy triethoxy)-*p*-phenylene-vinylene] (BTEM-PPV), poly[2-(nona-oxy)-5-(methoxy-triethoxy)-*p*-phenylene-vinylene] (NTEM-PPV) as well as two PTV derivatives, *i.e.* non-substituted poly(thienylene vinylene) (PTV) and poly[3,4-diphenyl-2,5-thienylene vinylene] (DiPh-PTV) have been studied (figure 4-1). The polarity of the side chains in the four PPV polymers, which range from apolar alkyl to polar oligo(oxyethylene) groups, exhibits substantial variation. All PPV-type polymers have been synthesized *via* the sulfinyl precursor route, whereas the PTV-type polymers have been prepared *via* the dithiocarbamate precursor route. In this chapter also the both IR vibrational frequencies in the neutral state and those obtained during the p-doping process of selected PPV derivatives will be compared with frequencies obtained from *ab initio* calculations, which have been performed in cooperation with Professor M. Deleuze (Hasselt University).

4.2 In situ UV-Vis-NIR Spectro-Electrochemistry

4.2.1 Introduction

Electrochemical oxidation and reduction of conjugated polymers lead to the formation of charge carriers, such as positive/negative polarons and bipolarons (radical cations/anions), delocalized along the polymer chain. These charge carriers exhibit peculiar electronic, vibrational and charge transport properties²⁵. The polarons and bipolarons induce new electronic levels within the polymer π - π^* energy gap (band gap) and usually lead to an insulator-to-metal transition at a critical doping level. The oxidation and reduction processes involving the formation of positive and negative charge carriers in conjugated polymers are described, in analogy to inorganic semiconductors, as p- and n-doping processes, respectively.

A powerful and convenient approach to couple spectroscopic methods with electrochemical experiments is based on *in situ* spectro-electrochemistry. It appears that the possible optical transitions mentioned in the discussion of charge carriers in conjugated polymers in chapter 1, can be readily observed by the absorption of visible and infrared light. These optical measurements are performed during the electrochemical processes and are therefore referred to as '*in situ*'. Upon electrochemical doping, absorption features of the neutral polymer are reduced and polaronic transitions, which are markedly red shifted as compared to the initial band, appear. The start of the bleaching of the main absorption band in the visible spectrum potentially gives additional confirmation of the onset values determined with cyclic voltammetry.

4.2.2 Experimental

The *in situ* UV-Vis-NIR spectro-electrochemical measurements have been carried out with a conventional three-electrode spectro-electrochemical cell (figure 4-2). The employed electrochemical cell consists of a quartz cuvette with 1 cm path length. An Indium-Tin Oxide (ITO) coated glass has been used as working electrode, an Ag wire as reference electrode and a Pt wire as counter electrode. The Ag quasi reference electrode was calibrated with ferrocene. The reduction potential of ferrocene is located at 4.662 V vs. Vacuum. The electrolyte solution is 0.1 mol/L TBAPF₆ in anhydrous CH₃CN for thin film spectro-electrochemical measurements and 0.1 mol/L TBAPF₆ in anhydrous CH₂Cl₂ for solution spectro-electrochemical measurements. All measurements were performed under a nitrogen atmosphere. The *in situ* UV-Vis-NIR absorption spectra were recorded using a VARIAN CARY 500 UV-Vis-NIR spectrophotometer (scan rate: 600 nm/min) in the wavelength range of 300 nm to 2600 nm. The required potentials for oxidation/reduction have been applied with Eco Chemie Autolab PGSTAT 20 Potentiostat/Galvanostat. For thin film measurements, each of the polymers was coated onto an ITO coated glass substrate from a CHCl₃ solution (5 mg/mL).

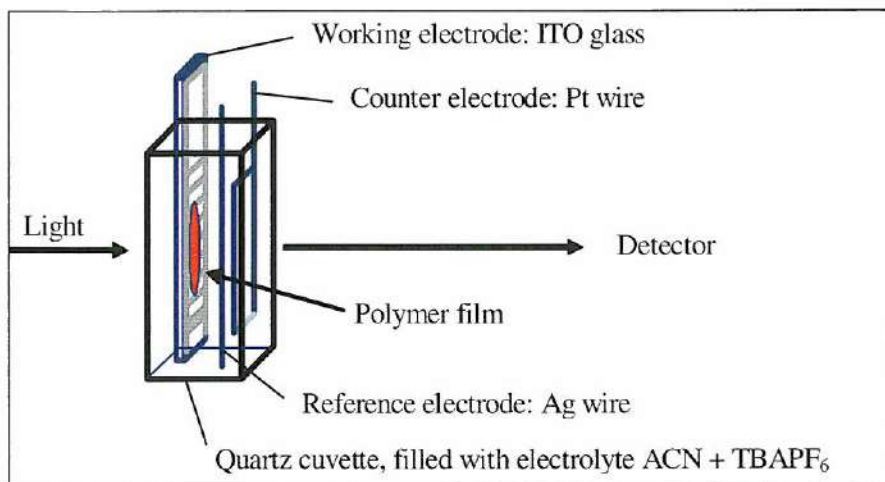


Figure 4-2: *In situ UV-Vis-NIR spectro-electrochemical cell*

4.2.3 *In Situ* UV-Vis-NIR Spectro-Electrochemistry of MDMO-PPV

✓ *Electrochemical doping of MDMO-PPV film*

MDMO-PPV polymer has been coated onto an ITO coated glass substrate and optical absorption spectra have been recorded during the electrochemical p-doping of the resulting polymer film. Figure 4-3 shows the optical absorption spectra of MDMO-PPV at different potentials during oxidation. Before the application of a bias to the ITO electrode, a typical absorption is observed at 509 nm (2.44 eV). This band is the π - π^* transition associated with the neutral polymer, which is correlated to the average conjugation length in the polymer chain and to the degree of delocalization of the π -electrons (*cf.* chapter 3). In the neutral state, MDMO-PPV has an orange color. In addition, to the π - π^* transition, on ITO substrates also two broad additional absorption features can be seen at 891 and 1232 nm, which are not observed on, for example, non-conductive quartz substrates. It is believed that these features are associated with (partial) charge transfer phenomena between

the ITO substrate and the conjugated polymer. When the applied voltage reaches a potential of 0.7 V vs. the Ag reference electrode, the p-doping process of MDMO-PPV commences, *i.e.* oxidation of the polymer film occurs. The electrochemical doping of the MDMO-PPV film results in bleaching of the π - π^* transition with a simultaneous growth of two broad bands around 809 nm (1.53 eV) and 1917 nm (0.65 eV). This oxidation process can also visibly be observed, since the color of the film turned green upon electrochemical doping. At a potential of 1 V vs. Ag, the p-doping process is complete and the color of the polymer film becomes deep blue.

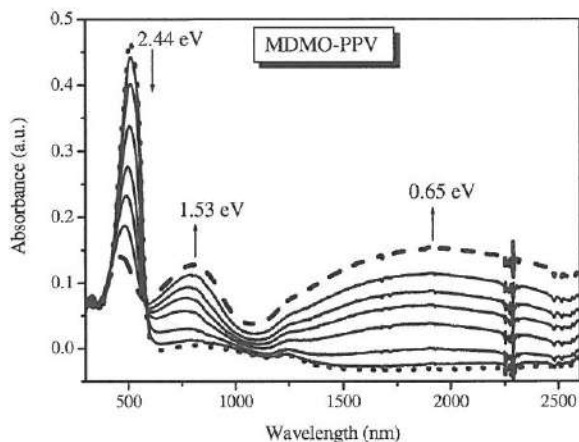


Figure 4-3: UV-Vis-NIR spectro-electrochemistry of a thin film of MDMO-PPV in the potential window 0 V to 1 V vs. Ag.

(dotted line: neutral state, dashed line: state with the highest doping level)

The two new doping bands at 1.53 eV and 0.65 eV are due to two new polaronic electronic transitions induced upon p-doping. As mentioned in chapter 1, during the p-doping process new charge carriers, *i.e.* polarons (radical cation) and/or bipolarons (spinless cation) are created together with two new electronic states in the π - π^* band gap of the polymer. The previously discussed schematic band structure diagram is repeated in figure 4-4. The dotted arrows indicate new possible optical transitions, independent whether they are allowed by symmetry or not.

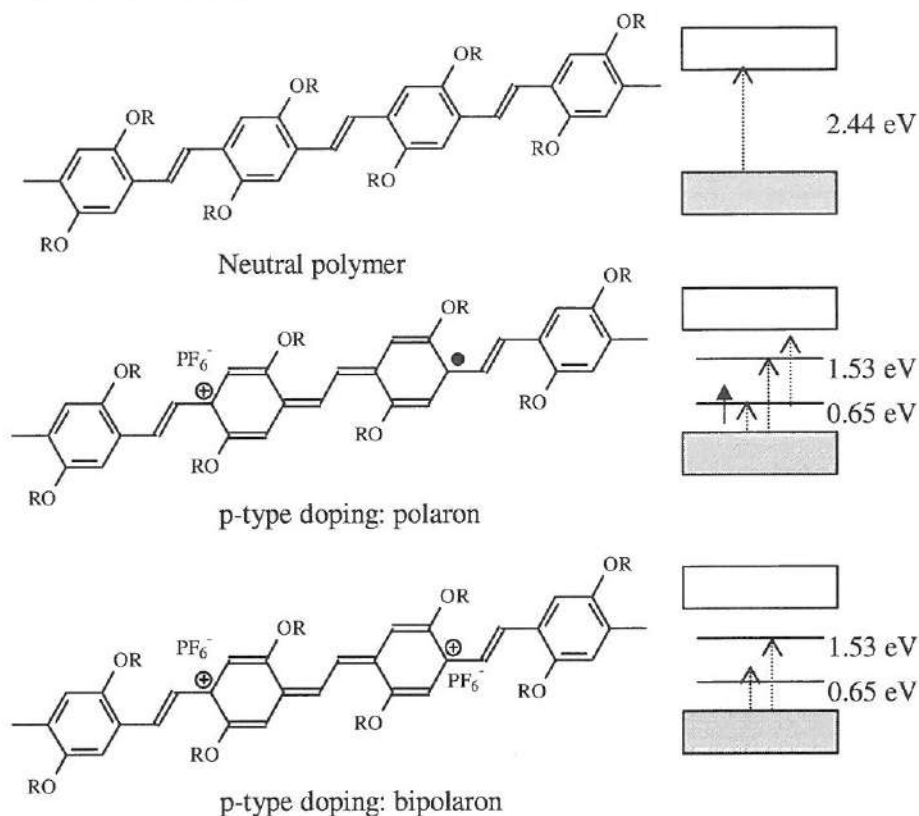


Figure 4-4: Polaron and bipolaron structures as observed in poly(*p*-phenylene vinylene) and the corresponding electronic states in the band gap.

Dotted arrows indicate possible optical transitions to and from the mid-gap states.

In theory, only transitions for levels with an odd parity to levels with an even parity in the wave function or *vice versa* are allowed. The parity of the wave function is alternating with every energy level. The absorption band observed at 0.65 eV is an allowed transition from the valence band to the first new electronic state. However, the transition at 1.53 eV from the new electronic state to the conduction band or from the valence band to the second electronic state should not be allowed. Apparently, there is considerable disorder in the polymeric material and as a result this transition is no longer entirely forbidden. However, the somewhat lower intensity may well reflect these parity issues. It can be observed

that the distance between the valence band and the first new electronic state is almost equal to the distance from the second new electronic state to the conduction band. Hence, it can be concluded that the two absorption bands observed in figure 4-3 represent the creation of stable polarons and/or bipolarons as illustrated in the band structure diagram of figure 4-4.

✓ *Electrochemical doping of MDMO-PPV in solution*

It is also possible to dope the conjugated polymers electrochemically in solution. In this way, the behavior of the solvated but otherwise isolated conjugated polymers can be compared with the solid state case in which the conjugated polymers have significant interactions with neighboring polymers. Figure 4-5 shows the UV-Vis-NIR absorption spectra of MDMO-PPV in dichloromethane solution in the potential window 0 V to 0.85 V vs. the Ag reference electrode. The spectra have been registered after reaching equilibrium at a given potential.

Before the application of the positive bias to the ITO electrode, only the absorption band at 506 nm (2.45 eV) is observed, which is associated with the π - π^* transition of the neutral polymer. This transition is similar to that observed for the thin film of MDMO-PPV coated on an ITO glass substrate. Figure 4-5 shows that the oxidation of MDMO-PPV in CH_2Cl_2 solution also leads to the formation of two new absorption bands. The first band is located at 790 nm (1.56 eV) and the second band is very broad with a maximum in the range 1250-2600 nm dependent on the doping level. The presence of these bands confirms that the formation of polarons and/or bipolarons also occurs in solution. It is noteworthy that in contrast to the thin film measurements no distinct maximum is observed for the second doping band. This is possibly a result of the fact that in solution the polymer chains are more flexible and an additional broadening of the electronic states occurs. The polymer is fully doped at a potential of 0.85 V vs. Ag at which the original π - π^* -transition transition has mostly disappeared.

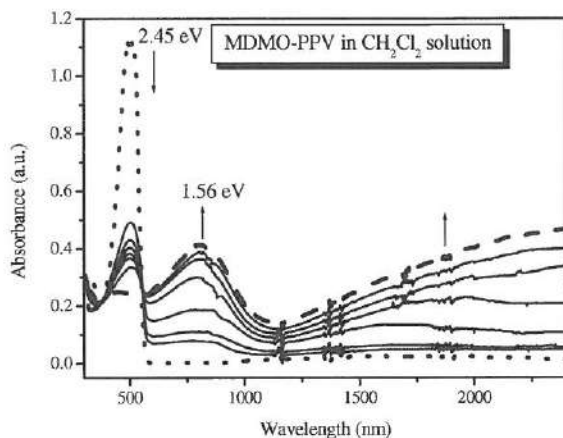


Figure 4-5: UV-Vis-NIR spectro-electrochemistry of a CH_2Cl_2 solution of MDMO-PPV in the potential window 0 V to 0.85 V vs. Ag.

(Dotted line: neutral state, dashed line: state with the highest doping level)

✓ Chemical doping of the MDMO-PPV film

The transition from semi-conducting (undoped) into a conducting (doped) state can not only be performed electrochemically but also chemically²⁶. For example, p-doping can be performed chemically by using oxidants such as H_2SO_4 , FeCl_3 , I_2 etc.^{16, 27} It is of interest to compare the chemical doping with the previously discussed electrochemical processes. To this end the chemical oxidation of MDMO-PPV was carried out in two different ways: by dipping the polymer film in a $\text{FeCl}_3/\text{CH}_3\text{CN}$ solution and by exposing the film to I_2 vapor. The doping process was followed with UV-Vis-NIR absorption spectroscopy. After doping, the polymer was dedoped by exposing it directly to air.

The thin film absorption spectra of the chemical doping processes of MDMO-PPV are displayed in figure 4-6. The absorption spectra of MDMO-PPV obtained *via* chemical doping exhibit the same general trends as those obtained with spectro-electrochemistry. In the neutral state, the π - π^* transition is observed at 509 nm

(2.44 eV). After submersion of the polymer film into FeCl_3/ACN solution or exposing it to the I_2 vapor, two doping bands at 824 nm (1.50 eV) for both doping processes and 2217 nm (0.56 eV) for doping with FeCl_3/ACN and 807 nm (0.65 eV) for doping with I_2 vapor are observed and the π - π^* transition peak has mostly disappeared. Before doping the MDMO-PPV film is orange, whereas the doped film is blue. This is the same color as observed for fully electrochemically doped MDMO-PPV films. After dedoping by exposing to air, the film returns to its original orange color. The two doping bands in the absorption spectra correspond to the transitions due to polaronic and/or bipolaronic charge carriers. The peaks observed at 0.56 eV and 0.65 eV represent transitions from the valence band to the first new electronic state and the transition of 1.50 eV from the second new electronic state to the conduction band or from the valence band to the second new electronic state. The positions of the bands in the thin film absorption spectrum obtained *via* chemical doping and electrochemical doping of MDMO-PPV are essentially the same. The main advantage of electrochemical doping as opposed to the chemical method is the control of the doping level. This can easily be done electrochemically *via* the applied voltage giving highly reproducible results. In contrast, with chemical doping attempts to reach intermediate doping levels often result in inhomogeneous and poorly controlled doping.

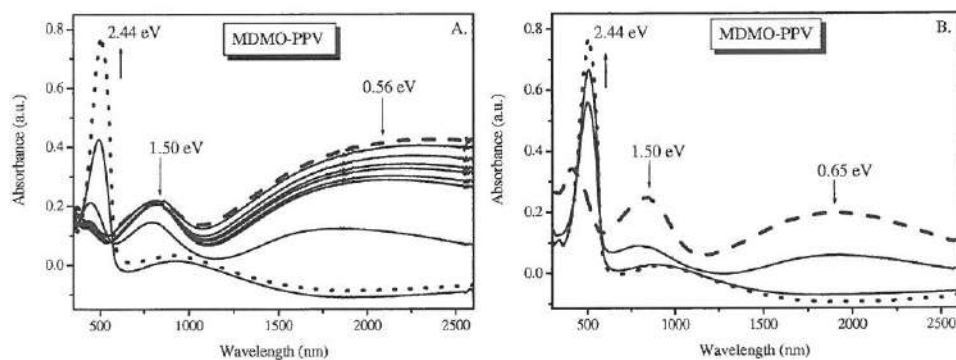


Figure 4-6: UV-Vis-NIR spectroscopy of a thin film of MDMO-PPV film upon exposure to oxidizing agents (A: FeCl_3 in acetonitrile; B: I_2 vapor) (Dotted line: neutral state, dashed line: state with the highest doping level)

4.2.4 In Situ UV-Vis-NIR Spectro-Electrochemistry of MTEM-PPV and BTEM-PPV

✓ *Electrochemical doping of MTEM-PPV and BTEM-PPV in solution*

As mentioned in chapter 2, MTEM-PPV and BTEM-PPV are conjugated polymers with one or two oligo(oxyethylene) side chains attached onto the phenylene ring. The influence of the variation of the polarity of the side chains, *i.e.* oligo(oxyethylene) and alkyl substituents, on the doping characteristics has been examined. It should be noted that it has not been possible to perform the thin film doping measurements for MTEM-PPV and BTEM-PPV. The oligo(oxyethylene) side chains make these polymers highly soluble and as a result they are also partially soluble in acetonitrile, which is used for the electrolyte solution. Therefore, the electrochemical doping has been performed in solution with MTEM-PPV and BTEM-PPV being dissolved in dichloromethane/TBAPF₆.

In figure 4-7, the evolution of the electronic spectra are compared for both PPV derivatives in a CH₂Cl₂ solution during the p-doping process. With increasing potential, two new bands can be observed with a concomitant decrease of the π - π^* transition, which is situated around 2.55 eV for this type of polymers. The maximum energy of the first doping band is 1.56 eV for both polymers. There is no maximum observed for the second doping band. This behavior is similar to that of solutions of MDMO-PPV (*vide supra*). As shown in figure 4-7, the π - π^* transition does not fully disappear when the potential is increased. Apparently, it is not possible to dope MTEM-PPV and BTEM-PPV fully. In addition, the doping bands of MTEM-PPV and BTEM-PPV are smaller than the bands observed for MDMO-PPV. Evidently, the doping process is more difficult when the polymer has oligo(ethylene oxide) side chains. This is reflected in the fact that the doping bands of BTEM-PPV, which has two oligo(ethylene oxide) side chains, have the lowest intensity. Possibly this is a result of the fact that due to a different solvation of the polymer chains, the charge transfer process at the electrodes is to some degree hampered and an overpotential is necessary to achieve doping.

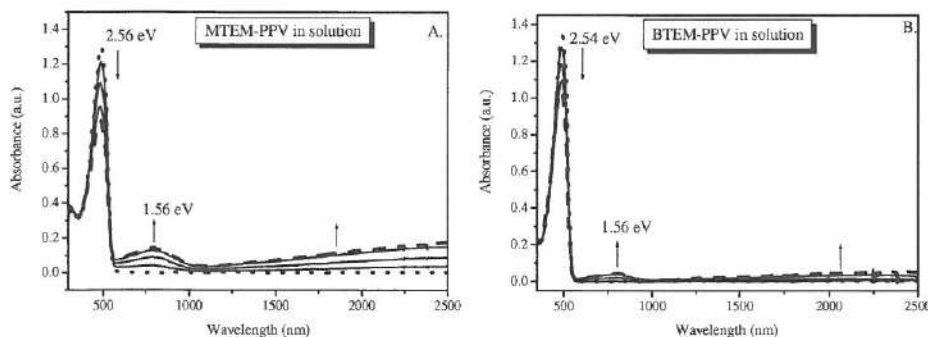


Figure 4-7: UV-Vis-NIR spectro-electrochemistry a $\text{CH}_2\text{Cl}_2/\text{TBAPF}_6$ solution of

A. MTEM-PPV in the potential window 0 V to 1.80 V vs. Ag

B. BTEM-PPV in from the potential window 0 V to 0.75 V vs. Ag

(Dotted line: neutral state, dashed line: state with the highest doping level)

✓ Chemical doping of MTEM-PPV and BTEM-PPV

Chemical doping of a thin film of the polar PPV derivatives with FeCl_3/ACN is not possible, because both polymers are partially soluble in acetonitrile. For that reason, MTEM-PPV and BTEM-PPV polymers can only be chemically doped by exposing the polymer film to I_2 vapor (figure 4-8). Before doping, as usual only the π - π^* absorption band is observed. After exposing the polymer films to I_2 vapor, the doping of the polymer films starts. The formation of two new absorption bands is clearly visible. They are positioned at 834 nm (1.49 eV) and 1940 nm (0.64 eV) for MTEM-PPV and at 806 nm (1.54 eV) and 2036 nm (0.61 eV) for BTEM-PPV. These bands confirm the formation of polarons and/or bipolarons upon doping. There is also an absorption observed below 400 nm. However, this transition is not associated with the polymer but a result of traces of I_2 . After exposing the doped film to air, no I_2 is present anymore. When the polymers films are dedoped by exposing to air, the two doping bands decrease in intensity and the π - π^* absorption band becomes again more pronounced. From these measurements it can be seen that thin film chemical doping is more readily achievable than electrochemically

doping in solution. This is as expected, since in this case no charge transfer processes at an electrode interface take place.

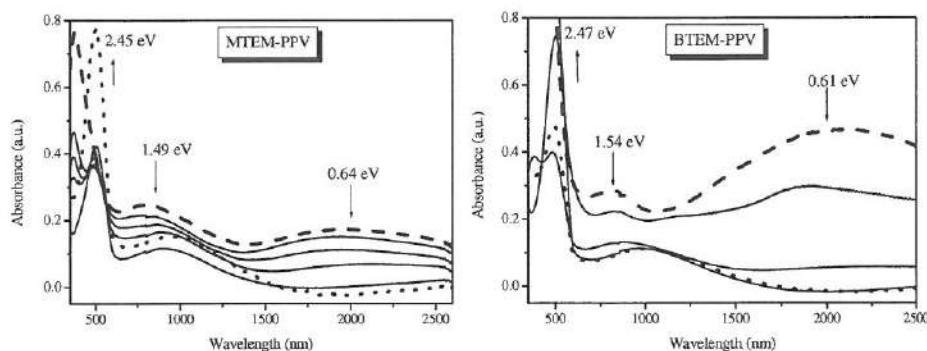


Figure 4-8: UV-Vis-NIR spectroscopy of thin films of MTEM-PPV and BTEM-PPV upon chemical doping with I_2 vapor and dedoping by exposure to air.
(Dotted line: neutral state, dash line: state with the highest doping level)

4.2.5 In Situ UV-Vis-NIR Spectro-Electrochemistry of NTEM-PPV

✓ Electrochemical doping of a thin film of NTEM-PPV

Since NTEM-PPV is not soluble in acetonitrile, this polymer can be investigated with thin film spectro-electrochemical measurements. In this way, at least one PPV-derivative with a polar side chain has been studied in this manner. Figure 4-9 shows a representative selection of UV-Vis-NIR spectra of NTEM-PPV during the electrochemical oxidation of the polymer. Before voltage was applied to the ITO electrode, as usual only the π - π^* transition associated with the neutral polymer is observed. In addition, the previously discussed broad absorption band at 1019 nm (1.22 eV) can be seen, which is associated with charge-transfer phenomena between PPV-type polymers and ITO substrates. When the applied voltage reaches 0.70 V vs. Ag, the bands, which are associated with the polarons and/or bipolarons become apparent, *i.e.* a band at 781 nm (1.59 eV) and another very broad band in

the NIR-range of the absorption spectrum with a maximum around 1911 nm (0.65 eV). Upon further oxidation by increasing the applied voltage, both (bi)polaron bands increase gradually in intensity. Concomitantly the band associated with the π - π^* transition decreases in intensity. The obtained results do not significantly differentiate from the other studied PPV-derivatives. Hence, it can be concluded that the polar side chains do not have a significant impact on the type of charge carriers formed upon doping.

In chapter 2, the cyclic voltammogram of NTEM-PPV has been discussed (figure 2-14) and it has been demonstrated that it is possible to oxidize the polymer (p-doping) and reduce the polymer (n-doping). Therefore also the n-doping process, *i.e.* reduction of the polymer film by decreasing the electrode potential, was studied by UV-Vis-NIR spectro-electrochemical measurements. The spectra was recorded at only one potential (-1.45 V vs. Ag; Figure 4-10). More stepwise scanning is not possible because it appears that under the experimental conditions employed the negative polarons and/or bipolarons are insufficiently stable.

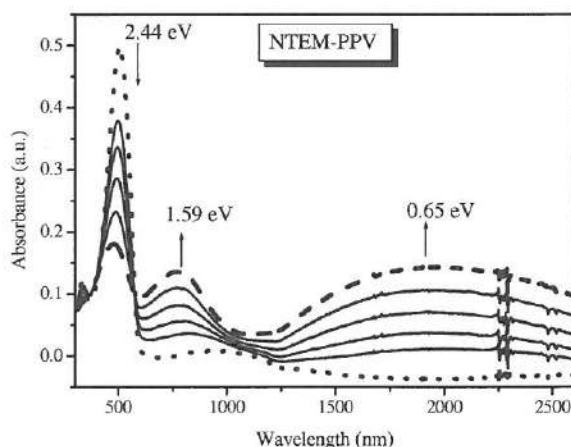


Figure 4-9: UV-Vis-NIR spectro-electrochemistry of a thin film of NTEM-PPV in the potential window 0 V to 0.90 V vs Ag.

(Dotted line: neutral state, dashed line: state with the highest doping level)

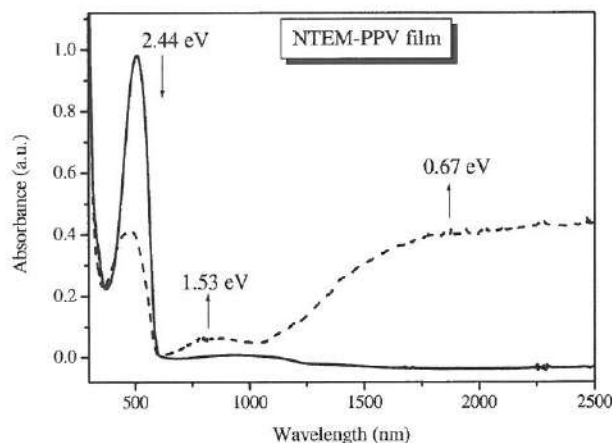


Figure 4-10: UV-Vis-NIR spectro-electrochemistry of a thin film of NTEM-PPV at 0 V and -1.45 V vs. Ag. *N*-doping occurs.

(solid line: neutral state, dashed line: state with the highest doping level)

During the *n*-doping process, negative polarons and/or bipolarons are formed (figure 4-11) and two new electronic states are created in the π - π^* band gap. The process is similar to that previously described for *p*-doping. Two doping bands are observed in the UV-Vis-NIR spectrum, which are associated with the two possible electronic transitions. The transition of 0.67 eV is the transition from the second new electronic state to the conduction band. This transition is allowed. The band at 1.53 eV is the transition from the first new electronic state to the conduction band. This transition is in theory not allowed but is still visible as a result of the disorder of the polymer chains in the film. However, its intensity is significantly lower. When figure 4-9 (*p*-doping) and figure 4-10 (*n*-doping) are compared, we can see that the positions of the doping bands are very similar. This can be readily understand by comparing the band structure diagrams of a negative (bi)-polaron and a positive (bi)-polaron. From these diagrams it is evident that the distance between the valence band and the first new electronic state is equal to the distance between the conduction band and the second new electronic state.

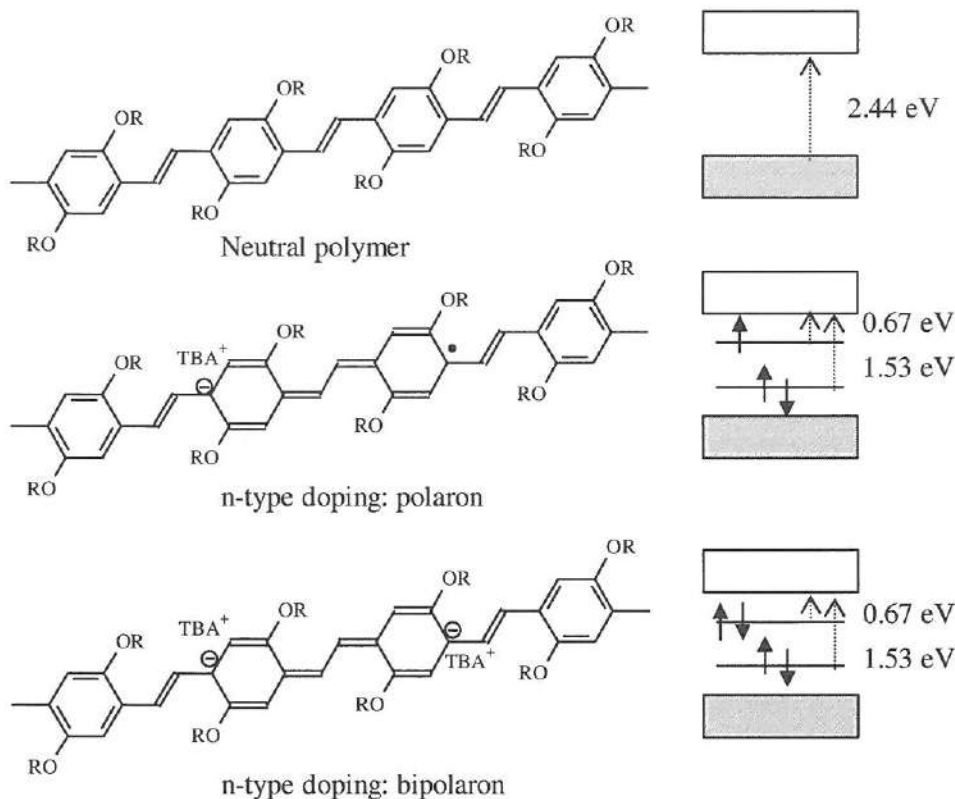


Figure 4-II: Polaron and bipolaron structures as observed in poly(*p*-phenylene vinylene) and the corresponding electronic states in the band gap. Dotted arrows indicate possible optical transitions to and from the mid-gap state.

For the other three 2,5-di-alkoxy PPV derivatives, MDMO-PPV, MTEM-PPV and BTEM-PPV, it was not possible to follow the n-doping process with UV-Vis spectroscopy. MDMO-PPV polymer has two apolar side chains attached onto the phenylene ring, which cannot complex any counter ions stabilizing charges on the conjugated backbone. This makes electrochemical doping more difficult and apparently n-doping virtually impossible. Already with cyclic voltammetry, no distinct reversible n-doping processes were observed for this polymer (*cf.* chapter 2). Furthermore, MTEM-PPV and BTEM-PPV are partially soluble in acetonitrile,

which is used for the electrolyte solution. Therefore, the electrochemical n-doping in a thin film of these two polar PPV-derivatives is also not achievable.

✓ Electrochemical doping of NTEM-PPV in solution

In the same manner as the three other PPV derivatives, it is also possible to dope NTEM-PPV electrochemically in a dichloromethane solution (figure 4-12). Before applying a voltage, the π - π^* transition peak is observed at 495 nm (2.51 eV). During the oxidation process of NTEM-PPV, two new doping bands appear. The most pronounced one is at a wavelength of 796 nm (1.56 eV) and the other one is extremely broad covering most of the NIR range, extending from 1100 nm to well over 2600 nm. There is no maximum observed for the second doping peak. This was also the case for the other three PPV derivatives during electrochemical doping in solution. Similar to other polar PPV-derivatives, the electrochemical doping process in dichloromethane solution does not result in a full doping of the conjugated polymers, *i.e.* the π - π^* transition remains visible.

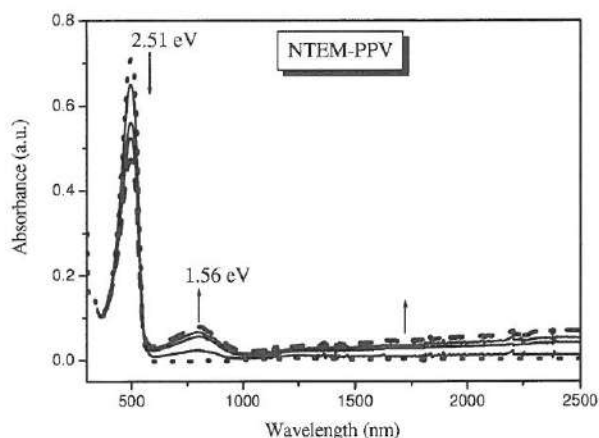


Figure 4-12: UV-Vis-NIR spectro-electrochemistry of a CH_2Cl_2 solution of NTEM-PPV in the potential range 0 V to 1 V vs. Ag.

(Dotted line: neutral state, dashed line: state with the highest doping level)

✓ *Chemical doping of NTEM-PPV film*

Finally, also for NTEM-PPV it is possible to achieve chemical doping. NTEM-PPV coated on an ITO glass has been chemically p-doped *via* two different, *viz.* by submersion of the film in a FeCl_3/ACN solution or by exposing the polymer film to I_2 vapor (figure 4-13). The same behavior is observed as was previously found for the other PPV-type polymers.

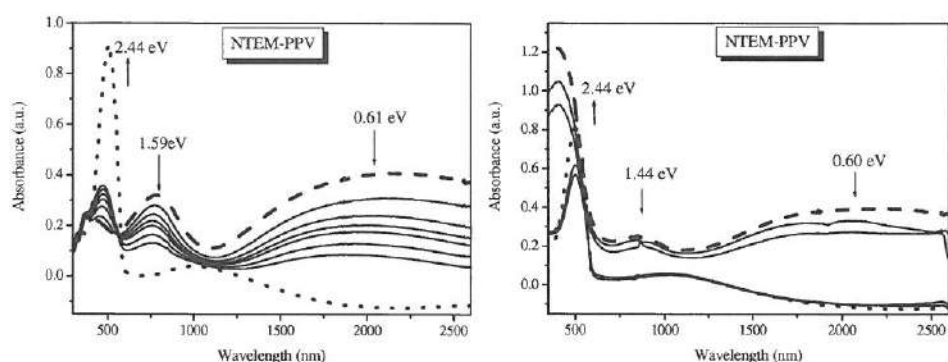


Figure 4-13: UV-Vis-NIR spectroscopy of a thin film of NTEM-PPV upon exposure to oxidizing agents (A: FeCl_3 in acetonitrile; B: I_2 vapor)
(Dotted line: neutral state, dashed line: state with the highest doping level)

4.2.6 In Situ UV-Vis-NIR Spectro-Electrochemistry of PTV and DiPh-PTV

✓ *Electrochemical doping of PTV and DiPh-PTV film*

The final two polymers, which are studied with *in situ* UV-Vis-NIR spectro-electrochemistry, are non-substituted PTV and poly(3,4-diphenyl-2,5-thienylene vinylene) (DiPh-PTV). Both polymers are low-band gap polymers, with a band gap lower than 1.8 eV. This in contrast to the previously described PPV-type polymers. Hence, it is of interest to understand whether this low band gap character will affect the spectro-electrochemical properties.

Figure 4-14 shows the UV-Vis-NIR-spectro-electrochemistry of PTV and DiPh-PTV coated onto an ITO glass substrate. Before applying a voltage to the ITO working electrode, a typical transition at 559 nm (2.22 eV) for PTV and 557 nm (2.23 eV) for DiPh-PTV is observed, due to the interband excitation of the polymer (π - π^* transition). Also for this type of polymers an additional broad band is observed which is associated with charge transfer phenomena with the ITO substrate. The neutral polymer films have a blue color. At low doping states, the interband absorption of both polymers decreases and concomitantly a very broad band develops at longer wavelength (maximum at about 0.97 eV for PTV and 0.75 eV for DiPh-PTV). Obviously this band is associated with the upon doping generated charge carriers on the conjugated polymer backbone²⁸. This band gradually becomes larger with increasing doping level. The heavily doped films have a light yellow color.

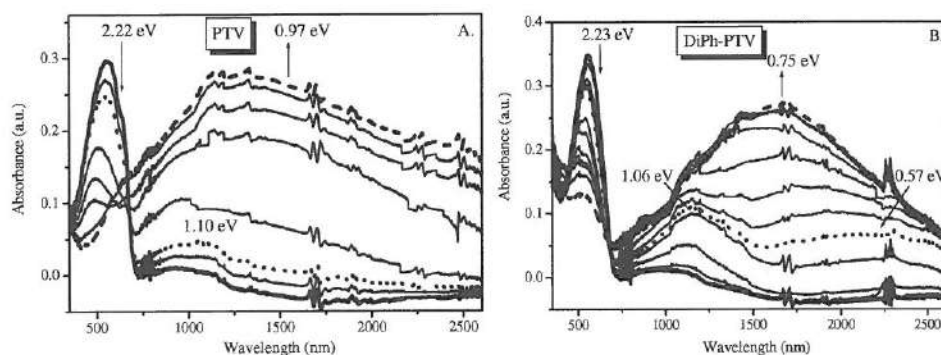


Figure 4-14: UV-Vis-NIR spectro-electrochemistry of

A. A thin film of PTV (potential window 0 V to 0.82 V vs. Ag)

B. A thin film of DiPh-PTV (potential window 0 V to 0.80 V vs. Ag)

(solid line: neutral state, dotted line: lightly doped state, dashed line: state with the highest doping level)

As seen in figure 4-14, the UV-Vis spectra of both polymers display a higher noise level than the previously discussed spectra of the PPV-type polymers. This is due to the fact that the thin films of the PTV-type polymers, which are needed for the

spectro-electrochemical measurements, have been obtained by a thermal conversion of thin films of the corresponding precursor polymers. Whereas the PPV derivatives are soluble in chloroform in their conjugated form, this is not the case for the PTV derivatives. Hence, the thickness and the purity level of the PTV films are more difficult to control.

At first sight, the UV-Vis-NIR characteristics of electrochemically doped PTV derivatives are different from those observed for the PPV-type polymers, since for the PTV-type polymers only one broad doping band is observed instead of two. However, a carefully examination of the spectra reveals that when both PTV-type polymers are lightly p-doped, two doping bands are observed (dotted line in figure 4-14). These transitions have the same (bi)polaronic origin as those observed in the PPV-type polymers. When the PTV-type polymers are more heavily doped, additional charge carriers are created. This results in a broadening of the new electronic states (figure 4-15C). As mentioned before, the band gap of PTV derivatives is comparatively small. Apparently, with increasing doping levels overlap between the new doping bands may occur (figure 4-15D). This is the origin of the fact that for heavily doped PTV-derivatives only one absorption band is observed at 0.97 eV for PTV and 0.75 eV for DiPh-PTV.

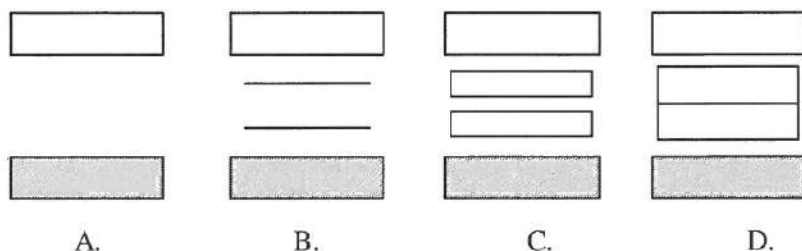


Figure 4-15: Schematic overview of the band models.

- A. Neutral polymer
- B. Lightly p-doped polymer
- C. Fully p-doped conventional conjugated polymer
- D. Fully p-doped low band gap conjugated polymer

It is worth mentioning that the electrochemical doping in solution for PTV and DiPh-PTV is obviously not possible because both polymers are insoluble in common organic solvents (chapter 2).

4.2.7 Conclusions

It is demonstrated that it is possible to dope selected conjugated polymers both chemically and electrochemically. The doping process can accurately be followed up with UV-Vis-NIR spectroscopy. For all polymers in the neutral state, only the π - π^* transition is visible. This transition can be used for the calculation of the optical band gap of a polymer (chapter 2). Electrochemical doping of the PPV and PTV derivatives film results in a reduction in intensity of the π - π^* transition. At the same time two doping bands develop at longer wavelength. The observation of the two doping induced transitions can be attributed to sub-gap transition due to the formation of polarons and/or bipolarons. For the low band gap PTV-type polymers, the doping bands overlap, when the polymer is full doped and only one broad band is observed in the UV-Vis-NIR spectrum.

A comparison of the maxima of the bands observed in the UV-Vis-NIR spectra indicates that there is no significant difference between the electrochemical and chemical doping processes. An advantage of electrochemical doping is that this doping method provides a better control over the extent of doping by adjustment of the electrode potential. Also no significant difference is observed for the solution and thin film doping processes. The only observation which can be made is that for the solution doping processes more broad doping bands are observed, possibly due to the absence of ordering phenomena, which are usually present in polymer films. Finally it is noteworthy that the measurements on the series of PPV-type polymers with side chains with different polarities reveal that the polarity, of these side chains has no significant impact on the spectro-electrochemical properties. Apparently, also in this case the conjugated polymer opto-electronic properties are

determined by the polymer backbone (and substituents which have a direct electronic effect on this backbone).

4.3 In Situ ATR-IR Spectro-Electrochemistry

4.3.1 Introduction

✓ *Attenuated Total Reflectance Spectroscopy*

A further technique, which can be used to provide valuable information related to the chemical structure of polymer films is known as internal reflection spectroscopy or attenuated total reflectance (ATR) spectroscopy. This technique is based on the propagation of infrared radiation through an infrared transmitting crystal (internal reflection element) and the reflection at the interface between the internal reflection element and the medium in contact with it. To this end, the sample material is coated or pressed onto the transmitting crystal. Suitable materials for the internal reflection element are silverchloride, thalliumhalide, zinc selenide or germanium. These materials typically have a high refractive index.

During the measurement, the infrared radiation from the spectrometer enters a trapezoidal crystal and is reflected several times at the surfaces of this crystal. During these reflections, the IR beam penetrates slightly into the sample. This penetration is called 'the evanescent wave' and is typically at a depth of a few micrometers. The internal reflection is conventionally called 'total' when the angle of incidence beam exceeds the so-called critical angle. After several reflections, the infrared beam is directed out of the crystal and back into the normal beam path of the spectrometer (figure 4-16). During its passage through the crystal, the infrared beam may undergo as many as 10-20 reflections. The intensity of the infrared beam is reduced (attenuated) by the sample in the spectral regions where the sample absorbs. It is this unique physical phenomenon that enables one to obtain infrared spectra of samples placed in contact with the internal reflection element.

✓ *In Situ ATR-IR Spectro-Electrochemistry*

In situ ATR-IR spectro-electrochemistry is a technique that can be used to visualize certain polaron and/or bipolaron transitions in the IR region during the doping process of a conjugated polymer. Not only these transitions become visible, but also new intense characteristic vibrational modes, the so-called infrared active vibration (IRAV) modes, appear when the polymer is in the doped state. These characteristic IRAV bands are situated between 1600 cm^{-1} and 700 cm^{-1} and potentially provide structural and electronic information about the conjugated polymer under investigation. However, a full interpretation and assignment of the IRAV bands is not always possible. Usually the IRAV bands are accompanied by a broad IR absorption band at a higher energy. This band has the same origin as the ones previously described in the section on UV-Vis-spectro-electrochemistry and are associated with the transitions related to the additional electronic levels created in the band gap by the doping process.

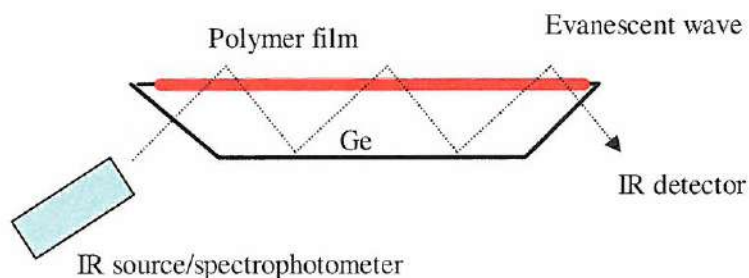


Figure 4-16: Attenuated total reflectance (ATR) of a polymer film on a germanium crystal

In the literature, several theoretical models have been developed to explain the IRAV bands, which are the spectral signatures of the charge carriers generated by the doping process. For example, the change in the charge density wave associated with the vibrational motion of the polymer backbone has been considered.^{29, 30} and a 'pinning parameter' as a quantification of the localization of the charges has been introduced. Furthermore, the IRAV bands have been explained by the IR activation

of the Raman active Ag modes in the pristine form of the polymer due to the local breaking of the symmetry around the charge carrier.³¹ In this model, the high intensity of the IRAV bands is explained by the large variation of the electric dipole momentum associated with the oscillation of the charge defects.^{17, 30, 32, 33}

4.3.2. Experimental

The infrared spectra were recorded using a Bruker IFS 66/S FT-IR spectrometer (resolution 20 cm^{-1} , 100 scans). Attenuated total reflection (ATR) FT-IR absorption spectra were recorded *in situ* during electrochemical potential measurements. The electrochemical equipment consisted of a galvanostat / potentiostat AUTOLAB PGSTAT 20 from Ecochemie. IR spectra are gathered at constant potential every 100 mV of a potential cycle starting at 0 V. The spectro-electrochemical measurements were carried out in a home-built small size ATR spectro-electrochemical three electrode cell made from Teflon (Figure 4-17). The central part of this method is a slightly n-doped germanium reflection element, which acts both as a wave-guide for the IR beam and as the working electrode. The Ge element was cleaned before the measurements by polishing. The counter electrode is a Pt gaze and the reference electrode is the same as for *in situ* UV-Vis-NIR spectro-electrochemistry, namely an Ag wire.^{32, 34, 35} The electrolyte solution was 0.1 M tetrabutylammonium- hexafluorophosphate (TBAPF₆) in anhydrous acetonitrile. The electrochemical cell was kept under nitrogen atmosphere to exclude moisture and oxygen during the electrochemical processes. All experiments were performed at room temperature. To visualize the specific spectral changes during the electrochemical doping, an IR spectrum just before the considered doping process was chosen as a reference. The subsequent spectra were compared to this spectrum.

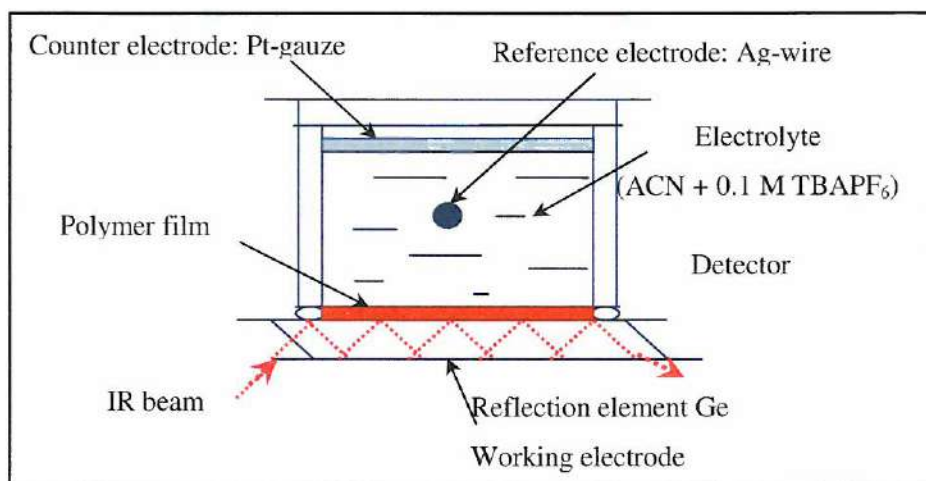


Figure 4-17: In situ ATR-IR spectro-electrochemical cell

4.3.3 In Situ ATR-IR Spectro-Electrochemistry of PPV

✓ Before doping

In the ATR-IR spectrum of neutral PPV a large number of bands is present. The strongest vibrations correspond to out-of-plane modes, with the induced dipolar moments being particularly strong (Figure 4-18, table 4-1). In this chapter, an attempt will be made to assign the infrared bands based on literature sources³⁶ and theoretical calculations.

Out-of-plane vibrations (cf. table 4-1)

In a substituted benzene ring, the C-H out-of-plane bending vibrations give rise to bands in the region 1000-700 cm⁻¹. In the case of PPV, this band appears at 834 cm⁻¹. This is the in-phase out-of-plane C-H bending for *para* substituted benzene.³⁶ The intense peak at 960 cm⁻¹ is due to the out-of-plane vibration of C-H of the *trans* vinylene double bond. This peak is typical for *trans* substituted olefins^{36 37,}

³⁸

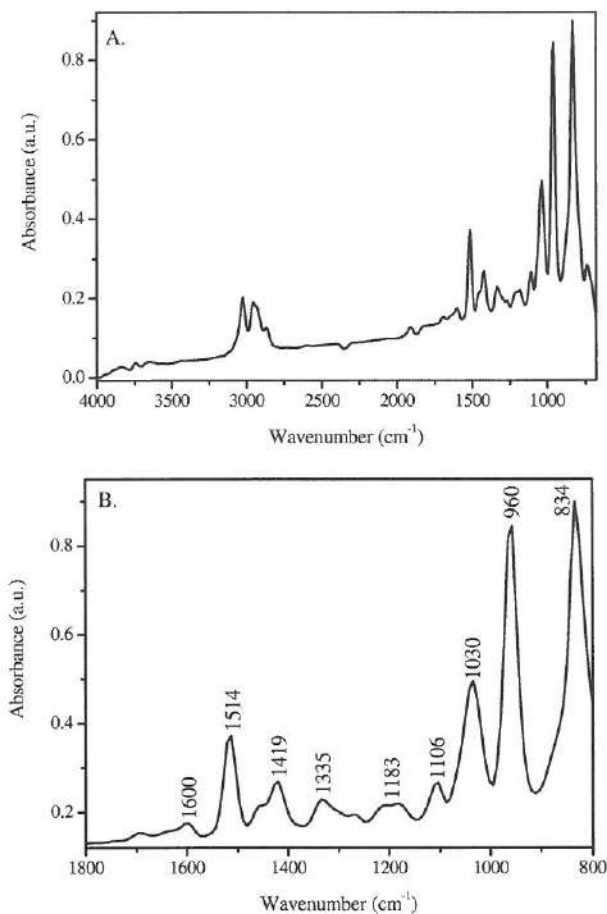


Figure 4-18: IR-spectrum of neutral PPV (top: full spectrum; bottom: enlargement)

In-plane vibrations (cf. Table 4-1)

The 1600 cm⁻¹ region

The weak vibration at 1600 cm⁻¹ mainly involves “*quadrant stretching*” of the ring C=C bonds. When a carbon moves tangentially clockwise, its hydrogen moves counterclockwise to some extent, but the vinylene double bond are nearly motionless. In benzene, the *semicircle stretching* of the carbon ring mixes strongly with C-H in plane bending. The vibration when a carbon moves tangentially clockwise and its hydrogen moves counterclockwise is observed at 1514 cm⁻¹.

When the hydrogen moves clockwise with its carbon, the semicircle stretching appears at 1419 cm^{-1} .³⁶ The peak at 1335 cm^{-1} is the vibration of the C-H bonds of the trans vinylene double bond, the C-H bonds rotate oppositely.

PPV (cm^{-1})		Assignment
834	vs	<i>p</i> -phenylene-ring C-H out-of-plane bend
960	vs	<i>trans</i> -vinylene C-H out-of-plane bend
1030	s	<i>p</i> -phenylene C-H in-plane bend (2,3 vs. 5,6)
1106	vw	<i>p</i> -phenylene C-H in-plane bend (2,6 vs. 3,5)
1183	vw	<i>p</i> -phenylene C-H in-plane bend (2,5 vs. 3,6)
1335	vw	<i>trans</i> -vinylene C-H in-plane bend
1419	m	semi circle C-C ring stretching
1514	m	semi-circle C-C ring stretching
1600	vw	quadrant C=C ring stretching

Table 4-1: IR bands of neutral PPV. Numbers are wavenumbers (cm^{-1}),
vs, very strong; s, strong; m, medium; w, weak; vw, very weak

The 1300-1000 cm^{-1} CH wag bands region

In the infrared spectrum, there are usually a number of medium-to-weak sharp bands in the $1300\text{-}1000\text{ cm}^{-1}$ region many of which involve in-plane C-H bending vibrations sometimes strongly mixed with C-C vibrations. The vibrational peak at 1030 cm^{-1} is a result of the C-H wag of the hydrogen of 2nd and 3th position with the 5th and 6th position (figure 4-19). The vibrational description of (2,3 versus 5,6) means that the 2th and 3th hydrogens tend to move clockwise while the 5th and 6th hydrogen tend to move counterclockwise. The peak at 1106 cm^{-1} corresponds to the (2,6 versus 3,5) C-H wag. Finally, the peak at 1183 cm^{-1} is the C-H wag with the

hydrogens at 2,5 versus 3,6.^{20 36} It should be noted that the above results are comparable to the results obtained on unsubstituted PPVs by others.^{12, 20, 37, 39,40}

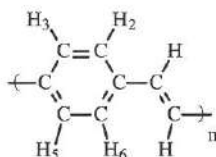


Figure 4-19: Molecular structure of PPV

✓ During *p*-doping process

Upon application of a positive bias to the conjugated polymer film, no changes were observed in the infrared spectrum until 500 mV vs. the Ag reference electrode. Therefore, the spectrum of the PPV-film recorded at 500 mV was used as the reference spectrum. At potentials higher than 500 mV, a new ATR-IR spectrum has been taken at every 100 mV step. Subsequently for each step after subtraction of the reference spectrum, the difference spectrum is obtained which only shows the infrared vibrational frequencies associated with the doped polymer, *i.e.* the spectral signatures of the polaron and/or bipolarons. This method of displaying is valid since the bands which occur upon doping have a significantly larger intensity than the bands associated with the polymer in the neutral form.

In a series of ATR-IR spectra of a thin film of PPV during the *p*-doping process two types of features can be identified (Figure 4-20). The first type is the appearance of a broad absorption band extending from 2100 cm⁻¹ to frequencies well over 4000 cm⁻¹. The second set of features comprise the previously mentioned intensive IR active vibrations (IRAV) bands, which appear in the wavenumber range 1800-700 cm⁻¹.

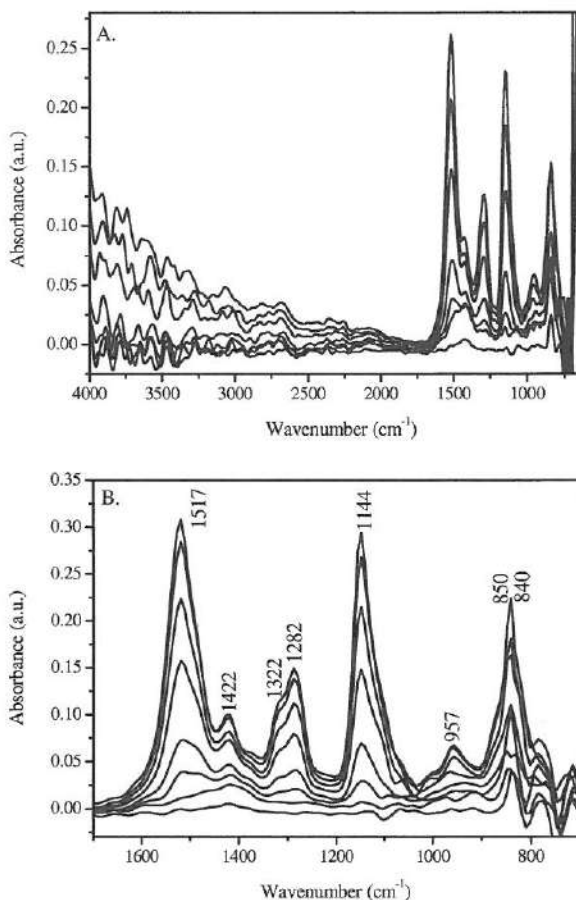


Figure 4-20: *In situ* FTIR difference spectra during p-doping of PPV
(top: full spectrum; bottom: enlargement showing IRAV bands)

The broad absorption band with a maximum around 4000 cm^{-1} (2500 nm) can be explained due to the sub-gap electronic transition due to the formation of polaronic and/or bipolaronic charged defects on the polymer chain. This broad and intense absorption band is found in most conjugated polymers in their conducting form⁴²
¹⁴ ⁴³ (figure 4-20A). This band has the same origin as those described in the previous section on UV-Vis spectro-electrochemistry.

As mentioned in the introduction, the infrared spectra of conjugated polymers in their conductive (chemically or electrochemically) states are characterized by intense infrared absorption bands (infrared active vibrations, IRAV bands), typically ranging from 1800 cm^{-1} to 700 cm^{-1} . The wavenumber range $1800\text{--}700\text{ cm}^{-1}$ of the spectra in figure 4-20A is shown in an enlarged scale in figure 4-20B. The p-doping induced IRAV bands increase in intensity with an increasing degree of oxidation of the PPV film. The positive charges which are created in the polymer chain, result in changes of the dipole moments of the vibrations. The p-doping induced IRAV effects are fully reversible. The vibrations become infrared active due to symmetry breaking and are strongly enhanced, because the charge distribution in the formed polaronic state causes large dipole moment changes during typical vibrations.^{17 30, 32, 33} Upon doping the intensities of the doping induced bands increase and some broadening occurs (figure 4-21)⁴⁴.

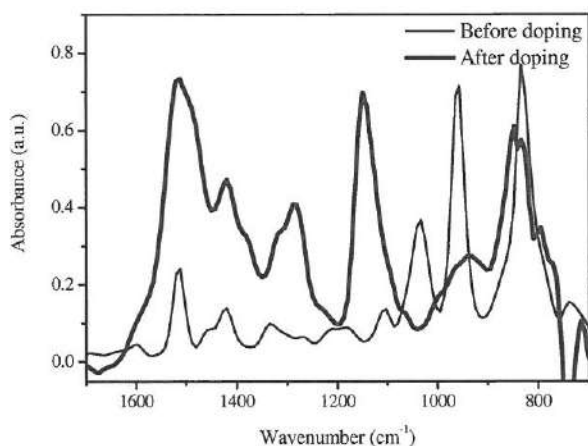


Figure 4-21: In situ ATR-FTIR spectrum before and the difference spectrum after p-doping of PPV (intensities are adjusted to enable a comparison of the spectra)

The different IRAV vibration frequencies of p-doped PPV film at 840 , 957 , 1144 , 1282 , 1322 , 1420 and 1517 cm^{-1} are absent in the spectrum of the neutral PPV-film (figure 4-18B). The strong band around 850 cm^{-1} is related to the PF_6^- electrolyte

ion which enters and leaves the polymer layer during the electrochemical reactions. The strong peak which almost coincides with this band at 840 cm^{-1} is likely due to an out-of-plane CH wag of the trisubstituted olefin,³⁸ which is a new structural element in the doped form of this polymer. It is not possible to straightforwardly assign the other IR bands of doped PPV because the radical cations during the p-doping process change the molecular structure and, as a result, other vibrations are possible. For that reason, theoretical calculations are necessary, which will be presented in the last section of this chapter.

4.3.4 In Situ ATR-IR Spectro-Electrochemistry of MDMO-PPV

✓ Before doping

In figure 4-22, the ATR-IR spectrum of a thin film of MDMO-PPV in the neutral state is shown. For comparison, also the infrared spectra of PPV and MDMO-PPV in the fingerprint region are overlaid in figure 4-23.

Out-of-plane vibrations (Table 4-2)

Both the PPV and MDMO-PPV spectra have a vibration around 960 cm^{-1} , which has been assigned to the in-phase out-of-plane vibration of C-H trans-vinylene bend.^{21, 38} MDMO-PPV has a tetra-substituted benzene with two hydrogens on position three and six, on the second and fifth position an alkoxy sidechain and on first and fourth position a trans vinylene bond. The C-H out-of-plane bending of a tetrasubstituted benzene give rise to a vibration at 854 cm^{-1} with the carbon and its hydrogen moving in opposite directions.³⁶

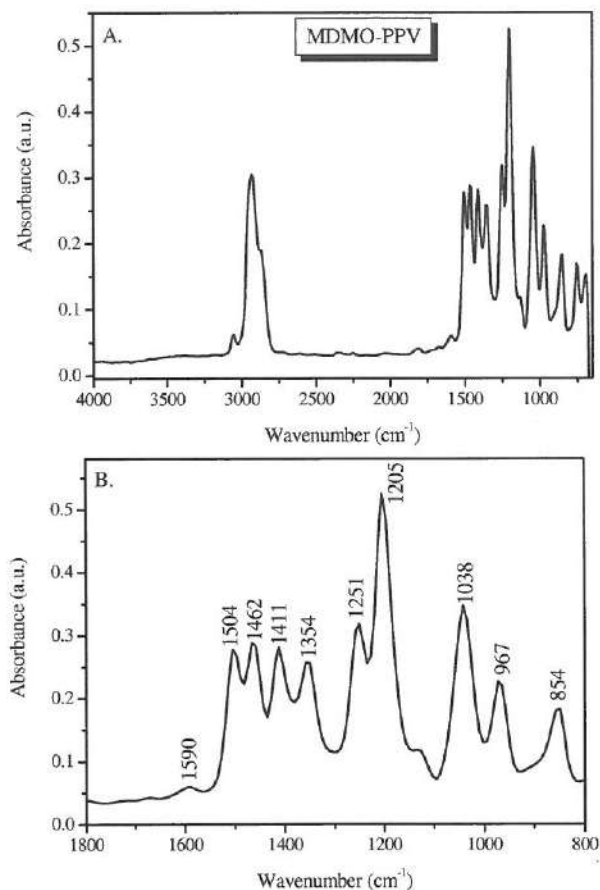


Figure 4-22: IR spectrum of neutral MDMO-PPV (top: full spectrum; bottom: enlargement).

In-plane vibrations (Table 4-2)

The 1600 cm⁻¹ region

The three vibrations at 1590, 1504 and 1411 cm⁻¹ in the MDMO-PPV can be correlated with the ring stretches at 1600, 1514, 1419 cm⁻¹ observed in PPV (table 4-1). The 1590 cm⁻¹ vibration involve the quadrant stretching of the ring C=C bonds, whereas the vibrations at 1504 and 1411 cm⁻¹ are correlated with the semicircle stretching of the carbon ring.

The 1300-1000 cm⁻¹ CH wag bands region

The vibrations at 1183, 1106 and 1030 cm⁻¹ in the spectrum of PPV arise from *para*-substituted phenylene C-H in-plane deformations. The phenylene C-H in-plane deformations in MDMO-PPV are expected to differ as compared to those in PPV, due to the fact that the MDMO-PPV phenylene ring is 1,2,4,5 tetra-substituted. While PPV lacks any strong vibrations in this region, this is an area of intense absorption for MDMO-PPV (figure 4-23). The intense peak at 1205 cm⁻¹ represents the C-H in-plane bend of the phenylene ring. The intense peak at 1354 cm⁻¹ corresponds to the in-plane vibration of the C-H bonds of trans-vinylene.

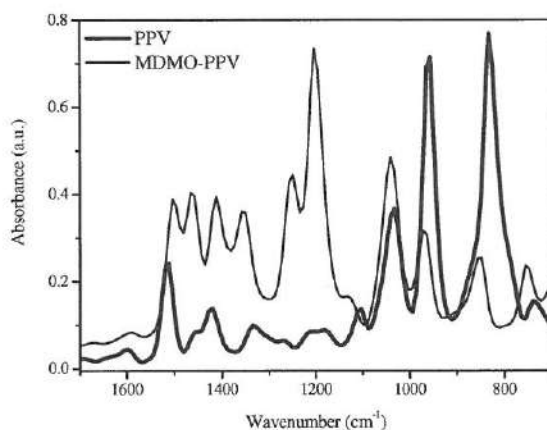


Figure 4-23: Comparison of the IR spectra of neutral PPV and MDMO-PPV.

Ether vibrations

The peak at 1462 cm⁻¹ is due to the symmetric CH₂ (alkyl) deformation of the aryl-ether-alkyl function in MDMO-PPV. Furthermore, an alkoxy chain attached to an aromatic ring usually gives rise to two correlated vibrations, in this case at 1251 cm⁻¹ and 1038 cm⁻¹. The vibration at 1251 cm⁻¹ may be looked upon as an aromatic carbon-oxygen asymmetric stretching frequency (like phenols), and the band at 1038 cm⁻¹ as the highest aliphatic carbon-oxygen asymmetric stretching frequency (like primary alcohols) ³⁸.

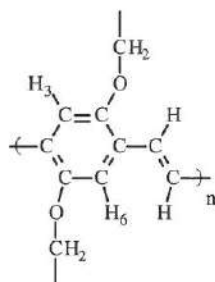


Figure 4-24: Molecular structure of MDMO-PPV

MDMO-PPV (cm^{-1})		Assignment
854	m	<i>p</i> -phenylene ring C-H out of plane bend
967	m	trans-vinylene C-H out of plane bend
1038	s	aliphatic C-O-aryl asymmetric stretch
1205	vs	<i>p</i> -phenylene C-H in-plane bend
1251	s	aromatic C-O-alkyl asymmetric stretch
1354	s	trans-vinylene C-H in-plane bend
1411	s	semi circle C-C ring stretching
1462	s	aliphatic C-O-aryl symmetric deformation
1504	s	semi-circle C-C ring stretching
1590	w	quadrant C=C ring stretching

Table 4-2: IR bands of neutral MDMO-PPV. Numbers are wavenumbers (cm^{-1}),
vs, very strong; s, strong; m, medium; w, weak; vw, very weak

✓ During *p*-doping process

Until a potential of 600 mV vs. Ag, no changes were observed in the ATR-IR characteristics of a thin film of MDMO-PPV. Therefore, the reference spectrum has been recorded at 600 mV. For comparison, also the *p*-doping process of

NTEM-PPV has been measured to enable a comparison with MDMO-PPV and PPV. In the same way as described previously for PPV, for both MDMO-PPV and NTEM-PPV at potentials higher than 600 mV, a new ATR-IR spectrum has been taken at every 100 mV step. Subsequently for each step after subtraction of the reference spectrum, the difference spectrum is obtained which only shows the infrared vibrational frequencies associated with the doped polymer, *i.e.* the spectral signatures of the polaron and/or bipolarons.

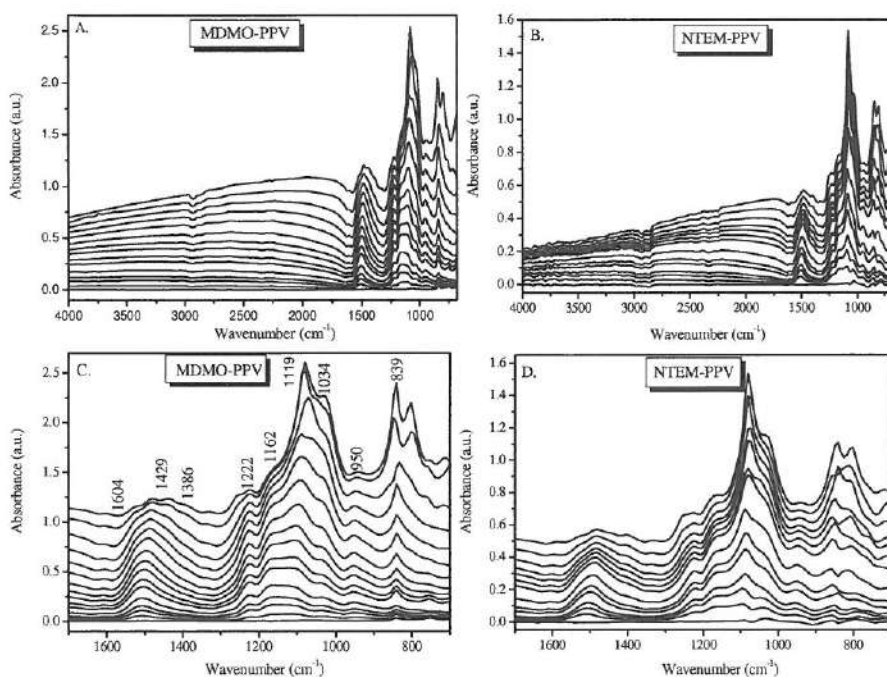


Figure 4-25: In situ FTIR difference spectra during the *p*-doping of MDMO-PPV (A and C) and NTEM-PPV (B and D).

When the ATR-IR spectra of electrochemical *p*-doped PPV (figure 4-20) are compared with those of *p*-doped MDMO-PPV and NTEM-PPV (figure 4-25) the resemblance is significant (figure 4-26). In all cases, a broad and intense absorption band is visible in the conducting state which extends from 2100 cm⁻¹ up to > 4000 cm⁻¹ and concomitantly IRAV bands are observed in the range

1800 cm^{-1} to 700 cm^{-1} . A more careful look at these IRAV bands reveals that upon doping, a broadening of the vibrational bands is observed and that there are also less vibrations present as compared to the neutral state (figure 4-27). The spectral signature of the IRAV modes is different from that of unsubstituted PPV but is similar to literature data on 2,5-substituted PPV-type polymers.⁴² This suggests that the presence of the alkoxy substituents has a significant impact on the IRAV bands, whereas the impact of the exact nature of these substituents (apolar *versus* polar or branched *versus* linear) is rather minimal. This is not surprising, since in the previous chapter it was already concluded that, for example, the introduction of the polar oligo(oxyethylene) substituents does not significantly alter the thin film opto-electronic properties as compared to their apolar counterparts.

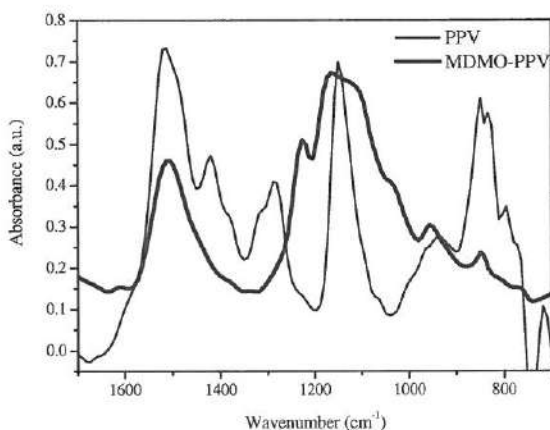


Figure 4-26: *In situ* ATR-FTIR difference spectra of *p*-doped PPV and MDMO-PPV

The most important IRAV bands in the electrochemically doped MDMO-PPV film are positioned at 950, 1160, 1225 and 1500 cm^{-1} . Also in this case, the strong band around 850 cm^{-1} is related to the PF_6^- electrolyte ion. It is not possible to assign the different infrared vibrations without the help of theoretical calculations.

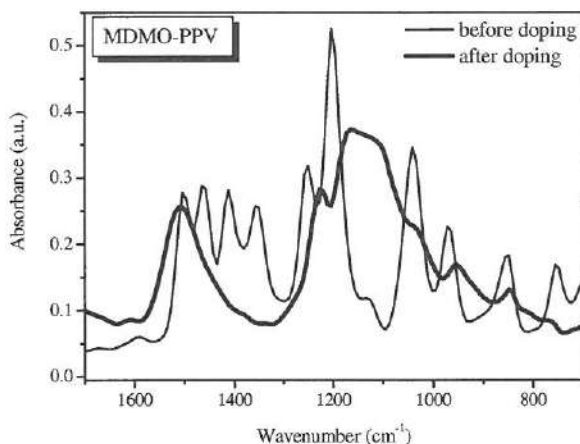


Figure 4-27: *In situ* ATR-FTIR difference spectra before and after p-doping of MDMO-PPV: IRAV range in the wavenumber range of 1700 cm^{-1} to 700 cm^{-1}

4.3.5 *In Situ* ATR-IR Spectro-Electrochemistry of PTV

Not only PPV-type polymers, but also two representative PTV-type polymers, *i.e.* unsubstituted PTV and 3,5-diphenyl-PTV, have been investigated with ATR-IR spectro-electrochemistry.

✓ *Before doping*

Figure 4-28 shows the infrared spectrum of a typical PTV film which was obtained after heat treatment of the corresponding precursor polymer at $160\text{ }^{\circ}\text{C}$.

Out-of-plane vibrations

In the IR spectrum of non-substituted PTV, there is an out-of-plane IR band at 928 cm^{-1} . This band is the C-H out-of-plane vibration of the trans vinylene double bond⁴⁵. This peak is comparable to the IR peak of vinylene bound in PPV at 960 cm^{-1} . The vibration of the thiophene ring appears at 823 cm^{-1} ⁴⁶.

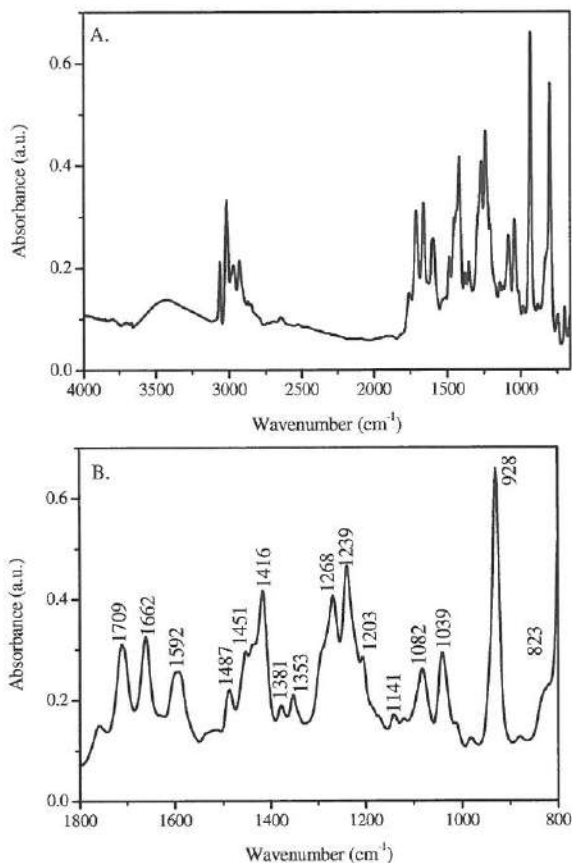


Figure 4-28: IR spectrum of neutral PTV (top: full spectrum; bottom: enlargement)

In-plane vibrations

The 1300 - 1600 cm⁻¹ region (Table 4-3)

In the region of 1300 and 1600 cm⁻¹, the five membered ring heteroaromatic compounds with two double bonds in the ring generally show three ring stretching bands since both C=C and C-C ring stretching vibrations are IR active. An intense peak attributed to C_α=C_β symmetric stretching occurs at 1451 cm⁻¹ followed by two weaker peaks around 1662 cm⁻¹ attributed to asymmetric C_α=C_β modes and at 1353 cm⁻¹, this peak is assigned to the C_β-C_β stretching vibration⁴⁷ (figure 4-29). The IR band around 1381 cm⁻¹ originates from the stretching of the C-S bond in the

thiophene ring ⁴⁸. The C=C stretching frequency near 1592 cm⁻¹ in vinylene hydrocarbons is a medium intensity band.

PTV (cm ⁻¹)		Assignment
823	w	thiophene vibration out-of-plane
928	vs	trans vinylene C-H out-of-plane
1039	m	C-H _{3,4} ring bending in-plane
1082	m	C-S stretching in-plane
1141	w	C-H _{3,4} ring bending in-plane
1203	w	dithiocarbamate leaving group
1239	s	thiophene ring deformation
1268	s	dithiocarbamate leaving group and trans vinylene C-H in-plane
1353	vw	C _β -C _β ring stretching
1381	vw	C-S ring stretching
1416	s	dithiocarbamate leaving group
1451	s	C _α =C _β symmetric ring stretching
1487	m	dithiocarbamate leaving group
1592	m	trans vinylene C=C stretching
1662	m	C _α =C _β asymmetric ring stretching
1709	m	dithiocarbamate leaving group

Table 4-3: IR bands of neutral PTV. Numbers are wavenumbers (cm⁻¹),

vs, very strong; s, strong; m, medium; w, weak; vw, very weak

The 1300-1000 region (Table 4-3)

The bands around 1039 cm⁻¹ and 1141 cm⁻¹ in the IR spectra of PTV are a result of the in-plane C-H ring bending. The peak at 1082 cm⁻¹ is the C-S stretching of the aryl-S-linkage. The band at 1239 cm⁻¹ is the deformation of the thiophene ring ⁴⁹. The peak at 1268 cm⁻¹ is the in-plane C-H stretching of the vinylene double bond.

The IR spectrum of PTV shows absorption bands at 1709, 1487, 1416, 1268 and 1204 cm^{-1} which all arise from the dithiocarbamate leaving group⁴⁵. This means that the conversion from the precursor polymer to the conjugated PTV polymer is apparently not complete.

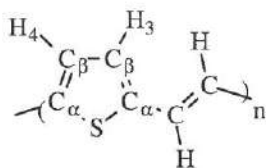


Figure 4-29: Molecular structure of PTV

✓ During *p*-doping process

The FTIR-ATR difference spectra recorded *in situ* during *p*-doping of a PTV film immersed in an acetonitrile/TBAPF₆ electrolyte solution are shown in figure 4-30.

As can be seen in figure 4-30, several new absorption bands appear during the *p*-doping process, which are not be found in the spectrum of the neutral form of PTV. The doping induced bands in the IR spectra start to appear at a potential where a current can be detected in the cyclic voltammogram, *i.e.* at 100 mV. The broad absorption band, starting at 1600 cm^{-1} and extending to higher wavenumbers, is similar the band observed for PPV-type polymers upon doping. Hence, also in this case it can be explained by electronic transitions due to the formation of charge carriers in the polymer chain. The doping induced infrared active vibrations (IRAV) as a result of the *p*-doping of the PTV film also originate from the formation of charge carriers on the polymer chain. As a result of doping, the dipole moment of the polymer repeating units changes and the typical increase in dipole moment will lead to an increasing interaction with the electromagnetic radiation and therefore to a strong increase in the absorption band intensity in the IR spectra²². Here the doping induced bands can be observed at 1533, 1370, 1177, 1090, 1011, 916, 824,

748 and 723 cm^{-1} . Also in this case, the strong band in the 800-850 cm^{-1} range is related to the PF_6^- electrolyte ion.

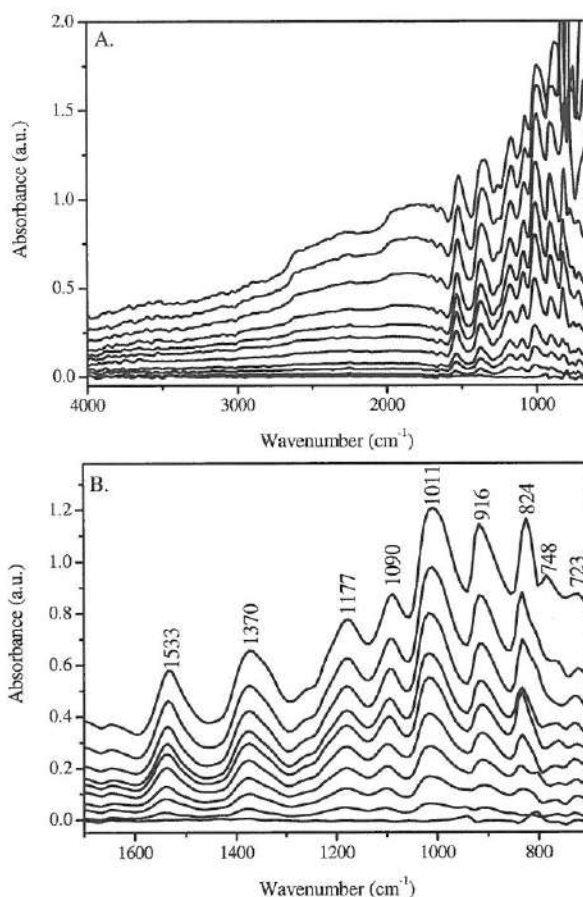


Figure 4-30: In situ FTIR difference spectra during *p*-doping of PTV
(top: full spectrum; bottom: enlargement showing IR bands)

4.3.6 In Situ ATR-IR Spectro-Electrochemistry of DiPh-PTV

The final polymer studied with ATR-IR Spectro-Electrochemistry is diphenyl-PTV. This is a PTV derivative with two phenyl side chains at the position three and four of the thiophene ring. The presence of these two side chains does not have a

significant impact on the cyclic voltammetry of this compound as compared to unsubstituted PTV (chapter 2). Hence, it is of interest to know whether the phenyl groups do influence the doping characteristics.

✓ *Before doping*

In figure 4-31, the IR spectrum of neutral DiPh-PTV is shown.

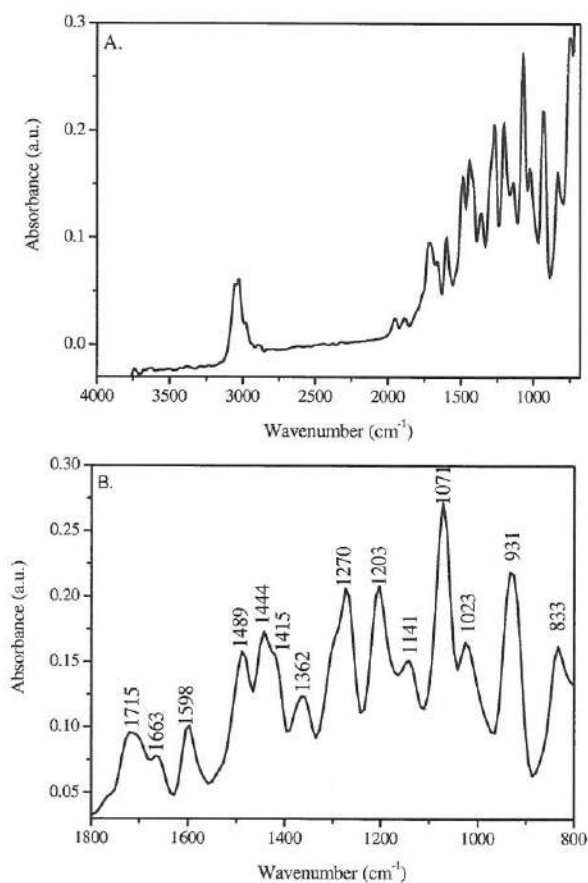


Figure 4-31: IR spectrum of neutral DiPh-PTV
(top: full spectrum; bottom: enlargement)

From the measurements it becomes clear that the IR bands of DiPh-PTV (table 4-4) are virtually identical to those of PTV (Table 4-3). Also for this polymer, the

conversion from the precursor polymer to its conjugated form is not complete, as can be seen from presence of the vibrations of the dithiocarbamate leaving group at 1203, 1270, 1415, 1489 and 1715 cm^{-1} . At 833 cm^{-1} and 931 cm^{-1} the out-of-plane vibrations of the thiophene ring and vinylene bound are found. At 1071 cm^{-1} the in-plane ring vibration of C-S of the thiophene ring is present. The peaks at 1270 cm^{-1} and 1598 cm^{-1} are the in-plane vibrations corresponding to the vinylene double bound, respectively the C-H bending and C=C bending. The IR bands at 1023 cm^{-1} , 1141 cm^{-1} , 1362 cm^{-1} , 1444 cm^{-1} and 1663 cm^{-1} are the in-plane stretching of the ring.

DiPh-PTV (cm^{-1})		Assignment
833	w	thiophene vibration out-of-plane
931	s	trans vinylene C-H out-of-plane
1023	m	C-H ring bending in-plane
1071	vs	C-S stretching
1141	w	C-H ring bending in-plane
1203	s	dithiocarbamate leaving group
1270	s	dithiocarbamate leaving group and trans vinylene C-H in plane
1362	w	C $_{\beta}$ -C $_{\beta}$ ring stretching
1415	m	dithiocarbamate leaving group
1444	s	C $_{\alpha}$ =C $_{\beta}$ symmetric stretching
1489	s	dithiocarbamate leaving group
1598	m	trans vinylene C=C stretching
1663	m	C $_{\alpha}$ =C $_{\beta}$ asymmetric stretch
1715	m	dithiocarbamate leaving group

Table 4-4: IR bands of neutral DiPh-PTV. Numbers are wavenumbers (cm^{-1}),

vs, very strong; s, strong; m, medium; w, weak; vw, very weak

When table 4-3 (PTV) and table 4-4 (DiPh-PTV) are compared, it can be concluded that the vibrations of both polymers are very similar, although some variations in the actual wavenumbers do exist. Only the peaks at 1239 cm^{-1} and 1381 cm^{-1} in the IR spectrum of PTV are not found in the spectrum of DiPh-PTV. The reason of the absence of the IR peak at 1381 cm^{-1} in DiPh-PTV is due to the broadness of the peak at 1362 cm^{-1} . This weak peak includes two vibrations, the $\text{C}_\beta\text{-C}_\beta$ ring stretching and the C-S ring stretching.

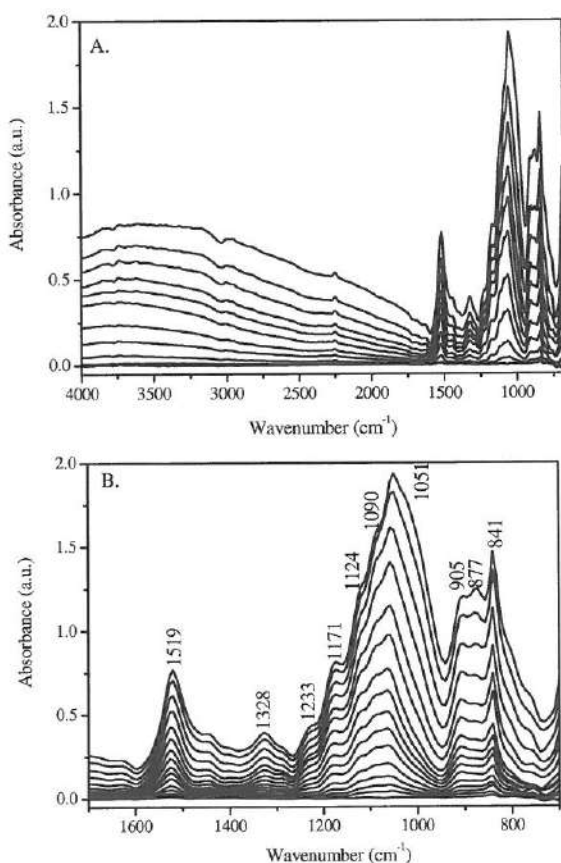


Figure 4-32: In situ FTIR difference spectra during p-doping of DiPh-PTV
(top: full spectrum; bottom: enlargement showing IRAV bands)

✓ *During p-doping process*

A series of FTIR spectra taken *in situ* during stepwise oxidation and reduction of DiPh-PTV film in 0.1 M TBAPF₆-acetonitrile solution are shown in figure 4-32. Spectra are gathered at constant potential every 100 mV. A spectrum of the DiPh-PTV film at 50 mV was used as a reference spectrum.

During the p-doping process positive charges are created in the polymer chain, resulting in changes in the dipole moment of vibrations followed by increasing interaction with electromagnetic radiation. The thus appearing infrared active vibrations (IRAV) of DiPh-PTV can be found at 1519, 1328, 1233, 1171, 1124, 1090, 1051, 905 and 877 cm⁻¹, with at 841 cm⁻¹ the vibration associated with the PF₆⁻ ion. Similar to all previously discussed spectro-electrochemical data on conjugated polymers also in this case a broad band is visible at frequencies above 1600 cm⁻¹ (figure 4-33).

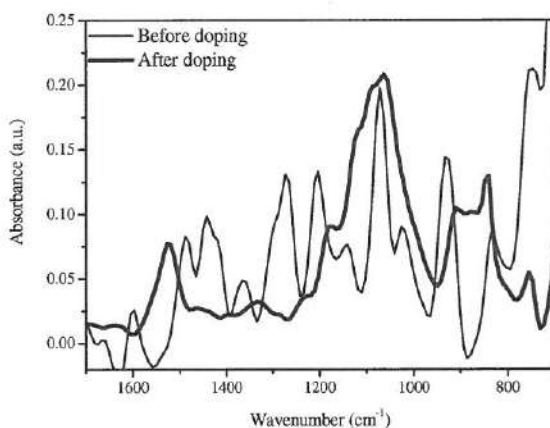


Figure 4-33: *In situ ATR-FTIR difference spectra before and after p-doping of DiPh-PTV*

To answer a final remaining question of this section whether the presence of the two phenyl side chains of DiPh-PTV has an impact on the doping characteristic, figure 4-34 is shown. From this figure it is clear that the presence of the two phenyl

rings does have a significant impact. This is most likely a result of the fact that the two phenyl rings have an aromatic character. Although optical and electrochemical measurements indicate that in the ground state these phenyl rings are mostly decoupled from the conjugated system (*cf.* Chapter 2), apparently this is not the case in the doped state.

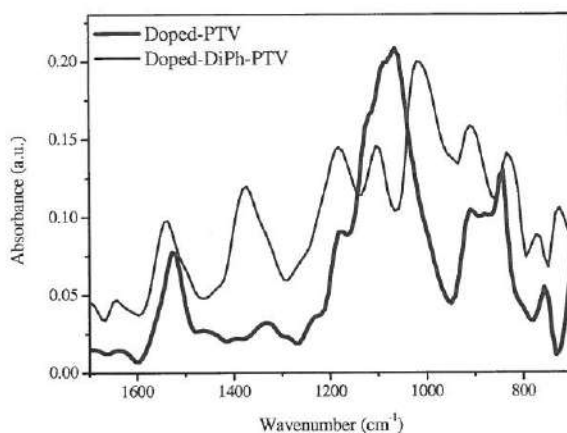


Figure 4-34: *In situ* ATR-FTIR difference spectra of *p*-doped PTV and DiPh-PTV.

4.3.7 Conclusions

ATR-IR spectroscopy measurements have been performed on three PPV and two PTV derivatives. It is readily possible to assign the vibrational IR frequencies of the neutral forms of these polymers using literature sources. Subsequent *in situ* ATR-IR spectro-electrochemistry during the oxidation of these polymers reveals a more complex behavior and two types of features can be observed in the resulting spectra. The most notable feature is the evolution of a broad absorption band extending from 1500–2000 cm^{-1} up to frequencies well above 4000 cm^{-1} . This broad absorption band originates from typical sub-gap electronic transitions due to the formation of polaronic and/or bipolaronic charge carriers on the polymer chain. This broad and intense absorption band is found in most conjugated polymers in

their conducting form. Concomitantly with the appearance of this broad band, new sharp intensive infrared active vibrations (IRAV) appear in the wavenumber range 1800-700 cm^{-1} . The p-doping induced IRAV bands grow in intensity with the degree of oxidation of the polymer film. This is a result of the fact that positive charges are created in the polymer chain. These charges induce changes in the dipole moments of the polymer repeating units, which results in an increasing interaction with electromagnetic radiation. The vibrations become infrared active due to symmetry breaking and are strongly enhanced, because the typical charge distribution in the formed polaronic state induces high dipole moment changes during vibration. At this stage, it is not possible to assign the IRAV bands conclusively without the help of theoretical calculations.

4.4 In Situ Raman Spectro-Electrochemistry

4.4.1 Introduction

✓ Raman spectroscopy

Raman spectroscopy is a spectroscopic technique used in the chemistry to study the vibrational, rotational and other low-frequency modes in a system. The obtained vibrational information is very specific for the chemical bonds in the molecules. Raman spectroscopy differs from other spectroscopy experiments because the scattering of radiation by the sample is used rather than the absorption or emission of radiation. Typically in Raman spectroscopy, the sample is illuminated with an intense monochromatic radiation, which is usually supplied by a laser. The laser light is dispersed onto a detector, which is orthogonal to the direction of the incident radiation, so as to observe only the scattered light.

When laser light is scattered from a molecule, most photons are elastically scattered. This process is called 'Rayleigh scattering' where the emitted photons have the same energy (frequency) and therefore, the same wavelength as the absorbing photons. However, Raman spectroscopy is based on the 'Raman effect',

which is the inelastic scattering of photons by molecules. The 'Raman effect' comprises a very small fraction, about 1 in 10^7 , of the incident photons. In Raman scattering, the energies of the incident and scattered photons are different. Raman scattering can occur with a change in vibrational, rotational or electronic energy of a molecule, with the vibrational Raman effect being the most important in the context of Raman spectroscopy.

Infrared (IR) and Raman spectroscopy are techniques, which both measure the vibrational energies of molecules, albeit with a difference in the use of the selection rules. For infrared spectroscopy, it is necessary for the molecule being analyzed to have a permanent electric dipole. A vibrational motion is IR active when the dipole moment of that molecule changes upon vibrating. This is not the case for Raman spectroscopy. Raman spectroscopy is useful for analyzing molecules without a permanent dipole moment. However, the polarizability of these molecules is important, which must vary with orientation. The combined evaluation of Raman and infrared spectra yields more information about molecular structure than when they are evaluated separately. But Raman spectroscopy can be more straightforward to use than IR spectroscopy. This is a result of the fact that, for example, water and glass are strong infrared absorbers whereas they are weak Raman scatters, making it is easier to produce quality Raman spectrum of an aqueous sample in a glass container.

To assess whether a vibrational frequency is active in Raman spectroscopy or infrared spectroscopy, group theory is essential. Hereby, the molecules are classified according to the symmetry elements or operations that leave at least one common point unchanged. All information about a point group is contained in a character table. An example of character table is shown in table 4-5 for the point group C_{2v} and C_{3v} .⁵⁰

C_{2v}	E	C_2	$\sigma_v (xz)$	$\sigma_v' (yz)$		
A_1	1	1	1	1	z	x^2, y^2, z^2
A_2	1	1	-1	-1	R_z	xy
B_1	1	-1	1	-1	x, R_y	xz
B_2	1	-1	-1	1	y, R_x	yz

C_{3v}	E	$2C_3$	$3\sigma_v$		
A_1	1	1	1	z	$x^2 + y^2, z^2$
A_2	1	1	-1	R_z	
E	2	-1	0	$(x, y) (R_x, R_y)$	$(x^2 - y^2, xy) (xz, yz)$

Table 4-5: Character tables of the point groups C_{2v} and C_3

An example of a molecule with the point group C_{3v} is $CHCl_3$, whereas CH_2Cl_2 is represented by the C_{2v} point group. In the left corner of the character table, the point group is identified. The symmetry operations of the point group are given in the first row of the character table. The letters in the left column represent the symmetry species that label the irreducible representations of the group. The numbers in the table show how the symmetry operation of the point group affect these axes. The R_x , R_y , and R_z in the table show how the symmetry operations of the point group affect rotation about these axes.

With the help of character tables one can find the IR active bands because a fundamental transition will be *infrared active*, if the normal mode involved belongs to the same symmetry representation as the Cartesian coordinates x , y and z . For example, for the C_{2v} point group if the symmetry representation of the normal mode is A_1 , B_1 or B_2 , it will be infrared active. The normal modes with the A_2 symmetry representation would be infrared forbidden. For the C_{3v} point group, this means that if the symmetry representation of the normal mode is A_1 or E, it will be infrared allowed. The normal modes with the A_2 symmetry representation would be

infrared forbidden. A fundamental transition will be *Raman active*, if the normal mode involved belongs to the same symmetry representation of the Cartesian components of the polarizability tensor of the molecule. (The symmetry label contains a product of x, y or z). For the C_{2v} point group, this means that all of the symmetry representations of the normal mode: A_1 , A_2 , B_1 and B_2 , will be Raman allowed. No normal modes for molecules in the C_{2v} point group will be Raman forbidden. For the C_{3v} point group, the symmetry representation of the normal mode A_1 or E is Raman allowed and A_2 symmetry representation would be Raman forbidden.

✓ *In situ Raman spectro-electrochemistry*

Raman spectroscopy is also well suited for spectro-electrochemical studies of conducting polymers. Electrochemical doping leads to changes in chain geometry and modification of the condition for Raman scattering.^{10, 14, 16, 17, 20, 23}

Two conjugated polymers have been studied with Raman spectro-electrochemistry, namely MDMO-PPV and PTV. In this way one example of a PPV derivative and one example of a PTV derivative have been investigated. Further research is necessary to establish the Raman characteristics of the other conjugated polymers used in this work.

4.4.2 Experimental

In situ FT-Raman spectra were measured on a Bruker IFS 66/S Fourier transform-IR spectrometer with a resolution 10 cm^{-1} , which was modified for Raman measurements. A continuous wave Nd:YAG laser was operated at 1064 nm for Raman excitation. Raman scattered radiation was collected with a 90° off-axis parabolic mirror in a backscattering configuration. A germanium detector operated at liquid nitrogen temperature was used. Raman spectra were measured with a laser line of 1064 nm at room temperature. Each spectrum is calculated from a co-

addition of 300 interferograms. Raman spectra were recorded *in situ* during the electrochemical potential measurements. The electrochemical equipment consisted of a galvanostat/potentiostat AUTOLAB PGSTAT 20 from Ecochemie. Raman spectra are gathered at constant potential every 100 mV of a potential cycle starting at 0 V. The spectro-electrochemical measurements were carried out in a home built Raman spectro-electrochemical three electrode cell made from glass (figure 4-35). A transparent glass electrode coated with indium tin oxide (ITO) was used as working electrode together with a Pt counter electrode and a reference Ag electrode. Each studied polymer was coated onto the working electrode from a CHCl_3 solution. For Raman spectro-electrochemistry it is important that the polymer film is sufficiently thick, as otherwise insufficient intensity of the Raman scattering was observed. Therefore, "thin films" were prepared from a solution with a higher polymer concentration (10 mg/mL), which was drop casted onto the ITO glass substrate. A 0.1 M electrolyte solution of tetrabutylammonium hexafluorophosphate (TBAPF_6) in anhydrous acetonitrile was used for the measurements. The electrolyte solution was prepared and kept under nitrogen atmosphere to exclude moisture and oxygen during the electrochemical processes.

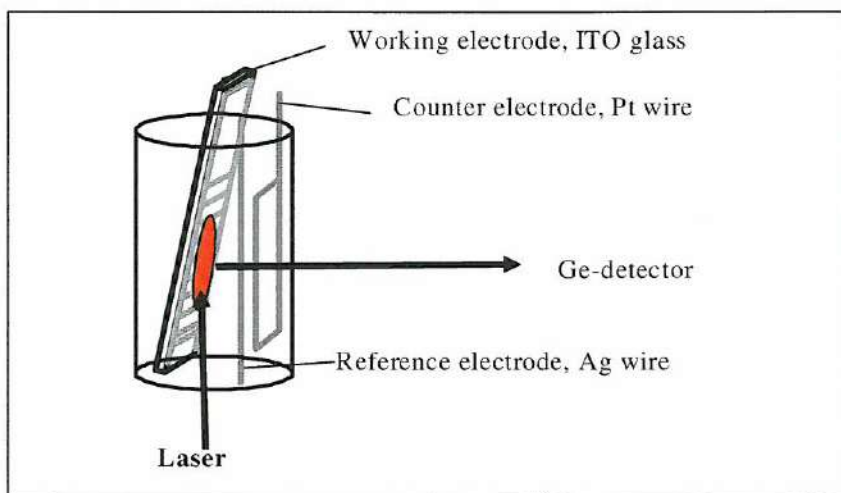


Figure 4-35: In situ Raman spectro-electrochemical cell

With *in situ* ATR-IR spectro-electrochemistry, it was possible to take a reference spectrum of the polymer before the electrochemical doping process to obtain specific spectral changes during the considered process. Unfortunately, with *in situ* Raman spectro-electrochemistry, it was impossible to obtain such a reference spectrum. Due to this fact, the vibrations of the electrolyte solution (ACN/TBAPF₆) and the neutral polymer are observed in each Raman spectrum. For reference, in figure 4-36, the Raman spectrum of the electrolyte solution is shown.

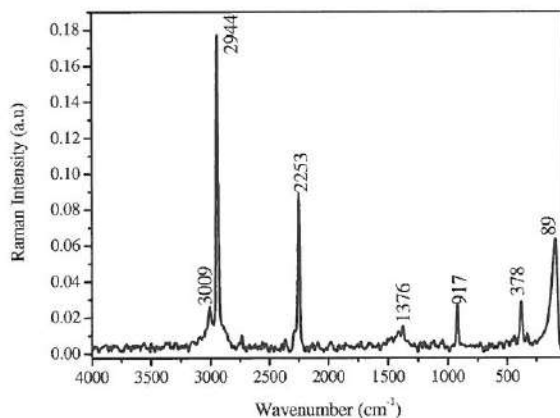


Figure 4-36: Raman spectrum of the electrolyte solution TBAPF₆ in acetonitrile.

4.4.3 *In situ* Raman Spectro-Electrochemistry of MDMO-PPV

The first polymer studied with Raman spectro-electrochemistry is MDMO-PPV. This is one of the most common PPV-type polymers and provides thus an excellent proof of principle for this analytical technique.

✓ *Before doping*

The Raman spectrum of MDMO-PPV is shown in figure 4-37. Three relatively sharp lines at 1583 cm^{-1} , 1310 cm^{-1} and 1112 cm^{-1} as well as some smaller peaks can be distinguished in the spectrum (Table 4-6).

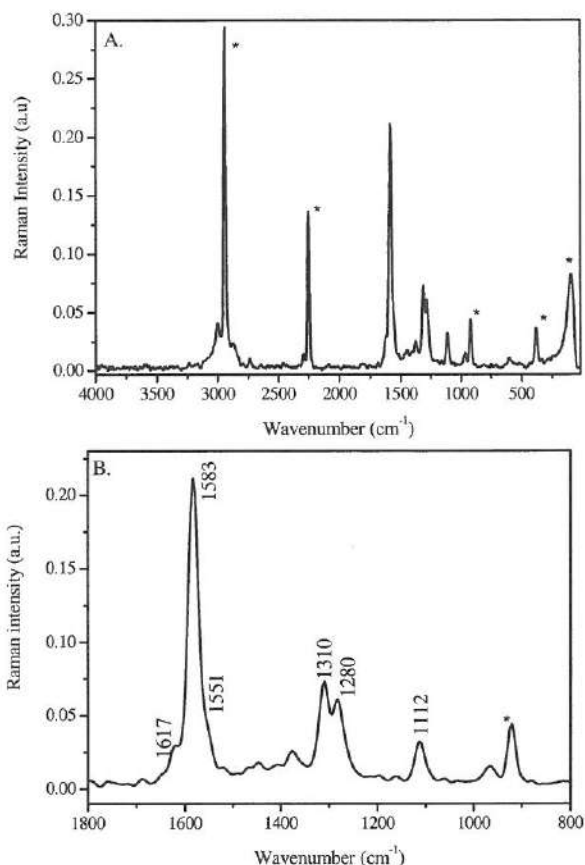


Figure 4-37: Raman spectrum of the MDMO-PPV before doping (top: full spectrum; bottom: enlargement; solvent/electrolyte peaks are designated by an asterisk)

In the upper frequency range, one strong band (1583 cm^{-1}) accompanied by two weak shoulders on the low and high frequency side (1617 and 1551 cm^{-1}) can be observed in the MDMO-PPV Raman spectrum. The band at 1617 cm^{-1} is due to a vibration mode of the vinylene group, *i.e.* the symmetric stretching vibration of the C=C bond. The other two peaks at 1583 and 1551 cm^{-1} correspond to vibrations of

the tetra-substituted benzene ring (C-C ring stretching).^{39, 51, 20, 47, 52-55} The second intense vibration at 1310 cm^{-1} in the Raman spectrum of MDMO-PPV also originates from the vinylene group. The C-H bonds stretch in the same direction and give this vibration. The third intense peak at 1112 cm^{-1} can be assigned to a mixture of the symmetric C-C stretching and C-H in plane bending vibrations. These bands are comparable to the bands observed in the literature for non-substituted PPV.^{39, 51, 20, 47, 52-54, 56} MDMO-PPV is a PPV derivative with on the 2nd and 5th position of the phenyl core an alkoxy side chain. This side chain is also observed in the Raman spectrum. The peak at 1280 cm^{-1} is known to be active for alkoxy PPV stretching ($\phi\text{-O-CH}_2$) presented by the alkoxy group attached to the phenylene rings..⁵⁷⁻⁵⁹

MDMO-PPV (cm^{-1})		Assignment
1112	m	symmetric C-C stretch C-H in plane bend
1280	m	phenylene-alkoxy stretch ($\phi\text{-O-CH}_2$) C-H in plane bend
1310	m	trans vinylene C-H in plane stretch
1551	w, sh	C-C ring stretch
1583	vs	C-C ring stretch
1617	w, sh	trans vinylene C=C stretch

Table 4-6: Band assignment and wavenumbers of Raman modes of neutral MDMO-PPV
(vs, very strong; s, strong; m, medium; w, weak; vw, very weak; sh, shoulder)

✓ During p-doping process

Raman spectra have been recorded with excitation line in the near infrared ($\lambda_{\text{exc}} = 1064 \text{ nm}$ or 1.17 eV) which is close in energy to electronic transitions of doped segments in order to fulfill resonance condition for the different species induced by

doping. *In situ* electrochemical doping shows different modifications of the Raman spectra. The bands observed in the Raman spectra are assigned with the help of a variety of literature sources. As mentioned before, with Raman spectroscopy, it is not possible to take a reference spectrum as was done for ATR-IR spectro-electrochemistry. During the doping process, the bands observed due to the electrolyte solution and the neutral MDMO-PPV remain therefore visible.

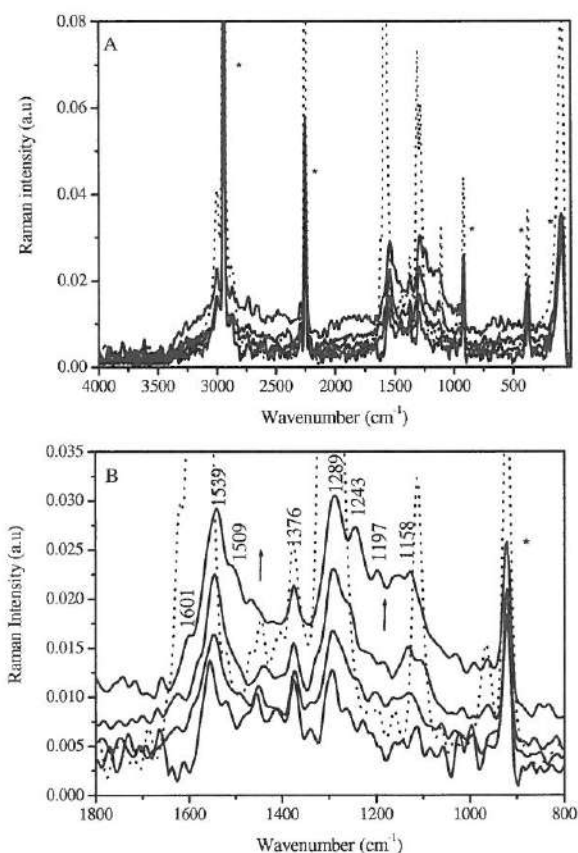


Figure 4-38: *In situ* Raman spectrum of the MDMO-PPV during the doping process (top: full spectrum; bottom: enlargement; solvent/electrolyte peaks are designated by an asterisk; dotted line: neutral MDMO-PPV)

Upon doping, *i.e.* increasing the potential from 0 to 1.4 V vs. Ag the three previously mentioned most intense polymer vibrations essentially disappear (Figure 4-38). The reasonably well-defined peaks transform into two broad features with low intensity. In addition, the Raman active vibrations exhibit shifts and broadening which can be explained by structural modifications along the polymer chain when the benzenoid (undoped) form is changed to the quinoid (doped) form of MDMO-PPV. The difference in shifts can be due to variations in distribution of the positive charge carriers and the resulting structure of the neighboring backbone environment ¹⁴.

The main changes in the Raman spectrum upon doping occur in the 1800-800 cm^{-1} range (figure 4-38B). The two most intense bands which are visible upon doping (maximum frequencies 1289 cm^{-1} and 1539 cm^{-1}) originate from the two strongest bands of neutral MDMO-PPV at 1310 cm^{-1} and 1583 cm^{-1} . They are somewhat shifted and broadened upon doping. In addition, several new bands appear at various other frequencies (Table 4-7)

In the Raman spectrum, one very strong band at 1539 cm^{-1} and two small shoulders at 1509 and 1601 cm^{-1} are clearly visible upon doping. The shoulder at 1601 cm^{-1} is assignable to the mode containing large contributions of the vinylene C=C stretch in the doped segments. The corresponding vibration is observed at 1617 cm^{-1} for neutral MDMO-PPV. The downshift on going from neutral MDMO-PPV to doped MDMO-PPV are due to the decreases in the bond order of the vinylene C=C bond. Literature reports ^{56, 60} describe a similar behavior with FeCl_3 doped PPV, which is attributed to the distortion to a quinoid structure upon doping. The peak at 1539 cm^{-1} and the shoulder at 1509 cm^{-1} are also attributable to the ring mode corresponding to the stretching of benzene ²⁰. This corresponds with the peak at 1583 cm^{-1} and the shoulder at 1551 cm^{-1} of the neutral state. Furthermore, the band at 1289 cm^{-1} arises from the C-H bending mode of the vinyl group, which corresponds with the band at 1310 cm^{-1} in the neutral form. The vibration at 1243

cm^{-1} in the doped state corresponds with the vibration at 1310 cm^{-1} and is the bending of C-H of trans vinylene. The vibration corresponding with the alkoxy stretching ($\phi\text{-O-CH}_2$) is situated at 1280 cm^{-1} in the neutral state and is shifted to 1243 cm^{-1} in the p-doped state. At 1158 cm^{-1} , 1197 cm^{-1} and 1376 cm^{-1} , new Raman vibrations are observed upon doping, which can be assigned to the C-C and C-H bending of the ring..^{10, 59 16, 47, 56, 60, 61}

Doped			Assignment
MDMO-PPV			
(cm^{-1})			
1158	w	*	ring C-H bending
1197	w	*	ring C-H bending
1243	m		phenylene-alkoxy stretching ($\phi\text{-O-CH}_2$)
1289	s		trans vinylene C-H bending
1376	w	*	C-C ring stretching
1509	w, sh		C=C ring stretching
1539	vs		C-C ring stretching
1601	w, sh		trans vinylene C=C stretching

Table 4-7: Band assignment and wavenumbers of Raman modes of doped MDMO-PPV

(vs, very strong; s, strong; m, medium; w, weak; vw, very weak; sh, shoulder,
new doping peaks are designated by an asterisk)

4.4.4 In Situ Raman Spectro-Electrochemistry of PTV

✓ Before doping

In figure 4-39, the Raman spectrum of a PTV film before doping is shown. As is clearly visible from this figure, the spectral features of PTV are significantly

different from that observed for PPV. In table 4-8, the observed bands of PTV are listed together with tentative assignments.

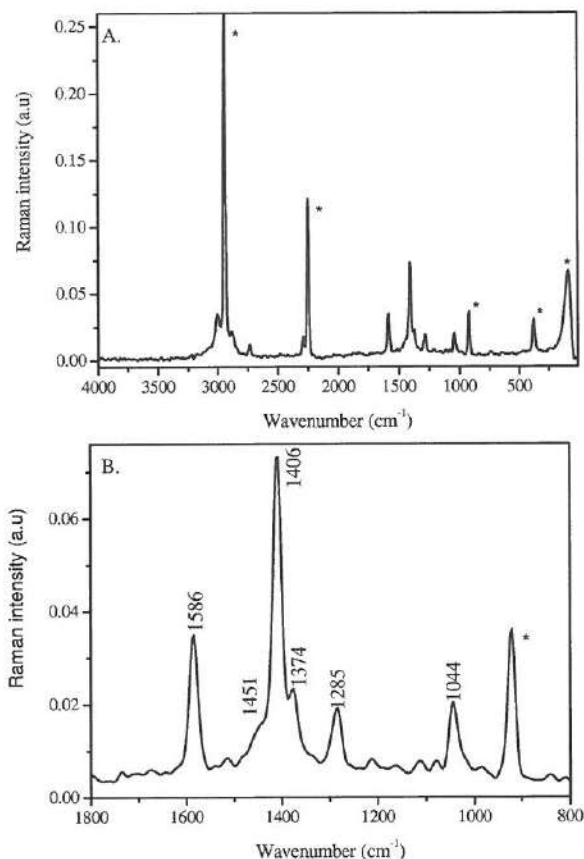


Figure 4-39: Raman spectrum of PTV before doping (top: full spectrum; bottom: enlargement; solvent/electrolyte peaks are designated by an asterisk)

The region around 1300-1600 cm⁻¹ is interesting because both the C=C and C-C stretching vibrations are active. The Raman lines observed at 1586 and 1285 cm⁻¹ for PTV are characteristic of the vinylene bonds⁴⁷. The line at 1586 cm⁻¹ almost purely corresponds to the C=C stretching of the spacer and the line at 1285 cm⁻¹ is associated with the in-plane symmetric bending of the vinylene C-H bonds. The most intense peak in the Raman spectrum of PTV appears at 1406 cm⁻¹ and is a

result of a symmetric C=C stretching vibration in the thiophene ring. The low intensity peak at 1374 cm^{-1} is due to the in-phase stretching of all the C $_{\beta}$ -C $_{\beta}$ bonds (figure 4-40). Finally the medium intensity peak at 1044 cm^{-1} can be assigned to C $_{\beta}$ -H bending vibrations.^{49, 55, 59, 62, 63}

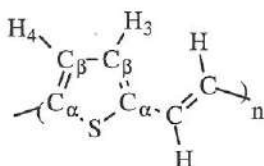


Figure 4-40: Molecular structure of PTV

PTV (cm^{-1})		Assignment
1044	m	C $_{\beta}$ -H ring bending
1285	w	trans vinylene C-H bending
1374	w, sh	C $_{\beta}$ -C $_{\beta}$ ring stretching
1406	s	C $_{\alpha}$ =C $_{\beta}$ ring stretching
1451	w, sh	C $_{\alpha}$ =C $_{\beta}$ ring stretching
1586	m	trans vinylene C=C stretching

Table 4-8: Band assignment and wavenumbers of Raman modes of a neutral PTV film
(vs, very strong; s, strong; m, medium; w, weak; vw, very weak; sh, shoulder)

✓ During *p*-doping process

The resonant Raman spectra of PTV upon electrochemical doping are displayed in figure 4-41. All peaks are broadened and several additional broad peaks in the 1500 cm^{-1} - 1100 cm^{-1} region are visible. These additional peaks are a result of typical vibrational modes stemming from localized, mid-gap lattice defects, *i.e.* polarons and bipolarons. The peak broadening is similar to that observed for MDMO-PPV.

⁵⁹ The observed vibrations are listed in table 4-9.

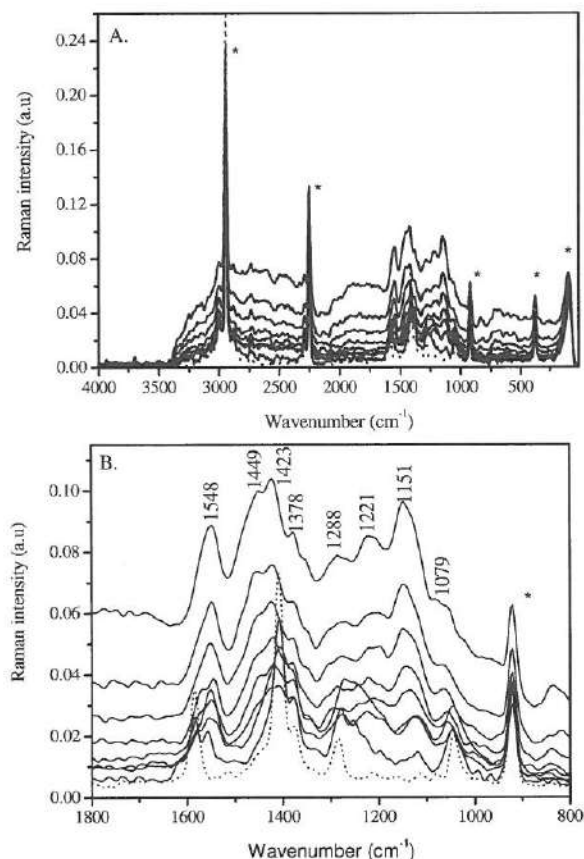


Figure 4-41: In situ Raman spectrum of PTV during the doping process (top: full spectrum; bottom: enlargement; solvent/electrolyte peaks are designated by an asterisk; dotted line: neutral PTV)

The peaks at 1548 cm^{-1} and 1221 cm^{-1} represent the vibrations for the vinylene group in PTV. The first vibration is the C=C stretch of the vinyl group and the 1221 cm^{-1} vibration is the C-H stretching of the same group. These two vibrations corresponds to the vibrations at 1586 and 1285 cm^{-1} in the neutral state. The downshift on going from neutral PTV to doped PTV are due to the decreases in the bond order of the vinylene C=C bond. The vibrations corresponding to the $C_{\alpha}=C_{\beta}$ stretching are situated at 1449 cm^{-1} and 1378 cm^{-1} . These vibrations are most likely comparable to the vibrations at 1451 and 1406 cm^{-1} in the neutral PTV. The in

phase $C_\beta-C_\beta$ stretching deformations of PTV in the neutral film is situated at 1374 cm^{-1} . This vibration is possibly shifted to 1350 cm^{-1} in the doped state. The bands observed at 1079 , 1151 , 1288 and 1423 cm^{-1} are new Raman vibrations created during the p-doping process of PTV. The peaks at 1079 and 1151 cm^{-1} are vibrations due to the C-H ring stretching and 1423 cm^{-1} is the C-C ring stretching.

55, 56, 59, 60, 64

Doped PTV (cm^{-1})			Assignment
1079	w	*	C-H ring stretching
1151	s	*	C-H ring stretching
1221	w		trans vinylene C-H bending
1288	w	*	C-H quinoid
1350	w		$C_\beta-C_\beta$ in phase stretching
1378	w		$C_\alpha=C_\beta$ stretching
1423	s	*	$C_\beta-C_\beta$ ring stretching
1449	w		$C_\alpha=C_\beta$ stretching
1548	s		trans vinylene C=C stretch

Table 4-9: Band assignments and wavenumbers of Raman modes of a doped PTV film
(vs, very strong; s, strong; m, medium; w, weak; vw, very weak
new doping peaks are designated by an asterisk)

4.4.5 Conclusions

In this part of chapter 4, it is shown that it is possible to do *in situ* Raman spectro-electrochemistry of PTV and PPV derivatives. However, these Raman measurements are still preliminary. Further work is necessary to do a more detailed study and to use additional examples of conjugated polymers. Notwithstanding, already from the Raman measurements presented in this section, some initial conclusions can be drawn. In the neutral state, comparatively sharp lines can be

distinguished. It is possible to assign the vibrational Raman frequencies of the neutral form of MDMO-PPV and PTV using literature sources. During the p-doping process, the reasonably well-defined peaks of the neutral state transform into broad peaks with low intensity and several additional broad peaks are visible in the 1800-800 cm^{-1} region. The shift and broadening of the existing bands in the Raman spectra of conjugated polymer can be explained by structural modifications along the polymer chain when the benzenoid (undoped) form is changed to the quinoid (doped) form of the polymer. The difference in shifts going from the neutral conjugated polymer to the p-doped polymer are due to gradual decreases in the bond order of the vinylenic C=C bonds upon doping. The additional peaks are the result of typical vibrational modes stemming from polarons and/or bipolarons. However, at this stage, it is not possible to assign the new Raman bands conclusively.

4.5 Theoretical Calculations

4.5.1 Introduction

A detailed vibrational analysis of conjugated polymers can provide a wealth of information about the molecular structure of these polymers and about the structural distortion caused by the charge transfer to or from the polymer chain upon doping. The structural rearrangement of the polymer atoms gives rise to a shift of IR and Raman frequencies and/or the appearance of new vibrational bands in the spectra of doped polymers. Although the Raman and infrared spectra of PPV films have been reported in the literature,^{20, 41, 47, 49, 55, 58, 61} further studies are necessary for the complete assignments of the observed spectral features. As was shown in the previous section, also for the assignment of the vibrations in the doped polymers, additional theoretical work is needed. Density functional theory (DFT) calculations can be very useful for the accurate prediction of vibrational frequencies of large molecules. Therefore, DFT calculations can be used to assign

the frequencies observed in the infrared spectra..^{41, 47, 49, 52, 65, 66} Structural parameters calculated by the DFT method also agree with experimental values. However, it is impossible to calculate vibrational frequencies of an infinite PPV chain by using the DFT method at present. However, no problem exists for smaller molecules. For example, the infrared vibrations of trans-stilbene⁶⁵, 1,4-distyrylbenzene⁵², and 4,4'-distyrylbenzene have been assigned on the basis of DFT calculations. Transstilbene is the smallest system that approaches the structure of PPV-oligomers, but whereas transstilbene is a monosubstituted benzene, the members of the PPV family are disubstituted benzenes possessing only terminal monosubstituted benzene units^{52 66}.

In this section a vibrational study is presented of two representative oligomers, in the neutral and p-doped state. One oligomer has an unsubstituted PPV like structure and the other oligomer has a typical 2,5-dialkoxy-PPV main chain structure. The oligomers have been studied using DFT theory calculations, which were performed by Prof. M. Deleuze (Hasselt University). Density functional theory (DFT) infrared spectral calculations for PPV derivatives were performed to support the assignments of infrared normal modes. Changes related to the presence of polaronic or bipolaronic defects can then be interpreted in terms of a perturbation of the pristine sample²⁰

4.5.2 Experimental

The vibrational frequencies and the infrared intensities for PPV and 2,5-di-alkoxy-PPV oligomers have been investigated by performing density functional theory (DFT) calculations with the B3LYP (Becke-3-parameters-Lee-Yang-Parr) functional. Two different basis sets were used in these calculations. These comprise the 6-31G basis set as well as Dunning's correlation consistent polarized valence double-zeta (cc-pVDZ) basis. All calculations have been carried out using

the Gaussian 03 program package. Calculated atomic displacements in each vibrational mode were depicted with cygwin.

In this study, the normal coordinate calculations of two oligomers with seven phenylene-rings and six vinylene moieties (figure 4-42) have been performed. The frequency mode for a long oligomer is assumed to be very close to that of the corresponding optically active vibration of the polymer. The effective conjugation length of the polymer estimated from the frequency dispersion plot is 8 repeating units⁵³. However, for certain systems this may be a low estimate^{33, 67}. On the other hand, it has also been shown that the effective conjugation length of the solid materials, as judged from the vibrational spectra of the oligomers, is not less than 7-9 units. Other reports^{61, 68}, suggest that the charged defects of a polymer extend over approximately 3 to 5 polymer units, in rough agreement with experimental estimates of the length of polarons and bipolarons as obtained by comparison with model compounds. Due to the above considerations, the calculations have been performed on oligomers with 7 repeating units.

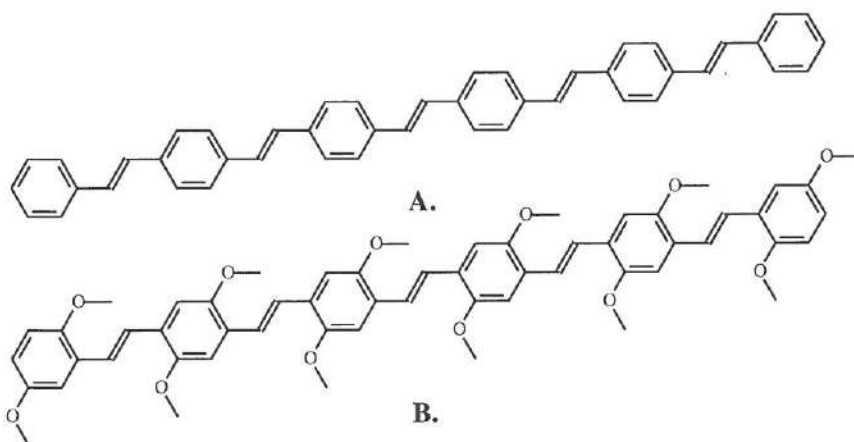


Figure 4-42: Structure of the used oligomers: PPV-7 (top) and OCC-PPV-7 (bottom)

Full geometry optimizations were performed under C_{2h} symmetry (table 4-10), assuming a planar structure. The in-plane and out-of-plane normal modes can be

separated into symmetric and antisymmetric modes with respect to the molecular plane. In the point group C_{2h} , the modes belonging to A_g and B_u symmetries are in-plane vibrations whereas those belonging to B_g and A_u are out-of-plane vibrations. The A_g and B_g vibrations are Raman active, whereas the A_u and B_u vibrations are infrared active ⁶⁶.

As shown above, the experimental IR and Raman vibrational frequencies of different PPV polymers have been measured both in the neutral and in the p-doped state. For that reason, the DFT theoretical calculations are done in neutral state but also with adding one radical cation to the oligomers (doped state). Due to this fact, the calculations will only give information on the vibrational frequencies as a result of polaronic doping and not bipolaronic doping. The theoretical vibration frequencies for oligomers PPV-7 and OCC-PPV-7 are compared with the experimental vibration frequencies of the polymers PPV and MDMO-PPV respectively. Even though MDMO-PPV has large side chains than the oligomer OCC-PPV-7, it is anticipated that the exact nature of the alkyl part of these side chains has no significant impact on the vibrational frequencies associated with the backbone.

C_{2h}	E	C_2	I	σ_h			
A_g	1	1	1	1	R_z	x^2, y^2, z^2, xy	
B_g	1	-1	1	-1	R_x, R_y	xz, yz	
A_u	1	1	-1	-1	z		$z^3, xyz, z(x^2-y^2)$
B_u	1	-1	-1	1	x, y		$xz^2, yz^2, x(x^2-y^2),$ $y(3x^2-y^2)$

Table 4-10: Character table of the point group C_{2h}

4.5.3 Theoretical Vibrations of PPV-7

✓ Before doping

For the comparison of the experimental Raman spectra of poly(*p*-phenylene vinylene) with the PPV-7 oligomer, only the calculated vibrational modes corresponding to an infinite polymer chain have been selected. The factor group of a planar infinite PPV chain is isomorphous to the point group C_{2h} . The fact that no imaginary value was obtained in the calculation of vibrational wavenumbers supports the planarity of the PPV oligomer. The repeating unit of the PPV chain consists of 14 atoms. Hence, PPV-7 contains 96 atoms. The modes belonging to the A_g and B_u symmetries are in-plane vibrations and those belonging to the B_g and A_u symmetries out-of-plane vibrations. As mentioned previously, the A_g and B_g vibrations are Raman active, whereas the A_u and B_u vibrations are infrared active. In this section only the infrared results will be evaluated.

The infrared spectrum of PPV film and the calculated infrared spectrum of PPV-7 are shown in figure 4-43. A list of characteristic IR vibrational frequencies with relative intensities was generated (table 4-11).

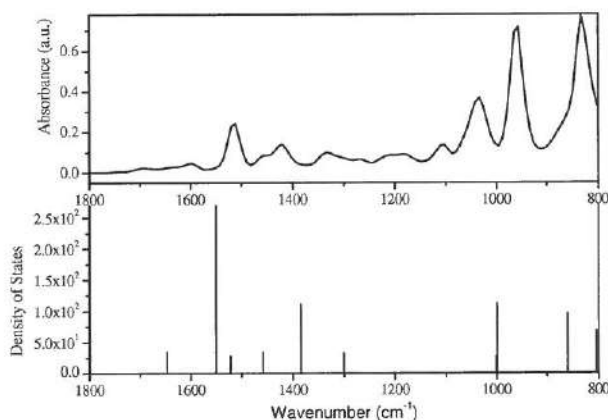


Figure 4-43: Infrared spectrum of neutral PPV (top) and calculated infrared spectrum of PPV-7 (bottom)

The infrared bands experimentally observed at 834 and 960 cm^{-1} are attributed to $\nu_1(\text{A}_u)$ and $\nu_2(\text{A}_u)$ respectively. Both frequencies are out-of-plane vibrations. The $\nu_1(\text{A}_u)$ band is assigned to the in-phase C-H out-of-plane bend of the phenylene ring. The $\nu_2(\text{A}_u)$ band is assigned to the in-phase C-H out-of-plane bend of the vinylene group. The theoretical frequencies of ν_1 and ν_2 were somewhat higher in energy (860 and 999 cm^{-1} respectively) than their corresponding experimental bands. The experimentally observed infrared bands at 1030, 1335, 1419 and 1514 cm^{-1} are attributed to $\nu_3(\text{A}_u)$, $\nu_5(\text{B}_u)$, $\nu_6(\text{B}_u)$ and $\nu_8(\text{B}_u)$ respectively. These bands likely correspond to the theoretical frequencies of 1002, 1385, 1458 and 1550 cm^{-1} for PPV-7. The $\nu_6(\text{B}_u)$ and $\nu_8(\text{B}_u)$ bands can be assigned to the C-C ring stretch in-plane. Finally, the IR band at 1335 cm^{-1} ($\nu_5(\text{B}_u)$) is associated with the C-H in-plane bending of the trans vinylene double bond and the C-H bending of the phenylene ring^{52, 66}. The atomic displacements of the PPV-7 for the bands attributed $\nu_2(\text{A}_u)$, $\nu_5(\text{B}_u)$, $\nu_6(\text{B}_u)$ and $\nu_8(\text{B}_u)$ are shown in figure 4-44.

	Symmetry	Experimental (cm^{-1})		Calculated (cm^{-1})	Intensity (DoS)
ν_1	Au	834	vs	860	96
ν_2	Au	960	vs	999	112
ν_3	Au	1030	s	1002	27
ν_4	Bu			1301	32
ν_5	Bu	1335	vw	1385	111
ν_6	Bu	1419	m	1458	33
ν_7	Bu			1522	28
ν_8	Bu	1514	m	1550	271
ν_9	Bu			1647	34

Table 4-11: Experimental and calculated IR frequencies in the wavenumber range of 800-1800 cm^{-1} for neutral PPV and PPV-7,

(Experimental bands: vs, very strong; s, strong; m, medium; w, weak; vw, very weak).

The vibrational frequencies of $\nu_4(\text{B}_u)$, $\nu_7(\text{B}_u)$ and $\nu_9(\text{B}_u)$ with the theoretical wavenumbers of 1301 cm^{-1} , 1522 cm^{-1} and 1647 cm^{-1} respectively, do not give a band in the experimental IR spectrum of PPV. The reason is that these vibrations are related to the terminal atoms of the oligomer (figure 4-45), which are obviously virtually absent in a high molecular weight polymer.

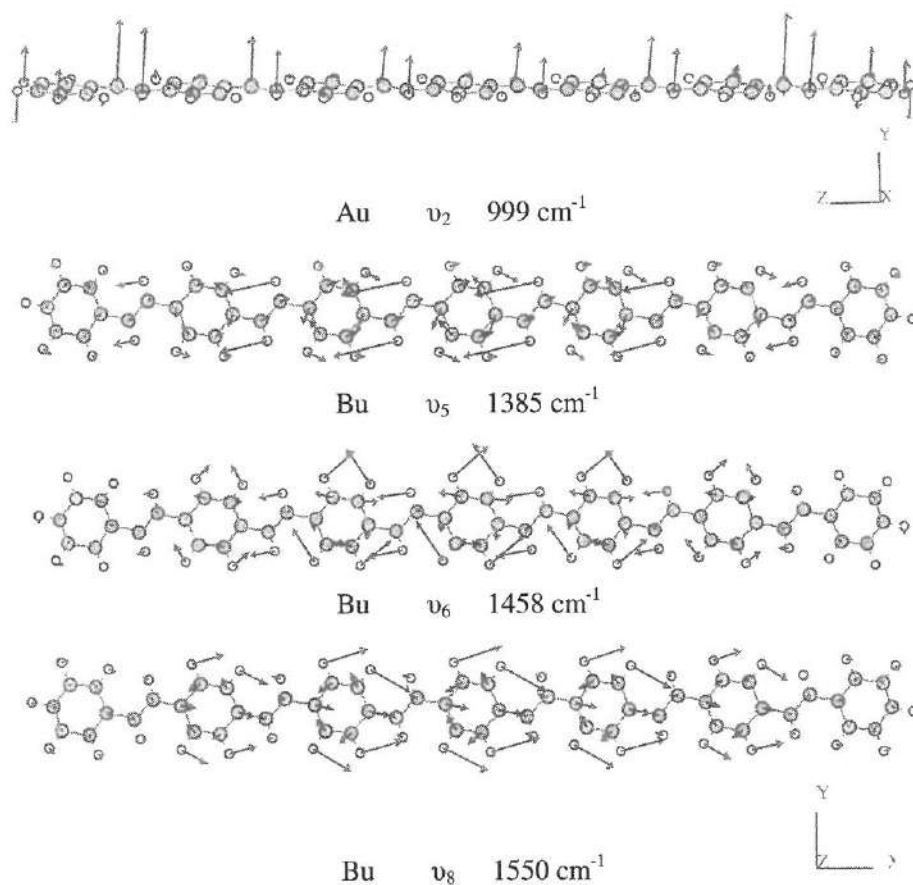


Figure 4-44: Selected *ab initio* vibrational displacements for the normal modes of PPV-7, which give rise to lines in the Infrared spectra of PPV

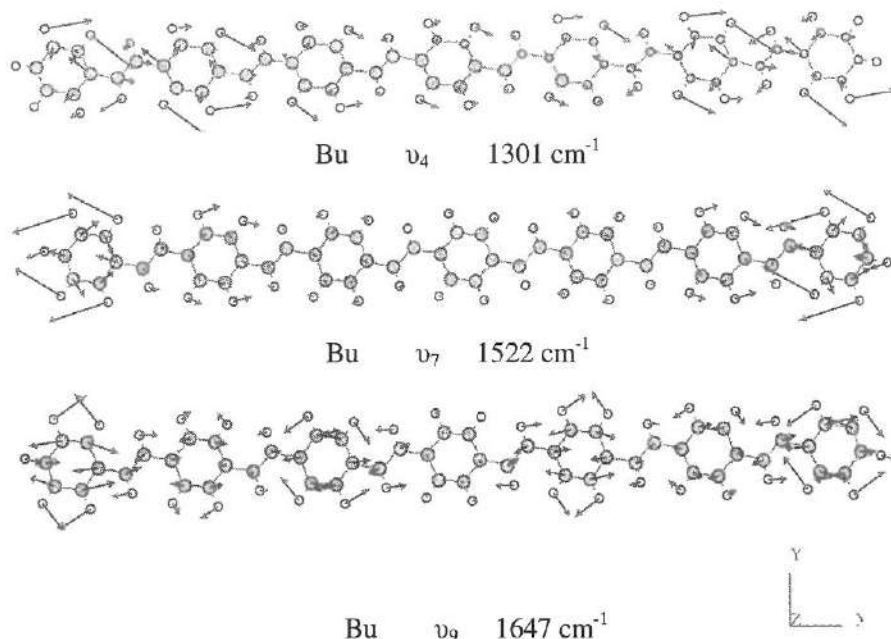


Figure 4-45: Selected *ab initio* vibrational displacements for the normal modes of PPV-7, which do not give rise to lines in the Infrared spectra of PPV

✓ After doping

To compare the experimental IR frequencies of the p-doped PPV polymer with the theoretical frequencies of the PPV-7 oligomer, theoretical calculations were also performed on the radical cation of PPV-7. It should be noted that in this way, only the effect of the formation of a polaron can be determined, not that of a bipolaron. Hence, only the experimental IR vibrations at the beginning of the p-doping process are compared to the theoretical IR vibrations. Also for the radical cation of PPV-7 all calculated frequencies have real values, thus validating the structure used for these calculations. The theoretical and experimental spectra are presented in figure 4-46 and the corresponding frequencies are listed in table 4-12.

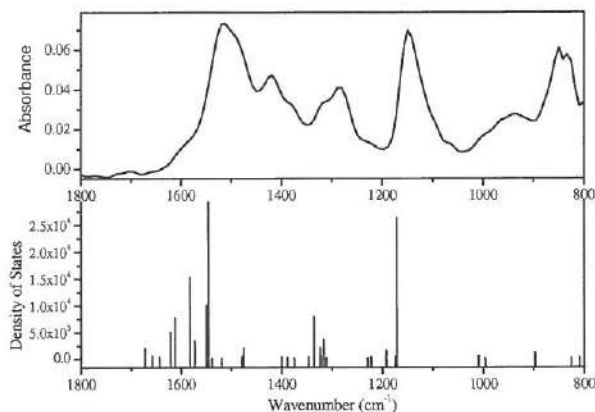


Figure 4-46: Infrared spectrum of *p*-doped PPV (top) and calculated infrared spectrum of the radical cation of PPV-7 (bottom)

Based on a review of table 4-12, two remarks can be made. The first is that by comparing the intensity of the theoretical infrared vibrations of the neutral state with those of the doped state, it can be concluded that the density of states of the doped state is much higher than that of the neutral state. Whereas the absorption frequency depends on the molecular vibrational frequency, the absorption intensity depends on how effectively the infrared photon energy can be transferred to the molecule, and this depends on the change in the dipole moment that occurs as a result of molecular vibration. Hence, one can conclude that the dipole moment of the doped state is, as expected, much higher than the dipole moment of the neutral state. This effect is also experimentally observed. The second remark is that all of the bands observed in the 1800-800 cm⁻¹ region have Bu symmetry. Apparently, due to the incorporation of the positive radical, there are only additional 'in-plane' vibrations, and no 'out-of-plane' vibrations. Hence, it can be concluded that IRAV bands are in-plane vibrations.

	Symmetry	Experimental (cm ⁻¹)		Calculated (cm ⁻¹)	Intensity (DoS)
ν_1	Bu			809	323
ν_2	Bu	840	s	897	1200
ν_3	Bu	957	w	1010	661
ν_4	Bu			1172	26294
ν_5	Bu	1144	vs	1175	510
ν_6	Bu			1193	1614
ν_7	Bu			1223	418
ν_8	Bu			1317	3650
ν_9	Bu	1282	m	1322	525
ν_{10}	Bu			1324	2127
ν_{11}	Bu	1322	m	1337	7945
ν_{12}	Bu			1347	444
ν_{13}	Bu			1400	434
ν_{14}	Bu	1422	w	1475	2152
ν_{15}	Bu	1485	m	1478	548
ν_{16}	Bu	1517	vs	1546	30555
ν_{17}	Bu			1549	10071
ν_{18}	Bu			1573	3423
ν_{19}	Bu	1590	m	1583	15265
ν_{20}	Bu			1613	7652
ν_{21}	Bu			1622	5020
ν_{22}	Bu			1643	389
ν_{23}	Bu			1657	637
ν_{24}	Bu			1672	1954

Table 4-12: Experimental and calculated IR frequencies in the wavenumber range of 800-1800 cm⁻¹ for *p*-doped PPV and the radical cation of PPV-7.

(Experimental bands: vs, very strong; s, strong; m, medium; w, weak; vw, very weak).

As can be seen in figure 4-46, the experimental infrared bands are broad. This means that multiple theoretical infrared vibrations can correspond with one broad experimental infrared band. Therefore, it is impossible to give one assignment to the IRAV bands because these bands are a combination of different vibrations. For example the $\nu_5(\text{Bu})$ vibration at 1172 cm^{-1} is a combination of C-H stretch of the phenylene ring, a C-C ring stretch and C-H stretch of the vinylene bond. A number of examples of the calculated atomic displacements are displayed in figure 4-47.

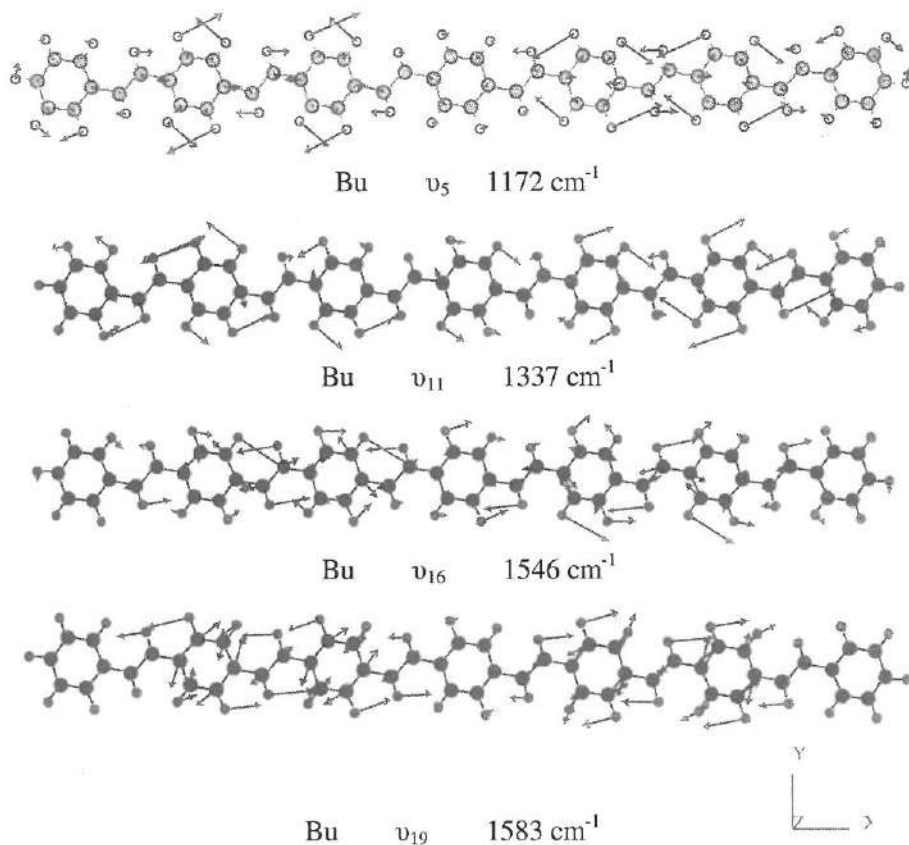


Figure 4-47: *Ab initio* vibrational displacements for selected normal modes of the radical cation of PPV-7, which give rise to lines in the infrared spectra of p-doped PPV.

The intense vibrations $\nu_{20}(\text{B}_u)$ and $\nu_{21}(\text{B}_u)$ with theoretical wavenumbers of 1613 cm^{-1} and 1622 cm^{-1} , do not appear in the experimental IR spectrum of p-doped

PPV. Similar to the neutral case, these vibrations are related to the terminal atoms of the oligomer (figure 4-48).

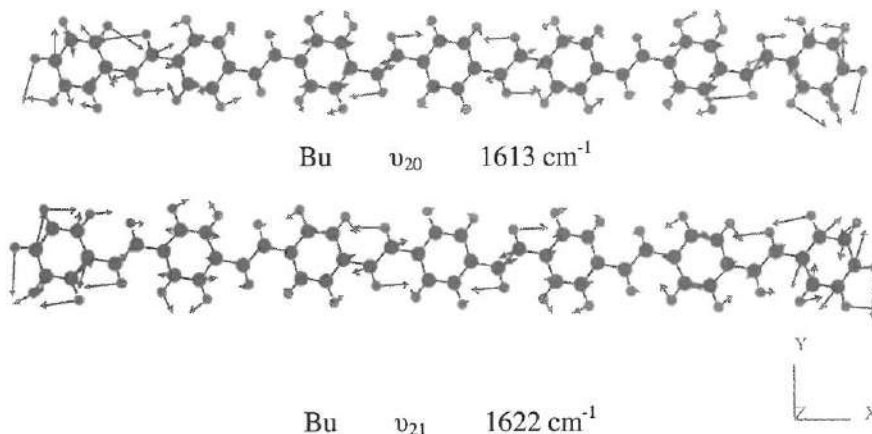


Figure 4-48: *Ab initio* vibrational displacements for selected normal modes of the radical cation of PPV-7, which do not give rise to lines in the infrared spectra of *p*-doped PPV.

4.5.4 Theoretical Vibrations of OCC-PPV-7

✓ Before doping

The infrared spectrum of a MDMO-PPV film and the calculated infrared spectrum of OCC-PPV-7 are shown in figure 4-49. The corresponding list of characteristic vibrational frequencies (theoretical and calculated) with relative intensities can be found in table 4-13.

The experimental infrared bands observed at 854 cm^{-1} and 967 cm^{-1} can be attributed to $\nu_1(\text{Au})$ and $\nu_2(\text{Au})$, respectively, which are theoretically predicted to appear at 882 cm^{-1} and 1009 cm^{-1} . Similar to the previous discussions, the theoretical frequencies are higher in energy than the experimental frequencies. The $\nu_1(\text{Au})$ corresponds to the out-of-plane C-H bending of the tetra-substituted benzene. The $\nu_2(\text{Au})$ band can be assigned to the out-of-plane vibration of C-H trans vinylene bend.

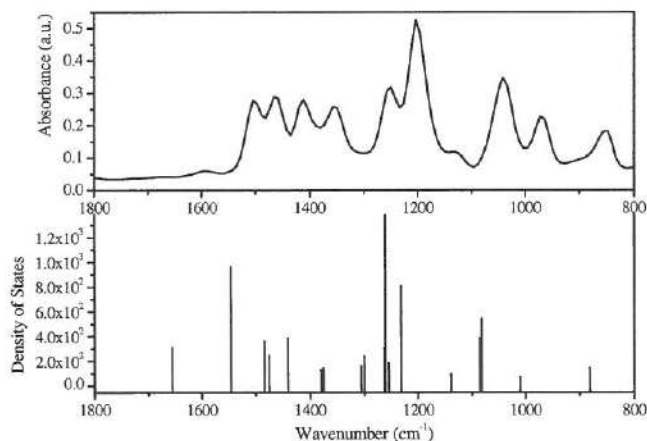


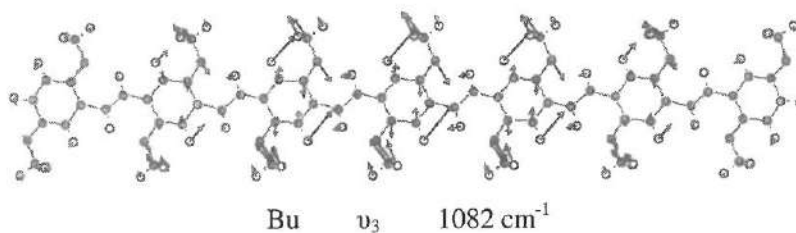
Figure 4-49: Infrared spectrum of neutral MDMO-PPV (top) and calculated infrared spectrum of OCC-PPV-7 (bottom)

In figure 4-50, the atomic displacements of the central part of OCC-PPV-7 for $\nu_3(\text{Bu})$, $\nu_5(\text{Bu})$, $\nu_6(\text{Bu})$, $\nu_{12}(\text{Bu})$, $\nu_{14}(\text{Bu})$ and $\nu_{15}(\text{Bu})$ are depicted. The most intense IR bands involve vibrations of the alkoxy side chains. As expected, the dipole moments and changes therefore are higher due to these side chains. The vibration corresponding to $\nu_3(\text{Bu})$ at 1082 cm^{-1} is the stretching of the ether-alkyl function attached onto the phenylene ring. This vibration is also dominant in the experimental spectrum. The theoretical vibrations corresponding to $\nu_{12}(\text{Bu})$ and $\nu_{14}(\text{Bu})$ at 1440 cm^{-1} and 1484 cm^{-1} are bands with symmetric and asymmetric stretch of the side chain on the second and fifth position of the phenylene ring. The calculated vibrations corresponding to $\nu_5(\text{Bu})$, $\nu_6(\text{Bu})$ and $\nu_{15}(\text{Bu})$ at 1232 cm^{-1} , 1251 cm^{-1} and 1546 cm^{-1} are more complex combined vibrations. Finally, $\nu_4(\text{Bu})$ at 1085 cm^{-1} is positioned at the terminal atoms of the oligomer (figure 4-51) and as a result is not observed in the experimental IR spectrum.

	Symmetry	Experimental (cm ⁻¹)		Calculated (cm ⁻¹)	Intensity (DoS)
ν_1	Au	854	m	882	145
ν_2	Au	967	m	1009	72
ν_3	Bu	1038	s	1082	545
ν_4	Bu			1085	385
ν_5	Bu	1205	vs	1232	804
ν_6	Bu	1251	s	1261	1389
ν_7	Bu			1262	303
ν_8	Bu			1300	242
ν_9	Bu			1305	163
ν_{10}	Bu	1354	s	1376	147
ν_{11}	Bu			1380	129
ν_{12}	Bu	1411	s	1440	388
ν_{13}	Bu	1462	s	1475	245
ν_{14}	Bu			1484	363
ν_{15}	Bu	1504	s	1546	963
ν_{16}	Bu	1590	w	1656	308

Table 4-13: Experimental and calculated IR frequencies in the wavenumber range of 800-1800 cm⁻¹ for MDMO-PPV and OCC-PPV-7.

(Experimental bands: vs, very strong; s, strong; m, medium; w, weak; vw, very weak).



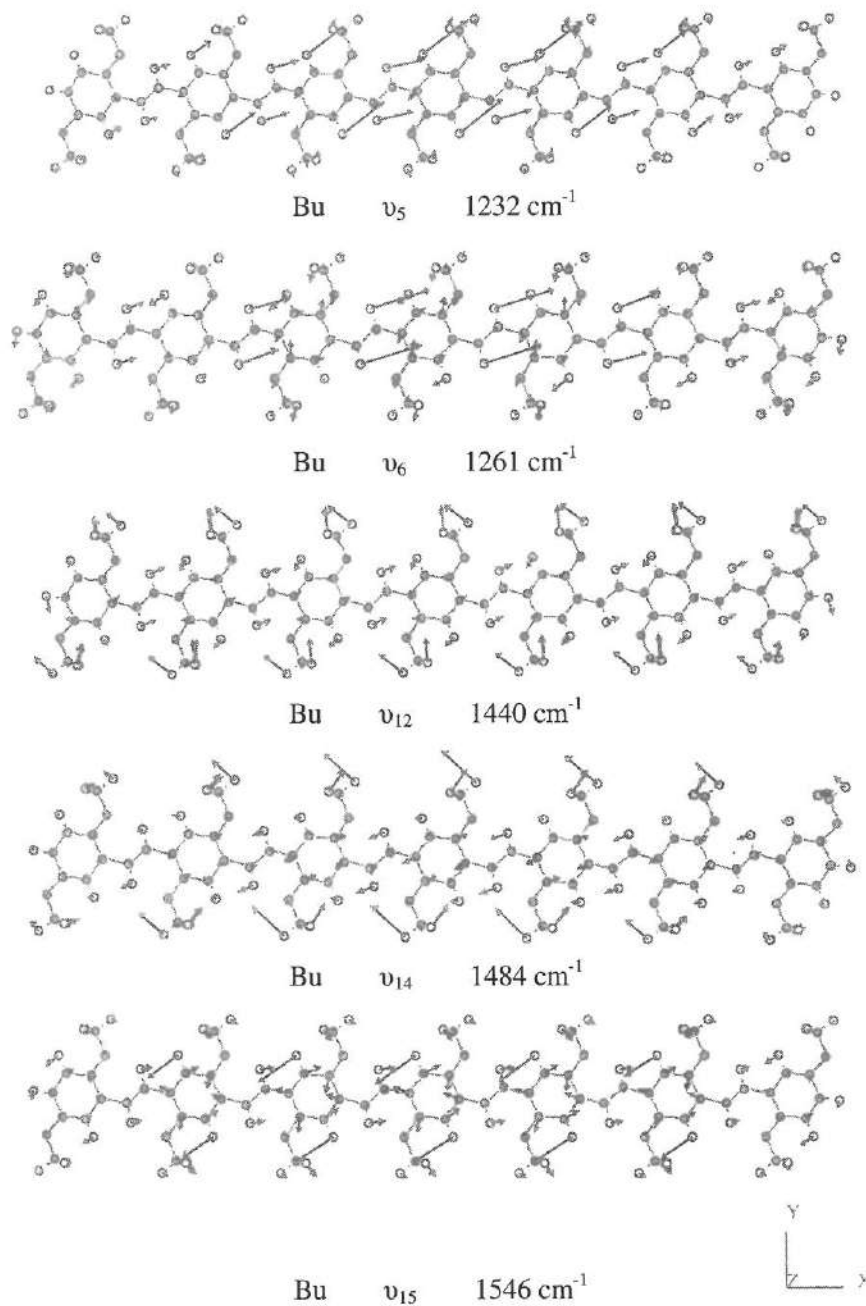


Figure 4-50: *Ab initio* vibrational displacements for selected normal modes of OCC-PPV-7, which give rise to lines in the infrared spectrum of MDMO-PPV.

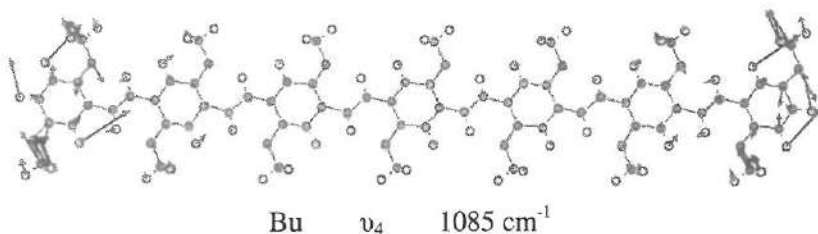


Figure 4-51: *Ab initio* vibrational displacements for a typical normal mode of OCC-PPV-7, which does not give rise to a line in the infrared spectrum of MDMO-PPV.

✓ After doping

The infrared spectrum of a p-doped MDMO-PPV film and the calculated infrared spectrum of the radical cation of OCC-PPV-7 are visualized in figure 4-52 and the characteristic vibrational frequencies are listed in table 4-14. Comparable to the theoretical calculations of PPV-7 in the doped state, only the effect of the formation of a polaron can be determined and not that of a bipolaron. Also in this case, the theoretical calculations for the vibrations of the radical cation of OCC-PPV-7 give real values.

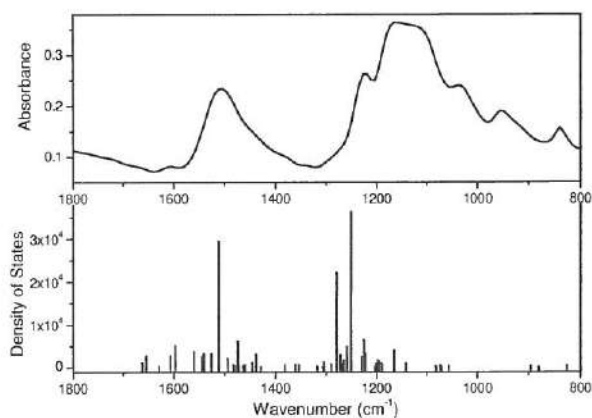


Figure 4-52: Infrared spectrum of p-doped MDMO-PPV (top) and calculated infrared spectrum of the radical cation of OCC-PPV-7 (bottom)

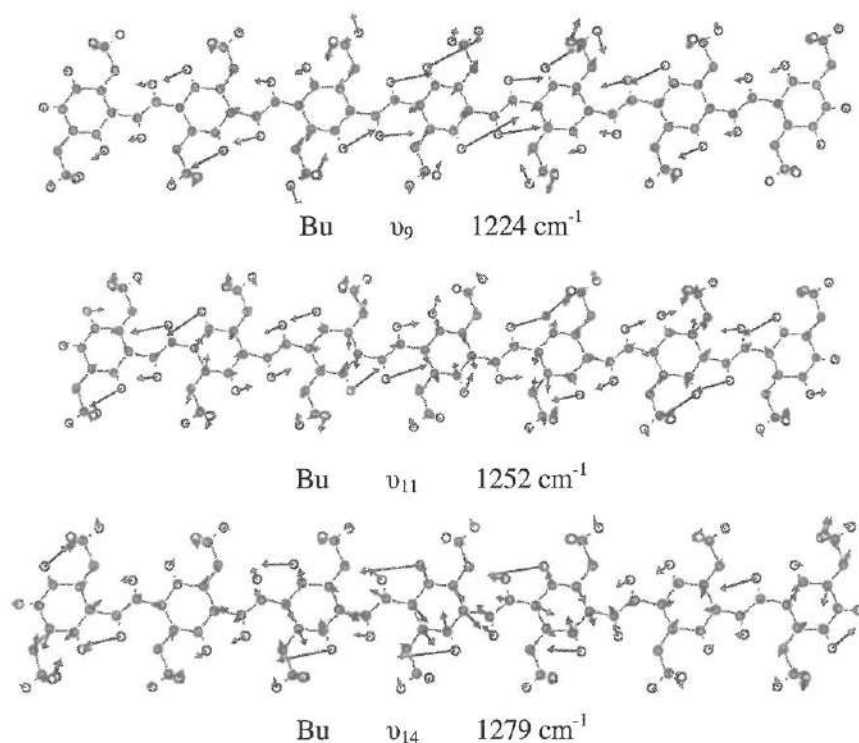
Symmetry		Experimental (cm ⁻¹)		Calculated (cm ⁻¹)	Intensity (DoS)
ν_1	Bu	839	s	828	503
ν_2	Bu	950	w	896	338
ν_3	Bu	1034	vs	1056	417
ν_4	Bu	1119	vs	1142	1049
ν_5	Bu	1162	w	1165	4011
ν_6	Bu			1195	1445
ν_7	Bu			1198	1780
ν_8	Bu	1222	w	1221	3413
ν_9	Bu			1224	6477
ν_{10}	Bu			1230	2600
ν_{11}	Bu			1252	36229
ν_{12}	Bu			1259	4884
ν_{13}	Bu			1271	2994
ν_{14}	Bu			1279	22182
ν_{15}	Bu	1386	w	1438	3156
ν_{16}	Bu	1429	m	1475	6200
ν_{17}	Bu			1494	2089
ν_{18}	Bu			1511	29406
ν_{19}	Bu			1526	3273
ν_{20}	Bu			1541	3377
ν_{21}	Bu			1545	2521
ν_{22}	Bu			1560	3788
ν_{23}	Bu			1597	5183
ν_{24}	Bu	1604	w	1606	2799
ν_{25}	Bu			1654	2877

Table 4-14: Experimental and calculated IR frequencies in the wavenumber range of 800-1800 cm⁻¹ for p-doped MDMO-PPV and the radical cation of OCC-PPV-7.

(Experimental bands: vs, very strong; s, strong; m, medium; w, weak; vw, very weak).

When figure 4-52 and table 4-14 of doped OCC-PPV-7 are compared with figure 4-49 and table 4-13 of the neutral state, it can be concluded that the intensity of the theoretical calculations of the doped state is also in this case significantly higher than that of the neutral state. This means that the dipole moment of the doped state is much higher than the dipole moment of the neutral state. This was also observed for PPV-7 oligomer. The next conclusion is that all the observed IR bands are in-plane vibrations, since they have a Bu symmetry. This supports our previous assessment that the IRAV bands correspond to in-plane vibrations.

In figure 4-53, a few examples of the *ab initio* vibrational displacements of the radical cation of OCC-PPV-7 are demonstrated. From these displacements it is evident that the IRAV bands consist of combinations of different vibrations. Hence, it is impossible to give one exact assignment to an individual IRAV band.



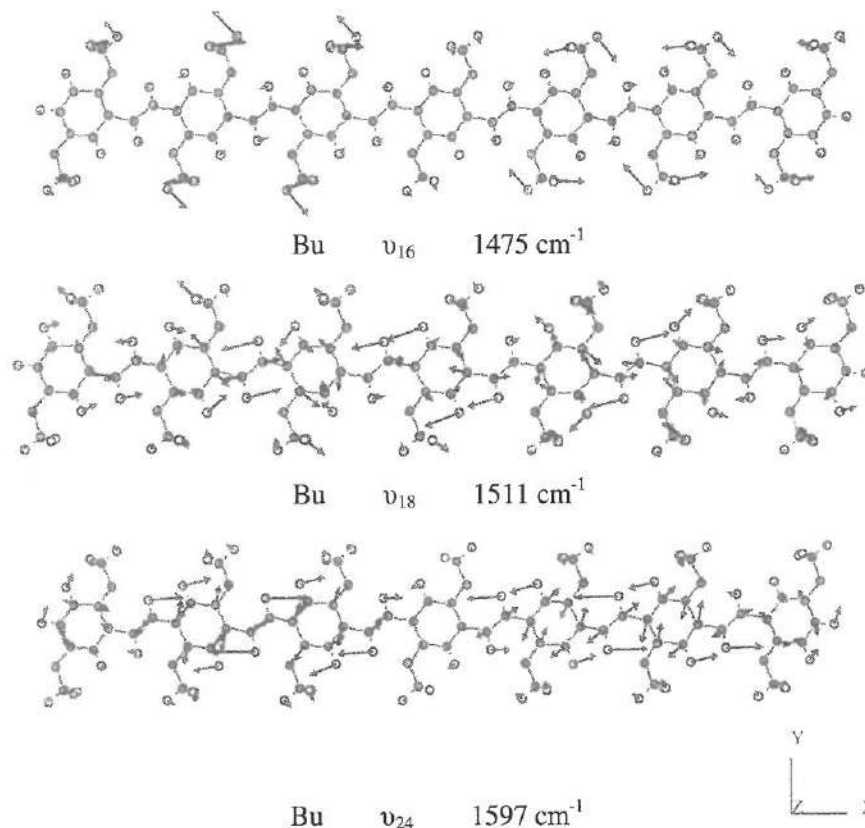


Figure 4-53: *Ab initio* vibrational displacements for selected normal modes of the radical cation of OCC-PPV, which give rise to lines in the infrared spectra of *p*-doped MDMO-PPV.

4.5.7 Conclusions

As demonstrated in this final section of chapter 4, it is possible to use DFT theoretical calculations as a tool for the assignment of the observed IR spectra of neutral and *p*-doped PPV-derivatives. For these normal coordinate calculations an oligomer was utilized with seven phenylene rings and six vinylene moieties. The assignment is possible using the *ab initio* vibrational displacements for the normal modes. Further research is necessary for the assignment of the infrared bands of PTV and its derivatives as well as the Raman bands for both PPV and PTV

derivatives. By comparing the theoretical vibrations with the experimental IR bands, it can be concluded that the theoretical frequencies are shifted to higher energy than the experimental IR vibrations. This can be attributed to the fact that a polymer has a significantly longer conjugated system than the model oligomer with the seven phenylene rings and six vinylene bounds.

Infrared active (IRAV) vibrations, the intense characteristic vibrational modes when the polymer is in the conductive state, are coupled vibrations consisting of a number of overlapping IR bands. It is impossible to give assignments to these bands without calculation first the vibrational displacements for the normal modes. After incorporation of one positive radical in the polymer backbone (in the conductive state), the IR vibrations bands are all in-plane. In contrast, in the neutral state, the IR vibrations are both in- and out-of-plane. It is noteworthy that the intensities (or density of states) of the infrared frequencies in the doped state are significantly higher than those in the neutral state. Whereas the frequency depends on the molecular vibrational frequency, the intensity depends on the change in the dipole moment that occurs as a result of molecular vibration. This means that, as expected, the dipole moment of the doped state is much higher than the dipole moment of the neutral state.

4.6 References

- 1 R. H. Friend, D. D. C. Bradley and P. D. Townsend, *Journal of Physics D: Applied Physics*, 20, **1987**, 1367.
- 2 L. S. Swansson, P. A. Lane, J. Shinar and F. Wudl, *Physical Review B*, 44, **1991**, 10617.
- 3 X. Wei, B. C. Hess, Z. V. Vardeny and F. Wudl, *Physical Review Letters*, 68, **1992**, 666.
- 4 C. Kvarnström and A. Ivaska, *Handbook of Organic Molecules and Polymers*, Vol 4, Wiley, New York, **1997**,

- 5 J. H. Burroughes, D. D. C. Bradley, A. R. Brown, R. N. Marks, K. Mackay, *Nature*, 347, **1990**, 539.
- 6 G. Gustafsson, G. Cao, G. M. Treacy, F. Klavetter, N. Colaneri, *Nature*, 357, **1992**,
- 7 R. H. Friend, R. W. Gymer, A. B. Holmes, J. H. Burroughes, R. N. Marks, *Nature*, 397, **1999**, 121.
- 8 A. J. Heeger, *Solid State Communications*, 107, **1998**, 673.
- 9 Y. Cao, I. D. Parker, G. Yu, C. Zhang and A. J. Heeger, *Nature*, 397, **1998**, 144.
- 10 M. Baïtoul, J. Wéry, J. P. Buisson, G. Arbuckle, H. Shah, *Polymer*, 41, **2000**, 6955.
- 11 R. Cervini, X. C. Li, G. W. C. Spencer, A. B. Holmes, S. C. Moratti, *Synthetic Metals*, 84, **1997**, 359.
- 12 H. Eckhardt, L. W. Shacklette, K. Y. Jen and R. L. Elsenbaumer, *Journal of Chemical Physics*, 91, **1989**, 1303.
- 13 D. A. M. Egbe, T. Kietzke, B. Carbonnier, D. Muhlbacher, H. H. Horhold, *Macromolecules*, 37, **2004**, 8863.
- 14 P. Damlin, C. Kvarnstrom, H. Kulovaara and A. Ivaska, *Synthetic Metals*, 135, **2003**, 309.
- 15 M. Al-Ibrahim, A. Konkin, H. K. Roth, D. A. M. Egbe, E. Klemm, *Thin Solid Films*, 474, **2005**, 201.
- 16 M. Baitoul, J. P. Buisson, S. Lefrant, B. Dulieu, J. Wery, *Synthetic Metals*, 84, **1997**, 623.
- 17 P. Damlin, C. Kvarnstrom, H. Neugebauer and A. Ivaska, *Synthetic Metals*, 123, **2001**, 141.
- 18 H. Neugebauer and Z. Ping, *Mikrochimica Acta*, 14, **1997**, 125.
- 19 H. Neugebauer, *Macromolecular Symposium*, 94, **1995**, 61.
- 20 I. Orion, J. P. Buisson and S. Lefrant, *Physical Review B*, 57, **1998**, 7050.
- 21 J. N. Wilking, B. Hsieh and G. A. Arbuckle-Keil, *Synthetic Metals*, 149, **2005**, 63.

- 22 P. Damlin, C. Kvarnstrom and A. Ivaska, *Journal of Electroanalytical Chemistry*, 570, **2004**, 113.
- 23 C. Kvarnstrom, H. Kulovaara, P. Damlin, T. Vuorinen, H. Lemmetyinen, *Synthetic Metals*, 149, **2005**, 39.
- 24 H. Neugebauer, *Journal of Electroanalytical Chemistry*, 563, **2004**, 153.
- 25 R. L. Elsenbaumer and J. R. Reynolds, *Handbook of Conducting Polymers*, 2nd edition, Marcel Dekker, New York, **1998**,
- 26 T. A. Skotheim, R. L. Elsenbaumer and R. J. Reynolds, *Handbook of Conducting Polymers*, Marcel Dekker, New York, **1998**,
- 27 M. R. Fernandes, J. R. Garcia, M. S. Schulz and F. C. Nart, *Thin Solid Films*, **2004**,
- 28 M. Onoda, S. Morita, T. Iwasa, H. Nakayama and K. Yoshino, *Journal of Chemical Physics*, 95, **1991**, 8584.
- 29 B. Horovitz, *Solid State Communications*, 41, **1982**, 729.
- 30 E. Ehrenfreund, Z. Vardeny, O. Brafman and B. Horovitz, *Physical Review B*, 36, **1987**, 1535.
- 31 G. Zerbi, M. Gussoni and C. Castiglioni, *Conjugated Polymers*, Kluwer, Dordrecht, **1991**, 435.
- 32 C. Kvarnstrom, H. Neugebauer, A. Ivaska and N. S. Sariciftci, *Journal of Molecular Structure*, 521, **2000**, 271.
- 33 B. Tian, G. Zerbi and K. Mullen, *Journal of Chemical Physics*, 95, **1991**, 3198.
- 34 A. Cravino, M. A. Loi, M. C. Scharber, C. Winder, H. Neugebauer, *Synthetic Metals*, 137, **2003**, 1435.
- 35 H. Neugebauer, C. Kvarnstrom, A. Cravino, T. Yohannes and N. S. Sariciftci, *Synthetic Metals*, 116, **2001**, 115.
- 36 N. B. Colthup, L. H. Daly and S. E. Wiberley, *Introduction to Infrared and Raman Spectroscopy*, Third edition, **1990**, 261.
- 37 D. R. Gagnon, J. D. Capistran, F. E. Karasz and R. W. Lenz, *Polymer Bulletin*, 12, **1984**, 293.

- 38 N. B. Colthup, L. H. Daly and S. E. Wiberley, *Introduction to Infrared and Raman Spectroscopy*, Third edition, **1990**, 250.
- 39 P. Damlin, C. Kvarnstrom and A. Ivaska, *Electrochimica Acta*, **44**, **1999**, 1919.
- 40 J. Obrzut and F. E. Karasz, *Journal of Chemical Physics*, **87**, **1987**, 6178.
- 41 D. D. C. Bradley, *Journal of Physics D-Applied Physics*, **20**, **1987**, 1389.
- 42 S. Srinivasan, H. Neugebauer and N. S. Sariciftci, *Synthetic Metals*, **84**, **1997**, 635.
- 43 H. Kuzmany, N. S. Sariciftci, H. Neugebauer and A. Neckel, *Physical Review Letters*, **60**, **1988**, 212.
- 44 C. Kvarnstrom, H. Neugebauer, S. Blomquist, H. J. Ahonen, J. Kankare, *Electrochimica Acta*, **44**, **1999**, 2739.
- 45 A. Henckens, K. Colladet, S. Fourier, T. J. Cleij, L. Lutsen, *Macromolecules*, **38**, **2005**, 19.
- 46 M. Onoda, H. Nakayama, K. Amakawa and K. Yoshino, *Ieee Transactions on Electrical Insulation*, **27**, **1992**, 636.
- 47 J. Y. Mevellec, J. P. Buisson, S. Lefrant, H. Eckhard and K. Y. Jen, *Synthetic Metals*, **35**, **1990**, 209.
- 48 V. Hernandez and F. J. Ramirez, *Journal of Chemical Physics*, **100**, **1994**, 114.
- 49 J. Y. Mevellec, J. P. Buisson and S. Lefrant, *Synthetic Metals*, **41-43**, **1991**, 283.
- 50 D. F. Shriver and P. W. Atkins, *Inorganic Chemistry*, Third edition, Oxford University, **1999**,
- 51 Q. G. Zeng, Z. J. Ding, X. Ju and Z. M. Zhang, *European Polymer Journal*, **41**, **2005**, 743.
- 52 T. Hrenar, R. Mitric, Z. Meic, H. Meier and U. Stalmach, *Journal of Molecular Structure*, 661-662, **2003**, 33.
- 53 T. P. Nguyen, V. H. Tran, P. Destruel and D. Oelkrug, *Synthetic Metals*, **101**, **1999**, 633.

- 54 T. P. Nguyen, S. H. Yang, J. Gomes and M. S. Wong, *Synthetic Metals*, 151, **2005**, 269.
- 55 Y. Furukawa, A. Sakamoto and J. Tasumi, *Journal of Physical Chemistry*, 93, **1989**, 5354.
- 56 S. Lefrant, J. P. Buisson and H. Eckhardt, *Synthetic Metals*, 37, **1990**, 91.
- 57 A. Mabrouk, S. Ayachi, B. Zaidi, J. P. Buisson, P. Molinie, *European Polymer Journal*, 39, **2003**, 2121.
- 58 E. Mulazzi, A. Ripamonti, J. Very, B. Dulieu, E. Faulques, *Synthetic Metals*, 101, **1999**, 196.
- 59 Y. Furukawa, H. Ohta, A. Sakamoto and M. Tasumi, *Spectrochimica Acta Part a-Molecular and Biomolecular Spectroscopy*, 47, **1991**, 1367.
- 60 S. Lefrant, E. Perrin, J. P. Buisson, H. Eckhardt and C. C. Han, *Synthetic Metals*, 29, **1989**, E91.
- 61 A. Sakamoto, Y. Furukawa and M. Tasumi, *Journal of Physical Chemistry*, 96, **1992**, 3870.
- 62 G. Louarn, J. Y. Mevellec, S. Lefrant, J. P. Buisson, D. Fichou, *Synthetic Metals*, 69, **1995**, 351.
- 63 P. M. Viruela, R. Viruela, E. Orti, J. Casado, V. Hernandez, *Journal of Molecular Structure*, 651, **2003**, 657.
- 64 Q.-T. Vu, M. Parlik, N. Hebestreit, U. Rammelt, W. Plieth, *Reactive and Functional Polymers*, 65, **2004**, 69.
- 65 H. Watanabe, Y. Okamoto, K. Furuya, A. Sakamoto and J. Tasumi, *Journal of Physical Chemistry A*, 106, **2002**, 3318.
- 66 K. Honda, Y. Furukawa and H. Nishide, *Vibrational Spectroscopy*, 40, **2006**, 149.
- 67 B. Tian, G. Zerbi, H. Schenk and K. Mullen, *Journal of Chemical Physics*, 95, **1991**, 3191.
- 68 P. Brendel, A. Grupp, M. Mehring, R. Schenk, K. Mullen, *Synthetic Metals*, 45, **1991**, 49.

Summary

Chapter 1 provides a general introduction on conjugated polymers. After a brief outline of the different applications of these materials, the charge transport in conjugated polymers is explained based on the concept of doping and different types of doping are described. The first type is chemical and/or electrochemical doping. This type of doping uses counter dopant ions, which can stabilize the charge on the polymer backbone introduced due to the doping. This type of doping is studied in the following chapters. Other types of doping are photo-doping and charge-injection doping, which both do not use counter dopant ions. At the end of this chapter, the aim and outline of the thesis are given.

In **chapter 2**, the electrochemical properties are presented for different PPV and PTV derivatives. For all studied polymers, the highest occupied (HOMO) and lowest unoccupied molecular orbitals (LUMO) energy levels are calculated. In the literature, a large variety of calculation methods exists to convert the experimental oxidation and reduction potentials to an absolute energy level (eV). The existing conversions have been evaluated and the most appropriate conversion is selected and used throughout this thesis. The selection of a uniform method allows for the comparison of the energy levels of a variety of polymers. This is important for the design of opto-electronic devices, such as organic solar cells.

For the available conjugated polymers, the influence of the introduction of different side chains on the electronic properties has been investigated. By introduction of an alkoxy side chain, the HOMO energy level exhibits a significant change, whereas the changes in the LUMO level are minimal. This results in a decrease of the electrochemical band gap. In contrast as demonstrated for PTV derivatives, the introduction of alkyl side chains has only a small effect on the electronic properties. Furthermore, the HOMO and LUMO levels will change when a bulky alkyl side chains is used. The same holds true for modifications of the conjugated system, for example by extension of the aromatic system.

Finally, the measurements have demonstrated that the HOMO and LUMO energy levels of the different type of conjugated polymers are also dependent on factors, which are not directly a result of the optoelectronic properties of the conjugated backbone. Especially, the ability of (electrolyte) ion transport through the thin conjugated polymer films and the stabilization of the electrolyte counter ion in the polymer film are important. As a result, in some cases the optical band gap is more accurate than the electrochemical band gap.

In **chapter 3**, the optical properties of a representative selection of four 2,5-di-alkoxy substituted PPV derivatives with side chains with different polarities as well as two PTV derivatives have been studied. It is well known that for certain conjugated polymers external stimuli such as heat (thermochromism), solvent (solvatochromism) or the presence of ions (ionochromism) can trigger conformational changes and as a result can have an impact on the optical properties.

In this chapter, the occurrence of thermochromism has been demonstrated for the PPV derivatives both in solution and in a thin film. In these polymers, upon cooling the effective conjugation length increases, which is reflected in a bathochromic shift of the maximum wavelength associated with the π - π^* transition. This thermochromic effect does not depend on the polarity and exact structure of the side chains. Even in the absence of side chains, *i.e.* for PTV, thermochromism is

observed. Hence, in contrast to previous literature reports, it has been demonstrated that the thermochromic effect in poly(arylene vinylene) polymers is associated with the conjugated backbone and not with phase transitions of the side chains. It is proposed that upon heating the segmental motions present in the polymers increase in number and amplitude. As a result, the average torsion angle of the backbone increases significantly and concomitantly the effective conjugation length decreases. In this way, the thermochromic effect can be correlated to the segmental motions present in the polymers. By using this correlation for thin polymer films, it is possible to accurately determine the glass transition temperature. Using this novel technique T_g values can be obtained, which are inaccessible using DSC. Above the T_g , the studied conjugated polymers exhibit virtually identical thermochromic behavior. At the T_g the backbone reaches a planar structure. Upon further cooling, the conformation of the backbone no longer changes and only ground-state aggregation phenomena are observed.

In addition to the effect of temperature, the influence of added ions on the optical properties, *i.e.* ionochromism, of thin films of PPV-type polymers has been demonstrated. These effects are based on the principle that the conformation of the conjugated polymer backbone can change due to complexation effects. The exact effect depends on the type of ion.

Whereas the occurrence of thermochromism is independent of the polarity of the side chains, the solubility as well as solution properties are significantly affected as a result of the introduction of polar substituents. For example, the accessible solvent range is considerably expanded by using not only apolar but also polar side groups. It appears that PPV-type polymers when dissolved in good solvents, do not display noticeable polymer-polymer interactions. However, particularly in poor solvents long-range aggregation phenomena are observed. Especially upon cooling inter- and intra-molecular interactions between individual conjugated segments become increasingly important. Dependent on the solvent/polymer combination used, upon cooling a planarization of the polymer backbone and aggregation phenomena can occur.

In **chapter 4**, the combined the electrochemical and optical properties of conjugated polymers have been investigated with *in situ* spectro-electrochemical techniques. As a first example, *in situ* UV-Vis-NIR spectro-electrochemistry is used to follow the doping process of selected conjugated polymers. For all conjugated polymers in the neutral state, the π - π^* transition is visible. Doping results in a reduction in intensity of the π - π^* transition. Concomitantly, two doping induced band appear, which can be attributed to sub-gap transition due to the formation of polarons and/or bipolarons. For the low band gap polymers, these doping bands overlap and when the polymers are fully doped only one broad band is observed in the UV-Vis-NIR spectrum. Furthermore, it can be concluded that the polarity of the side chains has no significant impact on the spectro-electrochemical properties, which are apparently entirely dependent on the conjugated backbone.

In addition to the optical properties of the doped polymers, also the vibrational properties have been studied. This is possible using *in situ* ATR-IR spectro-electrochemistry and Raman spectro-electrochemistry. In the neutral state, the polymers exhibit typical infrared and Raman vibrational frequencies, which can be assigned using literature data.

For Raman spectroscopy during the p-doping process, the reasonably well-defined peaks of the neutral state convert into broad peaks with low intensity. The Raman spectra exhibit shifts and broadening of existing bands, which can be explained by structural modifications along the polymer chain upon doping.

In contrast, upon doping two types of features can be observed in the IR spectra. The most notable feature is the evolution of a broad absorption band extending from 2100 cm^{-1} up to well above 4000 cm^{-1} . This band is associated with electronic transitions as a result of the formation of polaronic or bipolaronic charged defects on the polymer chain. Concomitantly with the appearance of this broad band, new sharp intensive infrared active vibrations (IRAV) appear in the wavenumber range $1800\text{--}700\text{ cm}^{-1}$. These IRAV bands are a result of the fact that positive charges are created in the polymer chain, which instigate an increasing interaction with electromagnetic radiation. The vibrations become infrared active due to symmetry

breaking and are strongly enhanced, because the typical charge distribution in the formed polaronic state induces high dipole moment changes during vibration.

In the final part of this chapter, DFT theoretical calculations are used as a tool for the assignment of the observed IR spectra of the neutral and p-doped PPV-derivatives. The assignment is possible using the *ab initio* vibrational displacements for the normal modes. After comparing the theoretical vibrations of a model oligomer consisting of seven phenylene rings and six vinylene bonds with the experimental IR bands, it can be concluded that the theoretical frequencies are shifted to higher energy than the experimental IR vibrations. This can be attributed to the fact that the actual polymers have a significantly longer conjugated system than the model oligomers. Using the theoretical calculations, it has been demonstrated that the characteristic infrared active vibrations (IRAV) of doped conjugated polymers are coupled vibrations consisting of a number of overlapping IR bands. Furthermore, these IRAV vibrations appear to be all in-plane. In contrast, in the neutral state, the IR vibrations are both in- and out-of-plane. Finally, the intensities of the infrared frequencies in the doped state are significantly higher than those in the neutral state. This indicates that, as expected, the dipole moments of the doped states are much higher than the dipole moments of the neutral states.

Samenvatting

In **hoofdstuk 1** wordt een algemene inleiding gegeven over geconjugeerde polymeren en daarbij wordt kort een aantal toepassingen van deze materialen aangehaald. Vervolgens wordt de ladingtransport in de geconjugeerde polymeren uitgelegd op basis van doperen en verschillende typen van doperen. Het eerste type is de chemische en/of de elektrochemische dopering. Dit type van dopering maakt gebruik van tegendoperingsionen die de lading, gecreëerd tijdens doperen in de polymeerketen, kan stabiliseren. Dit type van dopering wordt verder bestudeerd in de volgende hoofdstukken. Andere types van dopering zijn foto-dopering en lading-injectie dopering. Beide maken geen gebruik van tegendoperingsionen. Op het einde van dit hoofdstuk wordt het doel van de thesis besproken samen met een overzicht.

In **hoofdstuk 2** worden de elektrochemische eigenschappen van verschillende PPV en PTV derivaten behandeld. Voor alle bestudeerde polymeren worden de hoogst bezette (HOMO) en de laagst onbezette moleculaire orbitalen (LUMO) berekend. In de literatuur bestaan er vele soorten berekeningsmethoden om de experimentele oxidatie- en reductiepotentiaal om te zetten naar een absoluut energie niveau (eV). Deze verschillende soorten berekeningen worden vergeleken en geëvalueerd. Eén berekeningsmethode wordt gebruikt gedurende de hele thesis. Deze berekeningsmethode is belangrijk om de energie niveaus van alle bestudeerde

polymeren te vergelijken. Dit is dan weer belangrijk voor het ontwerpen van opto-elektronische devices zoals organische solar cells.

Daarnaast wordt voor de beschikbare geconjugeerde polymeren de invloed bestudeerd van het invoeren van zijgroepen op de elektronische eigenschappen. Door het invoeren van een alkoxy-zijketen verandert het HOMO energie niveau maar het LUMO niveau niet. Dit resulteert in een daling van de elektrochemische band gap. Voor PTV derivaten is er aangetoond dat de invoering van alkyl zijketens een minimaal effect heeft op de elektronische eigenschappen. Maar de HOMO en LUMO niveaus veranderen wel beiden als er een grote alkyl zijketen wordt gebruikt. Hetzelfde effect is waargenomen wanneer er grotere aromatische systemen worden gebruikt.

In dit hoofdstuk is er ook aangetoond dat de HOMO en LUMO energie niveaus van de verschillende typen geconjugeerde polymeren ook afhankelijk zijn van andere factoren, die niet direct het resultaat zijn van opto-elektronische eigenschappen van de geconjugeerde ruggengraat. Vooral de mogelijkheid van het transport van het elektrolyte ion door de dunne geconjugeerde polymeer film en de stabilisatie van de electrolyte tegenionen in de polymeer film is belangrijk. In deze gevallen is de optische band gap meer accuraat dan de elektrochemische band gap.

In **hoofdstuk 3** worden de optische eigenschappen bestudeerd van twee PTV derivaten en vier 2,5-di-alkoxy gesubstitueerde PPV derivaten die van elkaar verschillen door de zijketens met andere polariteiten. Het is gekend dat voor bepaalde geconjugeerde polymeren externe factoren zoals warmte (thermochroïsme), solvent (solvatochromisme) en de aanwezigheden van ionen (ionochroïsme) een invloed hebben op de conformationele veranderingen en zodoende de optische eigenschappen beïnvloeden.

In dit hoofdstuk wordt thermochromie gedemonstreerd voor PPV derivaten in oplossing en in een dunne film. Tijdens het koelen van deze polymeren stijgt de effectieve conjugatie lengte. Deze wordt waargenomen door een bathochrome shift van de maximale golflengte die geassocieerd is met de π - π^* transitie. Dit

thermochroom effect is niet afhankelijk van de polariteit en de structuur van de zijketen. Zelfs in afwezigheid van de zijketens zoals in PTV wordt het thermochromisch effect waargenomen. In tegenstelling tot verschillende artikels in de literatuur is er aangetoond dat de thermochromie in poly(aryleen vinyleen) polymeren afhankelijk is van de geconjugeerde ruggengraat en niet van de fase transities van de zijketens. Tijdens het opwarmen stijgen de segmentale bewegingen in de polymeerketens samen met de amplitude. Dit resulteert in een stijging van de gemiddelde torsie hoek van de ruggengraat waardoor de effectieve conjugatie lengte daalt. Dit wil zeggen dat het thermochromisch effect afhankelijk is van de segmentale bewegingen aanwezig in de polymeren. Door deze correlatie te gebruiken voor dunne polymeer filmen is het mogelijk om de glas transitie temperatuur van een polymeer accuraat te bepalen. Door deze nieuwe techniek te gebruiken kunnen er Tg waarden verkregen worden die niet kunnen bepaald worden door DSC metingen. Boven de Tg vertonen de bestudeerde geconjugeerde polymeren hetzelfde thermochroom gedrag. Op de Tg bereikt de ruggengraat een planaire structuur. Bij verder afkoelen verandert de conformatie van de ruggengraat niet langer en enkel een grondtoestand aggregatie wordt waargenomen.

Naast het effect van de temperatuur wordt de invloed van toegevoegde ionen op de optische eigenschappen nagegaan bij dunne PPV filmen. Dit is ionochroïsme. Dit effect is gebaseerd op het principe dat de conformatie van het geconjugeerde polymeer ruggengraat kan veranderen door de complexatie effecten. Het juiste effect hangt af van de grootte van het ion.

Zoals al eerder werd aangehaald is het thermochromisch effect onafhankelijk van de polariteit van de zijketens, maar de oplosbaarheid en de oplosningseigenschappen kunnen wel beïnvloed worden door de invoering van polaire substituenten. De solventen range kan bijvoorbeeld uitgebreid worden door gebruik te maken van apolaire en polaire zijgroepen. Wanneer PPV type polymeren worden opgelost in goede solventen spelen de polymeer-polymeer interacties geen rol. Maar in slechtere solventen worden lange range aggregatie fenomenen waargenomen. Vooral tijdens het afkoelen spelen de inter- en intra-moleculaire

interacties tussen individuele geconjugeerde segmenten een belangrijke rol. Afhankelijk van de gebruikte solvent/polymeer combinatie kan tijdens het afkoelen een planarizatie van de polymere ruggengraat en een aggregatie worden veroorzaakt.

In **hoofdstuk 4** worden de elektrochemische en optische eigenschappen van geconjugeerde polymeren gecombineerd door *in situ* spectro-electrochemische technieken. *In situ* UV-Vis-NIR spectro-elektrochemie wordt gebruikt om het doperingsproces van geselecteerde geconjugeerde polymeren te volgen. In de neutrale toestand is er enkel de π - π^* transitie waarneembaar voor alle geconjugeerde polymeren. Gedurende het doperen wordt de π - π^* transitie piek kleiner. Tegelijkertijd ontstaan er twee doperingsbanden die toegeschreven zijn aan de sub-gap transitie door de vorming van polaronen en/of bipolaronen. Voor low-band gap polymeren wordt er een overlap van de doperingsbanden verkregen. Bij een volledige dopering van deze polymeren wordt er één brede band waargenomen in het UV-Vis-NIR spectrum. Daarbij is er waargenomen dat de polariteiten van de zijketens geen invloed hebben op de spectro-electrochemische eigenschappen, die enkel afhankelijk is van de geconjugeerde ruggengraat.

Naast de optische eigenschappen van gedopeerde polymeren worden ook de vibrationele eigenschappen bestudeerd. Dit is mogelijk door gebruik te maken van *in situ* ATR-IR spectro-electrochemie en Raman spectro-electrochemie. In de neutrale toestand vertonen de polymeren typische infrarood en Raman vibrationele frequenties die benoemt kunnen worden door gebruik te maken van de literatuur.

Tijdens het p-doperen worden de scherpe Raman pieken van de neutrale toestand omgezet tot brede pieken met lage intensiteit. De bestaande Raman banden worden tijdens het doperen vergeschoven en verbreed. Dit kan verklaard worden door structurele veranderingen in de polymeer keten tijdens het doperen. Bij IR spectroscopie worden er twee kenmerken waargenomen tijdens het doperen. Het eerste kenmerk is de evolutie van een brede absorptie band die zich uitstrekt van 2100 cm^{-1} tot boven 4000 cm^{-1} . Deze band is geassocieerd met de elektronische

overgangen die het resultaat zijn van polaron en bipolaron geladen defecten in de polymeer ketens. Samen met deze brede band ontstaan er ook nieuwe scherpe intense infrarood actieve vibraties (IRAV) tussen 1800 cm^{-1} en 700 cm^{-1} . Deze IRAV banden zijn het resultaat van het feit dat positieve ladingen gecreëerd worden in de polymeer ketens. De vibraties worden infrarood actief door de symmetrie breking. Daarbij zijn deze banden sterk door de typische ladingdistributie van de gevormde polaron toestanden die een hoge dipoolmoment induceren die verandert gedurende de vibratie.

In het laatste deel van dit hoofdstuk worden DFT theoretische berekeningen uitgevoerd om de waargenomen IR spectra van de neutrale en de p-gedopeerde PPV derivaten te benoemen. Deze benoeming is mogelijk door gebruik te maken van *ab initio* vibrationele verplaatsingen van de normale modes. Na het vergelijken van de theoretische vibraties van een model oligomeer bestaande uit zeven fenyleen ringen en zes vinyleen bindingen met de experimentele IR banden, kan er geconcludeerd worden dat de theoretische frequenties opgeschoven zijn naar hogere energie in vergelijking met de experimentele IR vibraties. Dit komt omdat de werkelijke polymeren een langer geconjugeerd systeem hebben dan de model oligomeren. Door gebruik te maken van de theoretische berekeningen is er ook aangetoond dat de infrarood actieve vibraties (IRAV) van de gedopeerde geconjugeerde polymeren gekoppelde vibraties zijn bestaande uit een aantal overlappende IR banden. Daarbij zijn de IRAV banden allemaal vibraties in het vlak. Dit is in tegenstelling tot de neutrale toestand waar de IR vibraties in- en uit het vlak zijn. Tot slot is er nog waargenomen dat de intensiteiten van de infrarood frequenties in de gedopeerde toestand hoger zijn dan die in de neutrale toestand. Dit geeft aan dat het dipoolmoment van de gedopeerde toestand veel hoger is dan het dipoolmoment in de neutrale toestand.

List of Abbreviations

Chapter 1: Introduction: Conjugated Polymers

σ	Electrical conductivity
PA	Poly(acetylene)
PPV	Poly(<i>p</i> -phenylene vinylene)
PEDOT	Poly(ethylenedioxythiophene)
PT	Polythiophene
PTV	Poly(thienylene vinylene)
MDMO-PPV	Poly(2-methoxy-5-(3,7-dimethyloctyloxy)- <i>p</i> -phenylenevinylene)
DiBPh-PTV	Poly(3,4-bis(4-butylphenyl)-2,5-thienylene vinylene)
FET	Field-Effect Transistors
LED	Light-Emitting Diodes
LEC	Light-Emitting Electrochemical Cells
VB	Valence Band
CB	Conductance Band
E _g	Energy gap or band gap
eV	Electron Volt
p-doping	Oxidation
n-doping	Reduction

Chapter 2: Electrochemistry: Cyclic Voltammetry

CV	Cyclic Voltammetry
Pt	Platinum
NHE	Normal (also termed standard) Hydrogen Electrode
SCE	Saturated Calomel Electrode
Ag/AgCl	Silver/Silver Chloride (Ag/AgCl) electrode
Ag wire	Silver wire electrode
ITO	Indium-Tin-Oxide
a	Activity
ACN	Acetonitrile
TBAPF ₆	TetraButylAmmoniumhexaFluoroPhosphate
eV	Electron Volt
EA	Electron Affinity
IP	Ionisation Potential
HOMO	Highest Occupied Molecular Orbital
LUMO	Lowest Unoccupied Molecular Orbital
Fc	Ferrocene
E	Energy (in J)
h	Planck constant (6.626×10^{-34} Js)
c	Speed of light (3×10^8 ms ⁻¹)
ν	Frequency (in s ⁻¹ or Hz)
λ	Wavelength (in nm).

Chapter 3: UV-Vis-NIR Absorption Spectroscopy

UV-Vis-NIR	UltraViolet-Visible-Near InfraRed
MDMO-PPV	Poly(2-methoxy-5-(3,7-dimethyloctyloxy)-p-phenylenevinylene)

MTEM-PPV	Poly(2-methoxy-5-(triethoxymethoxy)- <i>p</i> -phenylenevinylene)
BTEM-PPV	Poly(2,5-bis(triethoxymethoxy)- <i>p</i> -phenylenevinylene)
NTEM-PPV	Poly(2-(<i>n</i> -nonyloxy)-5-(triethoxymethoxy)- <i>p</i> -phenylenevinylene)
λ_{\max}	Optical absorption maximum
DSC	Differential Scanning Calorimetry
T _g	Glass transition Temperature
MD	Molecular Dynamics
PTV	Poly(2,5-thienylene vinylene)
H-PTV	Poly(3-hexyl-2,5-thienylene vinylene)
CHCl ₃	Chloroform
THF	Tetrahydrofuran
E _T N	Polarity
AFM	Atomic Force Microscopy
PL	Photoluminescence

Chapter 4: *In Situ* Spectro-Electrochemistry

UV-Vis-NIR	UltraViolet-Visible-Near InfraRed
FTIR	Fourier Transform Infrared
ATR	Attenuated Total Reflection
Ge	Germanium
IRAV	Infrared Active Vibration
ν	Vibrational frequency
DFT	density functional theory
B3LYP	Becke-3-parameters-Lee-Yang-Parr functional
DOS	Density Of States

